Inelastic Behavior of Direct RC Column to CFST Pile Connections

Spencer Lindsley

A thesis

submitted in partial fulfillment of the

requirements for the degree of

Master of Science in Civil Engineering

University of Washington

2021

Reading Committee:

Dawn E. Lehman

Charles W. Roeder

Marc O. Eberhard

Program Authorized to Offer Degree:

Civil and Environmental Engineering

University of Washington

Abstract

Inelastic Behavior of Direct RC Column to CFST Pile Connections

Spencer Lindsley

Co-Chairs of the Supervisory Committee:
Dawn E. Lehman
Civil and Environmental Engineering
Charles Roeder
Civil and Environmental Engineering

Concrete filled steel tubes (CFSTs) are a composite structural component consisting of a steel tube with concrete infill. Prior research has shown that CFST structural elements have greater strength and stiffness than typical reinforced concrete structural elements of similar size, result in economical structures, and also provide accelerated bridge construction. CFST members are quite suitable for piles and drilled shafts for deep foundations in bridge construction. While there has been both analytical and experimental research into CFST member behavior, there has been little research on connections of RC columns to CFST piles and drilled shafts. This research is an experimental study of a new connection between RC columns and CFST piles. In this research, half-scale column-to-pile connections were tested to evaluate their inelastic behavior under seismic

loading. Four specimens were tested with the primary focus on the effects of (i) column reinforcement embedment depth, (ii) pile size, and (iii) the addition of a supplemental rib inside the pile. The nonlinear behavior was evaluated and the effects of these key parameters on the resistance, ductility, and deformation capacity were determined. The transfer of the force and moment from the RC column to the CFST pile were closely monitored. The experimental results were compared to nonlinear analyses performed with LS-Dyna computer program to calibrate models for future study and establish the accuracy of the models. The experiments found showed that the connections have excellent strength, ductility, and inelastic deformation capacity. The moment and force of the RC column were effectively transferred to the CFST pile with a nominal development length of the reinforcing bar. The test suggests that connections with a larger pile or a supplemental rib inside the pile, showed improved seismic performance, compared to connections with a smaller pile and no supplemental rib.

TABLE OF CONTENTS

LIST OF FIGURES

LIST OF TABLES

ACKNOWLEDGEMENTS

I would like to thank my advisors, Professor Dawn Lehman and Professor Charles Roeder for their support and expertise throughout this research. I would like to especially thank them for their patience and understanding during all aspects of the project. I would also like to thank Professor Marc Eberhard for serving on my committee.

I would like to thank all the students that helped me with this research both inside and outside the laboratory: Austin Anderson, Will Bergendahl, Clayton Black, Michelle Chang, Joe Kaldestad, Will Krause, Danielle Voytko, Jason Wells, and Ray Yu. Without their help, I would still be trying to figure out how to tie rebar. I owe a big thank you to Vongsant (Vince) Chaijaroen, who helped me with the research but also with life.

This project was funded by the Pacific Earthquake Engineering Research (PEER) Center and the Accelerated Bridge Construction University Transportation Center (ABC-UTC).

Chapter 1. INTRODUCTION

1.1 RESEARCH MOTIVATION

Concrete filled steel tubes (CFSTs) are a composite structural element that combines the compressive strength of concrete with the tensile strength and ductility of steel. They have been shown to provide greater strength and stiffness than traditional reinforced concrete (RC) elements of comparable size. CFSTs have significantly larger shear resistance than RC members of comparable size, and therefore CFSTs are very suitable for piles and drilled shafts in deep foundations at sites with liquefaction or lateral spreading of soil. CFSTs do not require formwork, shoring, or internal reinforcement, which accelerates construction and reduces cost.

In recent years, the seismic design forces on bridges have increased, which has led to increased demand on the structural resistance of bridge substructures. The use of CFSTs piles with RC columns provides the bridge with strength, stiffness, ductility, and energy dissipation for large lateral loads and deformations on the column and the pile. This combination also leads to accelerated construction and cost savings.

However, connections between RC columns and CFST piles and the mechanism of force and moment transfer between the two components are not well understood. This research is an experimental study focused on understanding these connections, their transfer mechanisms, and how these mechanisms affect moment, axial, and shear forces on the connection behavior.

Prior analytical research, suggests that the bond between the RC column reinforcement and the concrete, and the bond between the tube and concrete are important elements of the transfer mechanism. The bond between the reinforcement and the concrete is dependent on the embedment depth of the reinforcement into the pile and the relative diameters of the column and

pile. The bond between the tube and the concrete is affected by the type of steel tube used, with spirally welded tubes having shown to have more bond stress capacity than straight seam welded tubes. Adequate development length may be required to transfer the forces and moments of the RC column to the CFST pile. A steel rib welded to the interior of the tube may also aid in this force and moment transfer.

This research is an experimental study to investigate a direct RC-column-to-CFST-pile connection. Four half-scale experiments are performed. The specimens are designed to consider the critical parameters noted above. The specimens are loaded under cyclic inelastic deformation and their inelastic behavior is measured and observed. The data is analyzed and the results are compared to determine the relative importance of the variables considered in the study. The results are also compared to results of nonlinear analyses performed using LS-Dyna, an FEA computer program, so the finite element model can be calibrated and improved and the accuracy of the model estimated. This will allow the extension of this work through future nonlinear analysis studies.

1.2 RESEARCH OBJECTIVES

The experimental investigation of these specimens was done to characterize the behavior of a direct CFST pile to RC column connection under cyclic loading and to provide design recommendations. To meet this goal, the following objectives were set:

- Experimentally investigate the inelastic behavior response of the reinforcement development length in a direct CFST pile-to-column connection.
- Experimentally investigate the inelastic behavior response of different pile diameters in a direct CFST pile-to-column connection.

- Experimentally investigate the inelastic behavior of a direct CFST pile to column connection with the additional mechanical bond mechanism.
- Experimentally investigate the inelastic response of a direct CFST pile to column connection under long-duration cyclic loading.
- Compare and validate the simulated FEA model results of the connection with the experimental measured results.

1.3 ORGANIZATION OF THESIS

This report includes 7 chapters.

Chapter 2, is a literature review, which provides an overview of previous research that has been conducted on connections between cased shafts or concrete-filled tubes and reinforced concrete columns, and other related work to this experimental research.

Chapter 3, provides an overview of the four specimens in the test program. It also describes the design and construction process for each specimen, as well as the testing apparatus and process, and instrumentation.

Chapter 4, describes the experimental measured and observed response of the four tests, looking at the strain in the reinforcement, the specimen damage, and overall specimen behavior.

Chapter 5, discusses the data interpretation and analysis of the four tests based on measured responses from testing instrumentation. This chapter includes force-displacement plots, as well as strain distribution, curvature profiles, energy dissipation, and displacement contributions.

Chapter 6, compares the experimental results of the four tests to the analytical finite element model of Zhao. This chapter includes comparisons of force-displacement hysteretic curves, strain distributions, and specimen damage.

Chapter 7, summarizes the work and the conclusions and recommendations from this work.

Chapter 2. LITERATURE REVIEW

2.1 INTRODUCTION

Prior research into direct column to pile connections was used to develop the research program described herein. This chapter provides a summary of related research, both analytical and experimental, to connections between reinforced concrete (RC) columns and substructure subassemblies. The objectives of the chapter are to:

- Investigate similar types of column-to-pile connections being used in high seismic regions
- Investigate the behavior of similar connections through prior experimental research
- Understand how prior analytical research affected this experimental research's design and process

This chapter contains an overview of current column-to-pile connections used in high seismic regions along with code requirements used by the Washington Department of Transportation (WSDOT) and the California Department of Transportation (Caltrans). Following this overview, are the experimental test programs that investigated the force-transfer mechanisms of these types of connections. Table 2.1 summarizes the different research programs and their focus. The final section is on the Finite Element Analysis (FEA) of a RC column to CFST pile connection, which is the basis of this research.

Table 2.1. Research Programs Reviewed

Title	Researcher	Year	Research Focus
Lateral Behavior of RC Columns Supported on Type II Shafts	Liu	2012	Column Ductility and Plastic Hinge Formation
Performance of Steel Pipe Pile-to-Concrete Cap Connections Subjected to Seismic or High Transverse Loading	Kappes	2013	CFST Column to RC Cap Beam Connections
Design Expressions and Dynamic Evaluation of CFST Bridges Subjected to Seismic Hazards	Stephens	2016	CFST Column to Precast Cap Beam Connections
Seismic Performance of Bridge Column-Pile-Shaft Pin Connections for Applications in Accelerated Bridge Construction	Mehraein	2016	Pipe-Pin and Rebar-Pin Connections on RC Column to Shaft Connection
Analytical Investigation of A New Direct Column-to-Cased Shaft Connection	Zhao	2020	CFST Pile to RC Column Connections
Seismic Performance of Column-to-Drilled Shaft Connections in Reinforced Concrete Bridges	Chang	2021	RC Drilled Shaft to CIP Column Connections

2.2 Connection Types and Code Provisions

There are two general types of column-shaft connections that are used in high seismic regions by Caltrans and WSDOT: ones that transfer axial and shear force while permitting rotation, and ones that transfer moment, axial, and shear forces while restraining rotation.

Pin connections between column-shaft assemblies only transfer shear and axial force. This is done by having a reinforcement cage, pipe, or solid steel section as the pinned connection between the top of the shaft and the column base. A general pin connection diagram is shown in Figure 2.1. The main code requirements for this type of connection is that a) the shafts are designed to be capacity protected members, b) if using a reinforcement cage pin, the pin must be developed in both the column and the shaft, c) if using a pipe or solid steel pin, the pin must be developed in the shaft (Caltrans SDC). Mehraein investigates two types of pin connections, Rebar-Pin and Pipe-Pin, in his research.

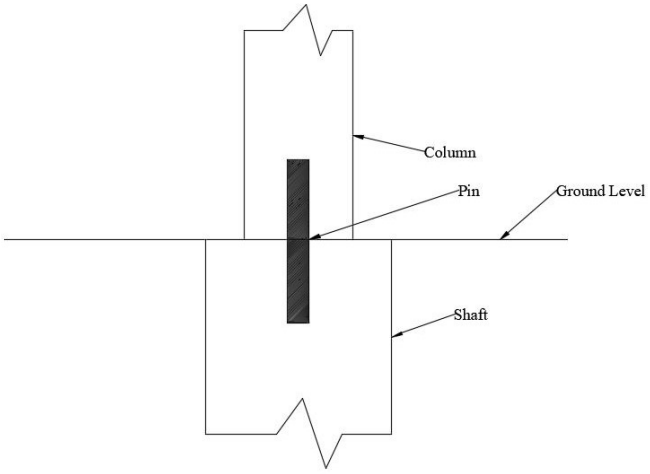

Figure 2.1. General Pin Connection

There are a few types of connections that transfer moment, shear, and axial force. The first type is a socket or drilled shaft connection, which uses RC for both the shaft and the column. The other type is a direct connection between a CFST and a RC column.

The socket connection is dependent on the embedment of the column reinforcement cage into the pile-shaft and the transverse reinforcement in the shaft. A general socket connection diagram is shown in Figure 2.2. The difference between Type 1 and Type II shafts is that Type I shafts have an increased amount of concrete cover below ground, while Type II shafts have both an increased diameter and a separate reinforcement cage from the column.

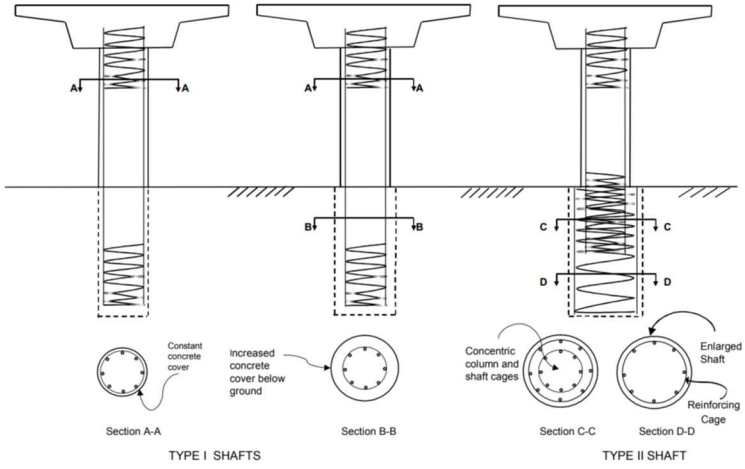

Figure 2.2. Column-Shaft Connection Types (Caltrans)

This connection also requires the shaft to be a capacity-protected member of the assembly, but Caltrans and WSDOT have differing requirements for the embedment length of the column reinforcement and the amount of required transverse reinforcement in the shaft.

Caltrans requires that the column longitudinal bar embedment length meet the following equation (Caltrans SDC Table 8.3.2-1):

$$l_e = \begin{Bmatrix} D_{c,max} + 42d_{bl} & for\ \#11\ bars\ and\ smaller \\ D_{c,max} + 48d_{bl} & for\ \#14\ and\ \#18\ bars \end{Bmatrix}$$

L_e = required embedment length of column longitudinal bar (in.)

$D_{c,max}$ = largest cross-sectional dimension of the column (in.)

d_{bl} = nominal diameter of column longitudinal bar (in.)

Caltrans requires the shaft transverse reinforcement to meet the following requirements based on a minimum volumetric ratio and maximum allowable spacing. This is shown in Table 2.2 (Caltrans SDC Table 5.4.5-1).

Table 2.2. Minimum Volumetric Ratio of Transverse Reinforcement in Caltrans Type II Shafts (Caltrans SDC)

Location	Minimum Volumetric Ratio of Transverse Reinforcement	
	CISS or CIDH with permanent casing	All other Shafts
Top 2 feet of Shaft	50% of that required at the base of the column	Same as that required at the base of the column
Between the bottom end of column cage and 2 ft. below the top of Type II shaft		50% of that required at the base of the column

WSDOT requires that the column longitudinal bar embedment length meet the following equation (WSDOT BDM 7.3.5):

$$l_e = l_s + e$$

l_s = the larger of $1.7l_{ac}$ or $1.7l_{d,c}$. The 1.7 factor represents a Class C lap splice modification factor from previous versions of AASHTO Bridge Design Specifications (BDS)

l_{ac} = development length (in.) from AASHTO Guide Specifications for LRFD Seismic Bridge Design (SGS) Section 8.8.4 for column longitudinal reinforcement (in.)

$l_{d,c}$ = tension development length from AASHTO BDS Section 5.11.2.1 for column longitudinal reinforcement (in.)

e = eccentricity distance between shaft and column longitudinal reinforcement (in)

WSDOT requires the shaft transverse reinforcement to meet the following equation (WSDOT BDM eq. 7.8.2-1), which is also used in AASHTO BDS:

$$\frac{A_{tr}}{s} = \frac{kA_l f_{u,l}}{2\pi f_{y,tr} l_s}$$

A_{tr} = area of transverse reinforcement (in.^{2})

S = spacing of the transverse reinforcement (in.)

k = factor representing the ratio of column tensile reinforcement to total column reinforcement at the nominal bending resistance

A_l = Total area of longitudinal column reinforcement (in.^{2})

$f_{u,l}$ = Specified minimum tensile strength of column longitudinal reinforcement (ksi)

$f_{y,tr}$ = the yield stress of the transverse reinforcement (ksi)

l_s = lap splice length of column reinforcement (in.)

A direct connection between a CFST shaft or pile and a RC column is also dependent on the embedment depth of the column longitudinal reinforcement but uses a ring or rib attached to the pile to help with the transfer of the moment. This connection, like the other, requires that the shaft be a capacity-protected element, and prior research has shown that a CFST element has significantly more strength than a similarly sized RC element. A general layout of a CFST-to Column connection is shown in Figure 2.3.

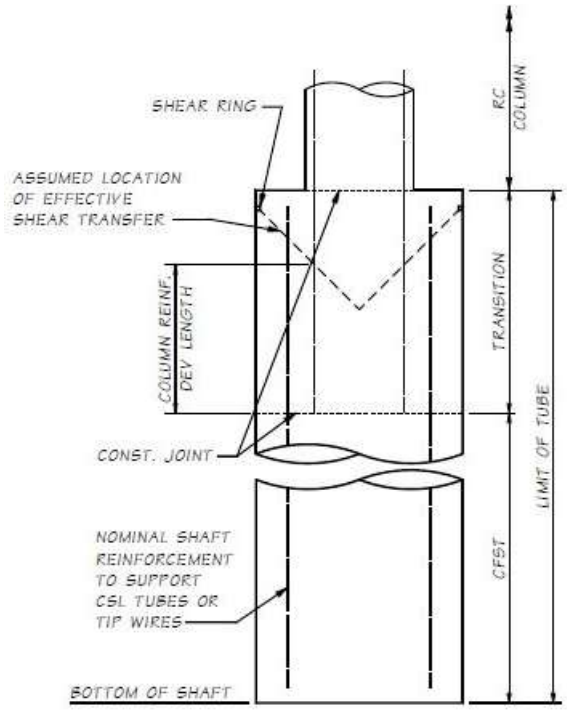

Figure 2.3. CFST-to Column Connection (WSDOT BDM)

WSDOT requires that a steel rib is welded to the inside of the steel tube 3 in. below the top of the tube and the column longitudinal bar embedment length meet the following requirements (WSDOT BDM 7.10.5):

$$l_e = maximum(0.5D + l_{d,bar}, 1.0D)$$

l_e = column longitudinal reinforcement embedment length (in.)

D = shaft diameter (in.)

$l_{d,bar}$ = column reinforcement development length (in.)

2.3 TEST PROGRAMS

Three different experimental test programs were reviewed to better understand the force-transfer mechanism used in the connection region and how the different study parameters affected the connection.

2.3.1 *Lateral Behavior of RC Columns Supported on Type II Shafts: Liu (2012)*

Liu constructed two large-scale specimens investigating a connection between a reinforced concrete (RC) column and a Type II cast-in-drilled-hole (CIDH) RC pile, as well as a finite element (FE) analysis of the column-pile system, interested in the lateral behavior. The FE analysis was to look at the influence of the soil-structure interaction on the lateral behavior and how it would affect the test specimen configurations to simulate the behavior without using soil. The experimental testing was to look at the column ductility capacity and the formation of the plastic hinge at the base of the column.

Liu tested two large-scale column-shaft subassemblies under cyclic lateral loading, the test matrix is shown in Table 2.3. All specimens had the same column diameter of 4 ft., and shaft diameter of 6 ft. The reinforcement of each specimen's column and shaft are shown in Figures 2.4 and 2.5. For both specimens, the shaft extends out of a RC footing, which is post-tensioned to the laboratory floor to prevent uplift. The footing is 14-ft long, 8-ft wide, and 4-ft deep and designed to allow interface shear transfer between the base of the footing and the laboratory door.

Table 2.3. LIU (2012) Test Program

Specimen	Shaft Height	Column Height	Specimen Height	Column Reinforcement Development Length	Longitudinal Reinforcing Bar Size	Transverse Reinforcement Spacing (in)	Transverse Reinforcing Bar Size
1	9 ft.	16 ft.	29 ft.	7.5 ft.	#14	6, 5, and 4	#5
2	8 ft.	18 ft.	30 ft.	6 ft.	#18	6, 4, and 7	#5

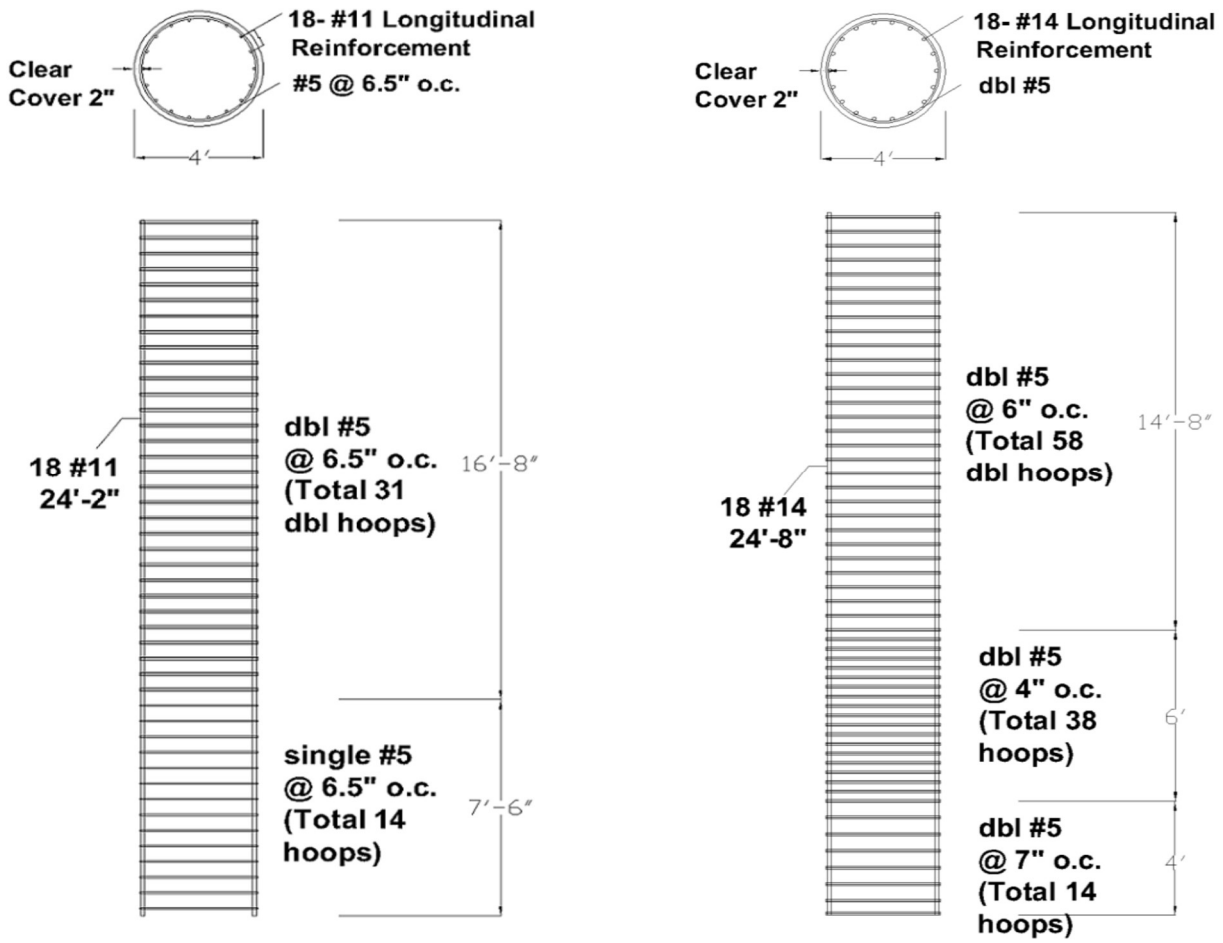

Figure 2.4. Liu (2012) Column Reinforcement Cages: a) Specimen 1 and b) Specimen 2

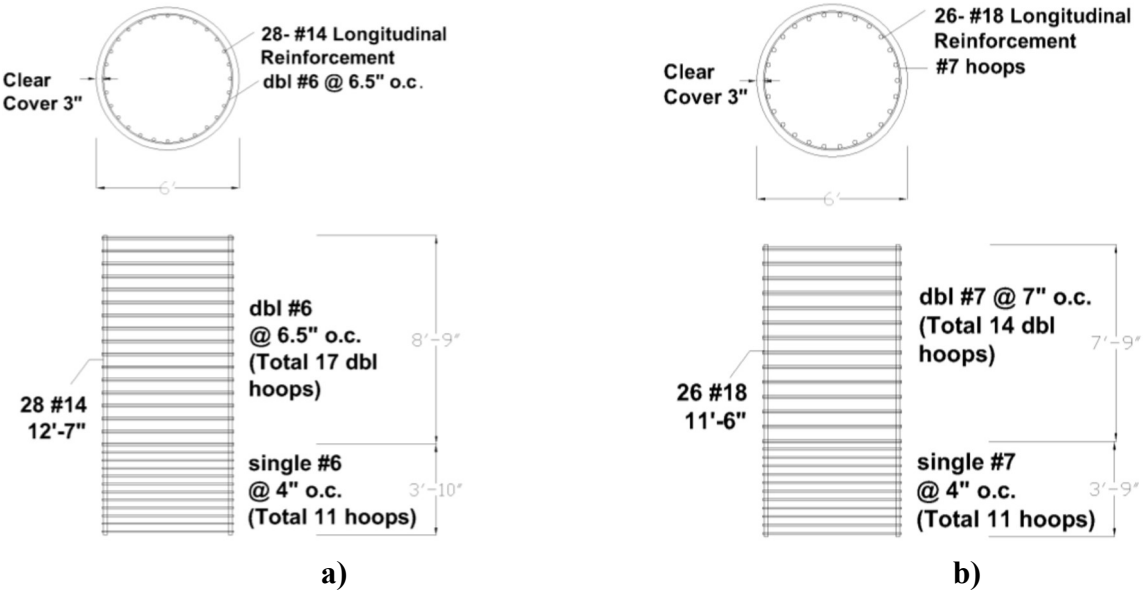

Figure 2.5. Liu (2012) Shaft Reinforcement Cages: a) Specimen 1 and b) Specimen 2

The specimens were post-tensioned to the laboratory floor to create a fixed base. The specimens were then loaded with a constant axial load and subjected to cyclic loading. Figure 2.6 shows the general test setup. The cyclic loading consisted of a lateral actuator subjecting the specimens to the prescribed force or displacement limit and returning the actuators back to the zero-force state. Specimen 1 reached a drift of 7% (+/-14 in.) and Specimen 2 reached a drift of 10.2% (+/-22 in.).

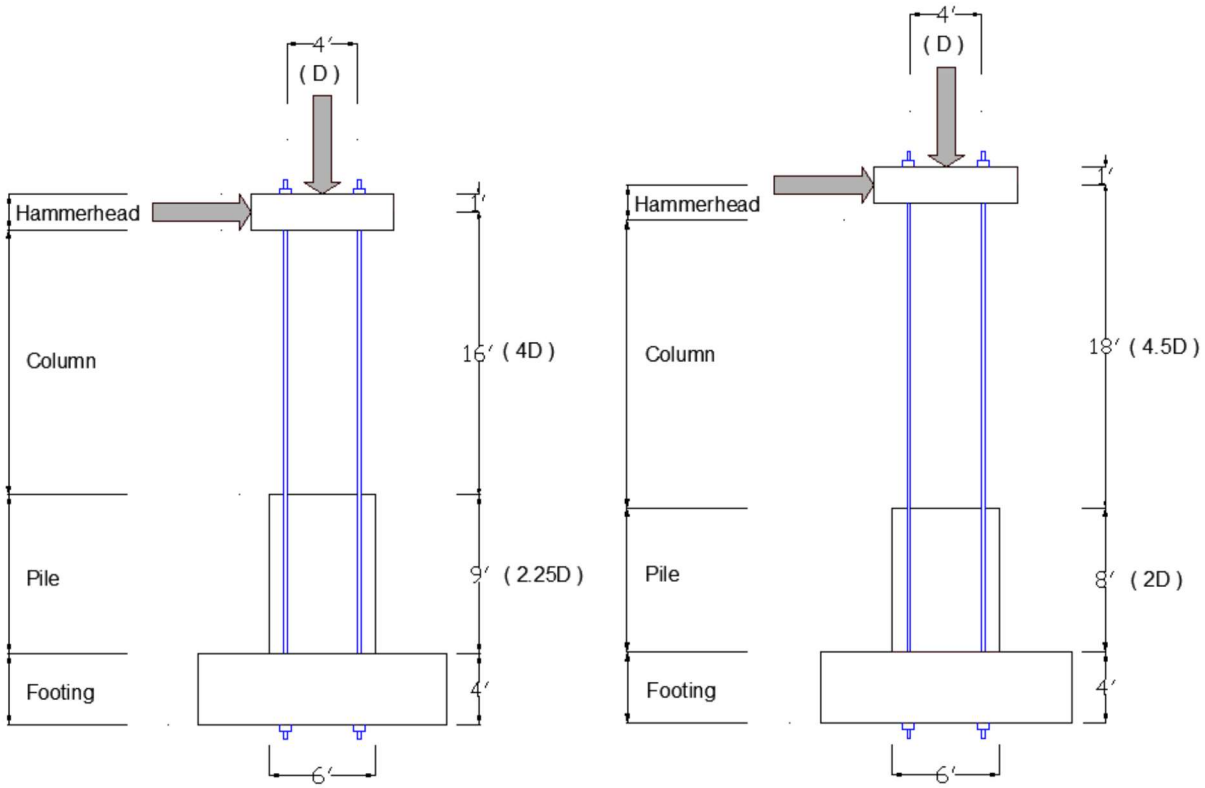

a) **b)**

Figure 2.6. Liu (2012) Test Setup: a) Specimen 1 and b) Specimen 2

Both tests were stopped after bar fracture occurred in the longitudinal reinforcement, shown in Figure 2.7. This occurred at cycle 14, (10.4 in. to -13.95 in.) for Specimen 1 and cycle 18 (21.54 in. to 22.46 in.) for Specimen 2.

a) b)

Figure 2.7. Liu (2012) Buckling and Fracture of Longitudinal Bars: a) Specimen 1 and b) Specimen 2

Figure 2.8 shows the force-displacement results of the two specimens. The specimens had similar results, with a loss in force after crushing and bar ruptures. Table 2.4 shows key ductility and strength values from the test.

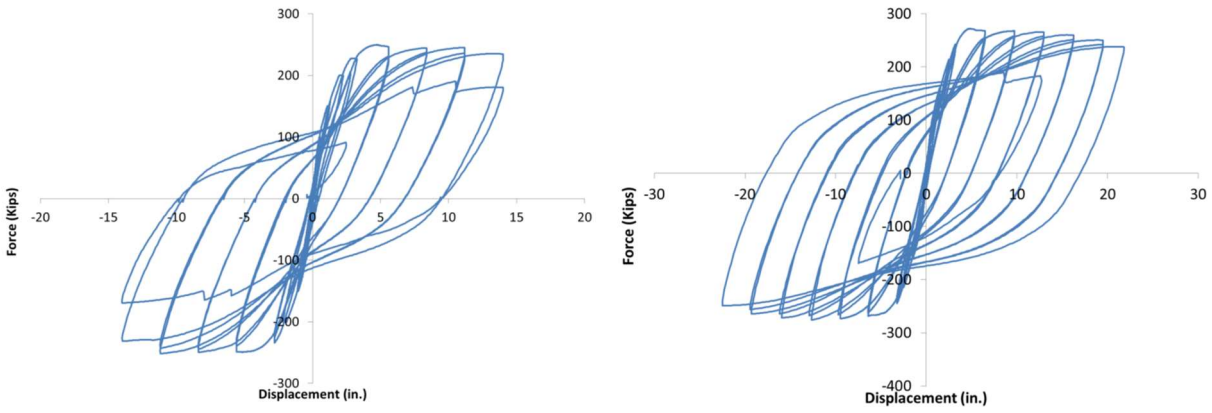

a) b)

Figure 2.8. Liu (2012) Overall Responses of Column-Shaft Assemblies including P-Δ Effects a) Test 1 and b) Test 2

Table 2.4. Displacement Ductility of the column-shaft assemblies (Liu 2012)

Specimen	First Yield Disp. (in.)		Effective Yield Disp. (in.)		Ultimate Disp. (in.)		Displacement Ductility (in./in.)		Peak Strength (kip)	
	Push	Pull	Push	Pull	Push	Pull	Push	Pull	Push	Pull
1	2.26	2.32	2.72	2.64	14.00	14.00	5.15	5.30	250	250
2	2.75	2.66	3.40	3.39	21.84	22.49	6.42	6.63	292	304

The relevant findings were as follows:

- The reduced embedment lengths, compared to current Caltrans standards, of the column reinforcing cages extending into the Type II shafts, is sufficient to fully develop the load resistance capacities of the columns
- The lateral displacements at the top of the columns were mainly contributed by column flexure (~50%) and base rotation (~40%) with the shear contribution (>5%) being negligible

2.3.2 *Seismic Performance of Bridge Column-Pile-Shaft Pin Connections for Applications in Accelerated Bridge Construction: Mehraein (2016)*

Mehraein investigated the seismic performance of two types of direct column-to-pile connections: (1) pipe-pin connections at column-pile shaft connections for CIP and precast constructions and (2) rebar-pin connections at column-pile shaft connections for CIP and precast constructions. Each Specimen would be tested with one precast column-pile and one CIP column-pile assembly, shown in Figures 2.9 and 2.10.

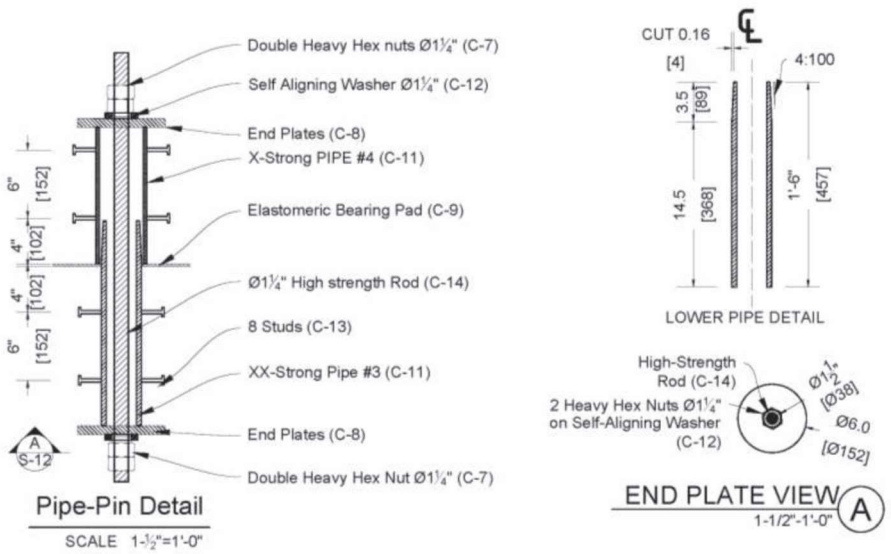

Figure 2.9. Mehraein (2016) BPSA Pipe-Pin Detail

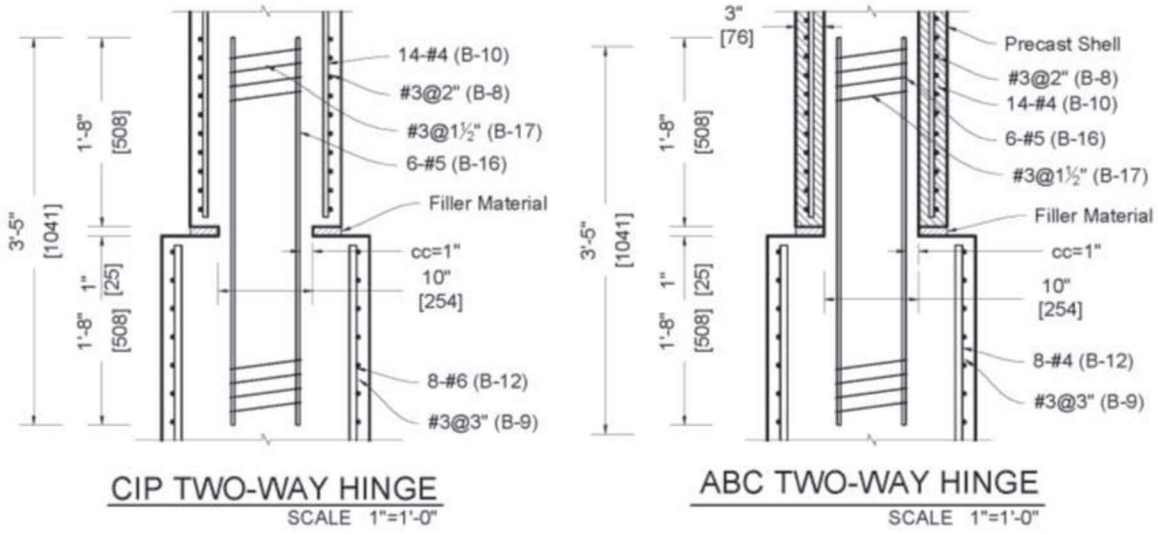

Figure 2.10. Mehraein (2016) BRSA Rebar Hinge Detail

Mehraein tested two 1/3.75 scale, two-column bent subassemblies, with one column as a precast shell filled with self-consolidating concrete and the other column being a Cast-In-Place concrete column, shown in Figures 2.11 and 2.12. The specifications and dimensions of the specimens are found in Table 2.5.

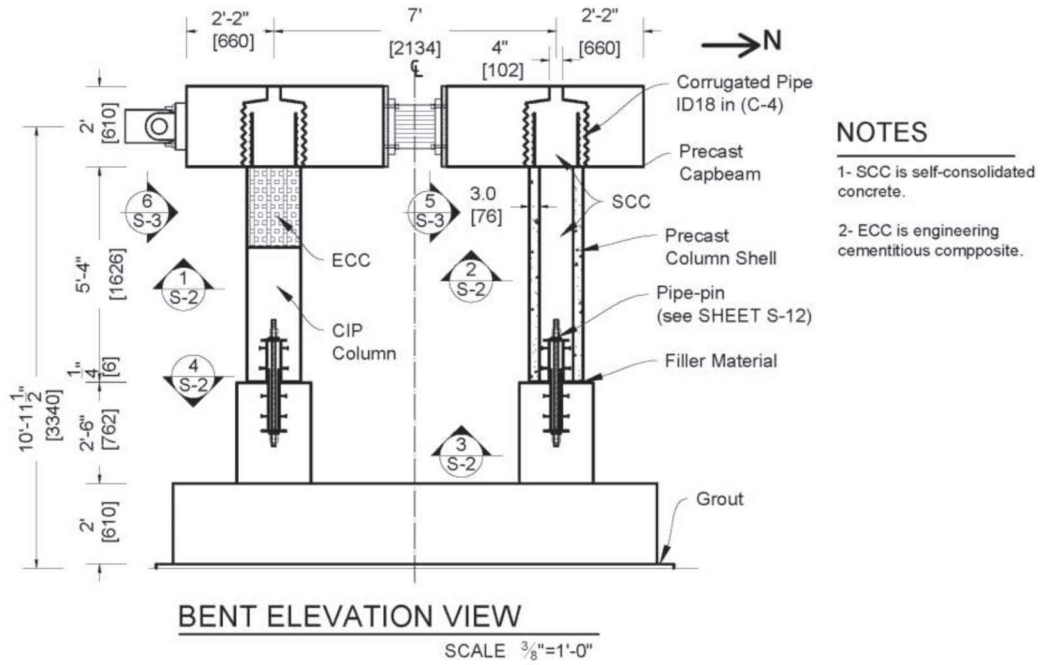

Figure 2.11. Mehraein (2016) BPSA Elevation View

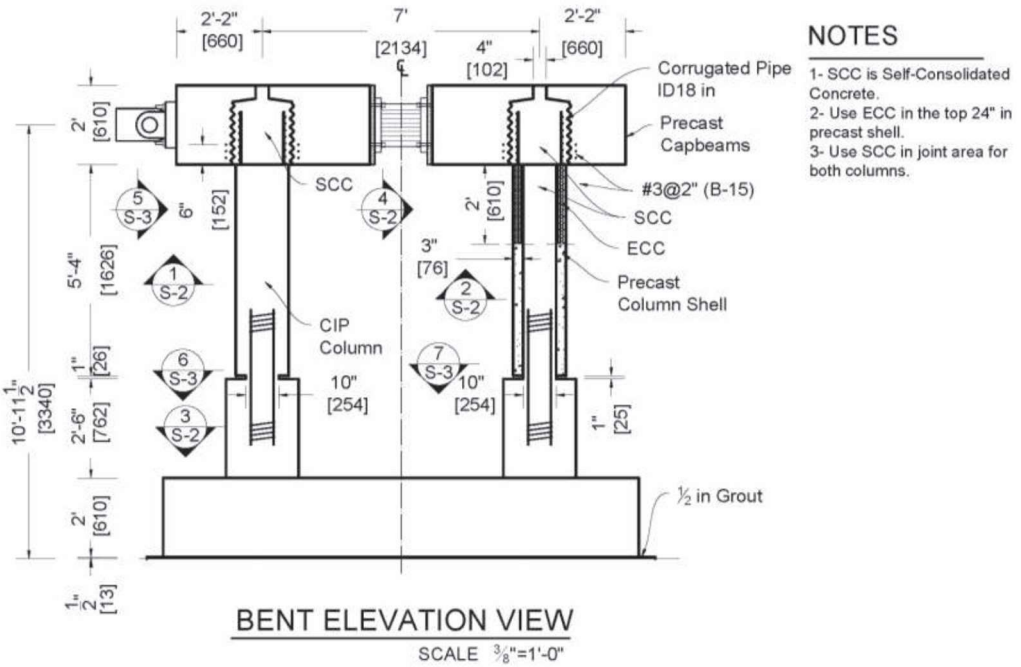

Figure 2.12. Mehraein (2016) BRSA Elevation View

Table 2.5. Mehraein (2016) Specifications of the Specimens

Model	BPSA	BRSA
Column Diameter	16 in.	
Column Longitudinal Reinforcement	14 - #4	
Column Spirals	W4 @ 2 in.	#3 @ 2 in.
Column Spiral Yield Strength	51 ksi	68 ksi
Pedestal Diameter	22 in.	
Pedestal Longitudinal Reinforcement	8 - #6	
Pedestal Spirals	#3 @ 3 in	

The specimens were subjected to the 142-degree of Sylmar Converter Station of the 1994 Northridge earthquake ground motions via a shake table as shown in Figure 2.13. The accelerations from these ground motions were filtered to create a symmetric ground motion and the time step of the acceleration was scaled to account for the specimen scale factor of 1/3.75. To account for the weight of the bent on the two columns, four blocks were placed on the mass rig. These four blocks on the mass rig provided the inertia force to the bent, a translational mass equivalent to 100 kips.

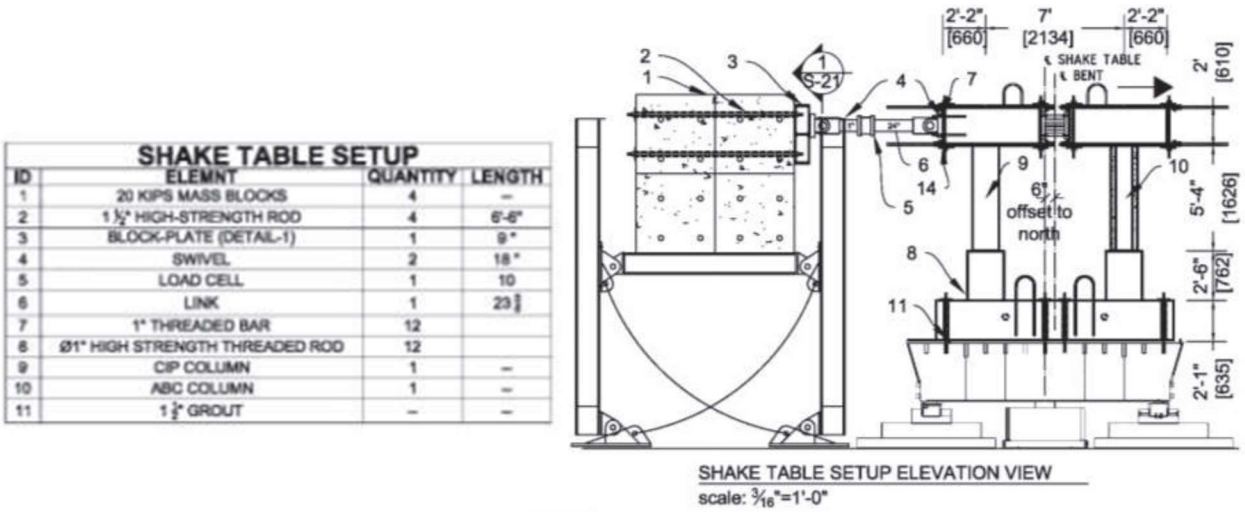

Figure 2.13. Mehraein (2016) Shake Table Setup

The BPSA specimen sustained 11 ground-motion runs before the test was terminated. The CIP components showed major cracking in the plastic hinge region of the column as well as buckled longitudinal reinforcement and ruptured spiral reinforcement. The pipe-pin had no observable damage. The PC components had similar results, with major spalling and buckled reinforcement. The pipe-pin connection also showed no damage. The BPSA CIP force-

displacement curve and the BPSA PC force-displacement curve are shown in Figure 2.14. The final state of the connection is shown in Figure 2.15.

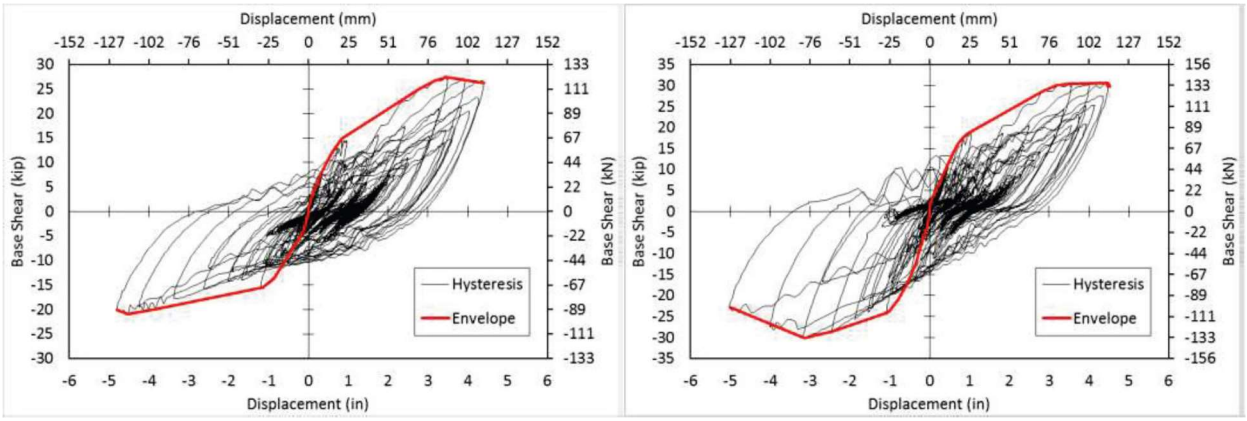

a) **b)**

Figure 2.14. Mehraein (2016) Force-Displacement Curve a) BPSA CIP and b) BPSA PC

a) **b)**

Figure 2.15. Mehraein (2016) BPSA Connection After Final Run a) CIP and b) PC

The BRSA specimen managed to do 6 ground-motion runs before the test was terminated. The CIP components showed major spalling at the top of the column. The concrete core of the column failed after run 6. The longitudinal bars also buckled. The spalling also caused the rebar-pin spiral to be exposed. The PC components had shear and flexural cracks which expanded in size after each run. There was a large flexural crack in the rebar-pin, which occurred during run-5, but

did not grow with the reaming runs. The BRSA CIP and the BRSA PC force-displacement curves are shown in Figure 2.16. The final state of the connection is shown in Figure 2.17.

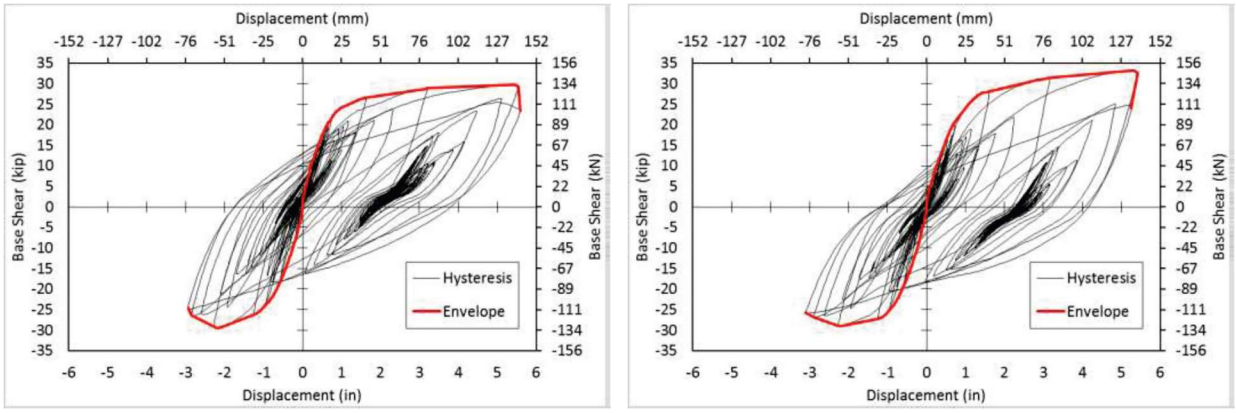

a) **b)**

Figure 2.16. Mehraein (2016) Force-Displacement Curve a) BRSA CIP and b) BPSA PC

a) **b)**

Figure 2.17. Mehraein (2016) BRSA Connection After Final Run a) CIP and b) PC

The relevant research findings are as follows:

- The design and detailing methods developed in this study for the reinforcing bar cage pins, pipe-pins, pocket connections, and the precast cap beams led to an effective ductile bridge bent.
- Moments were developed at both pin types, leading to an increase in the base shear by approximately 30%. Even the pipe-pins, without any tension members, and the rebar-pins, with very small core diameters, generated significant moments at the column base

- The damage in the pipe-pin connections was minimal because the strains in the pipes and longitudinal bars were well below the yield, and cracks in the column and pedestal were thin and few.
- The moment-rotation relationship of rebar-pins was stable even when the pins underwent large plastic deformations under many cycles of earthquake loading. The concrete near the hinge throat was damaged but the column and pedestal reinforcement did not yield near the rebar-pins.

2.3.3 *Seismic Performance of Column to Drilled Shafts: Chang (2021)*

Chang specifically investigated the effects of transverse reinforcement had on the performance of the connection under cyclic loading.

One 1/3.6-scale column-shaft subassembly was tested under cyclic lateral loading, working of prior research, where Hung (2015) had tested three similar subassemblies. Table 2.6 provides the experimental test matrix. The specimens had a column diameter of 20 in., column height of 60 in., shaft height of 30 in., embedment length of column reinforcement of 26 in., and the transverse reinforcement in the plastic-hinge region of column consisted of gauge-3 wire at 1.25 in.

Table 2.6. Chang (2021) Test Program

Researcher	Specimen	Shaft Diameter	Column Long. Reinf. Quantity and Bar Size	Shaft Long. Reinf. Quantity and Bar Size	Shaft Transverse Rein. Bar Size and Spacing
Hung	DS-1	30	10 #5	30 #3	2 gauge-9 wire @ 3 in
	DS-2	30	10 #5	30 #3	gauge-9 wire @ 3 in
	DS-3	26	16 #5	24 #4	3 gauge-9 wire @ 3 in
Chang	DS-4	30	16 #5	24 #4	gauge-9 wire @ 3 in

The loading of the specimens was a combination of an axial load of 10% of the nominal compressive strength of the column and a cyclic lateral load at the top of the specimen. Figure 2.18 shows the general test setup for each specimen. (This setup was also used in this test program). Each specimen failed at a specimen drift of approximately 10% and was defined as when the lateral

load resistance dropped by more than 50%. The moment-drift curve of DS-4 is also presented in Figure 2.19

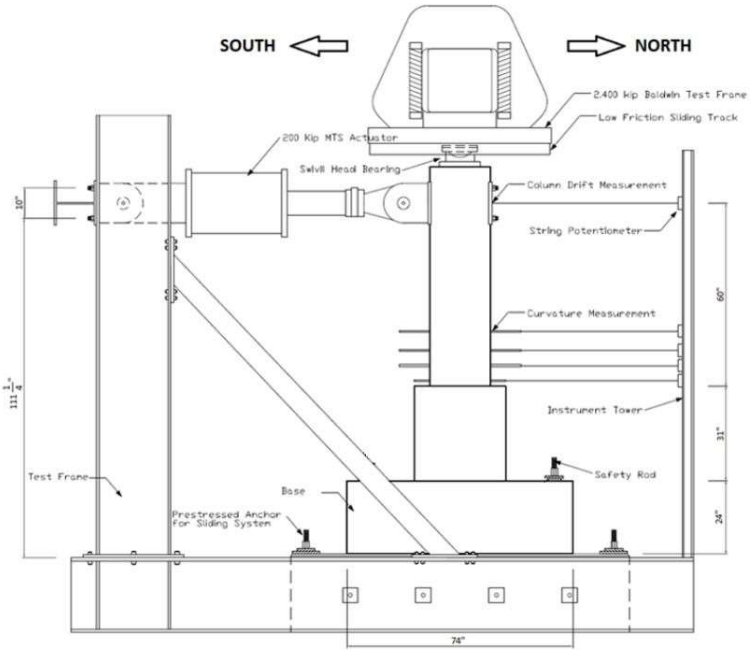

Figure 2.18. Chang (2021) Test Setup

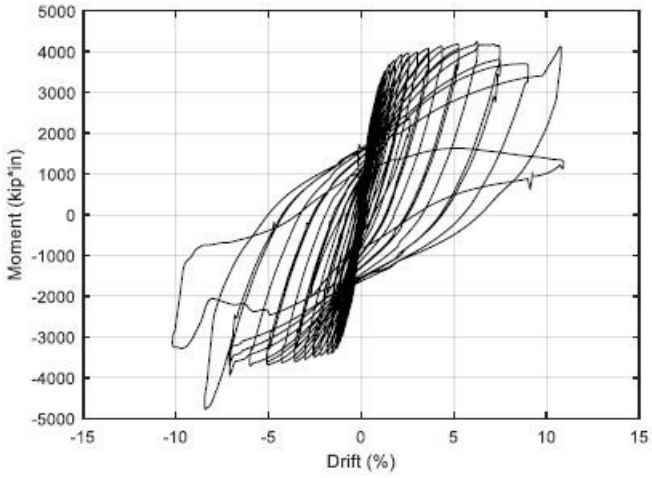

Figure 2.19. Chang (2021) Moment-Drift Response of DS-4

Specimens DS-1 and DS-3 failed by bar buckling and fracture in the column base. Specimen DS-2 and DS-4 failed due to prying occurring in the transition region, which is equivalent to the column embedment depth, the CIP concrete shell split open and the column was separated from the CIP shaft. The final states of these specimens are shown in Figure 2.20.

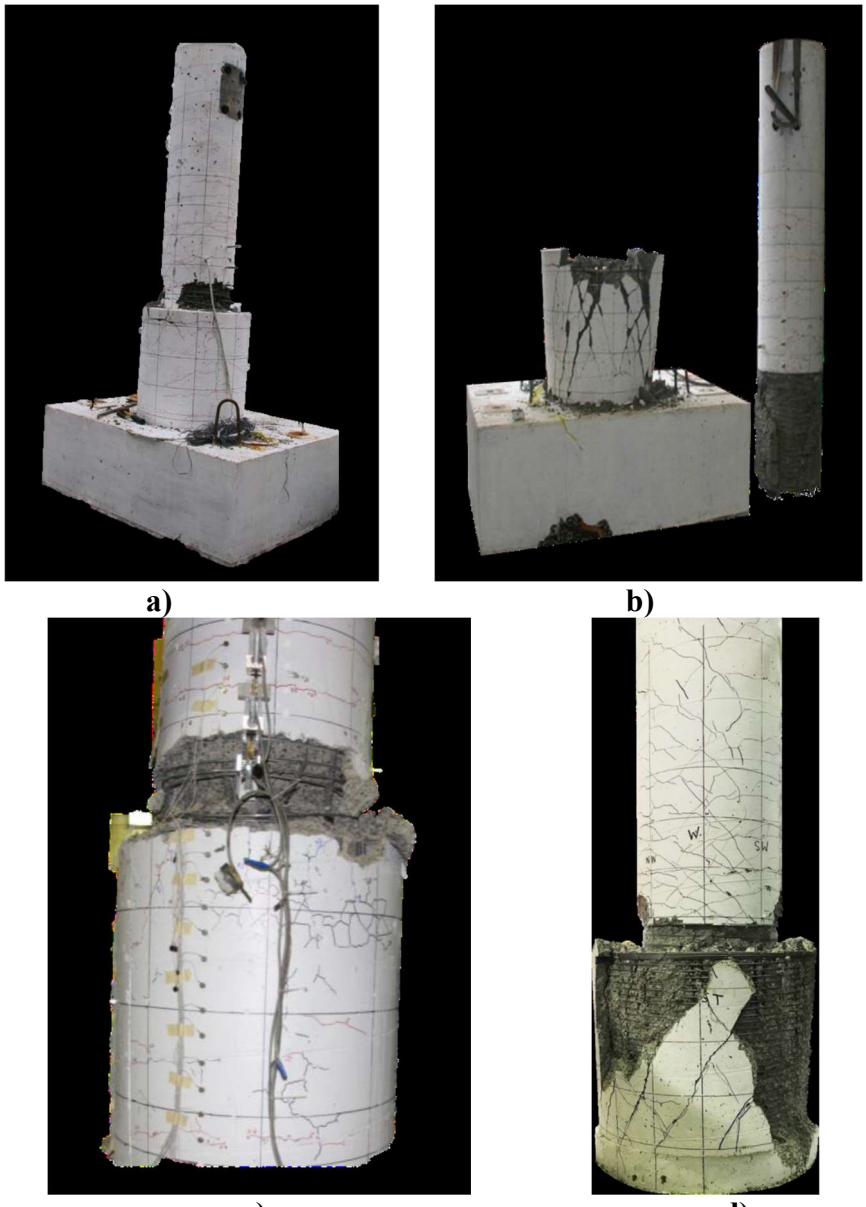

Figure 2.20. Final State of Specimens a) DS-1, b) DS-2, c) DS-3, and d) DS-4

The strain distribution in the shaft transverse reinforcement was not uniform throughout the specimens. The top regions of the spiral had a measured strain above the yield strain of the reinforcement, while the bottom spiral measured nearly zero strain.

The relevant findings were as follows:

- The current provisions (Caltrans and WSDOT) of the amount of spiral reinforcement required for conventional column-to-drilled shaft connections does not ensure the desired behavior for all configurations
- The amount of transverse shaft reinforcement can cause the failure mechanism to change from the column to the connection
- The tests specimens contained no external confining steel shell, such as a CFST, around the top of the transition region, and if one were used it would provide some of the benefits of additional spiral and may reduce the amount of spiral used

The research performed by Liu, Mehraein, and Chang help provide some insight into the behavior of different column-shaft connections, as well as how various parameters affect the connection's behavior. Liu and Chang show that the majority of specimen deformation is due to base rotation and column flexure. Liu demonstrates that the embedment depth of column longitudinal reinforcement into RC shafts can be reduced, while still developing the capacity of the column. Mehraein shows that, while the pin type connection leads to an effective bridge bent with minimal damage, moments are developed at both pin types, which leads to an increase in the base shear. Chang emphasizes the importance that shaft transverse reinforcement has on the type of failure for an RC drilled shaft, and the benefits that a CFST would have on such a connection.

2.4 CFST CONNECTIONS

Prior research into the connections between CFST element and RC elements has shown to develop a full strength connection between a tube and an RC element, such as a cap beam or a footing, requires an additional mechanical mechanism. Research programs performed at Montana State University (MSU) and the University of Washington (UW) studied these connections.

2.4.1 *Performance of Steel Pipe Pile-to-Concrete Cap Connections Subjected to Seismic or High Transverse Loading: Kappes (2013)*

The research performed by Kappes at MSU investigated the strength of an embedded CFST column-to-pier cap connection, as shown in Figure 2.21. This was done by extending the tube into the pier cap without the addition of a supplemental mechanical mechanism to enhance the bond between the two structural components. The key parameters of these tests were the CFT embedment length into the pile and the strength of the pile cap concrete.

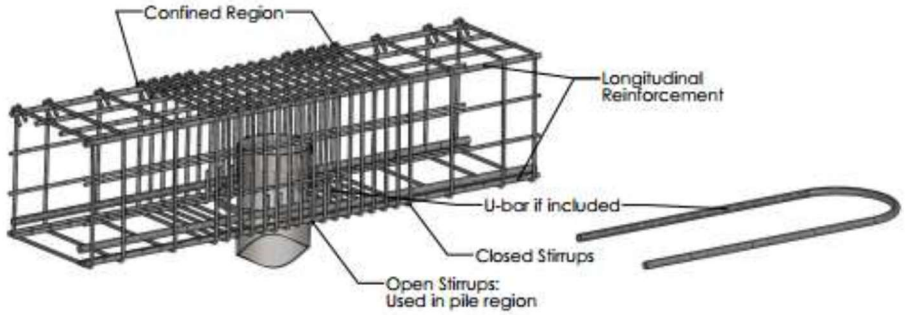

Figure 2.21. CFST to Pier Cap Connection (Kappes 2013)

Six ½ scale specimens were tested to evaluate the strength of the connection. Four specimens were subjected to monotonic loading to determine the ultimate strength of the connection. The other two specimens were tested under cyclic loading to determine the performance under multiple cycles of increasing load. Table 2.7 provides the experimental test matrix with the key parameters being investigated, Pile thickness, embedment length, and concrete strength. The RC pile cap, which was the same for all specimens, was 18 in. by 18 in. by 68 in. All the CFTs used had an outside diameter of 8.625 in.

Table 2.7. Kappes (2013) Test Program

Specimen	Loading	Pile Thickness	Embedment Length	Design Concrete Strength
VT1	Monotonic	0.25 in.	9.0 in.	6.25 ksi
VT2	Monotonic	0.50 in.	11.75 in.	4.0 ksi
VT2.5	Monotonic	0.50 in.	9.0 in.	6.25 ksi
VT3	Monotonic	0.50 in.	10.375 in.	4.0 ksi
CT1	Cyclic	0.73 in.	11.75 in.	4.0 ksi
CT2	Cyclic	0.73 in.	11.75 in.	4.0 ksi

As mentioned before, these connections were tested under monotonic and cyclic loading by applying lateral loads and a constant axial load of 15 kips to represent gravity loads through hydraulic jacks, as shown in Figure 2.22. The monotonic tests were loaded in the positive direction until a distinct loss in load-carrying capacity was observed. The process was then repeated to the same deflection in the negative direction. The maximum drifts reached for VT1, VT2, VT2.5, and VT3 are approximately 14%, 15%, 15%, and 14.5%, respectively. The cyclic tests were tested by displacing the pile over increasing drift cycles up to 11% drift.

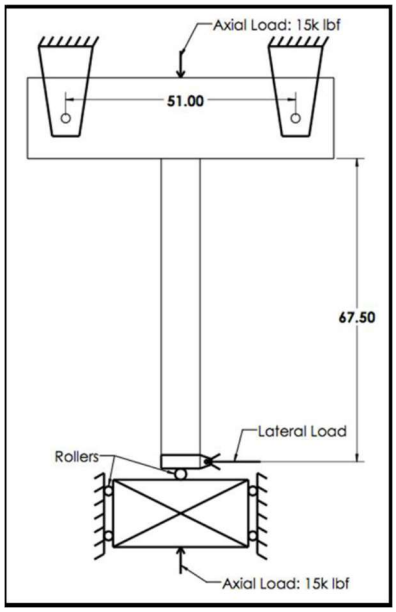

Figure 2.22. General Test Setup Layout (all lengths in units of in.) (Kappes 2013)

Specimen VT1 failed due to the formation of a plastic hinge in the CFT pile while all the other specimens failed due to fracturing in the pile cap. This change in failure mechanism is due to VT1 having a significantly smaller CFT. A summary of the test results is shown in Table 2.8.

Table 2.8. Kappes (2013) Summary of Test Results

	Test	U-bar Configuration	U-bar Location	Pile Embedment Length	Concrete Strength	Failure Mechanism	Maximum Moment at Failure
Monotonic	VT1	Single #7 U-bar in each direction	Exterior Only	9.0 in	6250 psi	Plastic hinge in steel pipe pile	119.2 ft·kip
	VT2	Single #4 and #5 U-bar in each direction	Exterior Only	11.75 in	3800 psi	Fracture of the concrete pile cap	173.8 ft·kip
	VT2.5	Single #7 U-bar in each direction	Exterior Only	9.0 in	6250 psi	Fracture of the concrete pile cap	138.5 ft·kip
	VT3	Single #7 U-bar in each direction	Exterior Only	10.375 in	4100 psi	Fracture of the concrete pile cap	151.7 ft·kip
Cyclic	CT1	Single #4 and #5 U-bar in each direction	Exterior Only	11.75 in	4200 psi	Fracture of the concrete pile cap	172.4 ft·kip
	CT2	Single #4 and #5 U-bar in each direction	Interior and Exterior	11.75 in	4200 psi	Fracture of the concrete pile cap	181.8 ft·kip

The final states of Specimen VT1 (plastic hinge) and CT2 (pile cap fracture) are shown in Figure 2.23. The moment-drift behavior of CT2 is shown in Figure 2.24.

a) **b)**

Figure 2.23. Final State of Specimens a)VT1 b) CT2 (Kappes 2013)

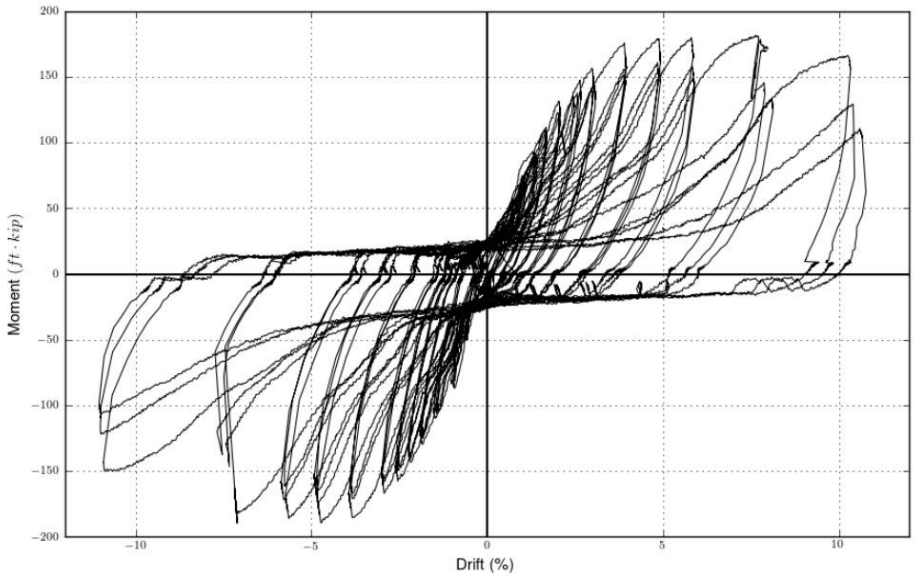

Figure 2.24. Moment-Drift of Specimen CT2 (Kappes 2013)

The relevant finding was as follows:

- An increase in the embedment depth of the CFT into the pile cap would reduce concrete crushing in the pile cap and increase the moment capacity of the column

2.4.2 *Design Expressions and Dynamic Evaluation of CFST Bridges Subjected to Seismic Hazards: Stephens (2016)*

The research performed by Stephens was built off of Kappes' work and previous research performed at UW to develop a full plastic moment connection of a CFST component to a RC component. Stephens investigated three types of connections for a CFST column into a RC cap beam: a) Embedded Ring (ER), b) Welded Dowel (WD), and c) Reinforced Concrete (RC), as shown in Figure 2.25. The ER connection uses a circular ring welded to the end of the tube that extends both inside and outside the tube. Four ER specimens were tested. The WD connection uses a ring of headed dowels, which are welded directly to the tube that extends into the cap beam. Three WD specimens were tested. The RC connection uses a reinforcing cage, with both

longitudinal and transverse reinforcement, which extends from the CFST into the cap beam. Only one RC specimen was tested.

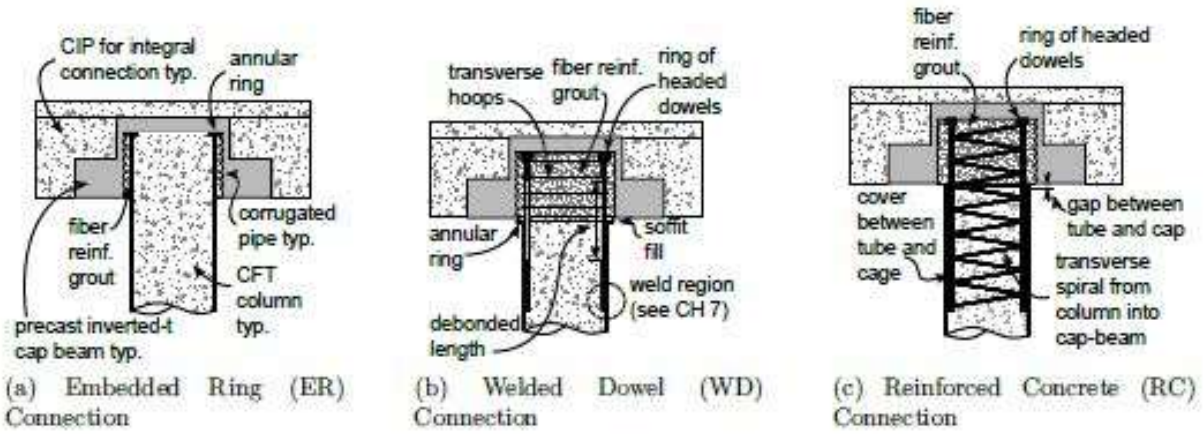

Figure 2.25. CFST to Pier Cap Connections (Stephens 2016)

The specimens were tested under axial and lateral loading similar to Chang's and this research's test program. The axial load was either 10% or 5% of the column capacity. The lateral loading was imposed displacement based on the column's yield displacement.

The ER connection was able to reach large strength, stiffness, and deformation capacities. The maximum drifts reached at 20% lateral strength degradation of the column ranged from 5% to 8.6% drift. The moment-drift behavior of the ER connection is shown in Figure 2.26. All ER connection specimens reached the plastic moment capacity of the CFST component. The failure mode for all specimens was ductile tearing at the column-to-cap beam interface. The ER connection has the advantage of reduced on-site construction time since no additional reinforcement is required.

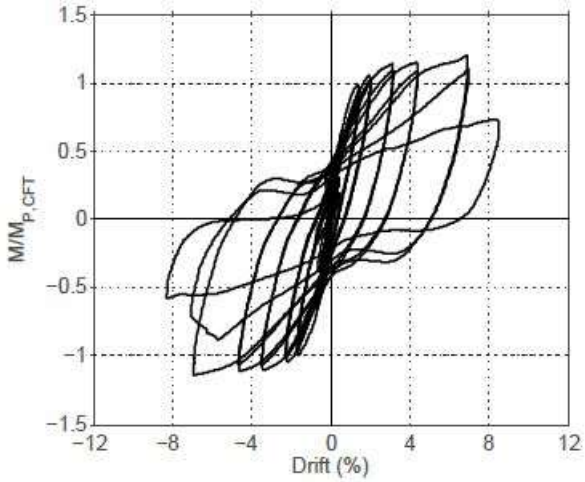

Figure 2.26. Moment-Drift Behavior of ER Connection (Stephens 2016)

The WD connection was also able to reach large strength, stiffness, and deformation capacities, however, the capacities were controlled by the effective reinforcing ratio of the dowels and therefore were smaller capacities than a comparable ER connection. The maximum drifts reached at 20% lateral strength degradation of the column ranged from 11.5% to 12.2% drift. The moment-drift behavior of the WD connection is shown in Figure 2.27. The two failure modes for this type of connection were cap beam failure due to the pullout of the headed dowels and yielding and fracture of the longitudinal dowels. The WD connection requires more on-site construction and labor and is not advantageous for accelerated construction.

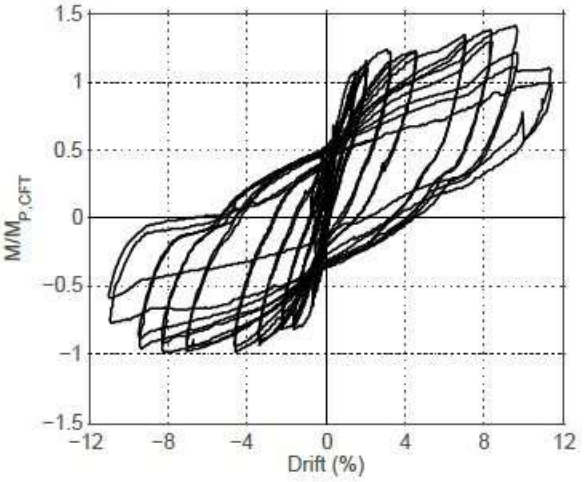

Figure 2.27. Moment-Drift Behavior of WD Connection (Stephens 2016)

The RC connection showed significantly lower strength and stiffness than the CFST component. The maximum drift reached at 20% lateral strength degradation of the column was 10% drift. The moment-drift behavior of the RC connection is shown in Figure 2.28The failure mode of this connection was the yielding and fracturing of the longitudinal reinforcement between the CFST and the cap beam. The RC connection is also not advantageous for accelerated construction due to the reinforcing cage that must be built on-site.

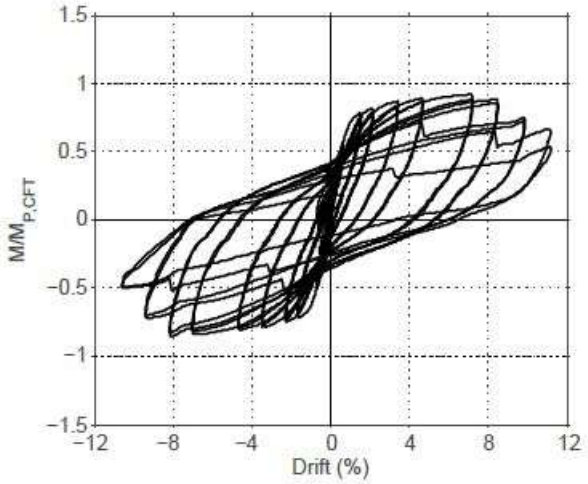

Figure 2.28. Moment-Drift Behavior of RC Connection (Stephens 2016)

The relevant findings are as follows:

- There is an increase in time and labor used for the construction of an RC or WD connection compared to the ER connection
- The ER connection showed improved seismic performance in ductility and strength compared to the RC and WD connections
- For the WD connection, extending the longitudinal dowels into the CFST would improve performance and steel stress distribution, and prevent damage to the tube

The research performed by Kappes and Stephens highlights the benefits of increased embedment depth and the addition of a rib into a CFST connection. The increased embedment

depth helps to develop the full capacity of the CFST member and the rib provides the tube with additional anchorage to the RC component and creates a strut for the reinforcing bars.

2.5 FINITE ELEMENT ANALYSIS OF CFST PILE CONNECTION

2.5.1 *Analytical Investigation of a Direct Column-to-Cased Shaft Connection: Zhao (2021)*

Zhao investigated the effects of different parameters on a Reinforced Concrete (RC) Column to Concrete Filled Steel Tube (CFST) Cased Shaft Connection. The objective of the research was to determine the adequate embedment depth of the reinforcement if a supplemental mechanical bond was not included, as well as the requirements for placing the supplemental mechanical bond, rib, and the location of the reinforcing bars for required development length. The parameters of the study included: the embedment depth (l_d), the rib size (b_{nR}), the rib location (l_R), the reinforcing bar diameter, and the tube diameter (D).

The LS-Dyna finite element computer program was used to study the connection with the various parameters. The model used concrete constitutive models and bond-slip between both the tube and the concrete fill and the reinforcement and concrete. The concrete was modeled using a constant-stress solid element (LS-Dyna: ELFORM=1) with the Concrete Damage Plasticity Model (LS-Dyna: MAT273) for the constitutive model. The tensile and compressive damage parameters of the concrete are defined in the following equation:

$$\sigma = (1 - w_t)\sigma_t + (1 - w_c)\sigma_c$$

σ = effective stress tensor (ksi)
σ_t = tensile effective stress (ksi)
σ_c = compressive effective stress (ksi)
w_t = tensile damage parameter, varies from 0 (undamaged) to 1 (fully damaged)
w_c = compressive damage parameter, varies from 0 (undamaged) to 1 (fully damaged)

The steel tube was modeled using the Belytschko-Tsay shell element with the trilinear constitutive model, PIECEWISE_LINEAR_PLASTICITY (LS-Dyna: MAT024). The reinforcing bars were modeled with the Hughes-Liu beam element with the combined kinematic model (LS-Dyna: MAT003). The reinforcement-concrete interface was modeled using the LS-Dyna function: BEAM_IN_SOLID, defining the bond-slip model proposed by Murcia-Delso (2015). The concrete fill-tube interface was modeled using the LS-Dyna contact element: AUTOMATIC_SURFACE_TO_SURFACE_TIEBREAK with Option = 9, which uses the cohesive material model MAT_COHESIVE_MIXED_MODE (LS-Dyna: MAT138). The interface between the tube rib and the concrete fill in the tube was modeled using the AUTOMATIC_SURFACE_TO_SURFACE contact with a coefficient of friction of 0.3. Figure 2.29 is the general schematic of the FE Model. The sizes of the elements were based on the diameter of their respective materials. The concrete element size was approximately d/15, with d being the diameter of the RC pier, or 1.33 in. The steel tube element size was approximately h_{CFST}/30 or 1.733 in. The steel rib element size was approximately D/30, with D being the diameter of the CFST, or 1 in. for the 30 in. diameter specimens and 1.6 in. for the 48 in. diameter specimens.

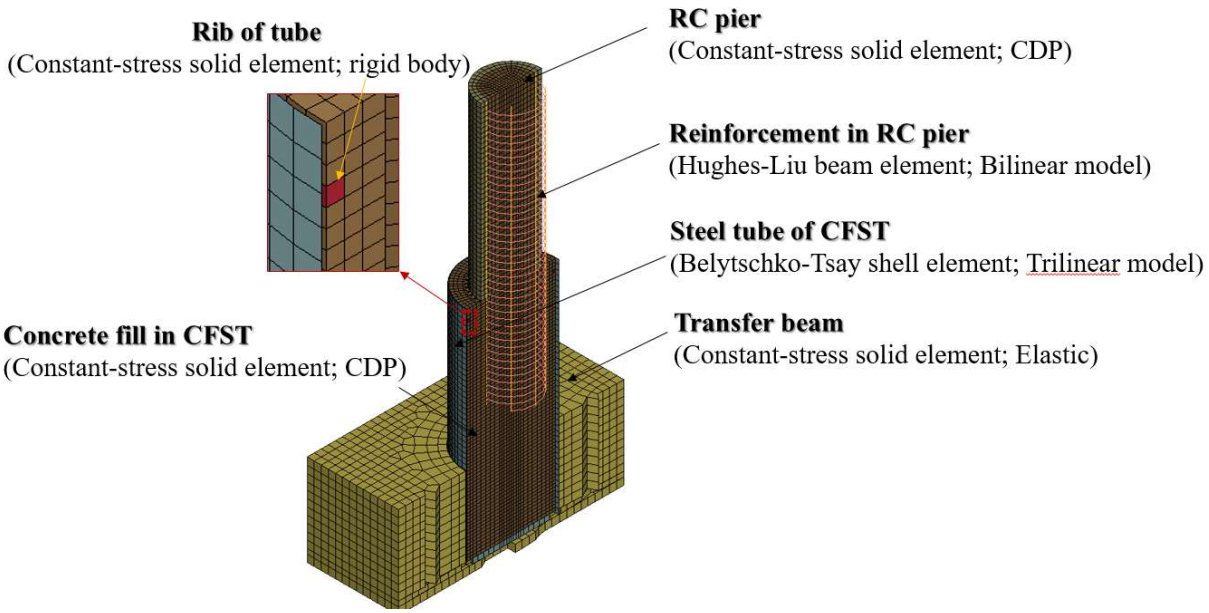

Figure 2.29. Zhao (2020) FE Model of RC Pier-to-Cased Shaft Connection

The model was verified by comparing the predicted and measured behavior to Xiao et al. (1998) and Han et al. (2016).

The parametric study showed the following results. Column longitudinal reinforcement embedment depths greater than 1.0D, one pile diameter, showed a full hysteretic response and sustained strength, while depths of 0.75D and 0.5D showed pinching in the response and loss of strength. The addition of a rib inside the pile leads to less concrete damage inside the pile and maximized the energy dissipation of the connection. The size of the reinforcing bar and location of the rib affected the strength degradation of the connection, with smaller reinforcement showing an improvement in strength degradation, which is due to the lower local bond demands. The larger tube diameter showed reduced concrete fill damage compared to the smaller tube diameter, and also had larger energy dissipation values.

The research produced by Zhao produced the following relevant conclusions:

- The embedment depth of the column reinforcing bars, for connections without a rib, must be equal to the greater of $l_{AASHTO,}$ AASHTO embedment length, and 1.0D
- The steel rib improves the structural performance of the connection and a rib size of b_{nR}=2/5 is recommended.
- The smaller reinforcing bar reduced the bond demand, concrete damage, and strength degradation of the connection.
- The rib should be located with $l_R \leq 0.3l_d$ to reduce concrete damage and strength deterioration.
- The larger diameter steel tube had less strength degradation and showed reduced damage to the concrete fill

Zhao's research was used as the basis for the specimen design of the experimental research described herein. Based on Zhao's findings, the important parameters to investigate were embedment depth, pile diameter size, and the addition of the embedded steel rib inside the pile. Additional FEA is done on the proposed connections and described in further detail in Chapter 6.

Chapter 3. EXPERIMENTAL TEST PROGRAM

A series of four half-scale CFST Pier to Pile connection specimens were tested to assess the cyclic, nonlinear response of the proposed connections. The reinforced concrete column or column was identical for all of the specimens, while the pile varied between the different specimens. The first three specimens were designed to evaluate the effects of reinforcement embedment depth, pile diameter, and the addition of an embedded rib inside the pile to enhance force and moment transfer. A fourth specimen was tested to evaluate the connection under a long-duration displacement history. This chapter presents the dimensions, reinforcements, and measured material properties of each specimen. The experimental test apparatus, loading, and instrumentation are described also.

3.1 Design of Prototype Structure and Specimens

The specimens were designed to represent a 40 in. diameter bridge column and the connection region of a 5 ft. or an 8 ft. diameter pile. A scale factor of ½ was used due to the constraints of the available testing equipment, available materials, and prior analytical research (Zhao 2020) done on these connections. This led to testing specimens consisting of a reinforced concrete pier extending out of a concrete-filled steel tube, which extended out of a reinforced concrete transfer block, with the column as the pier, the concrete-filled steel tube as the pile, and the transfer block being the mechanism that holds the pile.

The first specimen, Specimen 30-21, is a 30 in. diameter pile with a column reinforcement embedment depth of 21 in., the AASHTO development length of a #7 Reinforcing steel bar. The second specimen, Specimen 48-21, is a 48 in. diameter pile with a column reinforcement embedment depth of 21 in. The third specimen, Specimen 30-21-R, is a 30 in. diameter pile with

a column reinforcement embedment depth of 21 in. and a 2 in. rib embedded 2 in. into the pile. The fourth specimen, Specimen 30-21-LD is a 30 in. diameter pile with a reinforcement embedment depth of 21 in but tested under a long duration displacement history. The test matrix is shown in Table 3.1.

Table 3.1. Specimen Test Matrix

Specimen Name	Tube Diameter (in.) [mm]	Tube Diameter/ Tube Thickness	Reinforcement Bar Size	Embedment Depth (in.) [mm]	Rib Size (in.) [mm]	Rib Embedment Depth (in.) [mm]
30-21*	30 [762]	60	#7	21 [533]	NA	NA
48-21	48 [1219]	96	#7	21 [533]	NA	NA
30-21-R	30 [762]	60	#7	21 [533]	2 [50.8]	2 [50.8]
30-21-LD	30 [762]	60	#7	21 [533]	NA	NA

*Specimen 30-21 is reference specimen

The name convention of the specimens is as follows: The first number represents the pile or tube diameter. The second number represents the embedment depth of the column reinforcement into the pile. The third set of characters represents what is unique about the specimen, in these two specimen cases, the “R” stands for the Rib embedded into the pile, and the “LD” stands for the Long Duration displacement history the specimen was tested on.

All four of the specimen columns have the same dimensions and layout as shown in Figure 3.1. The total column length was 74 in., including the 12.25 in. extending above the point of lateral loading, but does not include the 21 in. embedment depth of the column reinforcement into the pile, and. The top 30 in. of the column was replaced with a 20 in. diameter, 0.375 in. thick steel tube, filled with concrete. This additional tube was added to prevent damage to the RC column when laterally loading during testing.

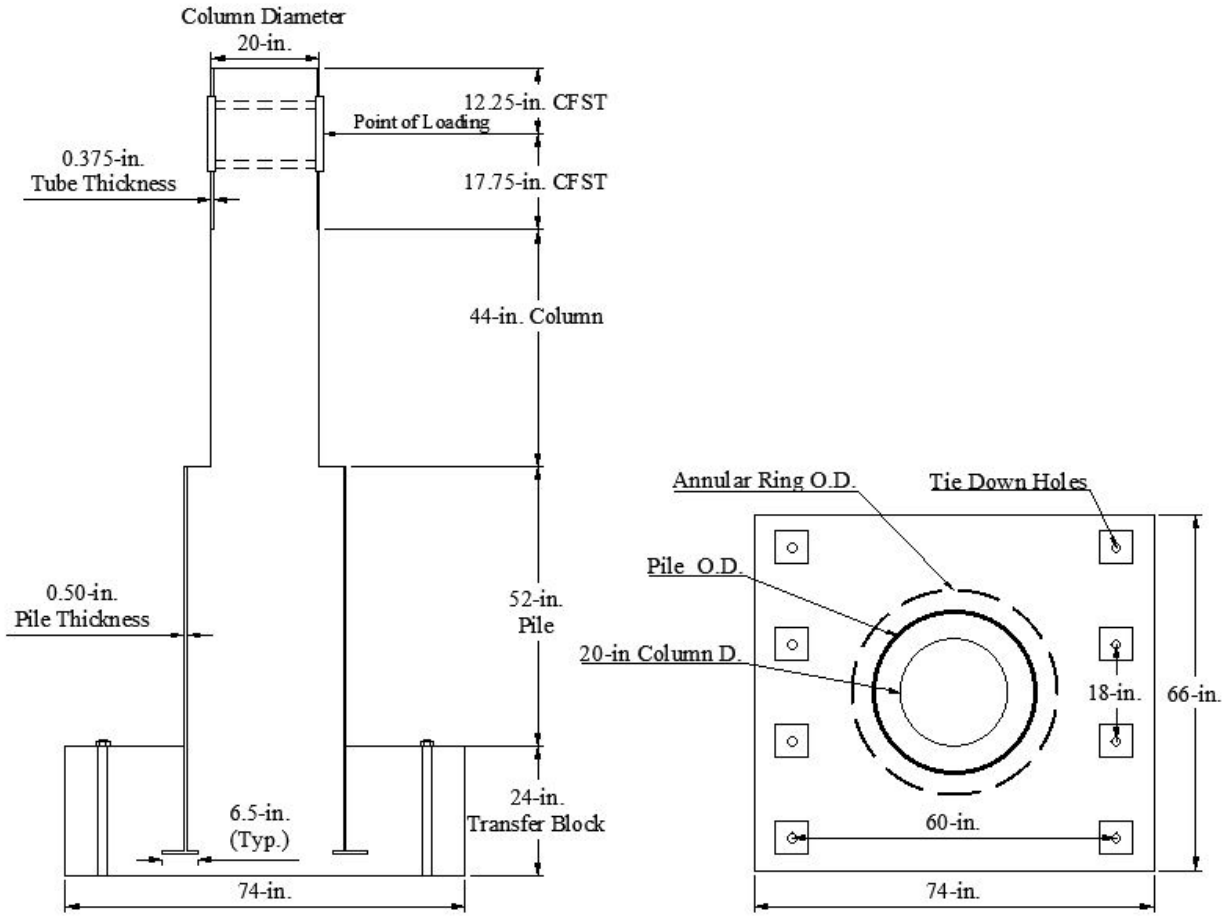

Figure 3.1. Specimen Layout and Dimensions a) Cross-section view b) Plan view

The pile had a diameter of 30 in. for specimens 30-21, 30-21-R, and 30-21-LD and 48 in for Specimen 48-21. All the tubes used for the piles had a thickness of 0.5 in, resulting in a D/t ratio of 60 for the 30 in. diameter tubes and 96 for the 48 in. diameter tube. The total tube length was 71.5 in. which included the bottom 19.5 in. embedded into the transfer block. A normal-strength steel (50 ksi yield stress) annular ring, 6.5 in wide by 0.5 in. thick, was welded to the base of each pile using a fillet weld. The rings projected 4 in. on the outside of the pile and 2 in. on the inside of the pile. For Specimen 30-21-R, a 2 in. wide by 0.5 in. thick rib was welded on the inside of the pile, 2 in. from the top of the pile using a fillet weld, which was the supplemental rib.

The test specimen for this research consisted of the RC column and the connection to the CFST pile. The force and moment transfer between the column and the CFST pile is the behavior

of interest. The pile was embedded in a 74" x 66"x 24" reinforced concrete transfer block to anchor the specimen to the test rig. The embedment depth of 19.5 in. and annular ring were chosen to assure the CFST pile could develop the required resistance without damage block and was based on previous research (Stevens 2015). The transfer block was designed to remain elastic throughout the test. The dimensions of the transfer block were limited by the anchor points and dimensions of the test rig. The locations of the tie-down rods for the transfer block were controlled by the location of the anchor holes on the lateral test rig. The two sets of holes were spaced 60 in. apart and each set's holes were 18 in. apart from each other. A total of eight tie-down rods were used, four on each side. The tie-down rods were 1 ¼-in Williams Form Engineering All-Thread high-strength steel bars.

3.2 SPECIMEN CONSTRUCTION

The test specimens were constructed in two phases, with two specimens being built simultaneously. The first two specimens built were specimens 30-21 and 48-21, followed by Specimens 30-21-R and 30-21-LD.

3.2.1 *Transfer Block Fabrication*

The reinforcement for the transfer block was designed so that the block would remain elastic if the column and pile reached their full predicted flexural capacity. The predicted capacity of the column was calculated using Response2000 and then increased to 1000 kip-ft. based on the additional height of the specimen from the point of loading to the transfer block to determine the moment that the transfer block would experience. To determine the amount of steel required, only 70% of the expected steel yield stress (72 ksi) and 50% of the expected concrete ultimate stress (6000 psi) were used. This resulted in using #7 bars at 3 in. for the bottom mat of reinforcement

and 12 #9 bars for specimens 30-21, 30-21-R, and 30-21-LD, and 8 headed #11 bars for Specimen 48-21 as shown in Figure 3.2. The required steel calculations can be found in the Appendix. Vertical cross ties were added for the 30 in. specimens, but not for the 48" specimen due to the size of the pile. While building the reinforcement cage, the locations of the testing rig tie-downs were accounted for by placing 2.875" diameter PVC pipes at the locations where the tie-down rods would be anchored.

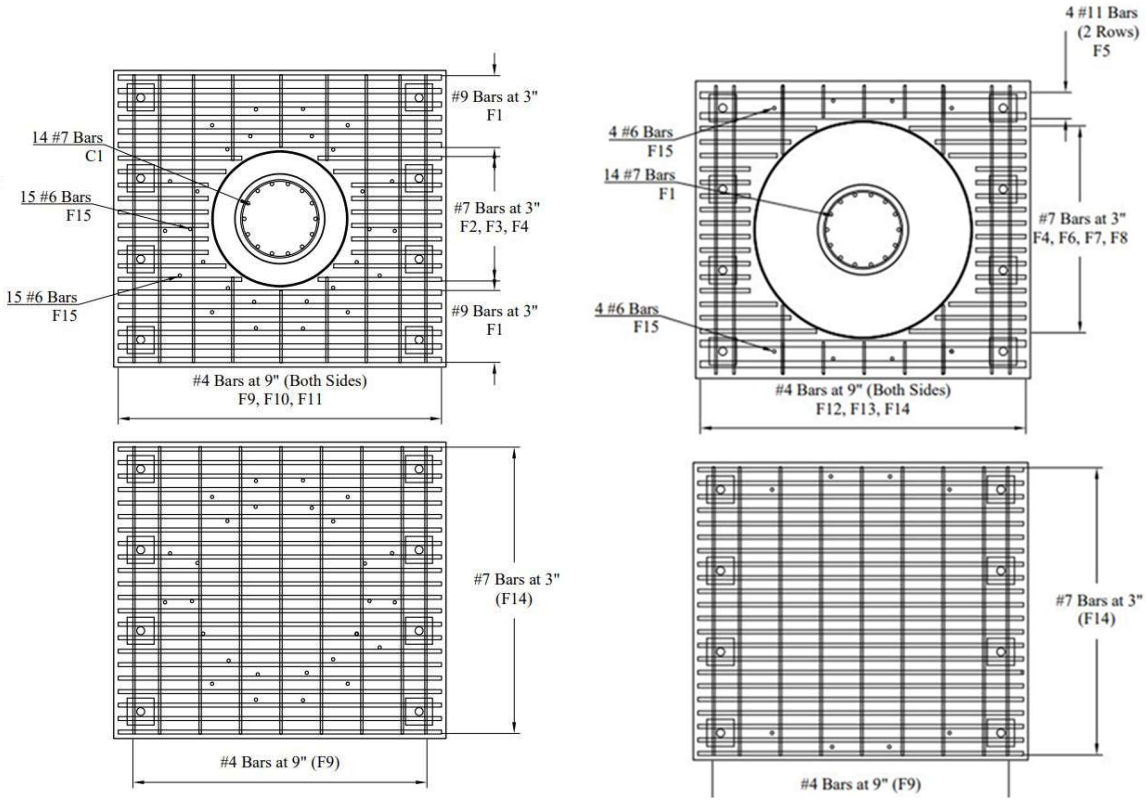

Figure 3.2. Transfer Block Reinforcement a) Specimens 30-21, 30-21-R, and 30-21-LD and b) Specimen 48-21

Figure 3.3. Specimen 30-21 Reinforcement

3.2.2 *Pile Fabrication*

The steel tube sections were cut on-site from a single piece of straight seam welded tube using an oxy-acetylene torch. Each section was cut to a length of 71.5 in. and the cut sides were ground down smooth. The annular rings were manufactured at a professional steel fabrication shop and then fillet welded to the tubes by a certified welder. For the 30 in diameter specimens, 30-21, 30-21-R, and 30-21-LD, all the fillet weld sizes were 0.625 in. and for Specimen 48-21 the fillet weld size was 0.5 in. On the outside flanges on the ring, 1.25 in. holes were drilled. Support screws

were then tack welded through these holes to act as supports to hold the base of pile 4 in. above the base of the transfer block.

3.2.3 *Column Fabrication*

The reinforcement for the column was consistent with WSDOT standards for a half-scale specimen. The longitudinal reinforcement consisted of 14 evenly spaced #7 steel bars, with a transverse reinforcement of 23 #3 hoops spaced at 3 in. in the plastic region of the column and spaced at 5 in. in the elastic region of the column. The column longitudinal reinforcement was placed after the application of strain gauges. The transverse reinforcement was then tied into place along the length of the column and the ends of the hoops were bent so that there was a 90-degree seismic hook at both ends of the hoop around the longitudinal reinforcement. The column reinforcement cage was then placed inside the pile, resting on rods such that the reinforcement was the correct depth, 21 in., inside the pile as shown in Figure 3.4.

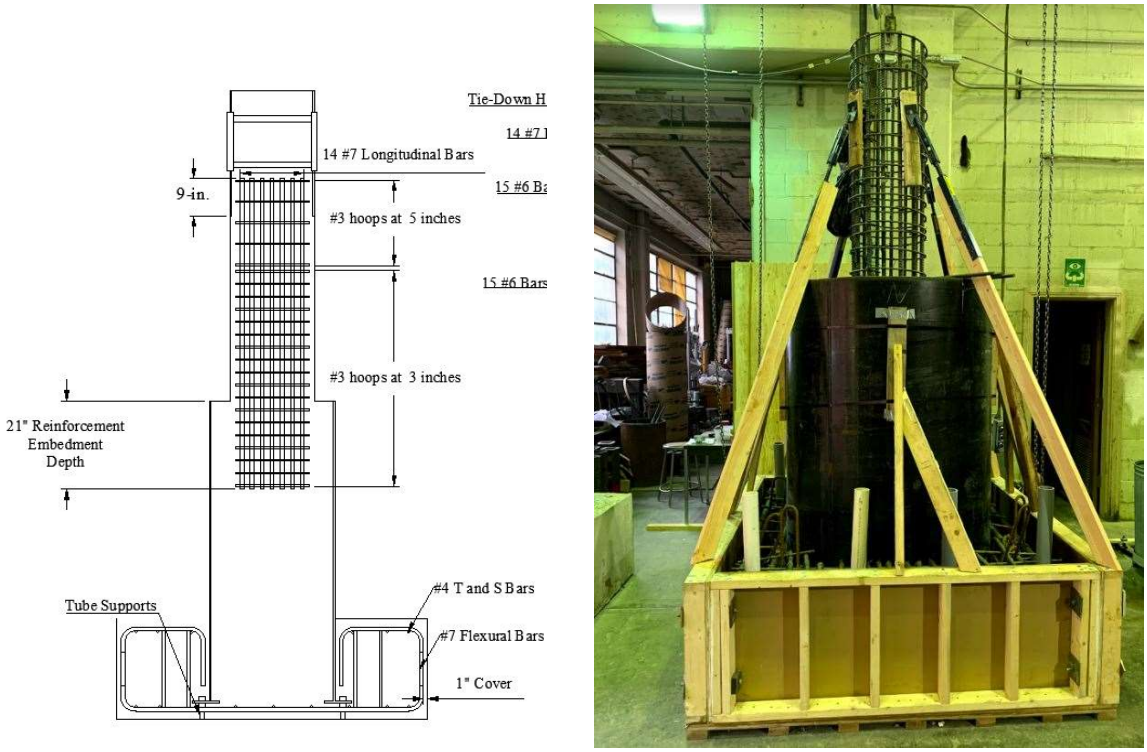

a) **b)**

Figure 3.4. Specimen Reinforcement a) Specimen Elevation and Reinforcement and b) Specimen 48-21 Completed Reinforcement Cage

3.2.4 *Casting*

A concrete mix design for structural applications (6000-A) was cast using a concrete pump truck. The casting procedure for each specimen was as follows.

Specimens 30-21, 30-21-R, and 30-21-LD all had the same procedure. The first cast was the transfer block and the up to the top of the pile. Wet burlap was placed on the exposed concrete to optimize curing. The second cast was for the column. This was done after a Sonotube and the top CFST were placed and secured around the exposed column reinforcement. The concrete was cured for a minimum of 28 days after casting before being tested.

For Specimen 48-21 the procedure was as follows. The first cast was the transfer block of the specimen. This cast used a self-consolidating concrete (SCC) mix as a different cast was being performed in the lab and the mix met the compressive strength requirements that the transfer block

would be subjected to. The second cast used the same mix as the other specimens (6000-A) and consisted of filling up the remaining height of the pile. The third cast was for the column. This was done after a Sonotube was placed and secured around the exposed column reinforcement. The concrete was cured for a minimum of 28 days after casting before being tested, except for the column concrete, which cured for 10 days before being tested but still met the compressive strength and elastic modulus requirements for testing.

3.3 SPECIMEN MATERIALS

Concrete used for the transfer blocks, piles, and columns was sourced from one supplier over eight distinct casts. All reinforcement bars were sourced from a single supplier and received in two separate shipments. These materials are summarized in Table 3.2, along with their respective specifications and supplying vendors.

Table 3.2. Material List

Item	**Designation**	**Vendor**
Concrete	6000-A, 4-ksi	Stoneway Concrete
Reinforcing Steel	A 706 Grade 60	Addison Supply
Straight Seam Steel Tubes	API 5L Grade B	Richards Pipe
Pile Annular Rings	A572 Gr. 50	Bloch Steel

3.3.1 *Concrete*

A total of eight casts were done. Two separate casts for Specimen 30-21. Three separate casts for Specimen 48-21. A total of three casts for Specimens 30-21-R and 30-21-LD, each one had a single cast separately and shared one cast.

Concrete was ordered from a single ready-mix plant in the Seattle area. A 4000 psi mix was specified with ¾ in. aggregate passing. A retarder was added to the first two mixes for Specimen 30-21 to enhance and maintain workability so proper finishing could be performed. For

each cast, 4 in. by 8 in. cylinders were made to track the strength of the concrete as it cured and for Day of Test material properties. Casts that were used for the transfer block only compressive cylinders were made. Casts that were used for the pile only compressive strength and tensile strength cylinders were made. For casts that were used for the column compressive strength, tensile strength, and elastic modulus cylinders were made.

All the test cylinders were stored in a calcium hydroxide water bath, per ASTM C511, until the various tests were performed. Cylinders used for elastic modulus tests were sulfur capped to ensure parallel loading surfaces. Compressive tests, splitting tensile tests, and elastic modulus tests were performed per appropriate ASTM standards as shown in Figure 3.5. The results of the compression, splitting tensile, and elastic modulus tests are summarized in Table 3.3.

Table 3.3. Day of Test Concrete Properties

Specimen ID	Mean Compressive Strength (psi)			Mean Splitting Tensile Strength (psi)		Mean Elastic Modulus (psi)
	Transfer Block	Pile	Column	Pile	Column	Column
30-21	8957		6742	526	431.9	4529
48-21	12040	5455	5127	402.1	432.4	4121
30-21-R	6685		5163	504.2	471.1	3811
30-21-LD	5508		6760	471.1	436.4	4178

a) **b)** **c)**

Figure 3.5. Tested Concrete Cylinders in a) Compression, b) Tension, and c) Elastic Modulus

3.3.2 *Reinforcing Bars*

Reinforcing bars were purchased from Addison Construction Supply in Tacoma, Washington, and were delivered at two separate times. The bars were A706 Grade 60 and it was requested that all reinforcement of the same size and grade be from the same heat.

The reinforcement was expected to yield from the lateral loading during the test. To determine the actual stress-strain relation of the reinforcement, steel from the longitudinal column reinforcement was tested in tension to ASTM 370 standards. The test setup is shown in Figure 3.6. The stress-strain relationship of the reinforcement was characterized using the stress and strain at the Yield, Ultimate, and Fracture points, which are shown in Table 3.4 below.

Table 3.4. Longitudinal Reinforcement Material Properties

	Specimens 30-21 and 48-21		**Specimens 30-21-R and 30-21-LD**	
	Average Stress (ksi)	**Average Strain**	**Average Stress (ksi)**	**Average Strain**
Yield	70	.0024	67.9	.0023
Ultimate	106.2	.06	111.6	0.1
Fracture	77.8	.155	87.2	0.237

Figure 3.6. Reinforcement Tensile Test Setup

3.3.3 *Steel Tubes*

The straight seam welded steel tubes are API 5L X52 for the 30 in. diameter tube, a 52 ksi yield strength, and API 5LB X42 for the 48 in. diameter tube, a 42 ksi yield strength. Tubes were purchased from Richards Pipe & Steel, Inc. in Pacific, Washington.

a) **b)**

Figure 3.7. a) 48 in. and b) 30 in. Diameter Steel Tubes Cut to Size

3.3.4 *Pile Annular Ring and Embedded Rib Plates*

The rings were purchased from and manufactured by Bloch Steel in Seattle, Washington. They are A572 Gr. 50 steel. The rings were fillet welded to the tubes using a 5/64 in. diameter Coreshield 8 E70 welding electrode. All structural welding was performed by a certified welder.

Figure 3.8. Annular Rings for Specimens 30-21 and 48-21

3.4 EXPERIMENTAL TEST SETUP

The test setup consisted of three main aspects. Secure the transfer block of the specimen so that uplift during testing would be negligent, apply vertical/axial loads to the column, and apply lateral loads to the top of the column. Figure 3.9 shows the components developed to meet these aspects of the setup. Lateral loads were applied using a combination of an MTS Actuator and a self-reacting test rig and axial loads were applied using a 2400-kip Baldwin Universal Testing Machine using a spherical bearing. To secure the transfer block of the specimen, eight high-strength Williams rods were used to tie down the specimen to the testing rig.

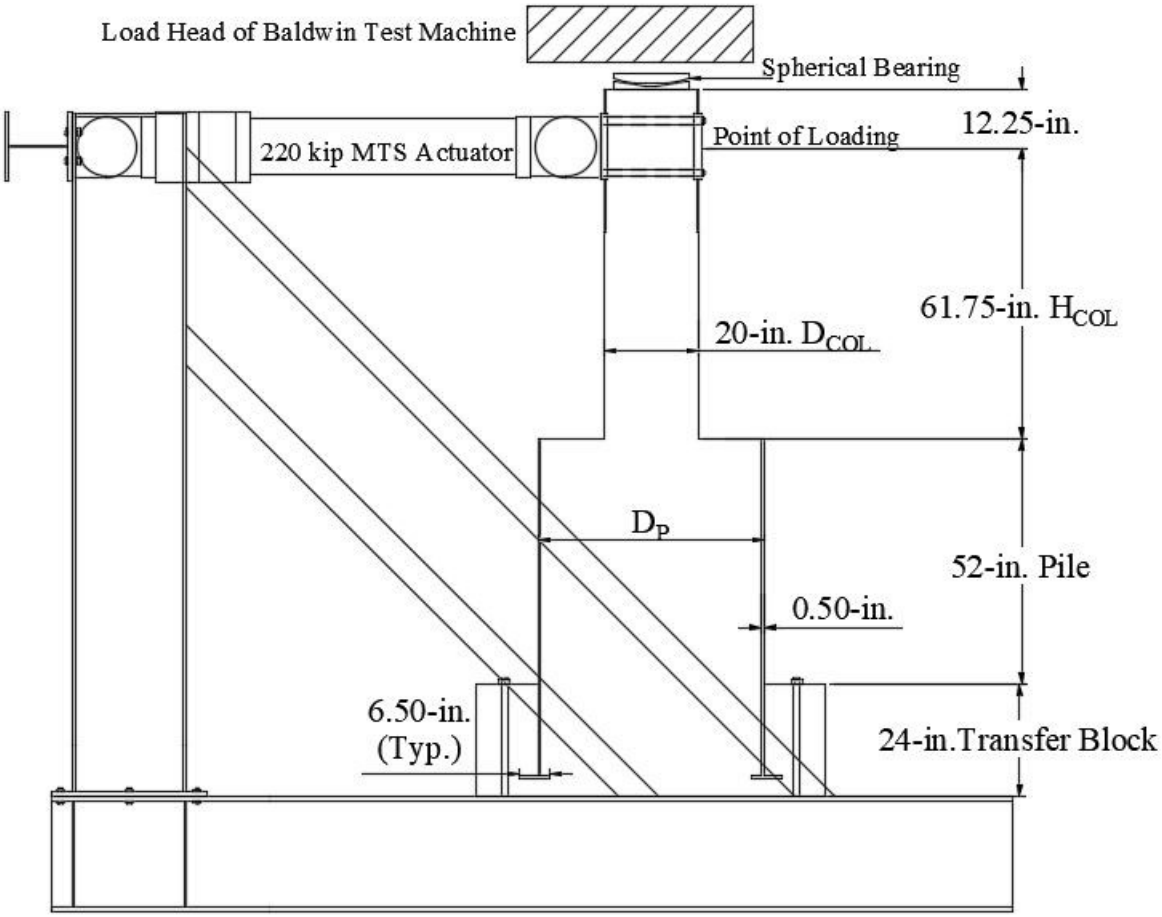

Figure 3.9. Experimental Setup Overview

3.4.1 *Lateral Load Application*

Lateral loads were applied using an MTS Actuator attached to a Self-Reacting Test Frame. The MTS Actuator has a capacity of 220 kips and a maximum stroke of +/- 10 in. The actuator applied a lateral load at the top of the column, which simulated increasing superstructure displacements and was operated under displacement control. For each test, the actuator was attached to the column using four 1 in high strength rods, a spreader plate, and rubber pads. The high-strength rods were tightened using 1 in. diameter bolts, which were tightened using a hydraulic torque wrench until a stress of 1000 psi was reached, to ensure the actuator head was

secured to the column throughout the test. The spreader plates and rubber pads distributed the applied force over an appropriate area to prevent localized damage.

The Self-Reacting Test Frame is used with the MTS Actuator to apply lateral loads to the specimen. The Self-Reacting Test Frame is moved under the Baldwin, before testing the specimen, and secured down to the laboratory floor.

3.4.2 *Axial Load Application*

Axial loads were applied to the column using the Baldwin Universal testing machine. The Baldwin Universal Testing Machine (Baldwin) has a maximum load of 2400 kips. For these tests, the Baldwin applied a constant load equivalent to 7.5% of the axial capacity of the column to the top of the column, simulating loading due to superstructure and the resultant P-Δ force. Due to the different day of test concrete strengths, the axial load was not the same for all 4 specimens. Specimen 30-21 had an axial load applied of 160 kips. Specimen 48-21 had an axial load applied of 120 kips. Specimen 30-21-R had an axial load applied of 120 kips. Specimen 30-21-LD had an axial load of 160 kips.

To allow the top of the column to displace while having a constant axial load, an assembly was used to act as a roller support at the top of the column and is shown in Figure 3.10. The critical components of this assembly were a spherical bearing and a low friction sliding surface. The assembly included additional components to restrict out-of-plane movements and evenly transfer the vertical load from the spherical bearing to the column.

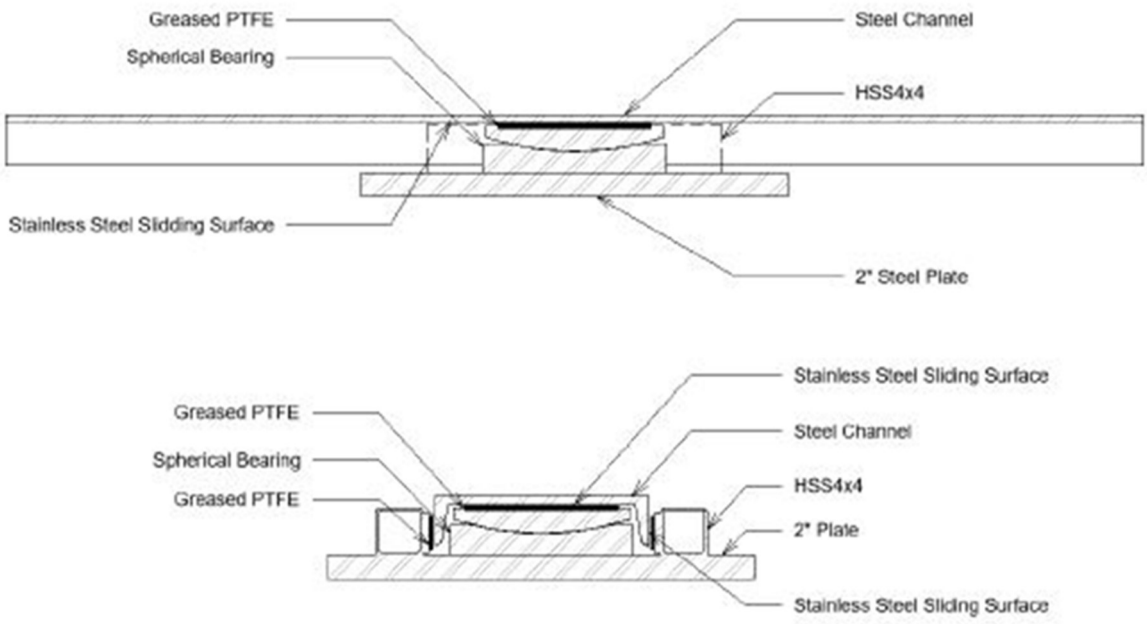

Figure 3.10. Axial Bearing Assembly for Specimen 30-21

The spherical bearing allows the top of the column to be displaced by the MTS Actuator while maintaining the Baldwin load. As shown, a piece of greased PTFE is embedded in the top of the spherical bearing. This provides a low friction sliding surface between the bearing and the channel, minimizing friction effects. The grease is a Methyl Siloxane lubricant.

The bottom 2 in. thick steel plate applies the axial force from the Baldwin evenly across the top of the column. The plate also has a track for the above channel made from a HSS and more greased PTFE, as shown in Figure 3.10, to prevent transverse displacement during testing.

The large steel channel is bolted to the head of the Baldwin and acts as the top track to prevent transverse displacement. The interior web of the channel and outside flanges are lined with stainless steel providing a smooth surface on which the greased PTFE slides.

This type of axial bearing was used for the Specimen 30-21's test. However, due to the short deformable length of the reinforced concrete column, this led to an unexpected increased rotation with the bearing. This caused the top channel to bind against the spreader plate at large displacements as shown in Figure 3.11. The effects of this binding will be addressed in later

chapters. Thus a new spherical bearing assembly, described below, was put together to be used for the remaining specimen tests.

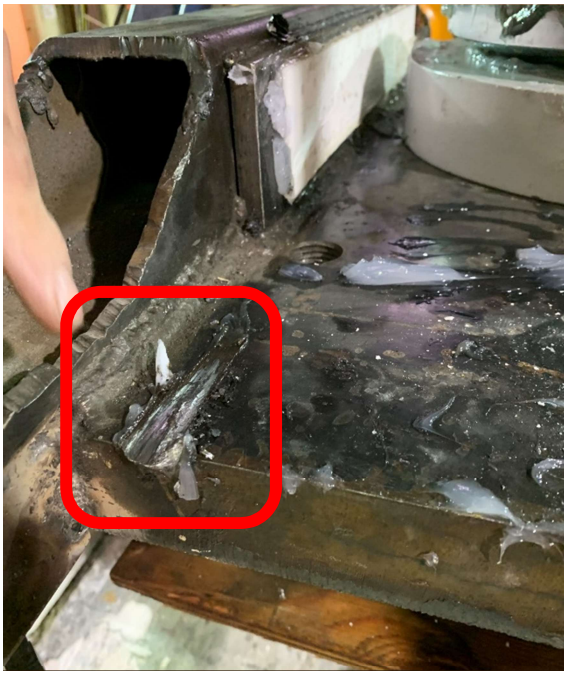

Figure 3.11. Spreader Plate Gouge Caused by Assembly Binding

To address this issue and new spherical bearing assembly was used for the remaining tests. The new assembly consisted of placing the spherical bearing inside the top of the column's steel tube. It was sat within the top 0.5 in. of the tube and had grout placed around it to prevent it from slipping. The top part of the assembly is the large steel channel described above. The interior web and flanges of the channel are lined with stainless steel that is greased providing a smooth surface for the axial bearing to slide back and forth on. The assembly used for the remaining tests can be shown in Figure 3.12.

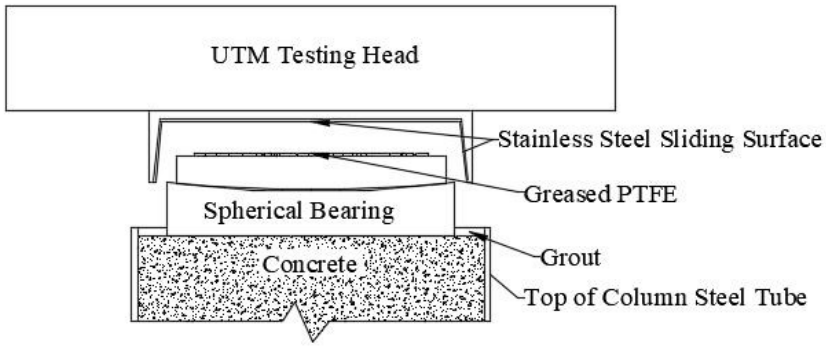

Figure 3.12. Axial Bearing Assembly for Specimens 48-21, 30-21-R, and 30-21-LD

3.5 SPECIMEN INSTALLATION

When the concrete had achieved sufficient strength, specimens were moved into the Self-Reacting Test frame, using a combination of cranes, forklifts, and the Baldwin Universal Testing Machine. The testing frame is also a strong floor that specimens can be tied down to. Each specimen was leveled, and grouted into place using Hydrostone, and the specimen was anchored and post-tensioned to the base of the test frame with four 1 1/4-in. Williams Form Engineering All-Thread high-strength steel bars on each side. Each one of the bars is post-tensioned to 33.3 ksi, resulting in a force greater than the predicted uplift force. Once all parts of the test setup were in place, instrumentation was connected to the specimen and the data acquisition system. Load cells, strain gauges, inclinometers, and different potentiometers were used, as well as an Optotrak camera and target system and a Vibrating Wire Gauge (VWG) system. The load cells, strain gauges, inclinometers, and potentiometers were all routed to a single data acquisition system while the Optotrak system and VWG system were each routed to separate systems. Instrumentation is discussed in more detail in Section 3.6.

3.6 INSTRUMENTATION

To characterize the response of test specimens to lateral loading, displacements, lateral load resistance, local displacements, curvature, and strains were recorded. The imposed displacements and lateral load response were used together to characterize and compare each specimen's force drift response. The general instrument layout is shown in Figure 3.13.

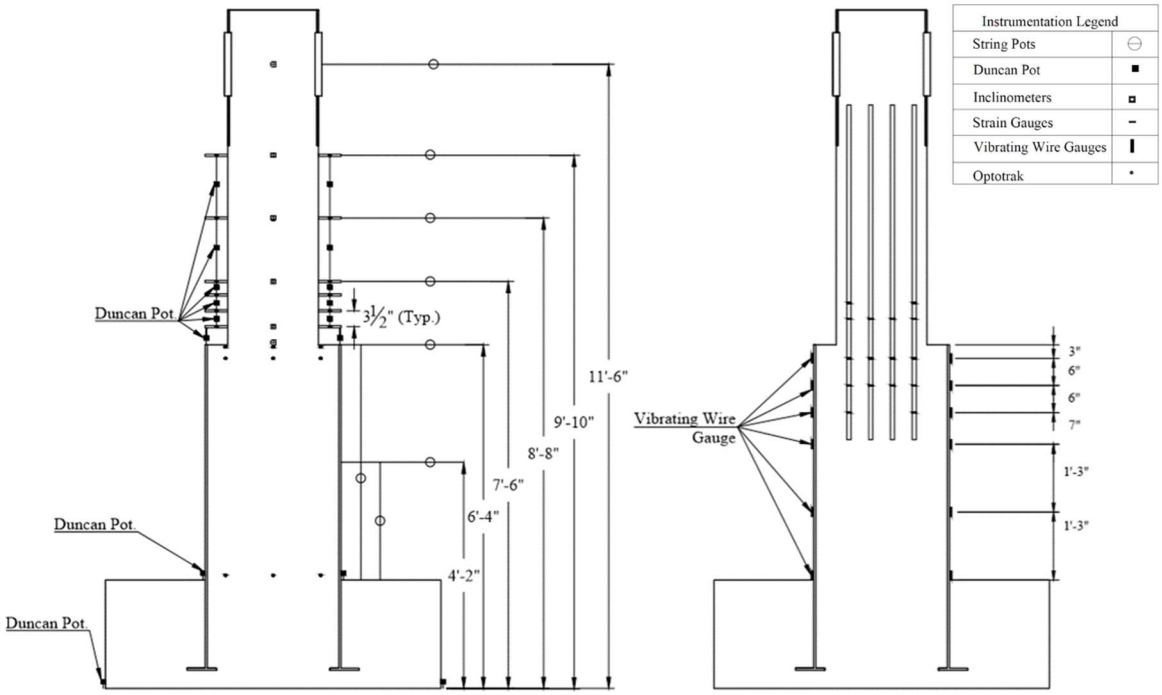

Figure 3.13. General Instrumentation Layout

3.6.1 *Lateral Load Response*

Lateral loads were recorded using the MTS Actuator load cell. To determine axial loads, The Baldwin Universal Testing machine's load cell was used to record loads, which were used to remove P-Δ effects during analysis.

3.6.2 *Crack Monitoring*

To monitor cracks in the concrete, all exposed concrete on the column and pile were painted white. The paint made it easier to see a formed crack. On top of the paint, a horizontal and vertical grid was drawn on, with 5 in. divisions. This was to give some general reference during the test to the size of the damage occurring. During the test, red and blue markers were used to mark cracks, red for when the column was in compression and blue for when the column was in tension.

For Specimens 30-21, 48-21, and 30-21-LD, a primer paint was used. Specimen 30-21-R used latex paint. This was due to the availability of paint in the structures lab at the time. The effects of latex paint are discussed in Chapter 4.

3.6.3 *Displacements*

Displacements at the level of lateral load application and displacements along the height of the column and pile were measured to determine the deformations of the specimens under lateral loading. Displacement at the point of lateral loading was used to develop the force-displacement and moment-drift response of the various connections. This response is used to compare the performance of connections and identify how the different connections perform under lateral loads.

To monitor the displacement at the level of lateral force application and the height of the column, a reference tower was placed to the north of the specimen and multiple string potentiometers were attached between the tower and the specimen. Though the MTS Actuator LVDT was measuring displacements, these displacements were not used due to the deformation of the setup.

An Optotrak system was used to capture displacement information for the pile and column as a backup. Optotrak targets were placed along the height of the column and pile, matching some of the points where the reference column string potentiometers were attached.

3.6.4 *Strains*

Knowing the yield behavior of reinforcement in relation to lateral loading was an important part of the evaluation of specimen performance.

To monitor these strains, strain gauges (TML YFLA (post-yield) strain gauges) were placed on a portion of flexural reinforcement inside the column. The strain gauge readings would be used to characterize the yield behavior and compare the results from various tests. To characterize the extent of yielding in longitudinal reinforcement across the height of the test specimens, a greater number of gauges were placed on reinforcement on the most northern and southern reinforcement through the column, while fewer gauges were placed on reinforcement on the northeast and southeast reinforcement.

The strain on the outside of the pile or tube was also monitored. This was done by placing both strain gauges (TML FLA (elastic) strain gauges) and Vibrating Wire Gauges (VWGs) along the height of the pile on the northern and southern faces. The locations of these gauges were at the same height on the pile but slightly offset to the left or right of each other.

VWGs were used due to the higher resolution of strain the VWG can detect compared to the regular strain gauges. Strains are measured using the vibrating wire principle: a length of steel wire is tensioned between two mounting blocks that are attached to the surface being studied. Deformations of the surface will cause the two mounting blocks to move relative to one another, thus altering the tension in the steel wire. The tension in the wire is measured by plucking the wire and measuring its resonant frequency of vibration. The wire is plucked, and its resonant frequency

measured, using an electromagnetic coil positioned next to the wire. The data acquisition system, used in conjunction with the gauge, provides the necessary excitation to pluck the wire and converts the measured frequency to display the reading directly in microstrains. The usable range of the strain gauge runs from around 1000 to 4000 microstrains. The mid-range reading for tension and compression is 1700. (Geokon, 2010)

To attach the Model 4000 VWGs to the pile, first, the mounting blocks were attached with spacer bars and tack welded to the tube, as shown in Figure 3.14, however for these tests the VWG was oriented vertically, not horizontally. Second, the Model 4000 vibrating wire strain gauges were inserted into the mounting blocks. The bottom end of the gauge was first slid through the top mounting block. The end of the strain gauge which had a V-groove in it was inserted into the mounting block that only had one set screw, and the screw was tightened hard. Third, the coil and thermistor housing were then attached to the center of the gauge, secured with a hose clamp. Fourth, the bottom end of the gauge, after making sure all readings were in the usable range of the strain gauge, was screwed into the other mounting block. Finally, the mounting blocks were tapped with the handle of a screwdriver to remove any installation strains and stabilize the reading.

Figure 3.14. Welding Sequence for the Mounting Blocks (Geokon, 2010)

3.6.5 *Curvature*

To monitor the curvature of the column, inclinometers and Duncan potentiometers were used. The inclinometers, that measure the rotation of the column, were placed along the height of

the column at the same heights that the string pots were attached to. At similar locations, rods going through the column were placed along its height. In between each set of rods, a Duncan potentiometer was placed to measure the deformation of the column between the rods. For the bottom rod, the rod extended out to the edge of the pile, where a Duncan potentiometer was attached and measured the difference between the rod and the top of the pile. Duncan potentiometers were also added at the base of the pile to measure any slip or uplift that the tube might experience.

3.6.6 *Global Instrumentation*

Duncan Potentiometers were placed horizontally and vertically at the base of the transfer block and the testing rig on both the north and south sides. They were used to measure any global uplift or slipping that might have occurred during testing. Additionally, a string potentiometer was placed on a reference tower to measure the lateral actuator's push back on the testing frame.

3.7 TESTING IMPLEMENTATION

Testing of Specimens 30-21, 48-21, 30-21-R, and 30-21-LD were carried out using the following test procedures written below. Before testing, an experimental checklist was completed. Once the checklist was completed and the lab manager verified test equipment was prepared the following procedure was performed:

Initializing:

1. Data acquisition systems were initialized

2. Axial load was applied to the column using the Baldwin Universal Testing Machine

For Each Target Displacement:

3. First cycle at the same target displacement was initiated and stopped at the first peak

4. Cracks were marked in red, crack sizes were recorded, and pictures were taken to record spalling, crushing, and bar buckling

5. The cycle was continued and halted at the second peak or valley

6. Cracks were marked in blue, crack sizes were recorded, and pictures were taken to record spalling, crushing, and bar buckling

7. The cycle was continued and halted when the MTS actuator read zero force

8. Residual displacement was recorded, and crack sizes were recorded

9. The cycle was completed

10. Steps 3-9 were repeated for a second cycle at the same target displacement

14. Steps 3 – 10 were repeated at increasing displacements until specimen failure was achieved or equipment limits were reached

Test Conclusion:

15. Axial load was removed from the column

16. Data acquisition systems were halted, and data was saved

17. Spalling was removed and more pictures were taken showing the specimen after testing concluded

Before the main test, a dry-run of the test setup takes place. For this dry-run, the specimen is displaced by a small elastic displacement. This is done to make sure the setup is secure and to verify that the instrumentation is working properly. Due to an error with the MTS Actuator controller, Specimen 30-21 dry run displacement was 1 in. instead of the 0.1 in. target displacement. The effects of this dry run will be explained in Chapter 4.

3.8 IMPOSED DISPLACEMENT HISTORIES

The specimens were cycled under displacement control using the displacement history described in previous sections. The target displacement included the flexibility of the test setup (including the reaction frame and actuator). The actual drift was measured using an independent string pot attached to a reference column. As such, the actual drift was nearly always less than the target. Target and actual drifts for each specimen are provided in Table 3.5.

Table 3.5. Target Displacements and Drifts

Series	Target Disp. (in)	Target Drift (%)	Number of Cycles per Specimen			
			30-21	48-21	30-21-R	30-21-LD
1	0.25	0.40	NA	2	2	NA
2	0.5	0.81	NA	2	2	NA
3	0.75	1.21	NA	2	2	2
4	1	1.62	3	2	2	NA
5	1.5	2.43	2	2	2	NA
6	2	3.24	2	2	2	6
7	3	4.86	2	2	2	1
8	4	6.48	2	2	2	10
9	6	9.72	2	2	4	2

While the target displacement history pattern was similar for all four specimens, each target displacement was cycled to 2 full cycles, there were some slight differences. For Specimen 30-21, due to incorrectly inputting the dry run test displacement, cycles less than 1.0 in. were not included. For Specimen 30-21-R, since the specimen was still maintaining lateral strength, an additional two cycles were run at the 6 in. displacement for a total of 4 full cycles. For Specimen 30-21-LD, which

was being tested under a long-duration displacement history, cycles at 0.25, 0.5, 1.0, and 1.5 inches were skipped. Additionally, there were 6 full cycles at 2.0 in., only 1 full cycle at 3.0 in., and 10 cycles at 4.0 in. The values listed above are the maximum drifts reached for each displacement. Figures 3.15-3.18 represent the target drift cycles for each specimen.

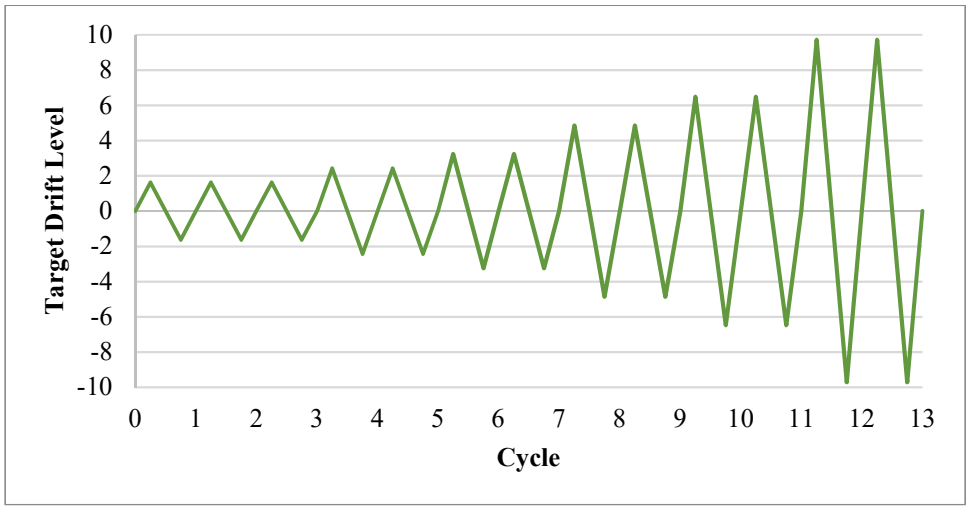

Figure 3.15. Specimen 30-21 Target Displacement History

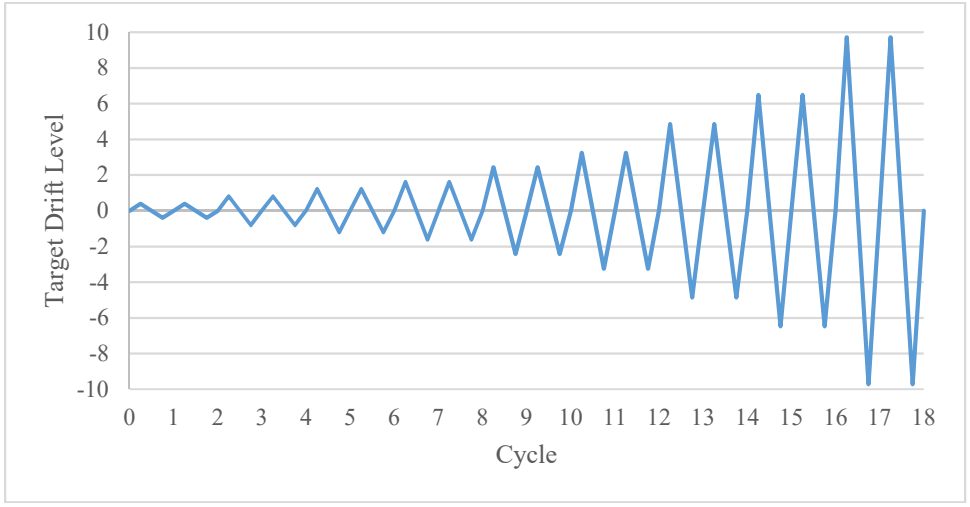

Figure 3.16. Specimen 48-21 Target Displacement History

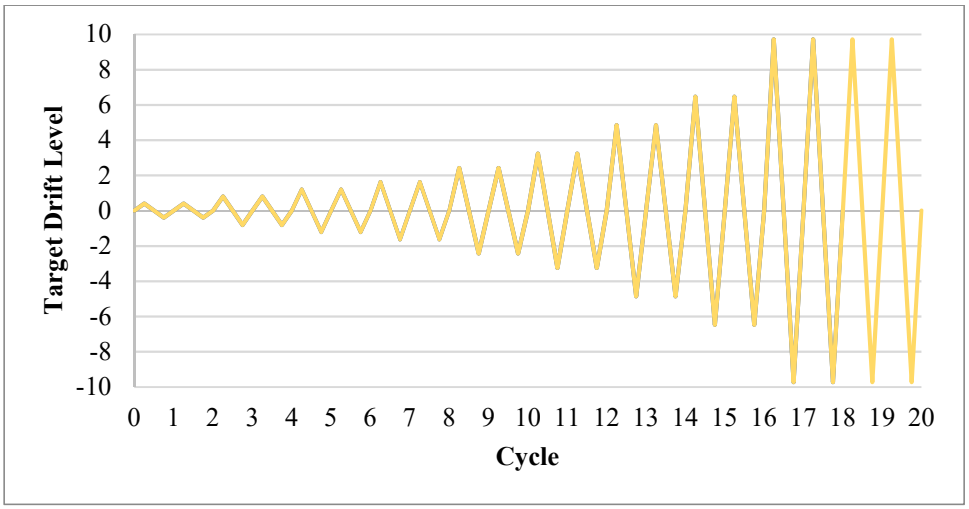

Figure 3.17. Specimen 30-21-R Target Displacement History

As mentioned before Specimen 30-21-LD was tested under a long-duration displacement history. This displacement history was based on results from research Kortum (2021) performed investigating the impacts of a Cascadia subduction zone M9 earthquakes on bridges in Washington State for single degree of freedom (SDOF) idealized bridge columns.

Kortum modeled SDOF bridge columns under M9 ground motions. Assuming a bridge column located in Seattle, Washington, with a Bridge Strength Ratio, Fy/W, the bridges lateral strength divided by its weight, of 15%, bridge effective periods of 1.0 and 2.0s, and with a soil site classification of D3, 60 different hysteric displacement curves were modeled. Using the results of Specimens 30-21 and Kortum's hysteric curves, it was determined that a typical bridge column would undergo 6 cycles at a ductility when first spalling would occur, μ=2.7 or a column drift of 2%, one cycle at a ductility when full spalling would occur, μ=4.2 or a column drift of 3%, and 6 cycles at a ductility when bar buckling would occur, μ=5.7 or a column drift of 4%. The ductility is based on the results of Specimen 30-21 since it was identical to Specimen 30-21-LD. Based on these results, a testing displacement history was put together that consisted of 1 cycle at the expected yield displacement, 0.75 in., 6 cycles at 2.0 in, 1 cycle at 3.0 in., and then cycle to

specimen failure, less than 50% of maximum strength at 4.0 in. This displacement history was slightly changed, as after 10 cycles at 6.5% drift the specimen had not failed, 2 cycles at 9.7% drift were run, as shown in Figure 3.18.

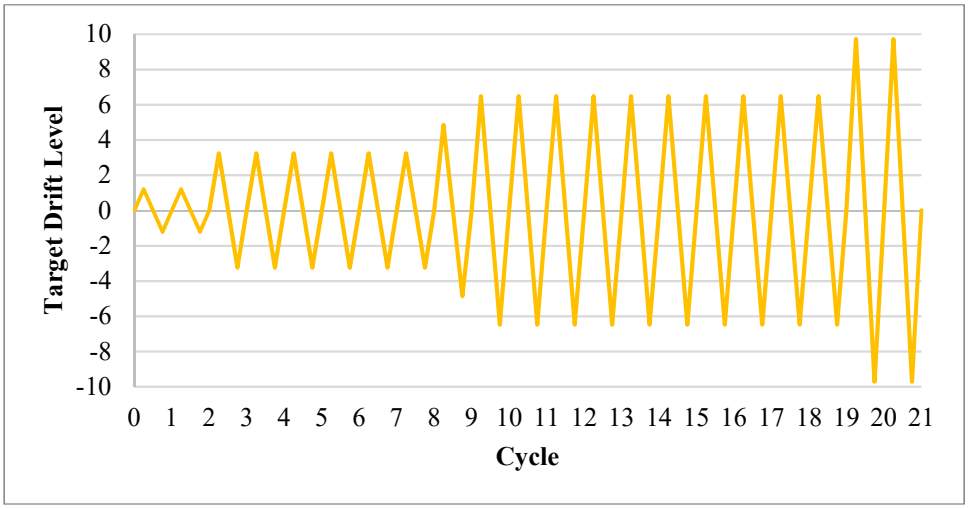

Figure 3.18. Specimen 30-21-LD Target Displacement History

Chapter 4. EXPERIMENTAL OBSERVATIONS AND RESULTS

4.1 INTRODUCTION

Experimental testing was conducted to assess the effects of pile diameter, reinforcement embedment depth, the addition of an embedded rib inside the pile, and displacement history on the cyclic, nonlinear performance CFST pile and RC column connections specimens. Each of the four specimens was tested using the test setup and target displacement history described in the last chapter to evaluate these parameters.

The first two specimens, Specimens 30-21 and 48-21 investigate the effect of pile diameter and embedment depth. The third specimen, Specimen 30-21-R, investigates the effect of the addition of the embedded rib inside the pile. The fourth specimen, Specimen 30-21-LD, investigates the performance of the connection under long-duration cyclic loading. The test matrix is shown in Table 4.1

Table 4.1. Specimen Test Matrix

Specimen Name	Tube Diameter (in.) [mm]	Tube Diameter/ Tube Thickness	Reinforcement Bar Size	Embedment Depth (in.) [mm]	Rib Size (in.) [mm]	Rib Embedment Depth (in.) [mm]
30-21*	30 [762]	60	#7	21 [533]	NA	NA
48-21	48 [1219]	96	#7	21 [533]	NA	NA
30-21-R	30 [762]	60	#7	21 [533]	2 [50.8]	2 [50.8]
30-21-LD	30 [762]	60	#7	21 [533]	NA	NA

*Specimen 30-21 is reference specimen

This chapter is divided into five sections. The first section summarizes the data used to describe each test. The remaining four sections are the experimental results and observations for each specimen based on the information used to describe the specimen in Section 4.2.

4.2 Data Provided for Each Specimen

For each specimen, the following information is described:

- Observed Overall Behavior
- Measured Response
- Observed Specimen Damage
- Strain Distribution of Connection

The measured column moment is determined by multiplying the lateral force by the height of the column to the point of loading. The moment, P-Δ, from the axial force, P, and the lateral displacement of the column, Δ, is then removed from the total moment, as shown in Figure 4.1.

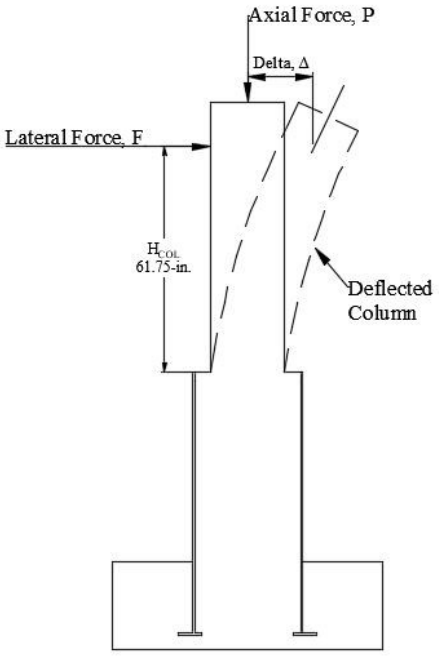

Figure 4.1. Deflected Column Shape with Applied Forces

The moments are then normalized using the nominal moment, $M_{n\text{-}Col}$, which was calculated using measured material strengths in the reinforced concrete sectional analysis program Response-2000. The lateral strength is normalized using the nominal force, $F_{n,}$ which is calculated using the following equation:

$$F_n = M_{n\text{-}Col} / H_{Col}$$

F_n = nominal force (kips)

M_{n_Col} = nominal moment calculated in Response 2000 (kip-ft.)

H_{col} = height of column to point of loading, 61.75 in.

This is followed by the sequence of damage that occurred in the pile and column, as observed during testing, is described at low drift ratios (0–1.5%), at moderate to high drifts (1.5%–4%), and at the final state (after 4 %). Damage to the specimen may consist of descriptions of cracks, concrete spall, and exposed reinforcement. For monitoring cracks, two cracks were identified during early test cycles and followed for the remainder of the test, measuring their length and maximum width with each new drift level. The monitored crack's location and width for each drift are tabulated for each drift level. The drift ratio is calculated using the following equation:

$$Drift_{COL} = \Delta_{\_Col} / H_{Col}$$

$Drift_{COL}$ = Drift Ratio of Column

$\Delta_{\_Col}$ = Lateral Displacement of Column (in.)

H_{col} = Height of Column to Point of Loading, 61.75 in. (in.)

Note: Displacement from pile deformation (displacement and fixed-end rotation) is removed from the lateral displacement of the column.

The strain distribution of the reinforcement and tube are shown for various drift levels. This is used to help exemplify the behavior of the reinforcement and to compare the observed

damage with the demand in the connection. Figure 4.2 shows a cross-sectional view of the specimen layout and identifies the locations of the strain gauges.

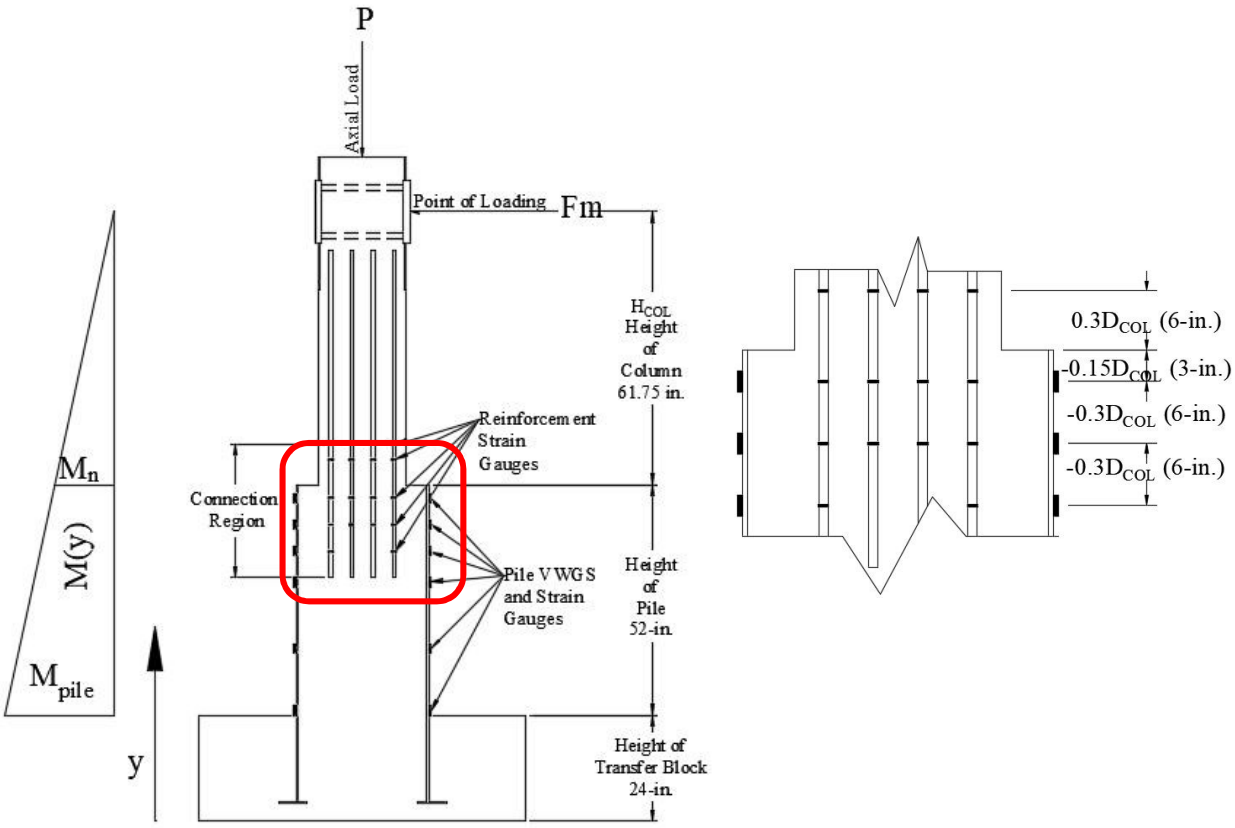

Figure 4.2. a) Cross-Section of Specimen Elevation with Gauge Locations Highlighted

Figure 4.3 shows a cross-section of the column and pile interface, which identifies the locations of the strain gauges on the reinforcing steel and tube. The vertical locations of the strain gauges will be referenced based on their location in terms of the column diameter, D_{COL}, and if there are above or below the column base. There are up to 6 vertical locations for each reinforcing bar: $0.45D_{COL}$ (9 in.) and $0.3D_{COL}$ (6 in.) are located above the base of the column and $-0.15D_{COL}$ (3 in.), $-0.3D_{COL}$ (6 in.), $-0.45D_{COL}$ (9 in.), and $-0.75D_{COL}$ (15 in.) are located below the base of the column. Figure 4.4 is an example of a strain distribution plot. The plots may consist of up to six points per height and drift level for each specimen. The tube strains are shown as filled circles, and while it may only appear like there is one mark per side, there are actually two at each location,

one from the strain gauge and one from the VWG. This is due to the strains measured on the tube being significantly smaller than the strains measured on the reinforcement. The reinforcement strains are shown as connected circles. There may be up to four points per specimen. If there are less than four points, this is either due to the middle reinforcement, North-East (NE), and South-East (SE) bars, not having a strain gauge at this location or a broken strain gauge at that location. On all plots, there is a horizontal line at the tension yield strain of the reinforcement, +/-.0024 in/in. The horizontal axis represents the horizontal distance the strain gauge is from the center of the column. It is normalized by the radius of the column, 10 in. The vertical lines at +/-1 represent the sides of the column.

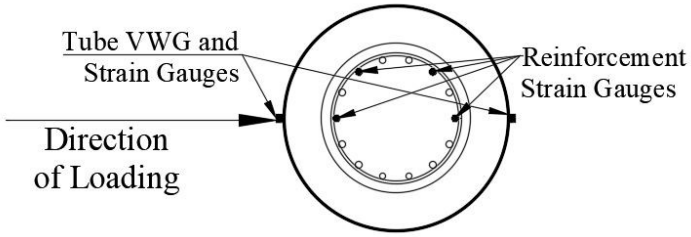

Figure 4.3. Cross-Section of Strain Gauge Locations

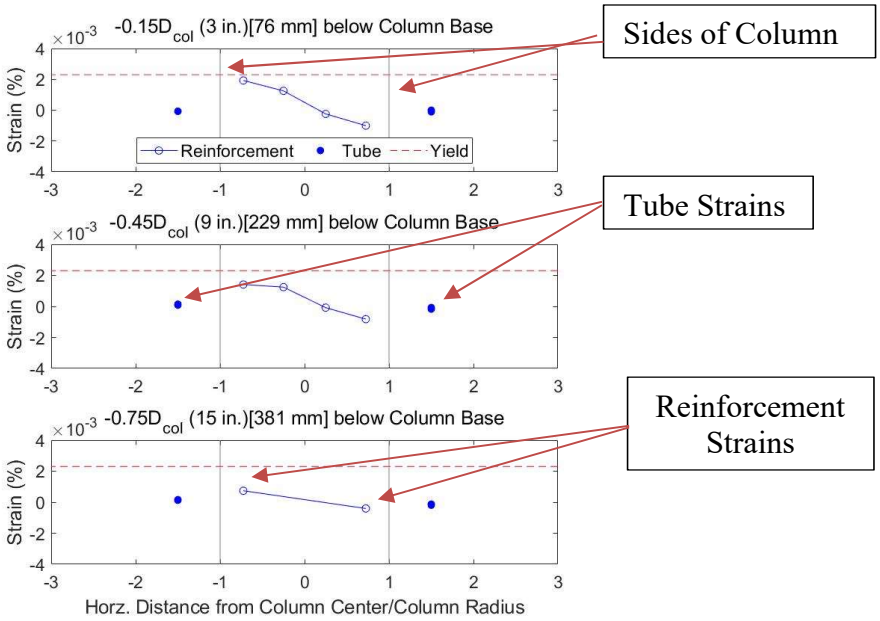

Figure 4.4. Example of Strain Distribution Plot

4.3 SPECIMEN 30-21

Specimen 30-21 was tested on February 11th, 2021 in the Structural Research Laboratory at the University of Washington. The test was performed 111 days after casting the transfer block and pile and 87 days after casting the column. The extended time between the specimen casts and testing was due to lab scheduling.

The maximum measured resistances and corresponding imposed drift of each cycle are provided in Table 4.2. The force-drift and moment-drift hysteresis curves of the column are shown in Figures 4.5-4.8. The constant axial load applied to this specimen was 7.5% of the axial capacity of the column, 160 kips.

Table 4.2. Maximum Resistances and Drifts in Each Cycle (30-21)

Target Drift	Cycle	Maximum Measured Resistance (kips)		Maximum Imposed Drift (%)	
		Tension	Compression	Tension	Compression
1.62%	1	77.93	63.14	1.11	1.06
	2	58.34	63.75	0.96	0.92
	3	65.54	63.14	0.94	0.93
2.43%	4	80.02	72.31	1.52	1.52
	5	81.07	77.13	1.55	1.54
3.23%	6	89.20	78.13	2.19	2.23
	7	86.89	74.84	2.25	2.30
4.86%	8	95.13	79.36	3.65	3.77
	9	85.09	80.38	3.71	3.82
6.48%	10	91.89	83.27	5.03	4.95
	11	86.28	78.30	5.13	4.98
9.72%	12	85.61	77.74	7.03	6.59
	13	48.61	18.16	7.51	8.06

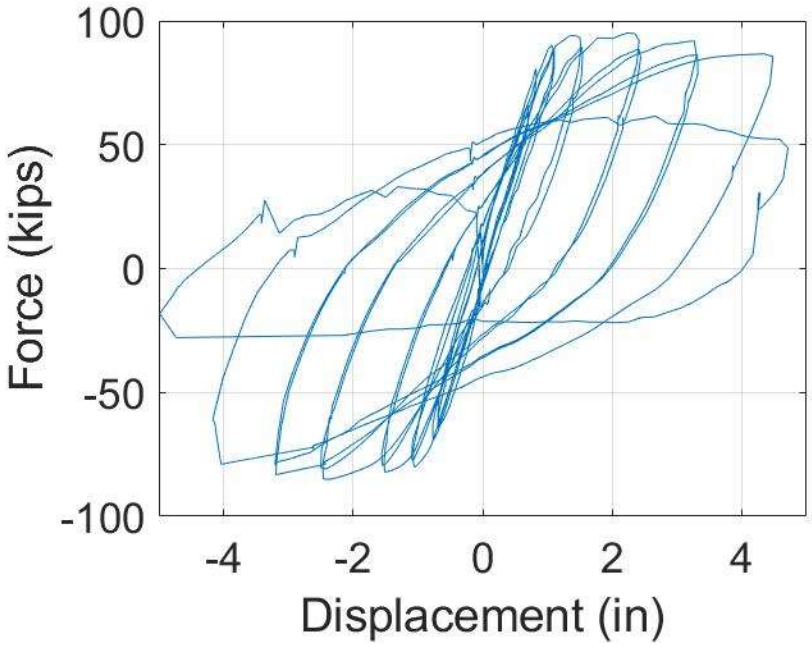

Figure 4.5. Specimen 30-21 Force-Displacement Curve

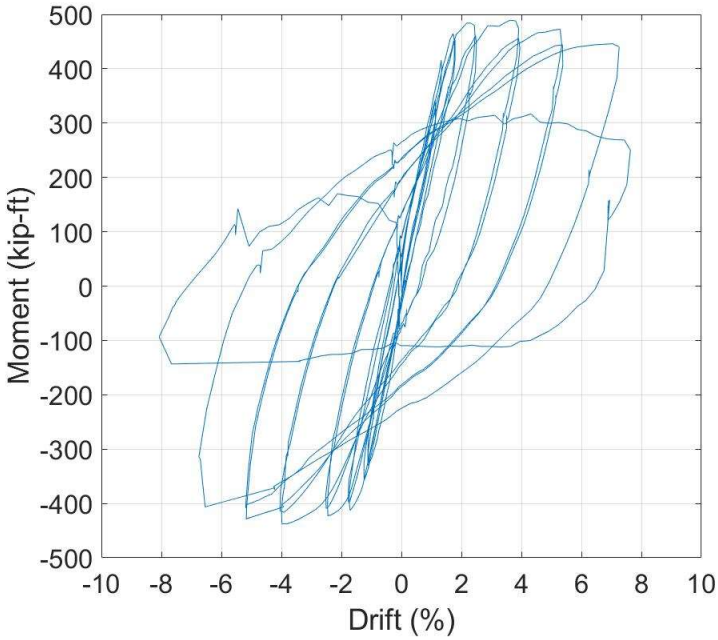

Figure 4.6. Specimen 30-21 Moment-Drift Curve with P-Δ Effects Removed

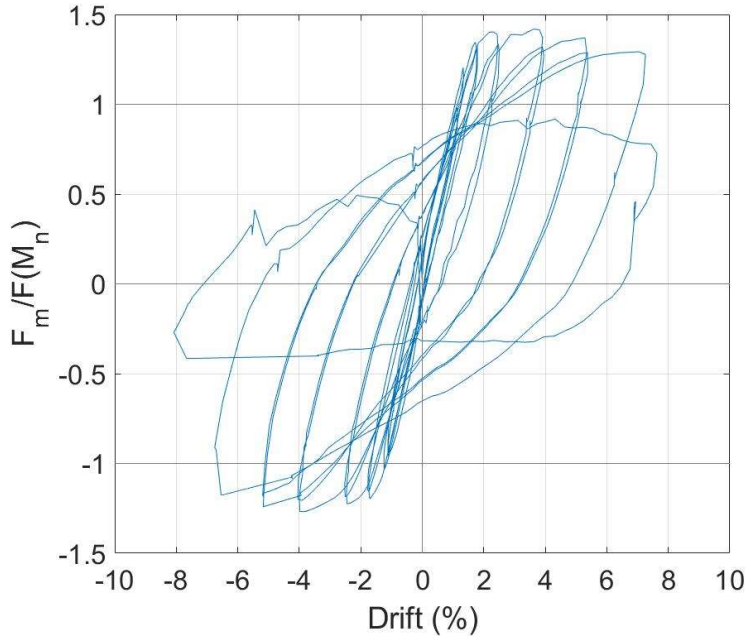

Figure 4.7. Specimen 30-21 Normalized by F_n Force-Drift Curve with P-Δ Effects Removed

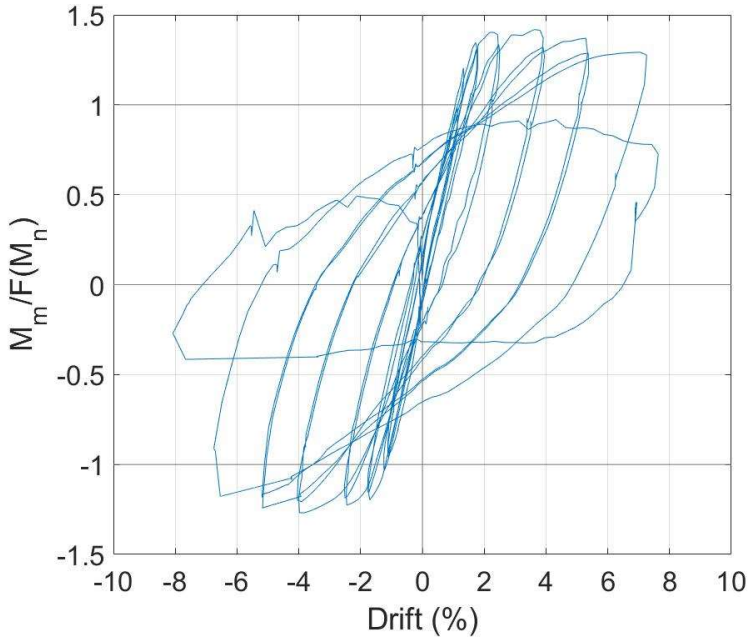

Figure 4.8. Specimen 30-21 Normalized by M_n Moment-Drift Curve with P-Δ Effects Removed

As shown in Table 4.1 and Figures 4.5 - 4.8, the largest moment, M_p, and corresponding drift reached by this specimen were 489.5 kip-ft or 1.42 M_n, at 3.7% drift. The nominal moment,

M_n, for Specimen 30-21 was 345.1 kip-ft. The strength degraded approximately 6% of M_p or 30 kip-ft with each of the following cycles at 5.0% and 7.3% drifts, and then substantially drops 40% of M_p or 190 kip-ft with the last cycle, which reached the largest drift of 7.5%. The behavior is similar on the negative drift side as well.

As mentioned previously, the dry run for this Specimen had a displacement of 1 in. instead of the planned 0.1 in. This caused the column and the column reinforcement to yield and to enter the inelastic region before originally planned. Due to this, displacements less than 1 in. were skipped for this specimen's displacement history. The results of the dry run were appended to the beginning of the test results.

Table 4.3 shows the width and location of the maximum and residual cracks measured for each drift level.

Table 4.3. Maximum Measured Crack Widths and Locations for Each Drift Level (30-21)

Drift Level	Maximum Crack		Residual Cracks	
	Width (mm)	Location	Width (mm)	Location
1.0%	0.5	Base of Column	0.1	11 in. above base
1.5%	1.0	Base of Column	0.3	5 in. above base
2.2%	2.0	Base of Column	0.9	5 in. above base
3.7%	3.0	Base of Column	1.0	11 in. above base
5.0%	3.0	Base of Column	2.0	5 in. above base
7.0+%	3.5	Base of Column	3.0	10 in. above base

4.3.1 *Low Drift Cycles (0-2.0% Drift)*

At approximately 1.1% drift, the lateral force ranged from -0.9 to 1.2 times the nominal force, $F_{n,}$ of 67.1 kips (-63.1 to 77.9 kips) as shown in Figure 4.9.

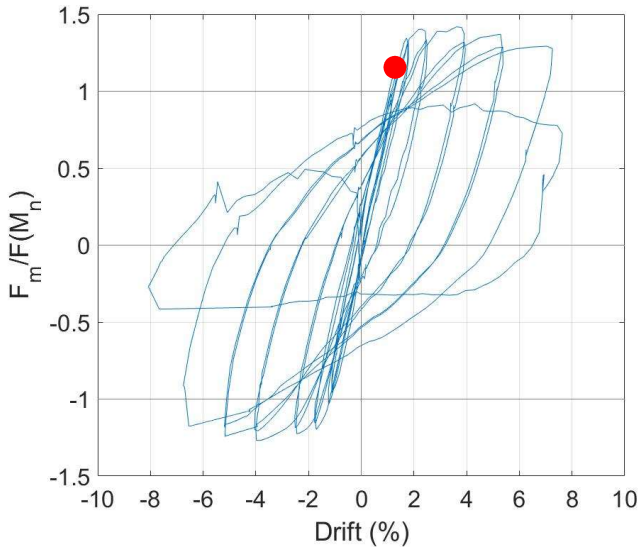

Figure 4.9. Specimen 30-21 Normalized Force-Drift Curve at 1.1% Drift

Small horizontal cracks, less than 0.5 mm in width, formed along the height of the column during this cycle, primarily on the northern and southern faces of the column, as shown in Figure 4.10.

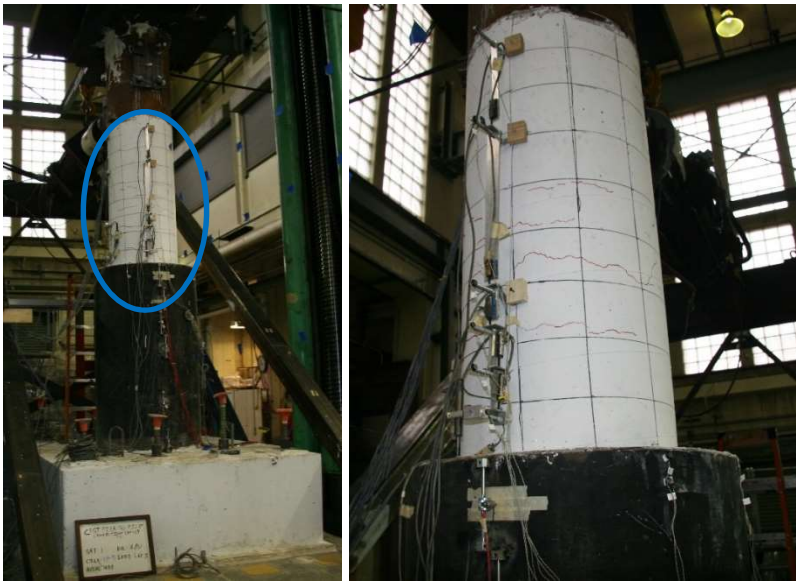

Figure 4.10. Specimen 30-21 Horizontal Cracks on North Column Face

During this cycle, the Northeast (NE), Southeast (SE), and Southern (S) longitudinal reinforcing bars in the column exceeded the reinforcement yield strain of 0.0024 in/in, from

$0.45D_{COL}$ to $-0.45D_{COL}$. Gauges below this range are in the elastic range. As shown in Figure 4.11, the reinforcement has yielded at multiple locations but had not yielded at $-0.75\ D_{COL}$.

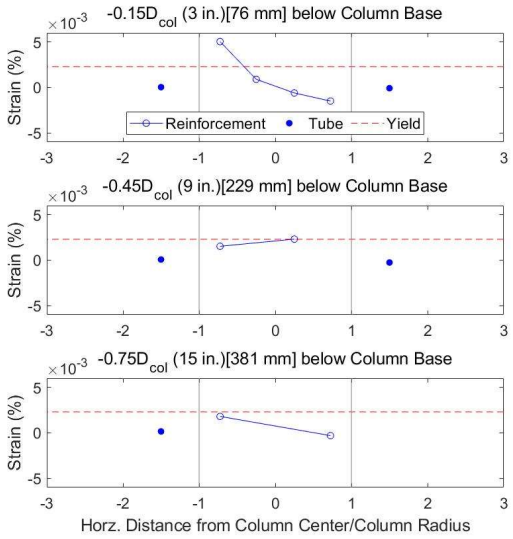

Figure 4.11. Specimen 30-21 Strain Distribution at 1.1% Drift

The next cycle was to 0.9% drift and was the first cycle during the actual testing and thus has a slightly smaller drift level than the previous cycle. At 0.9% drift, the lateral load had a range of -1.0 to $0.98F_n$ (-63.75 to 65.5 kips), which was a decrease of $0.1F_n$ from the previous cycle, shown in Figure 4.12.

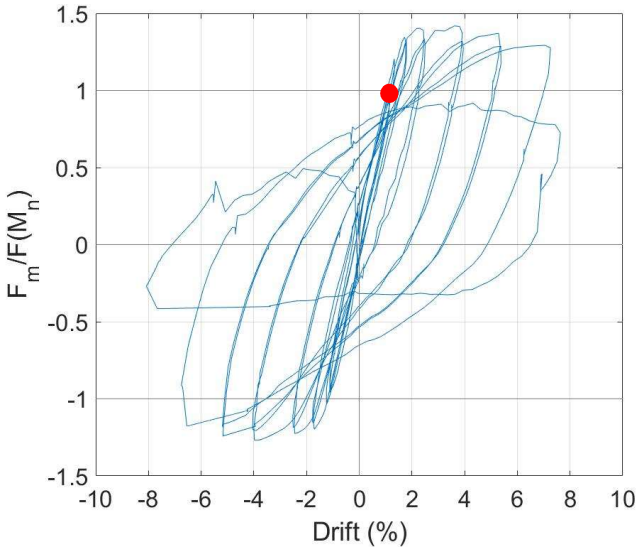

Figure 4.12. Specimen 30-21 Normalized Force-Drift Curve at 0.9% Drift

Horizontal cracks formed along the height of the column on both the north and south sides. The cracks, at the interface of the column and the top of the pile, ranged in width from 0.3mm to 0.5mm, shown in Figure 4.13.

Figure 4.13. Specimen 30-21 Interface Cracks on Southern Face at 0.9% Drift

The reinforcement at the peak of these cycles registered strains greater than yield in all the Northern (N), NE, and S bars, at locations -0.15D_{COL}, 0.30D_{COL}, and 0.45D_{COL} when the column was in tension. When the column was cycled in compression, no reinforcement strains measured were greater than the yield strain.

At 1.5% drift, the lateral load ranged from -1.1 to 1.21F_n (-77.1 to 81.1 kips), an increase of 0.2F_n from the previous cycle, shown in Figure 4.14.

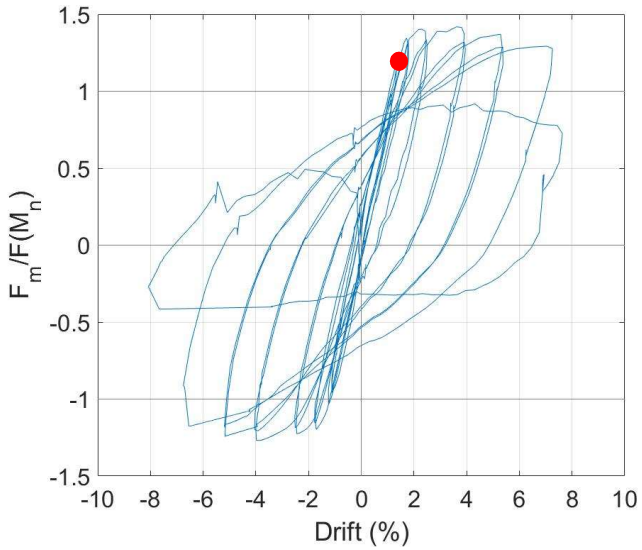

Figure 4.14. Specimen 30-21 Normalized Force-Drift Curve at 1.5% Drift

Radial cracks formed at three different locations on the top of the pile, going from the perimeter of the pile to the column, shown in Figure 4.15.

Figure 4.15. Specimen 30-21 Radial Cracks on North Face of Column

On the second cycle to 1.5% drift, diagonal cracks started to form $1.8D_{COL}$ (36 in.) above the base of the column, and the existing horizontal crack widths increased, with the largest width reaching 1 mm. During these cycles, when the column was in compression, all the strain gauge locations, except for $-0.75D_{COL}$ on the northern (N) bar reinforcement measured a strain greater

than yield, Figure 4.16. The same was true for the southern (S) bar reinforcement when the column was in tension.

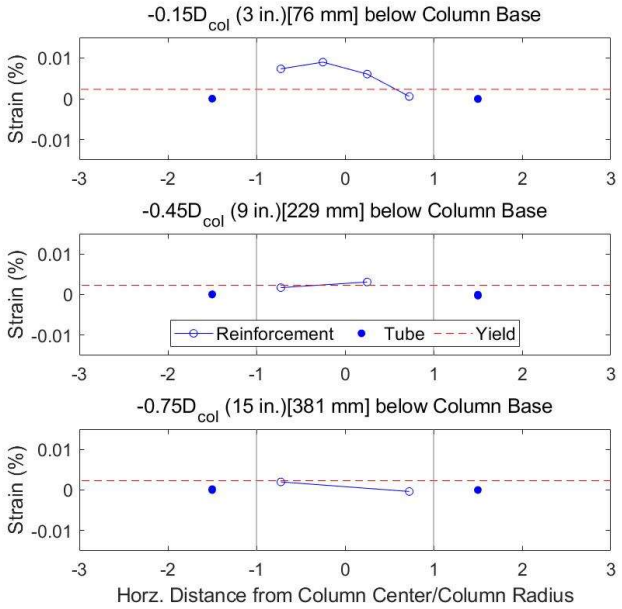

Figure 4.16. Specimen 30-21 Strain Distribution at 1.5% Drift

4.3.2 *Moderate Drift Cycles (2.0-4.0% Drift)*

At a drift of 2.2%, the lateral loads ranged from -1.2 to $1.3F_n$ (-78.1 to 89.2 kips), an increase of $0.1F_n$ from the previous cycle, shown in Figure 4.17.

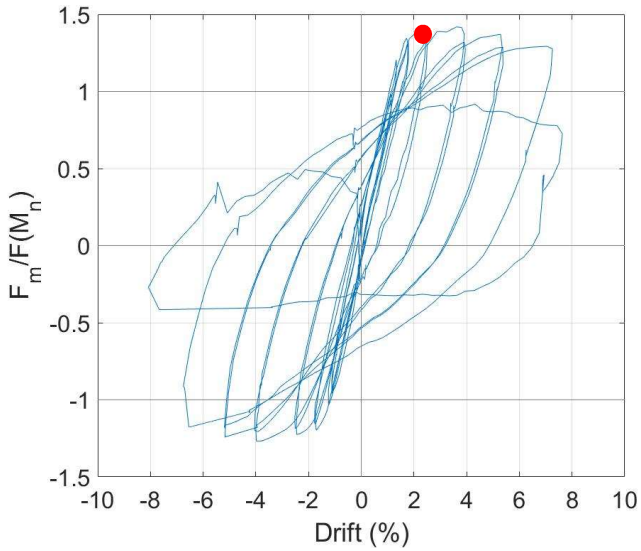

Figure 4.17. Specimen 30-21 Normalized Force-Drift Curve at 2.2% Drift

Spalling occurred at the bottom 2.5 in. of the column, but no reinforcing bars were exposed. The horizontal cracks increased to a maximum width of 2 mm, shown in Figure 4.18, with the largest cracks being at the interface of the column and the top of the pile, with the largest crack width being 1.75 mm.

Figure 4.18. Specimen 30-21 Initial Spalled Region on North Face at 2.2% Drift

At these peak drift levels, the reinforcement strain measured at the -0.75D_{COL} location stayed right at or below the yield strain. The rest of the measured strain locations (-0.30D_{COL}, -0.15 D_{COL}, 0.30D_{COL}, and 0.45D_{COL}) were well above the yield strain, reaching strains up to 0.016 in./in. when that side sustained tension, shown in Figure 4.19.

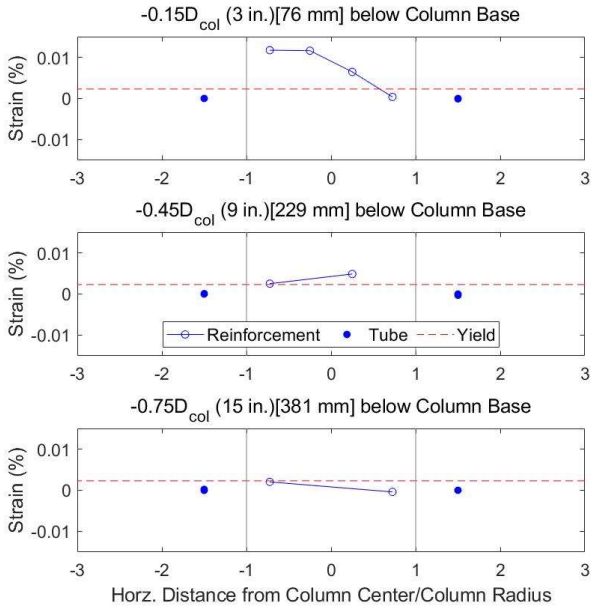

Figure 4.19. Specimen 30-21 Strain Distribution at 2.2% drift

At drift cycles of approximately 3.7%, the lateral loads ranged from -1.2 to 1.42F_n (-80.4 to 95.1 kips), approximately equal to the previous cycle, as shown in Figure 4.20. The 1.42F_n (95.1 kips) lateral load was the maximum lateral load the column experienced during this test. This occurred during the first cycle at this drift level.

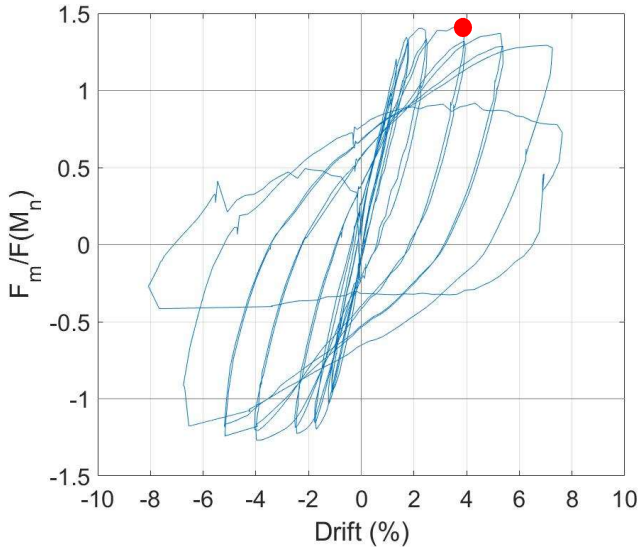

Figure 4.20. Specimen 30-21 Normalized Force-Drift Curve at 3.7% Drift

The crack widths at the column base continued to increase to a maximum width of 3 mm. The spalling increased to the point where transverse reinforcement, #3 hoops located approximately 3 in. from the base of the column, was exposed on the second cycle, shown in Figure 4.21.

Figure 4.21. Specimen 30-21 Spalled Region on Northern Column Face at 3.7% Drift

The stains measured at the peaks of this cycle all exceeded the yield strain, except for the S bar location at -0.75 D_{COL} as shown in Figure 4.22.

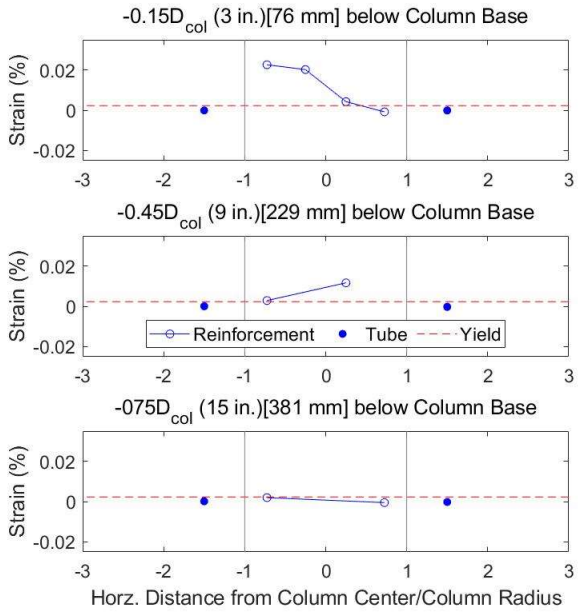

Figure 4.22. Specimen 30-21 Strain Distribution at 3.7% drift

4.3.3 *Large Drift Cycles (Greater than 4.0% Drift)*

At drift cycles of 5%, the lateral loads ranged from -1.2 to 1.37F_n (-83.3 to 91.9 kips), a decrease of approximately 0.05F_n from the previous cycle, which is shown in Figure 4.23.

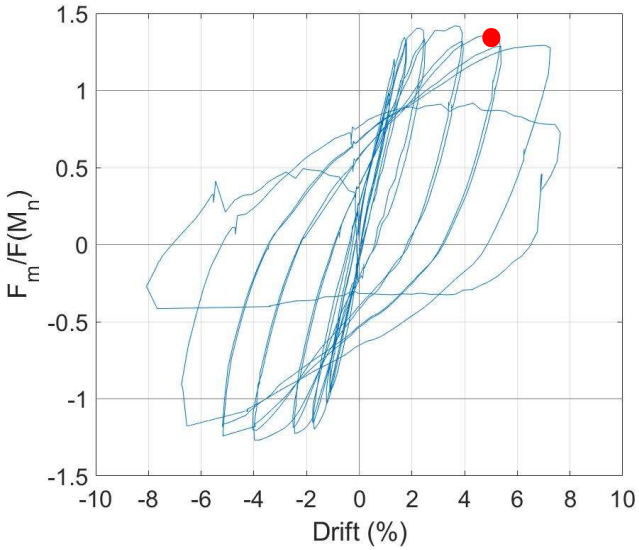

Figure 4.23. Specimen 30-21 Normalized Force-Drift Curve at 5.0% Drift

The spalled region increased to 0.50D_{COL} (10 in.) above the base of the column and multiple transverse reinforcement bars and the first longitudinal reinforcement were exposed on the northern face of the column, shown in Figure 4.24. There was a 3 mm wide crack at the interface of the column and the top of the pile.

Figure 4.24. Specimen 30-21 Exposed Longitudinal Reinforcement on South Face

As with the previous cycles at 3.7% drift, all the reinforcement strains measured were above the yield strain except for the S bar's -0.75D_{COL} location, which is shown in Figure 4.25.

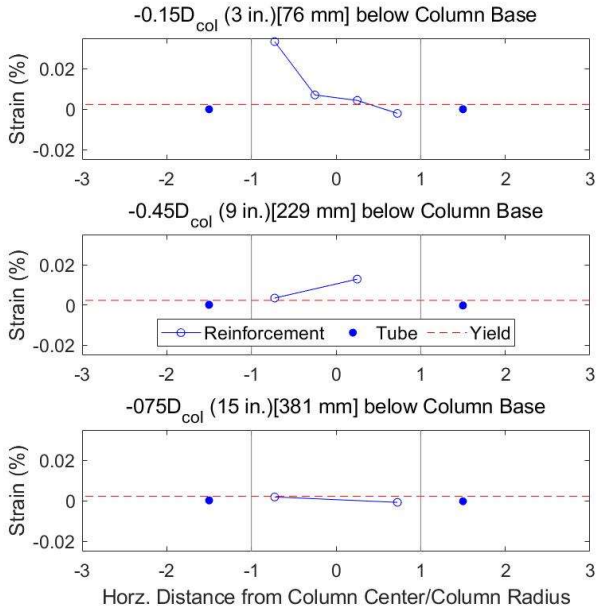

Figure 4.25. Specimen 30-21 Strain Distribution at 5% Drift

For this cycle at 5% drift and the remaining cycles that had equal or larger drifts, the axial binding issue of the bearing mentioned in Chapter 3 occurred. This was seen when plotting the original hysteretic force-displacement curve of the test. There were spikes in the measured lateral resistance due to this binding of the axial bearing assembly for the negative drift. These spikes in lateral force were removed from the data and estimated lateral resistances replaced these values. The lateral resistance estimates were based on how much the lateral resistance degraded during the positive drift at the same cycle. Figures 4.26-4.27 are a comparison of the moment-drift hysteresis curves before and after the lateral resistance corrections.

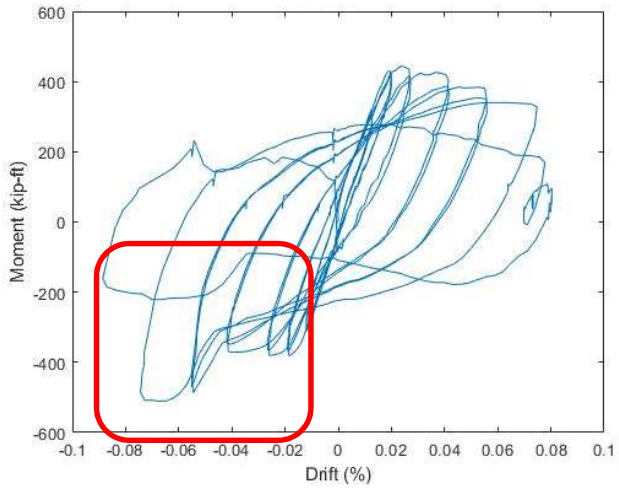

Figure 4.26. Specimen 30-21 Original Moment-Drift Curve

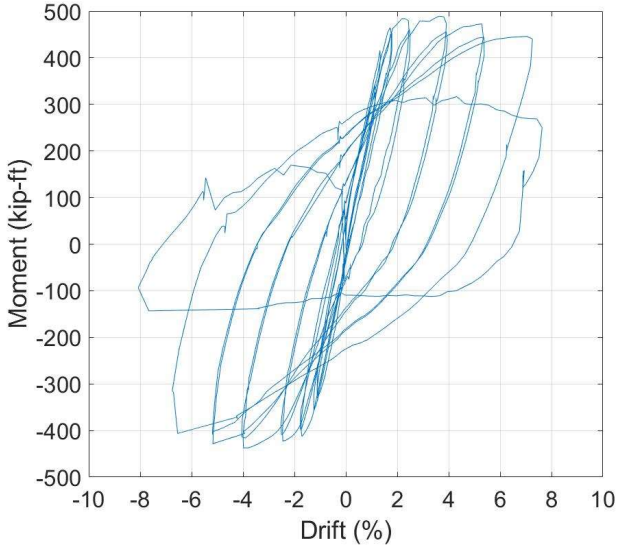

Figure 4.27. Specimen 30-21 Corrected Moment-Drift Curve

At 7.3% drift, the lateral loads ranged from -1.2 to $1.3F_n$ (-77.7 to 85.6 kips), a decrease of $0.1F_n$ from the previous cycle, shown in Figure 4.28.

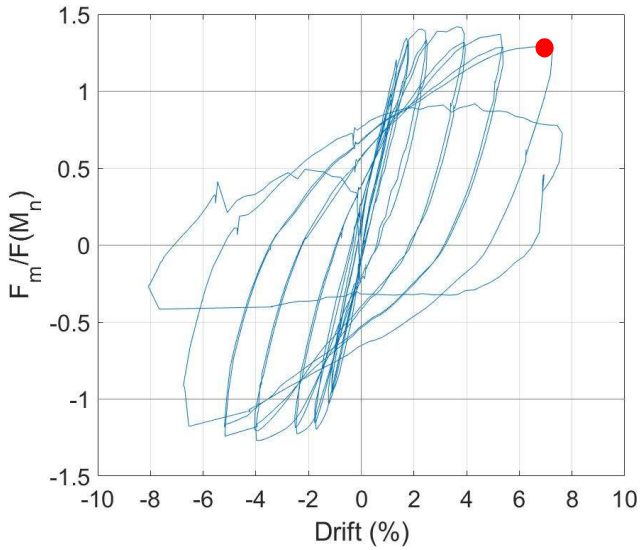

Figure 4.28. Specimen 30-21 Normalized Force-Drift Curve at 7.3 % Drift

The spalled region reached 0.875 D_{COL} (17.5 in.) on both the North and South sides. There was a 3+ mm wide crack at the base of the column. This crack was due to pullout failure of the reinforcing bars. This extensive spalled region and interface cracks are shown in Figure 4.29.

a) **b)**

Figure 4.29. Specimen 30-21 a) Major Spalled Region on Southern Column Face, b) Large Crack at Northern Column Interface at 7.3 % Drift

Loading was terminated after the second cycle at 8% drift when the longitudinal reinforcement bars had buckled when the column was both in tension and compression. The lateral load during this cycle reached a peak of $0.72F_n$ (48.6 kips), a $0.7F_n$ reduction in resistance from

the peak force. During this second cycle, the transverse reinforcement and concrete seemed to explode or pop out. Two of the transverse reinforcement hoops, at 4 in and 7 in from the base of the column, their ends, which had 90-degree hooks, opened. This happened as the column was cycled in both tension and compression. After the second cycle, the concrete at the base of the column had completely crushed, and there was no continuous concrete going from the base of the column above $0.15D_{COL}$ (3 in.) to the rest of the column. The final state of the column is shown in Figure 4.30.

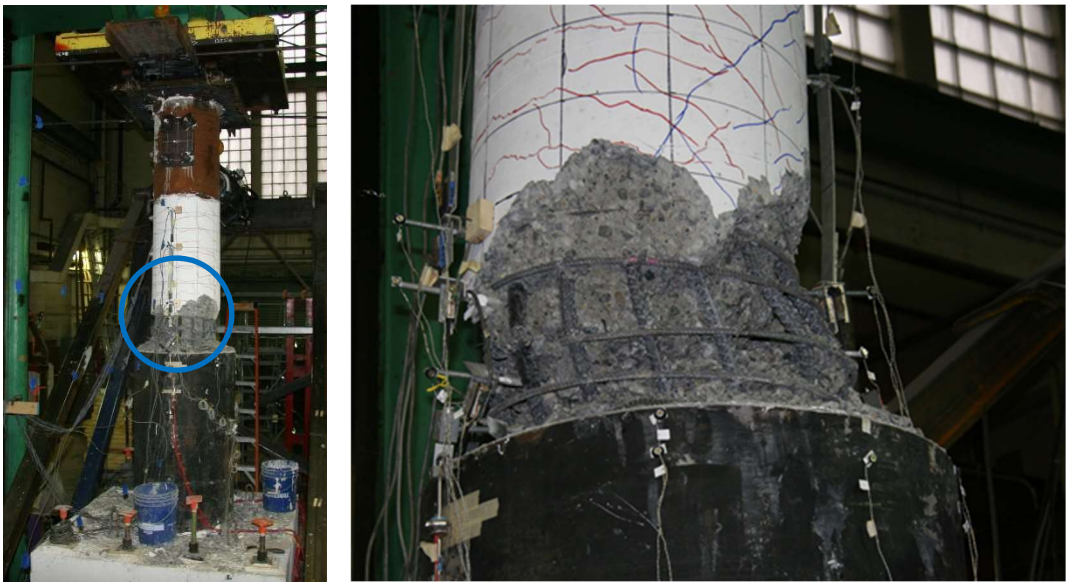

Figure 4.30. Specimen 30-21: Failed Specimen 30-21 at 8% Drift

Throughout all load cycles, the pile and transfer block showed no visible damage. There was no buckling or yielding of the pile. The largest measured tube strain was 0.0006 in/in, which occurred at 52 in. below the top of the tube, during the 3.7% drift cycles. There was no noticeable slip between the pile concrete in comparison to the edge of the steel tube at any point of the test. No cracks formed anywhere on the transfer block. After the test was finished, the column was removed from the top of the pile. As shown in Figure 4.31, except for the radial cracks and minor concrete damage around the base of the column, the top of the pile concrete appears to be largely undamaged.

Figure 4.31. Top of Specimen 30-21 Pile with Column Removed

4.4 SPECIMEN 48-21

Specimen 48-21 was tested on March 11th, 2021 in the Structural Research laboratory at the University of Washington. The test was performed 39 days after casting the transfer block, 32 days after casting the pile, and 10 days after casting the column. The column concrete had met the required design strength and was ready to be tested.

As stated before, Specimen 48-21 was identical to Specimen 30-21, except for the tube diameter, which was 48 in. instead of 30 in. An elastic cycle at 0.1 in. displacement was run on this specimen, as the dry run for the test. The maximum measured resistances and corresponding imposed drifts of each cycle are provided in Table 4.4. The force-displacement and moment-drift hysteresis curves of the column are shown in Figures 4.32 – 4.35. The constant axial load applied to this specimen was 7.5% of the axial capacity of the column, 120 kips.

Table 4.4. Maximum Resistances and Drifts in Each Cycle (48-21)

Target Drift	Cycle	Maximum Measured Resistance (kips)		Maximum Imposed Drift (%)	
		Tension	Compression	Tension	Compression
0.40%	1	32.6	30.8	0.20	0.12
	2	31.5	29.1	0.20	0.19
0.81%	3	54.0	49.9	0.49	0.48
	4	52.7	46.7	0.50	0.49
1.21%	5	67.4	62.6	0.75	0.76
	6	62.7	62.0	0.76	0.75
1.62%	7	74.0	73.7	1.11	1.10
	8	68.3	65.5	1.14	1.15
2.42%	9	81.9	80.5	1.82	1.82
	10	81.1	77.1	1.84	1.84
3.24%	11	82.2	83.8	2.62	2.57
	12	82.5	78.1	2.64	2.62
4.86%	13	84.8	8.6	4.22	4.10
	14	NA	79.1	NA	4.11
6.48%	15	84.7	84.8	5.91	5.65
	16	78.9	72.6	5.95	5.69
9.72%	17	37.1	37.1	9.52	8.53
	18	12.7	32.8	9.66	8.98

Due to operating error, the tension peak for cycle 14 was missed. When finishing the compression peak hold, the “Return to Zero” displacement button was accidentally hit which caused the cycle to end and the tension peak to be skipped.

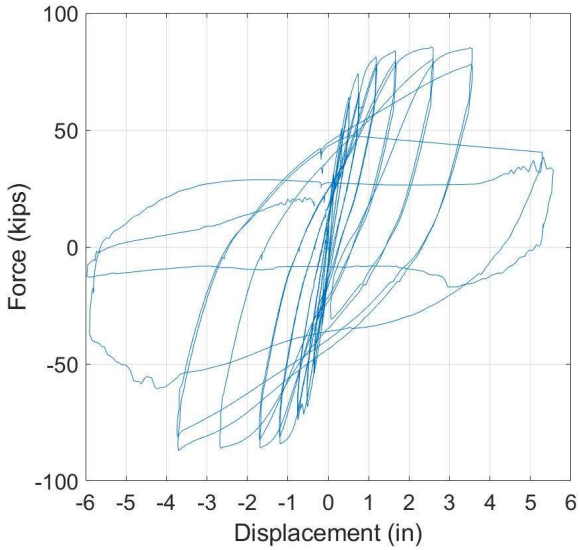

Figure 4.32. Specimen 48-21 Force-Displacement Curve

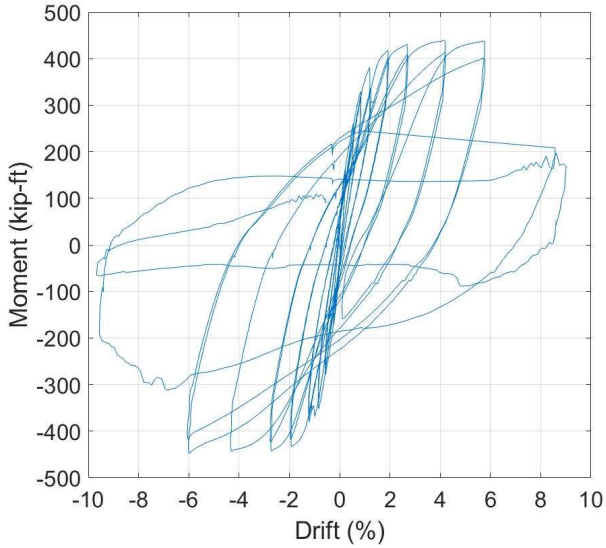

Figure 4.33. Specimen 48-21 Moment-Drift Curve with P-Δ Effects Removed

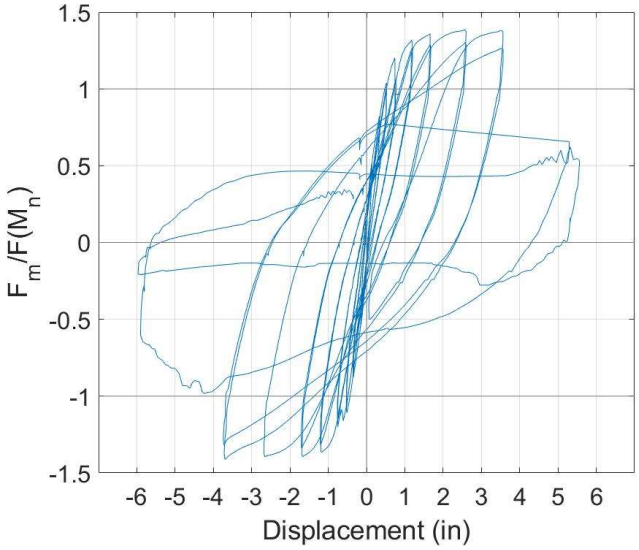

Figure 4.34. Specimen 48-21 Force-Displacement Curve with P-Δ Effects Removed Normalized by F_n

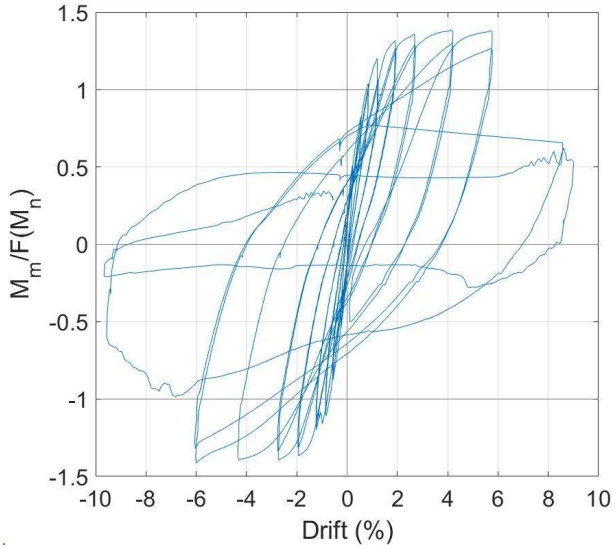

Figure 4.35. Specimen 48-21 Moment-Drift Curve with P-Δ Effects Removed Normalized by M_n

As shown in Table 4.4 and Figures 4.32-4.35, the largest moment, M_p, and corresponding drift reached by this specimen were 436.5 kip-ft or 1.38 M_n, at 5.5% drift. The nominal moment, M_n, was 317.3 kip-ft for Specimen 48-21. The lateral strength increased approximately 2% of M_p, or 10 kip-ft for each of the previous cycles at 2.6% and 4.1% drifts, and then substantially drops 46% of M_p or 200 kip-ft with the last two cycles, which reached the largest drift of 9.7%. The behavior is similar on the negative drift side as well. The largest moment, 436.5 kip-ft, does line up with the largest lateral resistance, 84.8 kips, when accounting for P-Δ delta effects.

Table 4.5 shows the width and location of the maximum and residual cracks measured for each drift level.

Table 4.5. Maximum Measured Crack Widths and Locations for Each Drift Level (48-21)

Drift Level	Maximum Crack		Residual Cracks	
	Width (mm)	Location	Width (mm)	Location
0.2%	0.2	9 in. above base	NA	NA
0.5%	0.5	Base of Column	0.1	Base of Column
0.8%	0.8	Radial top of Pile	<0.1	Base of Column
1.1%	1.5	Base of Column	0.1	Base of Column
1.8%	2.5	Base of Column	0.6	Base of Column
2.6%	3.5	Base of Column	0.5	Base of Column
4.2%	4.0	Base of Column	2.0	7 in. above base
6.0%	3.5	9 in. above base	Spall	Base of Column
9.0+%	Spall	Base of Column	Spall	Base of Column

4.4.1 *Low Drift Cycles (0-2.0% Drift)*

For drift cycles of approximately 0.2% and 0.5%, the lateral loads ranged from -0.5 to 0.5 times the nominal force, F_n, of 61.7 kips (-32.6 to 30.8) kips and -0.9 to 0.8F_n (-54.0 to 49.9 kips), respectively, as shown in Figure 4.36.

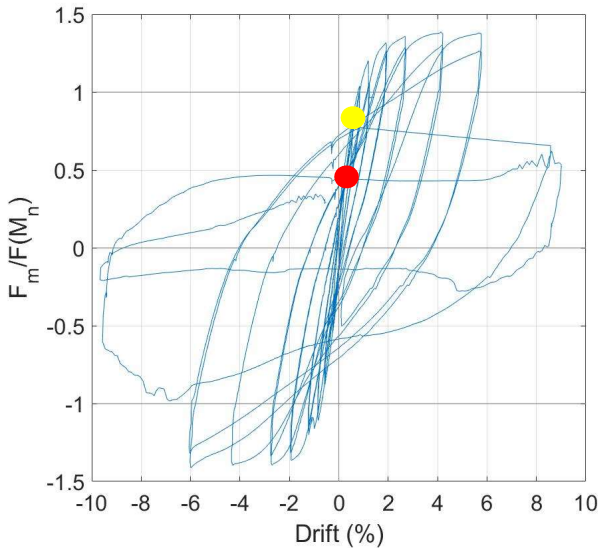

Figure 4.36. Specimen 48-21 Normalized Force-Drift Curve at 0.2% (Red) and 0.5% (Yellow) Drift

Small horizontal cracks formed 21 in. up the height of the column on both the northern and southern faces of the column, shown in Figure 4.37. The largest crack had a width of 0.5 mm wide. No residual cracks were measured at zero force.

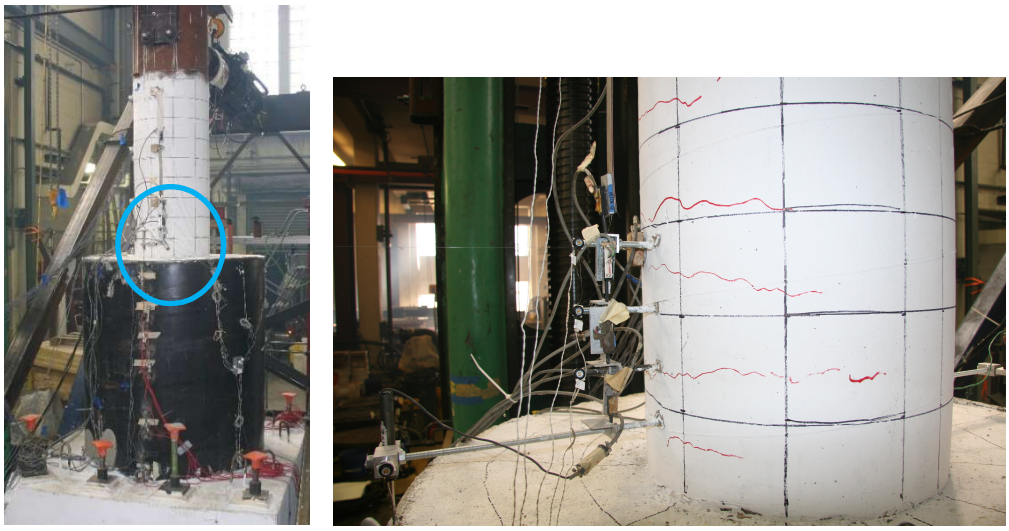

Figure 4.37. Specimen 48-21 Horizontal Cracks on North Column Face at 0.2% Drift

None of the longitudinal reinforcement strain measurements during the peak displacement exceeded the yield strain.

At 0.8% drift, the lateral load ranged from -1.1 to 1.0F_n (-67.4 to 62.6 kips), an increase of 0.2F_n from the previous cycle, shown in Figure 4.38.

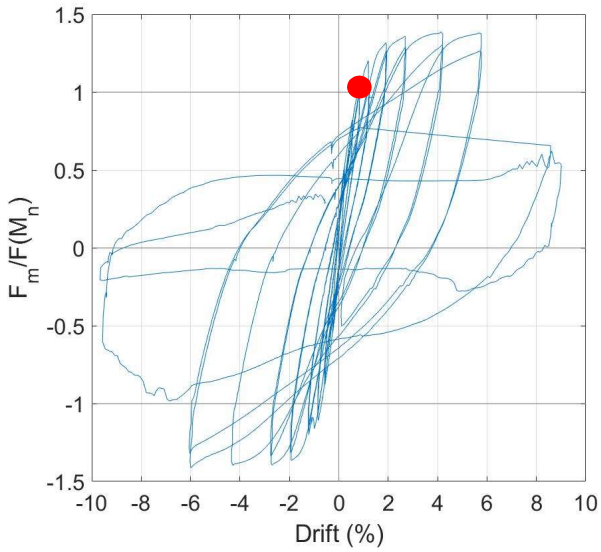

Figure 4.38. Specimen 48-21 Normalized Force-Drift Curve at 0.8% Drift

The already formed horizontal cracks continued to propagate circumferentially. The maximum width measured was 0.7 mm. New horizontal cracks formed 40 in. above the column base. Radial cracks were also measured at this displacement on the top of the pile shown in Figure 4.39. The radial cracks had a maximum width of 0.8 mm. From this point on additional radial cracks did not form and the already formed radial cracks did not expand in width.

Figure 4.39. Specimen 48-21 Radial Cracks on Top of Pile Concrete at 0.8% Drift

The column reinforcement strain exceeded the reinforcement yield strain of 0.0024 in/in at the peak displacement of this cycle. The largest strain was measured on the extreme Southern (S) bar of the column at $-0.15D_{COL}$, shown in Figure 4.40.

The strain distribution plots for Specimen 48-21 have a similar format to Specimen 30-21. However, the S bar strain gauges at the $0.3D_{COL}$ and $-0.45D_{COL}$ locations were broken before testing and no readings were able to be used from them, thus there are only 3 dots for the plot at $0.3D_{COL}$ and 1 dot for the $-0.45D_{COL}$ locations plot.

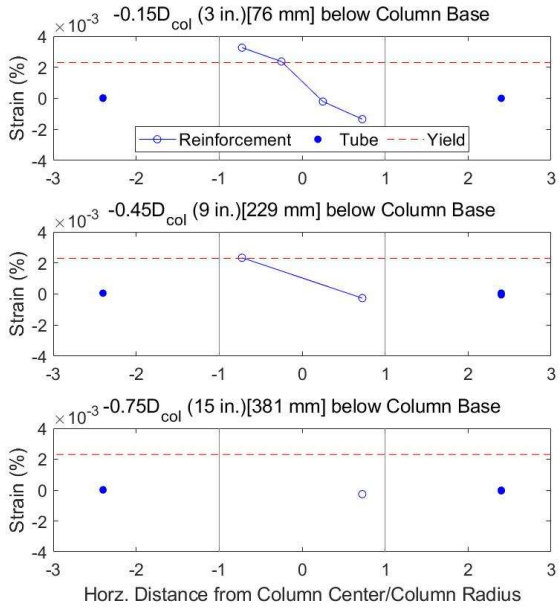

Figure 4.40. Specimen 48-21 Strain Distribution at 0.8% Drift

At drift cycles of 1.1%, the lateral load ranged from -1.2 to 1.2F_n (-74.0 to 73.7 kips), an increase of 0.15F_n as shown in Figure 4.41.

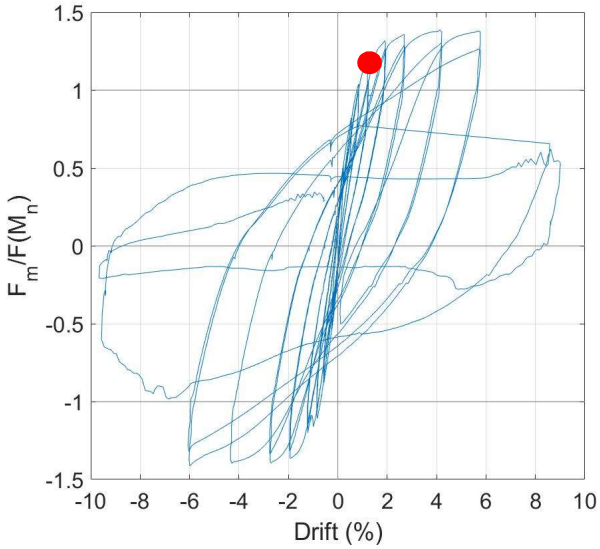

Figure 4.41. Specimen 48-21 Normalized Force-Drift Curve at 1.1% Drift

The horizontal cracks continued to widen to a maximum width of 1.5 mm, as well as audible cracking was heard. During zero force, small residual cracks were noted, having a maximum width less than 0.1 mm, shown in Figure 4.42.

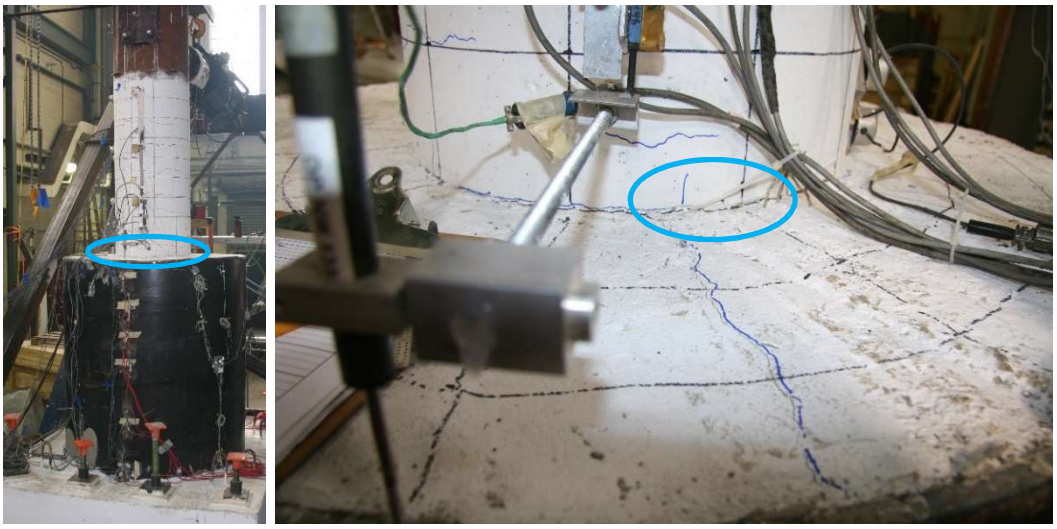

Figure 4.42. Specimen 48-21 Vertical Residual Force Crack at 1.1% Drift

The strains measured during the peak displacement of these cycles exceeded the yield strain at locations $0.3D_{COL}$, $-0.15\ D_{COL}$, $-0.3D_{COL}$, and $-0.45D_{COL}$ on both the N and S bars. The strain gauge located at $-0.75D_{COL}$ did not reach the yield shown in Figure 4.43.

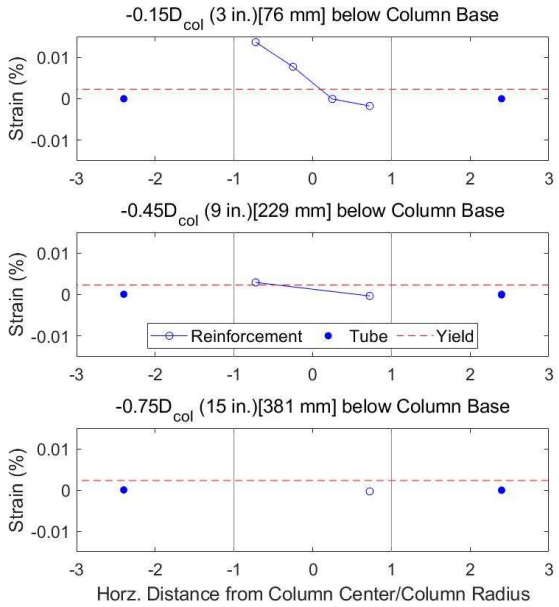

Figure 4.43. Specimen 48-21 Strain Distribution at 1.1% Drift

At drift displacements of 1.8%, the lateral load ranged from -1.3 to $1.3F_n$ (-81.9 to 80.5 kips), an increase of $0.1F_n$ shown in Figure 4.44.

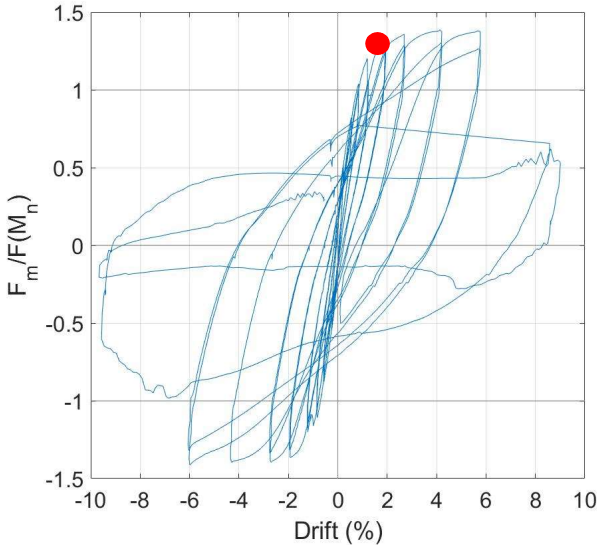

Figure 4.44. Specimen 48-21 Normalized Force-Drift Curve at 1.8% Drift

The already formed horizontal cracks expanded, with the maximum horizontal crack width measured at 2.5 mm. This crack was at the base of the southern face of the column shown in Figure 4.45.

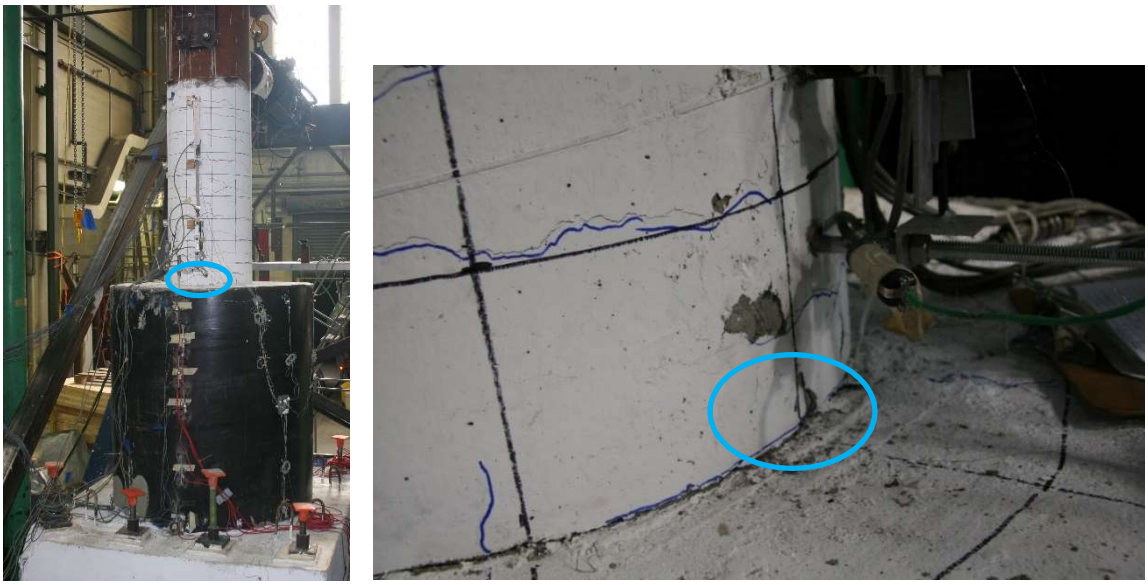

Figure 4.45. Specimen 48-21 Column Interface crack at 1.8% Drift

The strains measured at the peak displacement of these cycles all exceeded the yield of the reinforcement, with the largest strain, 0.015 in/in, occurring at $-0.15D_{COL}$ on the S bar, shown in Figure 4.46. The $-0.75D_{COL}$ location did not reach the yield strain.

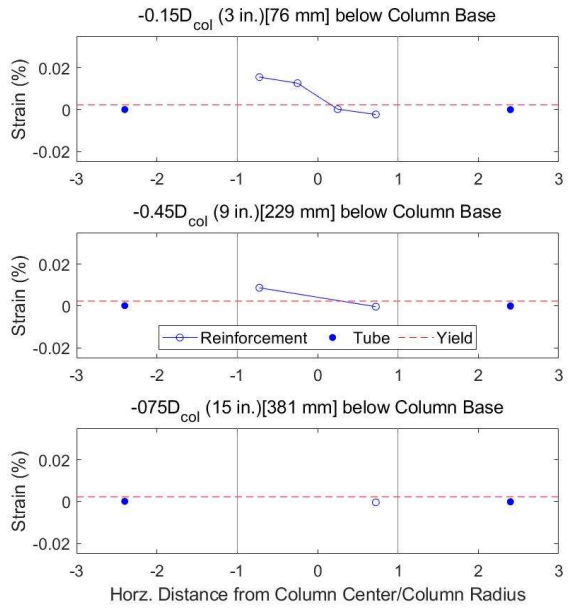

Figure 4.46. Specimen 48-21 Strain Distribution at 1.8% Drift

4.4.2 *Moderate Drift Cycles (2.0-4.0% Drift)*

On the following cycle, at 2.6% drift, the lateral loads ranged from -1.3 to $1.3F_n$ (-82.5 to 83.8 kips), approximately equivalent to the previous cycle as shown in Figure 4.47.

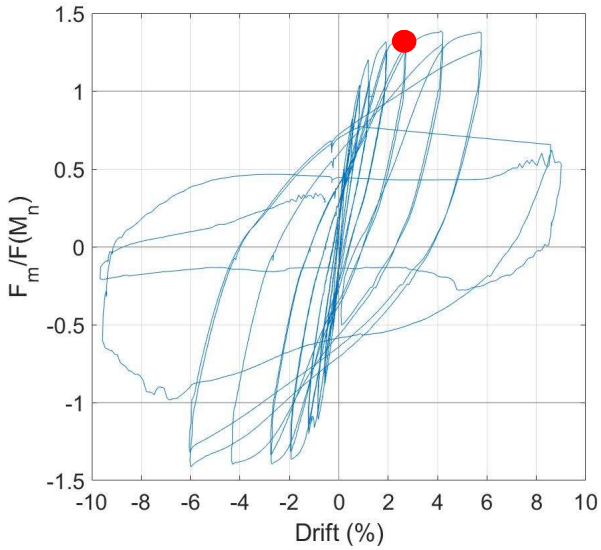

Figure 4.47. Specimen 48-21 Normalized Force-Drift Curve at 2.6% Drift

The horizontal cracks continued to expand, with the widest crack occurring at the base of the southern side of the column with a width of 3.5 mm. During zero force, a 1 in. section of

concrete spalled off on the northwestern face of the column. New residual cracks formed on the northern face, while the cracks on the southern face closed up. There was an increase in the spalling on both the northern and southern sides of the column continued to expand as shown in Figure 4.48.

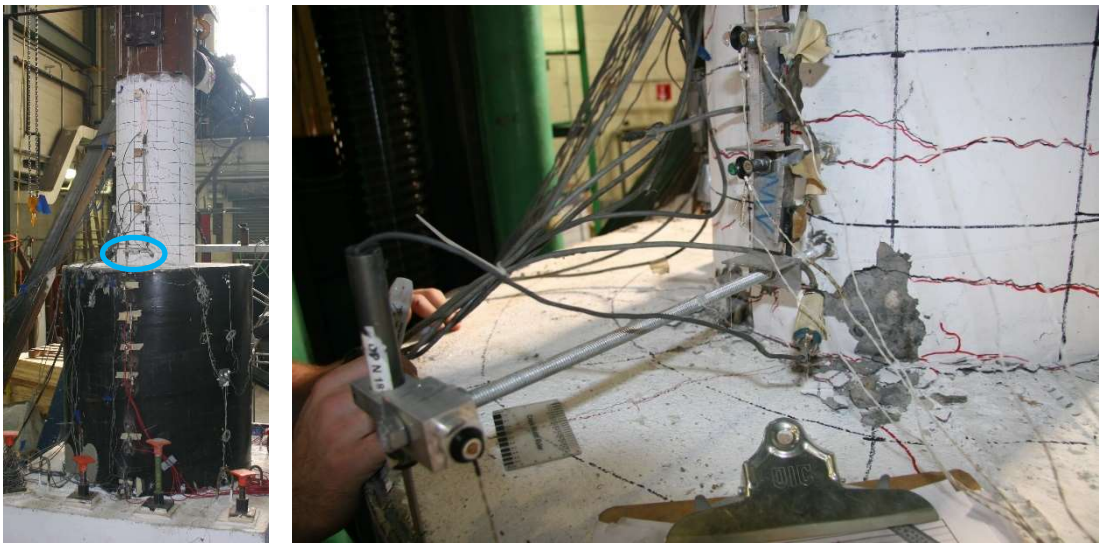

Figure 4.48. Specimen 48-21 Spalled Region at Base of North Face of Column at 2.6% Drift

The strains measured at the peak displacement of these cycles all exceeded the yield of the reinforcement, reaching a maximum strain of 0.022 in/in on the -0.15D_{COL} location on the S bar location. The -0.75D_{COL} location on the N bar did not reach the yield strain, as shown in Figure 4.49.

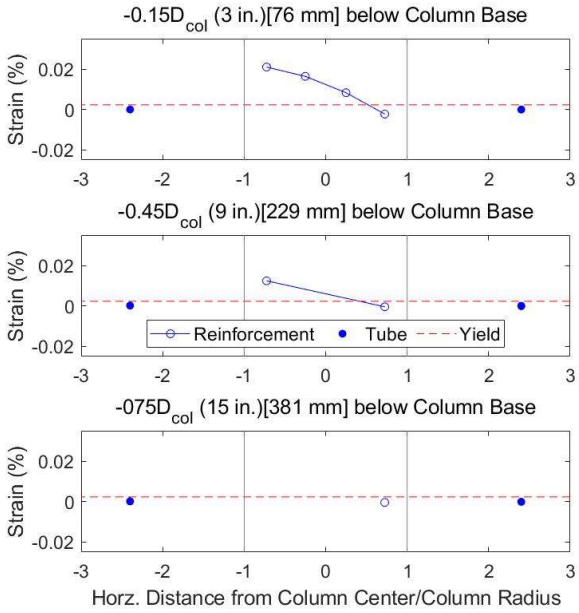

Figure 4.49. Specimen 48-21 Strain Distribution at 2.6% Drift

4.4.3 *Large Drift Cycles (Greater than 4.0% Drift)*

At drift cycles of 4.1%, the lateral load ranged from -1.4 to 1.4F_n (-84.8 to 84.6 kips), approximately equivalent to the last cycle as shown in Figure 4.50.

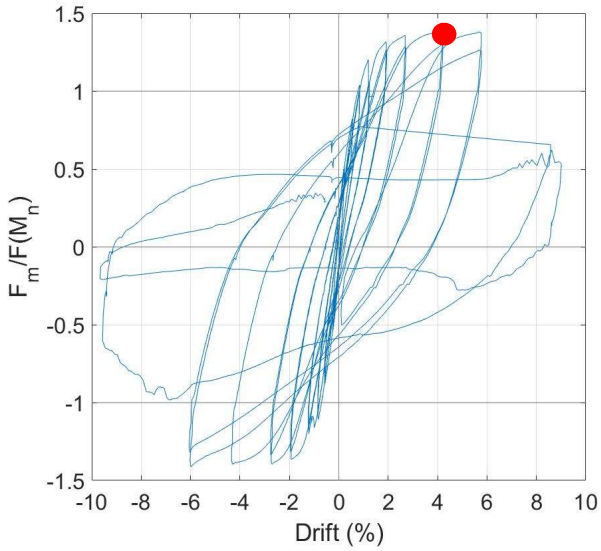

Figure 4.50. Specimen 48-21 Normalized Force-Drift Curve at 4.1% Drift

The spalling at the northern base of the column increased to the point where the column reinforcement, both transverse and longitudinal, was exposed as shown in Figure 4.51. The crack between the base of the column and the top of the pile continued to expand to a maximum width of 4 mm. During zero force, no new residual cracks formed or spall developed, unlike the previous cycle.

Figure 4.51. Specimen 48-21 Exposed Transverse and Longitudinal Reinforcement at 4.1% Drift

The strains measured at the peak displacement of these cycles all exceeded the yield of the reinforcement, reaching a maximum strain of 0.036 in/in at $-0.15D_{COL}$ on the S bar, shown in Figure 4.52. The $-0.75D_{COL}$ location did not reach the yield strain, with a max strain of .0020 in/in.

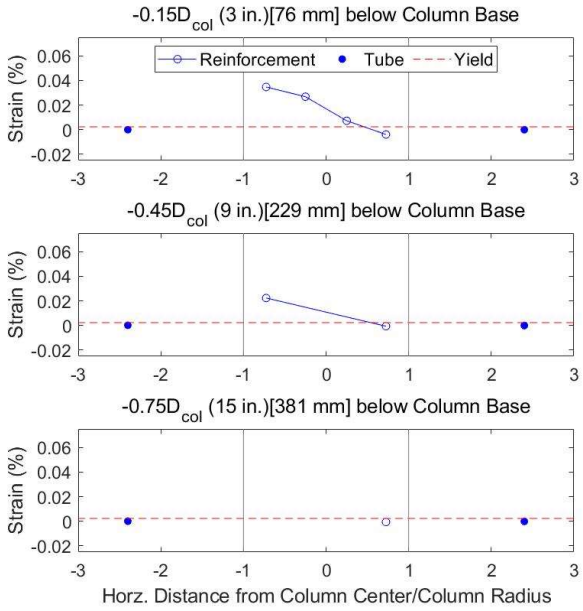

Figure 4.52. Specimen 48-21 Strain Distribution at 4.1% Drift

At drift cycles of 5.8%, the lateral load ranged from -1.4 to 1.4F_n (-84.7 to 84.8 kips), approximately equivalent to the last cycle as shown in Figure 4.53. The lateral load of 1.4F_n (84.8 kips) was the largest lateral load the column experienced during this test. During this cycle, the column experienced its largest moment, 1.4M_n or 436.5 kip-ft.

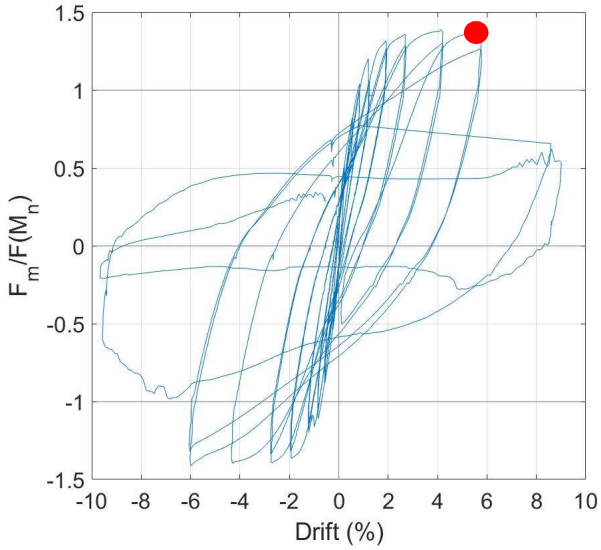

Figure 4.53. Specimen 48-21 Normalized Force-Drift Curve at 5.8% Drift

The concrete on the inside of the column transverse reinforcement spalled, which completely exposed the transverse reinforcement. Spalling on the north face increased to a point where longitudinal reinforcement bars, the two bars on the northern face, were exposed. The largest measured crack was again at the base of the column on the southern face and had increased in width to 5 mm. During the second cycle, the Northern column longitudinal reinforcement bar buckled approximately 5 in. from the base of the column as shown in Figure 4.54. While the picture makes it seem like the bar is not buckling, slight buckling was observed as the column was being pushed to the left in the photo, but the bar was still bent to the right.

Figure 4.54. Specimen 48-21 Buckled Longitudinal Reinforcement at 5.8% Drift

At 8.6% drift, the largest lateral load was $0.6F_n$ (37.1 kips) a decrease of $0.8F_n$ (48 kips) from the previous cycle, which was also the peak force, shown in Figure 4.55.

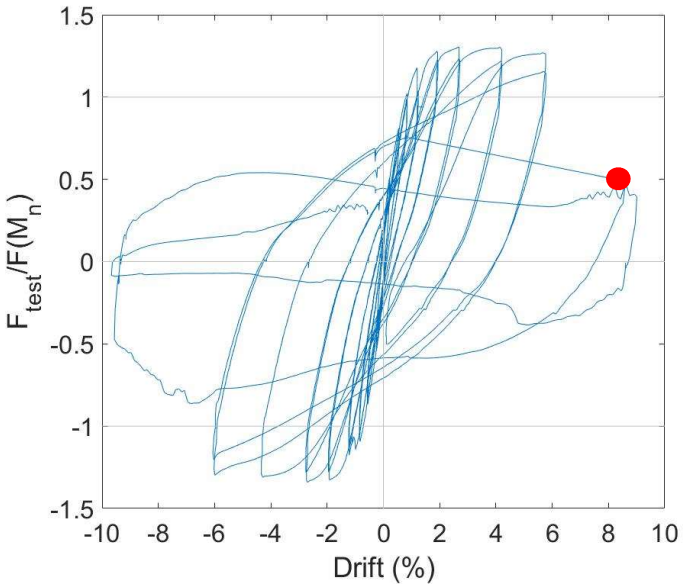

Figure 4.55. Specimen 48-21 Normalized Force-Drift Curve at 8.6% Drift

There was significant concrete crushing and the longitudinal bars buckled in both compression and tension, this is shown in Figure 4.56. The spalling was so widespread that horizontal cracks could not be measured.

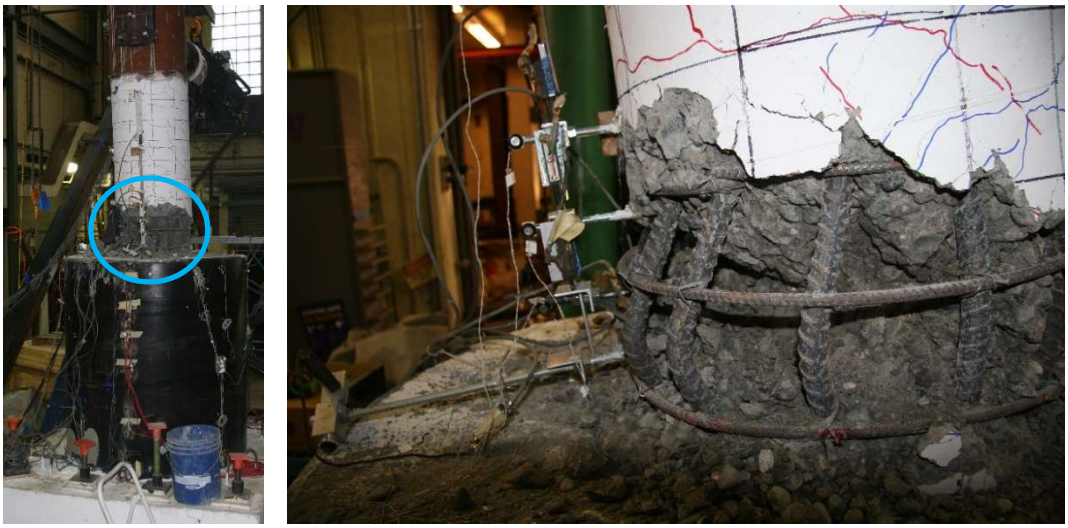

Figure 4.56. Specimen 48-21 North Face Severely Buckled Longitudinal Reinforcement Bars at 8.6% Drift

Loading was terminated after 9.7% drift, with all bars buckled and the concrete at the base of the column had completely crushed. The bottom $0.15D_{COL}$ (3 in.) of the column concrete separated from the rest of the pile. This cycle had a peak lateral load of $0.5F_n$ (32.8 kips) in

compression and $0.2F_n$ (12.7 kips) in tension, resulting in a force loss of 41 kips from the previous cycles at 6% drift or 70% loss in strength from the peak lateral load of 84.8 kips. Similar to Specimen 30-21, during both of these final two cycles, the concrete at the base of the column seemed to explode out, as did the transverse reinforcement at the base too. The final state of the specimen can be shown in Figure 4.57.

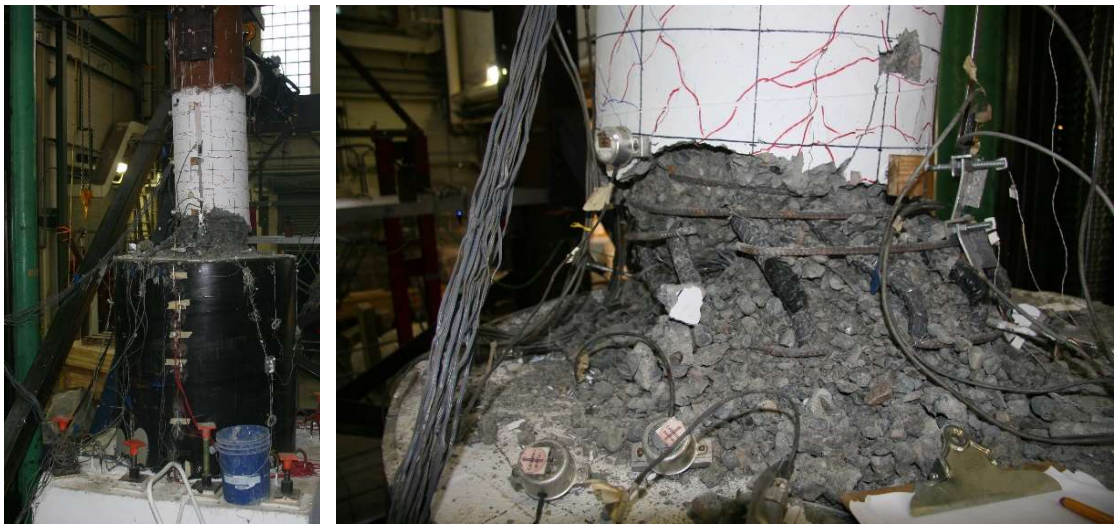

Figure 4.57. Final State of Specimen 48-21 after 9.7% drift

Throughout all load cycles, the pile and transfer block showed no visible damage. There was no buckling or yielding of the pile, with the largest measured strain being 0.00017 in/in, which occurred at 52 in. below the top of the tube, during the 4.1% drift cycles. No cracks formed anywhere on the transfer block. A 3 in. section of the transfer block did break off when moving the specimen onto the testing rig and was not related to the actual testing of the specimen. There was no noticeable slip between the pile concrete in comparison to the edge of the tube at any point of the test. As shown in Figure 4.58, except for the radial cracks, the top of the pile concrete appears largely undamaged.

Figure 4.58. Top of Specimen 48-21 Pile with Column Removed

Due to using the new axial bearing rig described in Chapter 3, there was no significant binding at the top of the column. The top of the column did shift to the East during the test due to the base of the column deforming, but any touching of the top of the column CFST and the guiding channel did not have noticeable effects during the test.

4.5 SPECIMEN 30-21-R

Specimen 30-21-R was tested on July 1st, 2021 in the Structural Research laboratory at the University of Washington. The test was performed 53 days after casting the transfer block and the pile, and 28 days after casting the column.

Specimen 30-21-R was identical with Specimen 30-21, except the tube now had a 2 in. wide steel rib welded inside 2 in. from the top of the tube.

Elastic cycles were run on this specimen, as the dry run for the specimen had a displacement of 0.1 in. The maximum measured resistances and corresponding imposed drifts of each cycle are found in Table 4.6. The normalized force-displacement and moment-drift hysteresis curves of the column and normalized versions are shown in Figures 4.59-4.62. The constant axial load applied to this specimen was 7.5% of the axial capacity of the column, 120 kips.

Table 4.6. Maximum Resistances and Drifts in Each Cycle (30-21-R)

Target Drift	Cycle	Maximum Measured Resistance (kips)		Maximum Imposed Drift (%)	
		Tension	Compression	Tension	Compression
0.40%	1	26.2	23.0	-0.20	0.15
	2	26.3	26.9	-0.20	0.19
0.81%	3	39.0	40.6	-0.45	0.47
	4	39.4	41.4	-0.45	0.46
1.21%	5	52.0	50.6	-0.76	0.73
	6	54.4	57.1	-0.78	0.77
1.62%	7	67.8	69.6	-1.05	1.05
	8	64.1	67.7	-1.08	1.06
2.42%	9	79.8	81.0	-1.74	1.69
	10	78.0	80.1	-1.78	1.69
3.24%	11	83.3	87.4	-2.51	2.35
	12	81.4	73.3	-2.53	2.40
4.86%	13	88.7	88.2	-4.06	3.93
	14	78.6	82.3	-4.10	3.97
6.48%	15	89.4	83.9	-5.66	5.44
	16	81.1	80.9	-5.72	5.49
9.72%	17	85.0	81.8	-8.90	8.35
	18	76.4	79.4	-9.03	8.39
	19	53.3	66.0	-9.30	8.53
	20	15.8	18.1	-9.82	8.95

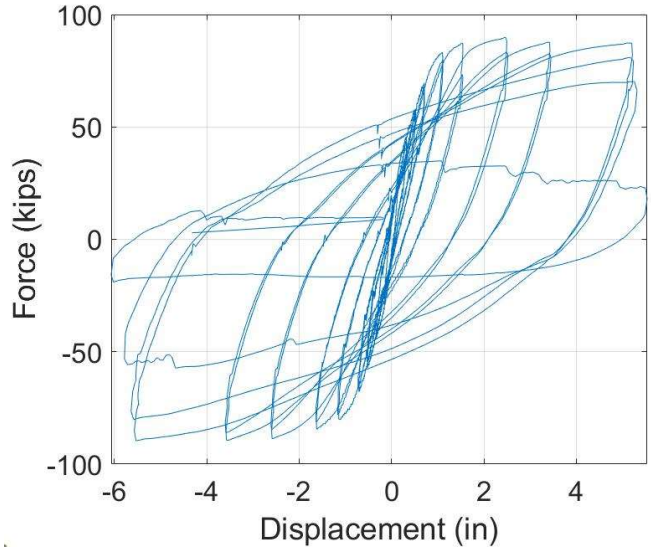

Figure 4.59. Specimen 30-21-R Force-Displacement Curve with P-Δ Effects Removed

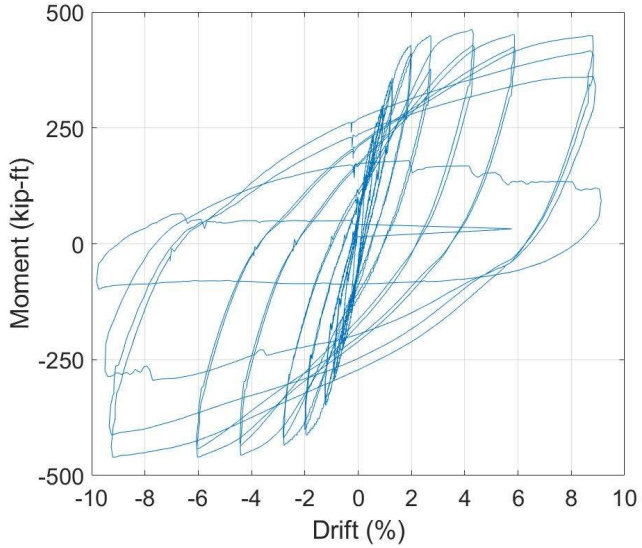

Figure 4.60. Specimen 30-21-R Moment-Drift Curve with P-Δ Effects Removed

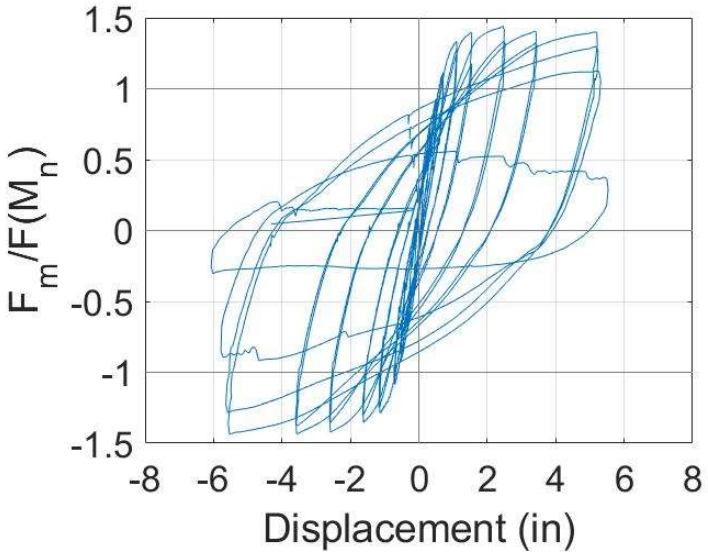

Figure 4.61. Specimen 30-21-R Force-Displacement Curve with P-Δ Effects Removed Normalized by F_N

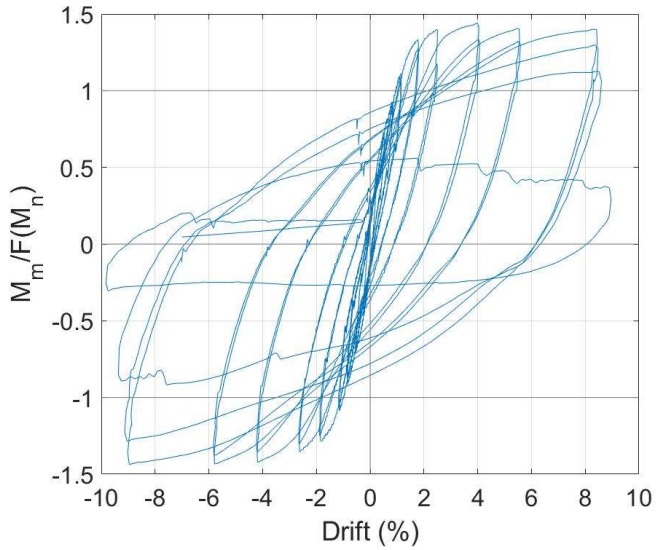

Figure 4.62. Specimen 30-21-R Moment-Drift Curve with P-Δ Effects Removed Normalized by M_n

As shown in Figures 4.59-4.62 and Table 4.6, the largest moment, M_p, reached was 460.2 kip-ft or 1.43M_n, at -5.7% drift. The nominal moment, M_n, was 321.1 kip-ft for Specimen 30-21-R The lateral strength increased approximately 2% of M_p, or 10 kip-ft for each of the previous cycles at -2.4% and -4.0% drifts. The lateral strength decreases 4% of M_p on the first cycle at -9.3% drift, 10% M_p on the second cycle, 26% M_p on the thirds cycle, and then substantially drops 40% of M_p or 193 kip-ft with the last cycle, which reached the largest drift of -9.8%. The behavior is similar on the positive drift side as well.

For the initial cycles of the test, it was difficult to see initial cracks being formed. This is due to the type of latex paint used on the column. Latex paint was used for this specimen as it was the only available paint in the structural laboratory at the time. For the other specimens, normal drywall paint was used, which made it easier to see the cracks form, and allowed the cracks to widen easier as well. Beyond this difficulty to see the initial cracking, the use of latex paint did not affect the behavior of the column.

Another detail about the testing of this specimen was the loading rate of the lateral actuator for the first ten cycles. The lateral actuator force seemed to increase in magnitude as a step function and not smoothly, as it did for the last ten cycles of the test. This is due to the short displacement that was occurring at the earlier cycles and the friction from the axial bearing assembly. The loading rate, one full cycle per 40 seconds, is constant for all the displacements, therefore smaller displacements have a slower velocity. This slower velocity affects the load cell in the lateral actuator, which is not able to overcome the friction from the testing assembly. The friction is due to the bearing coming into contact with the stainless steel on the sides of the guiding channel. For Specimens 30-21-R and 30-21-LD, a layer of PTFE was added to both of the sides on the inside of the channel, which reduced the space between the stainless steel and the side of the bearing. This reduction in space led to the contact between the stainless steel on the side of the channel and the axial bearing. This contact, along with slower velocity, is what caused the loading rate to fluctuate for the smaller cycles. At cycles larger than 1.75% drift, the loading rate did not fluctuate. Except for the loading having a step function, there was no noticeable impact on the peak loads or displacements, based on the measured response and small normal force between the bearing the stainless steel, and did not affect the results of the test.

Another visual observation from the actuator was that after a zero force-displacement hold, the actuator seemed to jump forward once restarted. While this was visually observed, there was no noticeable jump in any of the instrumentation, in terms of displacement or force.

Table 4.7 shows the width and location of the maximum and residual cracks measured for each drift level.

Table 4.7. Maximum Measured Crack Widths and Locations for Each Cycle (30-21-R)

Drift Level	Maximum Crack		Residual Cracks	
	Width (mm)	Location	Width (mm)	Location
0.2%	NA	NA	NA	NA
0.5%	0.1	7 in. above base	NA	NA
0.8%	0.3	8 in. above base	NA	NA
1.1%	0.6	7 in. above base	NA	NA
1.8%	1.0	7 in. above base	0.4	6 in. above base
2.5%	1.5	7 in. above base	1.0	6 in. above base
4.1%	2+	7 in. above base	0.8	11 in. above base
5.5%	2+	7 in. above base	1.5	11 in. above base
9.0+%	2+	7 in. above base	Spall	Base of Column

4.5.1 *Low Drift Cycles (0-2.0% Drift)*

For drift cycles of approximately 0.2%, the lateral load ranged from -0.4 to 0.4 (-26.2 to 26.9 kips) times the nominal force, F_n, which for this specimen was 62.4 kips, as shown in Figure 4.63.

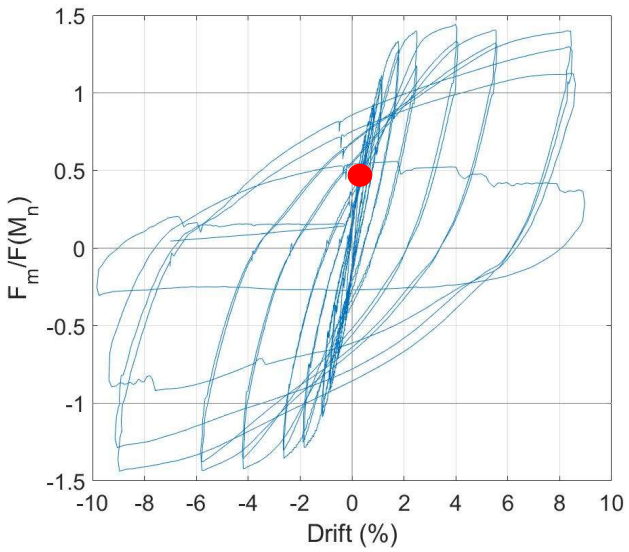

Figure 4.63. Specimen 30-21-R Normalized Force-Drift Curve at 0.2% Drift

As mentioned before, due to the latex paint no visible cracks were formed during this cycle. Strains measured during the peak displacement of the cycle were well within the reinforcement strain of 0.0023 in/in.

At drift cycles of 0.5%, the lateral load ranged from -0.6 to 0.7F_n (-39.4 to 41.4 kips), an increase of 0.2F_n from the previous cycle as shown in Figure 4.64.

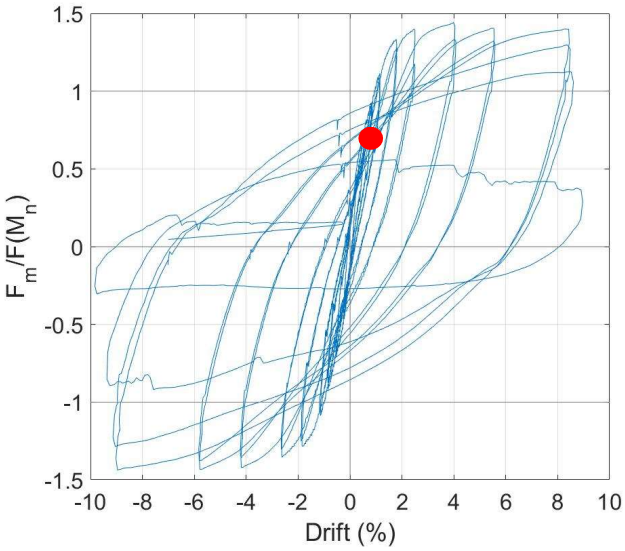

Figure 4.64. Specimen 30-21-R Normalized Force-Drift Curve at 0.5% Drift

A 0.1 mm wide horizontal crack formed 0.3D_{COL} (6 in.) from the base of the column on the northern face, shown in Figure 4.65. No residual cracks were measured at zero force displacements.

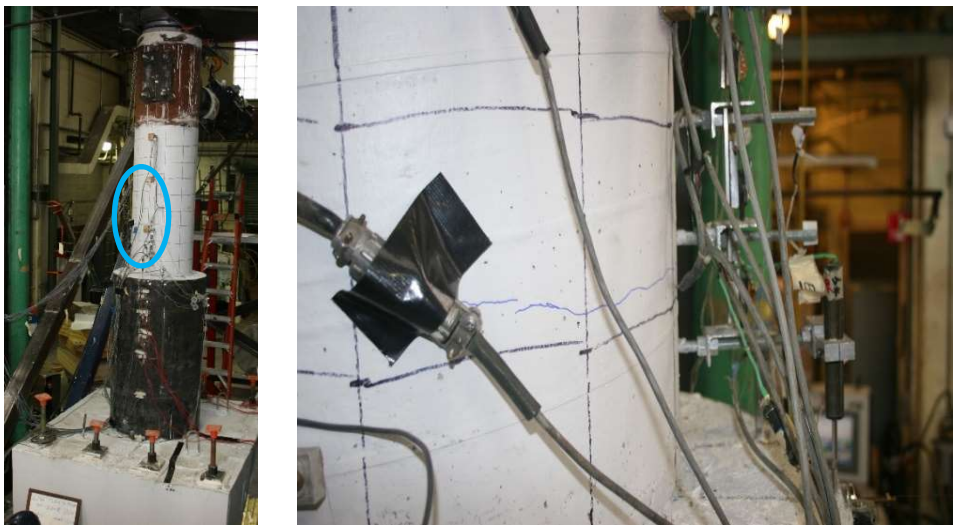

Figure 4.65. Specimen 30-21-R Horizontal Crack on Northern Column Face at 0.5% Drift

For this drift level, none of the longitudinal reinforcement strain measurements at peak displacement reached the approximate yield strain of 0.0023 in/in, with the largest strain, 0.0015 in/in, of these cycles, occurring on the $0.3D_{COL}$ location on the S Bar.

At 0.8% drift, the lateral load ranged from -0.9 to $0.9F_n$ (-54.4 to 57.1 kips), an increase of $0.3F_n$ from the previous cycle as shown in Figure 4.66.

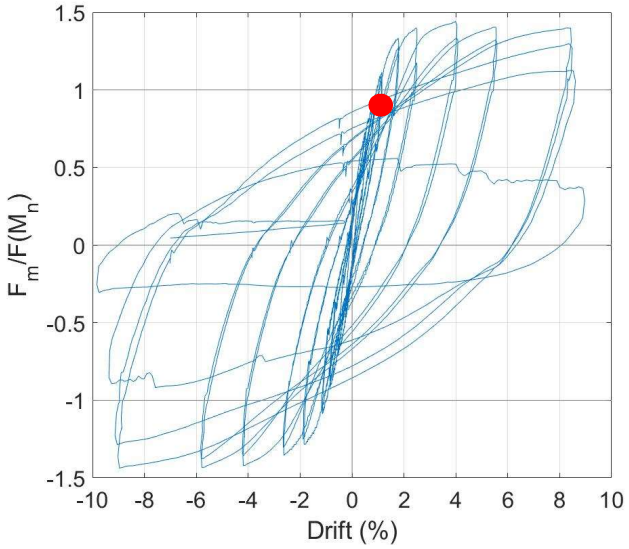

Figure 4.66. Specimen 30-21-R Normalized Force-Drift Curve at 0.8% Drift

Horizontal cracks on the northern and southern faces formed roughly every $0.25D_{COL}$ (5 in.) going up the height of the column, which can be shown in Figure 4.67, with the maximum width of the cracks being 0.3 mm, which occurred $0.3D_{COL}$ (6 in.) from the base on the North side of the column.

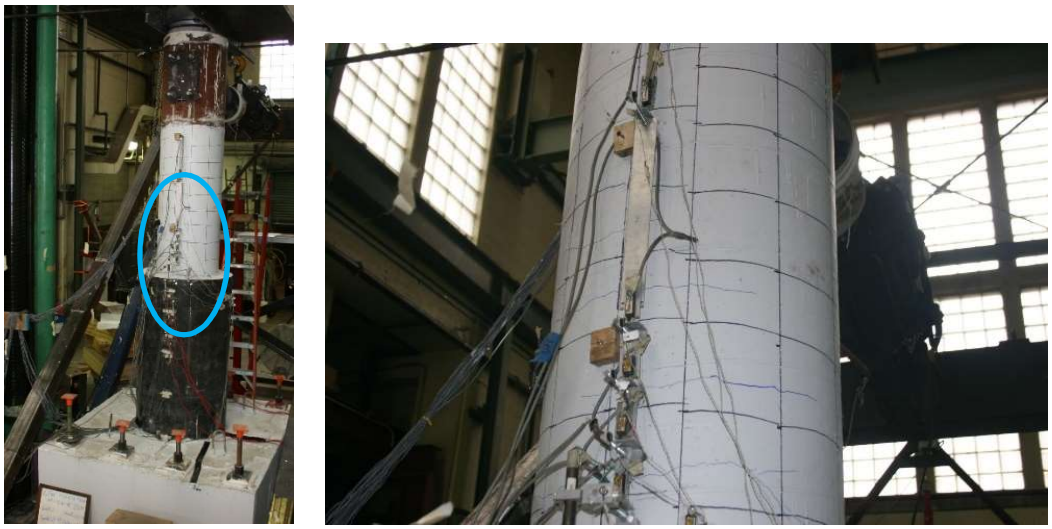

Figure 4.67. Specimen 30-21-R Horizontal Cracks on Northern Column Face at 0.8% Drift

During the first cycle at 0.8% drift, the column reinforcement strain exceeded the yield strain of 0.0023 in/in at $0.3D_{COL}$ on the S bar, during the peak displacement as shown in Figure 4.68.

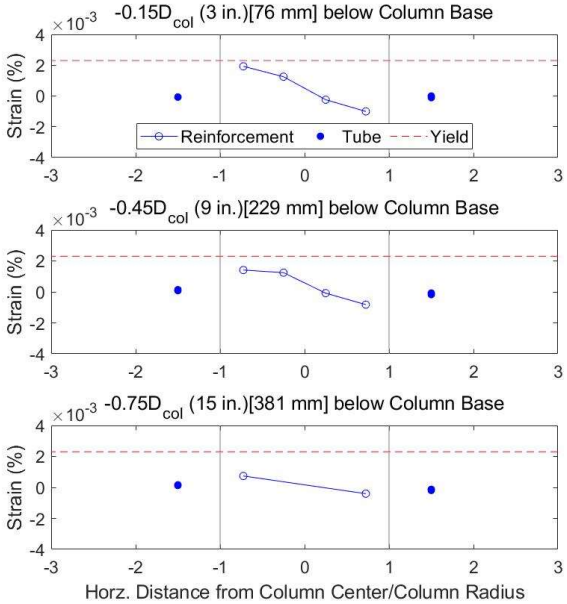

Figure 4.68. Specimen 30-21-R Strain Distribution at 0.8% Drift

At approximately 1.1% drift, the lateral load ranged from -1.1 to $1.1F_n$ (-67.8 to 69.6 kips), an increase of $0.2F_n$ from the previous cycle as shown in Figure 4.69.

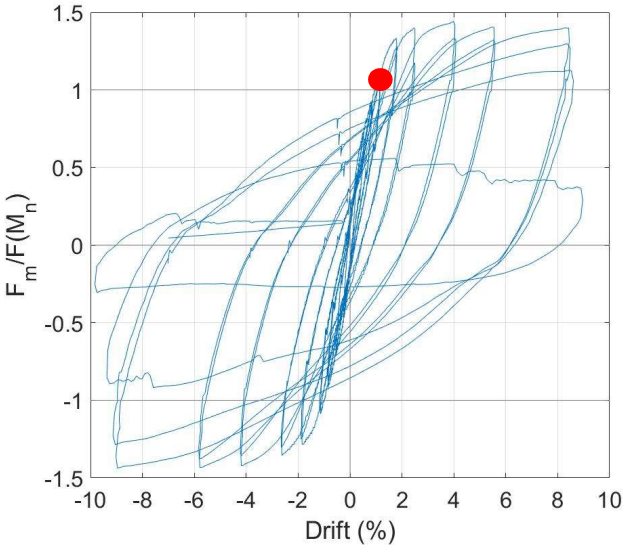

Figure 4.69. Specimen 30-21-R Normalized Force-Drift Curve at 1.1% Drift

The already formed horizontal cracks continued to lengthen, with the largest crack having a maximum width of 0.6 mm as shown in Figure 4.70. Additional horizontal cracks formed $1.5D_{COL}$ (30 in.) up on the column as well. During zero force, no residual cracks were visible, and the already formed cracks closed up.

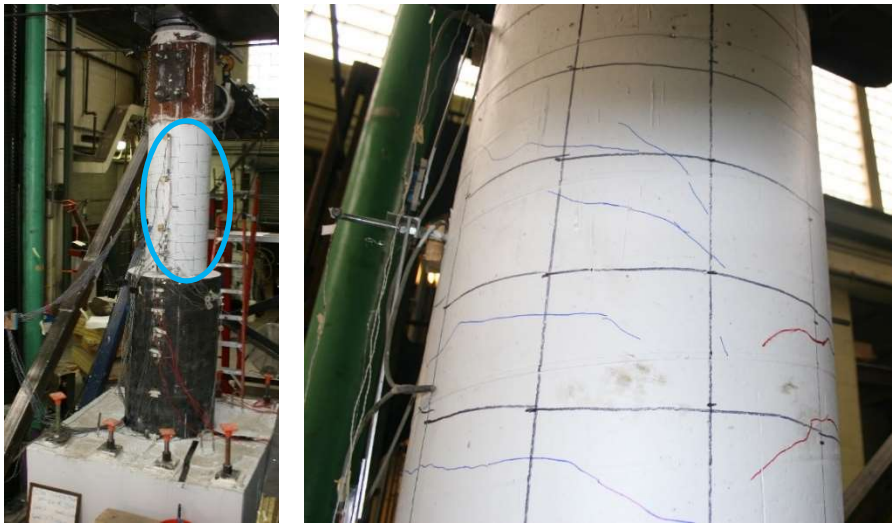

Figure 4.70. Specimen 30-21-R Horizontal Cracks at 1.1% Drift

The strains measured at the peak displacement of this cycle, exceeded the yield strain for all locations from $-0.45D_{COL}$ to $0.45D_{COL}$, shown in Figure 4.71. The strains reached 0.004 in/in, at $0.3D_{COL}$ on the S bar. The locations at $-0.75D_{COL}$ did not reach the reinforcement yield strain.

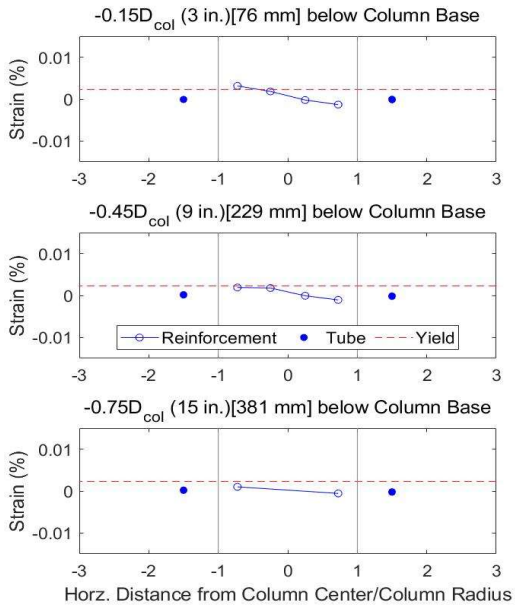

Figure 4.71. Specimen 30-21-R Strain Distribution at 1.1% Drift

At drift displacements of 1.75%, the lateral loads ranged from -1.3 to 1.3F_n (-79.8 to 81.0 kips) an increase of 0.1F_n from the previous cycle as shown in Figure 4.72.

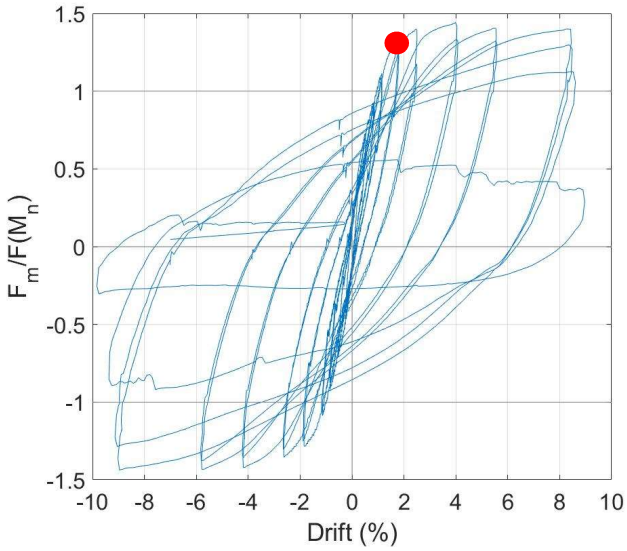

Figure 4.72. Specimen 30-21-R Normalized Force-Drift Curve at 1.75% Drift

The measured cracks widened noticeably to a maximum width of 1.0 mm. The largest cracks were located on the northern and southern faces, both 6 in. from the base of the column, as shown in Figure 4.73. During the zero-force displacements at this cycle, the southern cracks were

not visible at all, but the northern cracks 6 in. from the base of the column were visible and had a width of 0.4 mm.

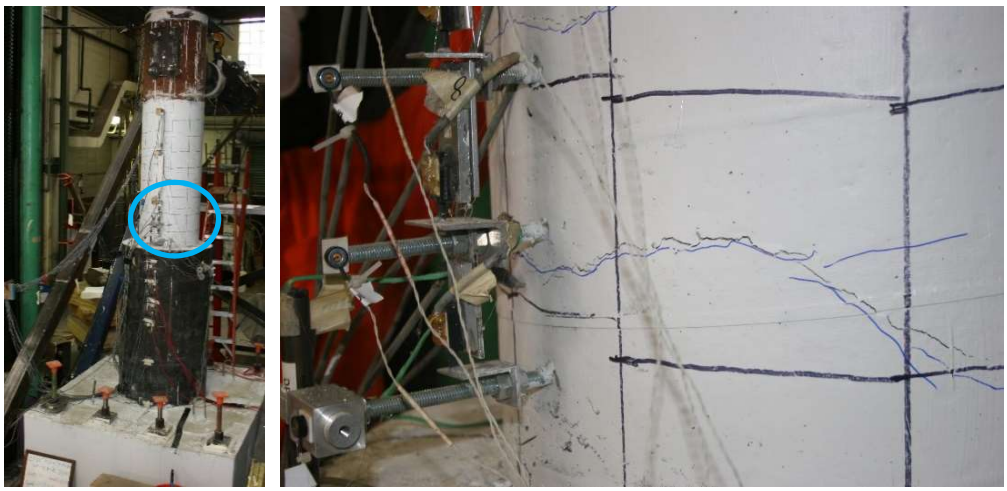

Figure 4.73. Specimen 30-21-R Column Northern Face crack at 1.75% Drift

Similar to the previous cycle, the strains measured at the peak displacement of this cycle, exceeded the yield strain for all locations from -0.45D_{COL} to 0.45D_{COL}, shown in Figure 4.74. The largest strain was 0.0091 in/in, which occurred at 0.3D_{COL} on the S bar.

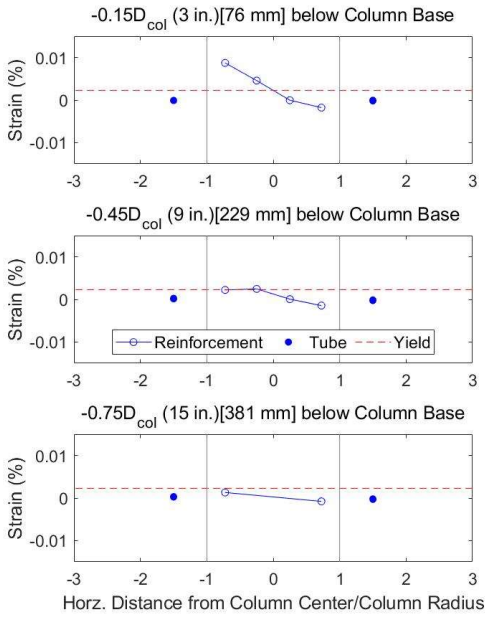

Figure 4.74. Specimen 30-21-R Strain Distribution at 1.75% Drift

4.5.2 *Moderate Drift Cycles (2.0-4.0% Drift)*

On the following cycle, at 2.4% drift, the lateral load ranged from -1.3 to 1.4F_n (-83.3 to 87.4 kips), an increase of 0.1F_n from the previous cycle as shown in Figure 4.75.

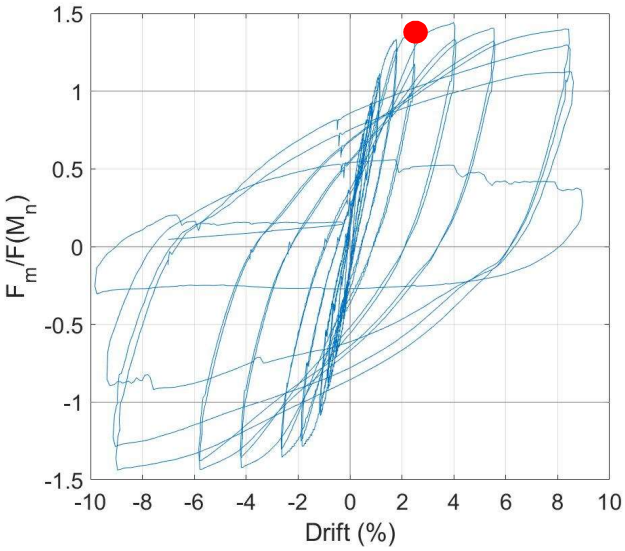

Figure 4.75. Specimen 30-21-R Normalized Force-Drift Curve at 2.4% Drift

The horizontal cracks continued to expand, with the widest crack occurring 0.3D_{COL} (6 in.) up from the base of the northern side of the column with a width of 1.5 mm. During this cycle, a small spalled region formed at the base of the northern face, which can be shown in Figure 4.76.

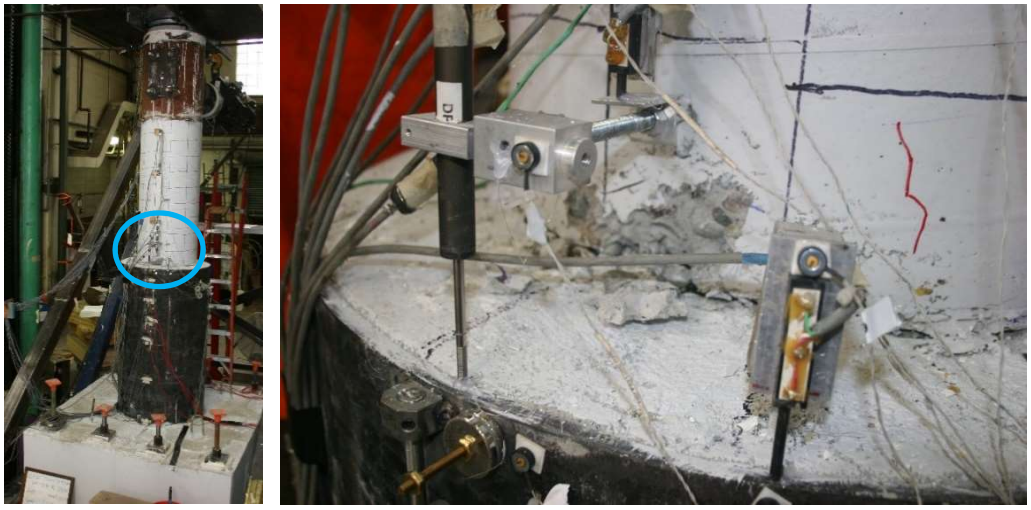

Figure 4.76. Specimen 30-21-R Spalled Region at Base of North Face of Column at 2.4% Drift

As with the previous cycle, the strains measured at the peak displacement of this cycle, exceeded the yield strain for all N and S bar locations, except -0.75$D_{COL,}$ as shown in Figure 4.77. The strains reached up to 0.014 in/in, which occurred on the S bar at 0.3D_{COL}.

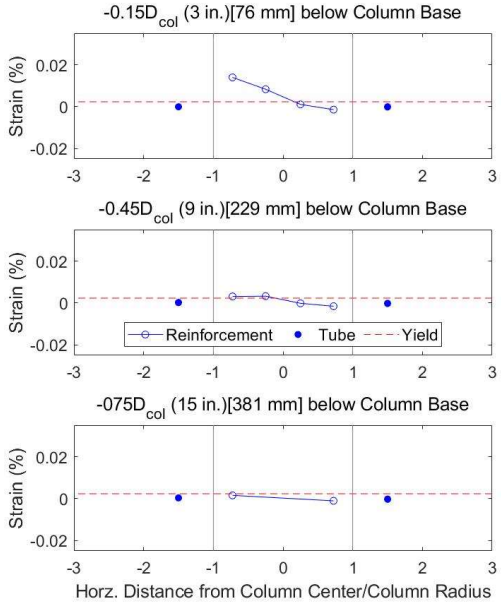

Figure 4.77. Specimen 30-21-R Strain Distribution at 2.4% Drift

At drift cycles of 4.0%, the lateral load ranged from -1.4 to 1.4F_n (-88.7 to 88.2 kips), which is approximately equivalent to the previous cycle as shown in Figure 4.78. It was during this cycle the column sustained its peak positive moment, 1.4M_n or 456.5 kip-ft when removing P-Δ effects.

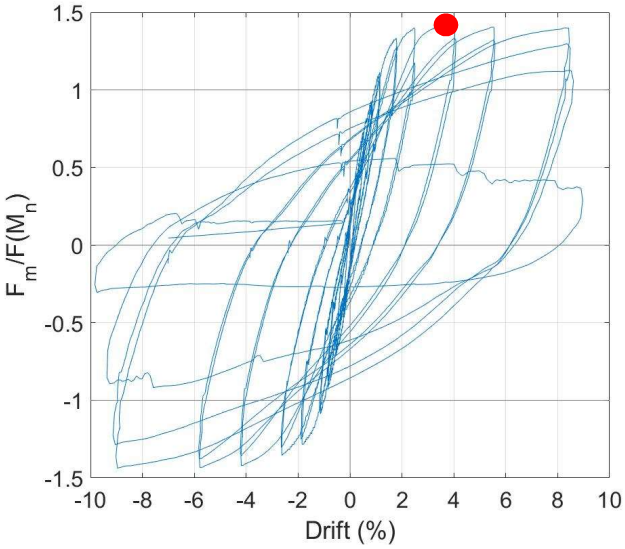

Figure 4.78. Specimen 30-21-R Normalized Force-Drift Curve at 4.0% Drift

The spalling region increased to a 10 in. by 7 in. area and the horizontal cracks at the base of the column increased to a maximum width of greater than 2 mm. The transverse column reinforcement was exposed as shown in Figure 4.77. The crack between the base of the column and the top of the pile expanded and had a depth of 2 in., as shown in Figure 4.80.

Figure 4.79. Specimen 30-21-R Exposed Transverse Reinforcement at 4.0% Drift

Figure 4.80. Specimen 30-21-R 2 in. Deep Crack at Northern Base of Column at 4.0% Drift

As with the previous cycle, the strains measured at the peak displacement of this cycle, exceeded the yield strain for all N and S bar locations, except for the N bar and S bar locations -0.75D_{COL}, as shown in Figure 4.81. The strains reached up to 0.028 in/in, which occurred on the S bar at 0.3D_{COL}.

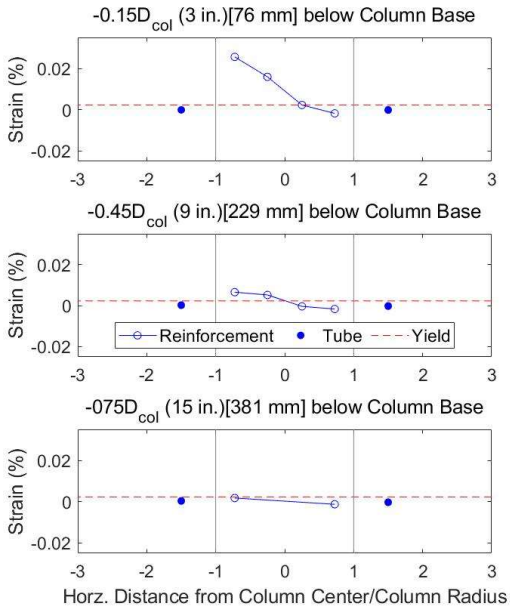

Figure 4.81. Specimen 30-21-R Strain Distribution at 4.0% Drift

4.5.3 *Large Drift Cycles (Greater than 4.0% Drift)*

At drift cycles of 5.5%, the lateral load ranged from -1.4 to 1.3 F_n (-89.4 to 83.9 kips) approximately equivalent to the last cycle as Figure 4.82 shows. At this drift level, in the negative direction, the maximum negative moment of $1.4M_n$ or 460.2 kip-ft.

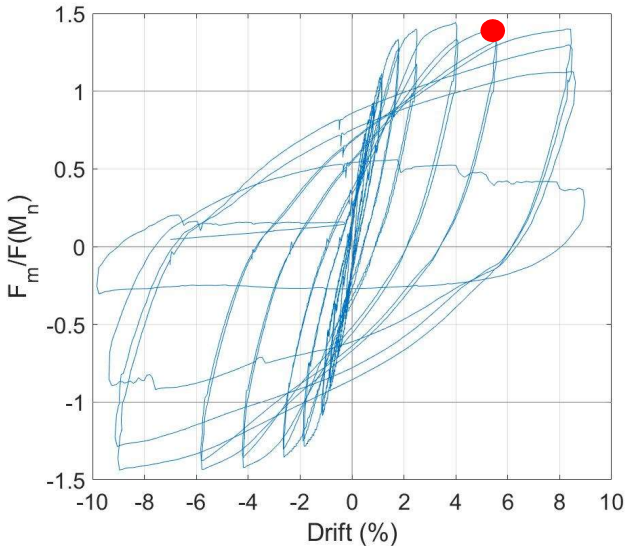

Figure 4.82. Specimen 30-21-R Normalized Force-Drift Curve at 4.0% Drift

The spalled region and the crack at the column base increased in size and exposed the longitudinal reinforcement on the northern face, shown in Figure 4.83. The spalled region now had an area of 20 in. by 8 in. on the north side and 10 in. by 5 in. on the south side. From this point on the cracks were too large to be measured, but all continued to increase in size and quantity.

Figure 4.83. Specimen 30-21-R Exposed Northern Longitudinal Reinforcement at 5.5% Drift

At 8.9% drift for the first cycle, the lateral load ranged from -1.4 to $1.3F_n$ (-85.0 to 81.8 kips) a decrease less than $0.1F_n$ from the previous cycle as shown in Figure 4.84.

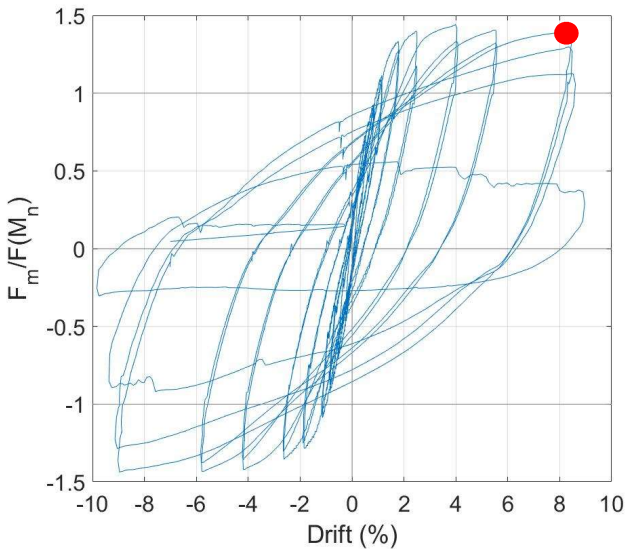

Figure 4.84. Specimen 30-21-R Normalized Force-Drift Curve at 8.9% Drift

The spalled region on both faces continued to increase with multiple longitudinal and transverse reinforcement being exposed. One of the longitudinal bars on the southern side buckled. There was also significant concrete crushing and the longitudinal bars buckled in both compression

and tension, this can be shown in Figure 4.85. The spalling was so widespread that horizontal cracks could not be measured.

Figure 4.85. Specimen 30-21-R South Face Buckled Longitudinal Reinforcement Bars at 8.9% Drift

On the second cycle at 8.9% drift, the lateral load ranged from -1.3 to 1.3F_n (-81.1 to 80.9 kips), a decrease less than 0.1F_n from the previous cycle as shown in Figure 4.86.

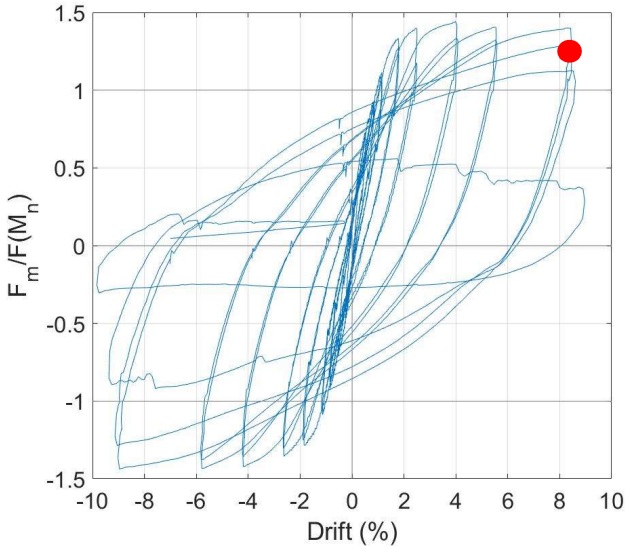

Figure 4.86. Specimen 30-21-R Normalized Force-Drift Curve at 8.9% Drift

The longitudinal reinforcement buckled in both compression and tension as shown in Figure 4.87. The spalled region on the northern side increased to an area of 25 in. by 15 in. and an area of 20 in. by 15 in. on the southern side.

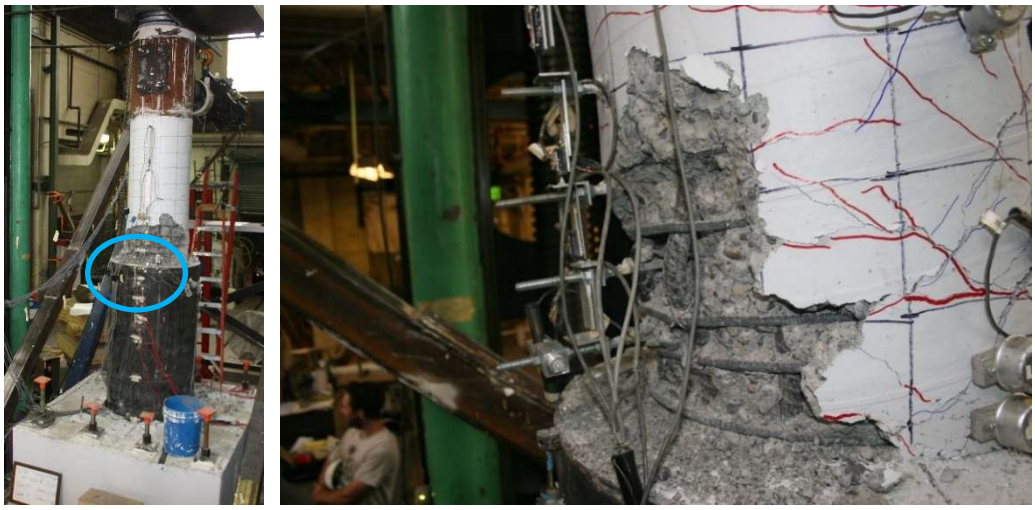

Figure 4.87. Specimen 30-21-R Buckled Reinforcement at 8.9% Drift

During the previous tests, loading was terminated after two cycles at 8.9% drift, however, since Specimen 30-21-R had not shown significant strength loss two more full cycles were run at 9.3% drift until the 50% strength loss had occurred. During the third cycle, a column drift of 9.3% was reached. The maximum lateral load was $1.1F_n$ (66 kips), a decrease in strength of $0.2F_n$ from the previous cycle or $0.4F_n$ from the peak strength of $1.4F_n$ (89.4 kips), as shown in Figure 4.88.

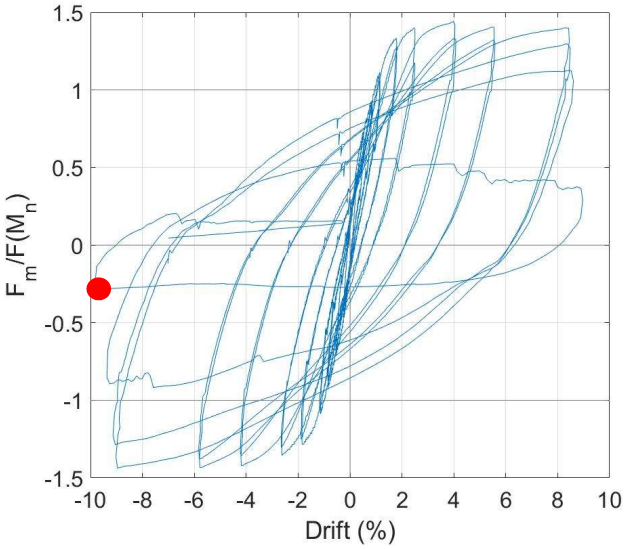

Figure 4.88. Specimen 30-21-R Normalized Force-Drift Curve at 9.3% Drift

During this cycle, concrete around the entire base of the column spalled off and the reinforcement continued to buckle, as shown in Figure 4.89.

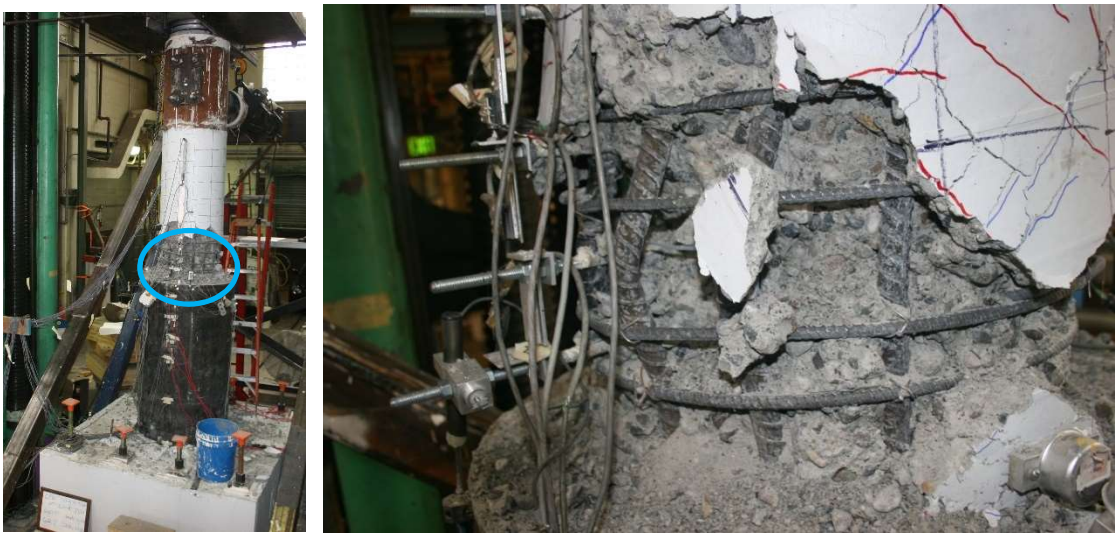

Figure 4.89. Specimen 30-21-R Base of Column at 9.3% Drift

Loading was terminated after 9.8% drift, with all bars buckled and the bottom $0.25D_{COL}$ (5 in.) of the column concrete separated from the rest of the pile. Similar to previous specimens, during the last cycle, the concrete at the base of the column seemed to explode out, as did the transverse reinforcement at the base too. The final state of the specimen can be shown in Figure

4.90. The lateral load on the last cycle was $0.3F_n$ (18.1 kips), a decrease of $0.8F_n$ (48 kips) from the previous cycle, or a decrease of $1.1F_n$ (71.1 kips) from the peak force.

Figure 4.90. Final State of Specimen 30-21-R after 9.8% Drift

Throughout all load cycles, the pile and transfer block showed no visible damage. The largest measured strain in the pile was 0.008 in/in, which occurred 52 in. below the top of the tube, during the 4.0% drift cycles. No cracks formed anywhere on the transfer block. There was no noticeable slip between the pile concrete in comparison to the edge of the tube at any point of the test. The Duncan potentiometer measuring the slip had a maximum uplift of 0.003 in. As shown in Figure 4.91, the top of the pile concrete appears largely undamaged. Unlike Specimens 30-21 and 48-21, no radial cracks formed on the top of the pile concrete.

Figure 4.91. Top of Specimen 30-21-R Pile with Column Removed

The day after the test, when working on removing the specimen from the testing rig, it was noticed that the most extreme southern longitudinal reinforcing bar had fractured overnight. No applied loads had occurred between now and the end of testing, but the fracture was caused by the weight of the column resting overnight. The fractured bar is shown in Figure 4.92.

Figure 4.92. Specimen 30-21-R Fractured Longitudinal Reinforcement

4.6 SPECIMEN 30-21-LD

Specimen 30-21-LD was tested on July 13th, 2021 in the Structural Research laboratory at the University of Washington. The test was performed 40 days after casting the transfer block and the pile, and 33 days after casting the column. The design of Specimen 30-21-LD was identical with Specimen 30-21, with the difference being the testing displacement history described in Chapter 3.

Elastic cycles were run on this specimen, as the dry run for the specimen had a displacement of 0.1 in. The maximum measured resistances and corresponding imposed drifts of each cycle are found in Table 4.8. The force-displacement and moment-drift hysteresis curve and the normalized curves of the column are shown in Figures 4.93 - 4.96. The constant axial load applied to this specimen was 7.5% of the axial capacity of the column, 160 kips.

Table 4.8. Maximum Resistances and Drifts in Each Cycle (30-21-LD)

Target Drift	Cycle	Maximum Measured Resistance (kips)		Maximum Imposed Drift (%)	
		Tension	Compression	Tension	Compression
1.21%	1	50.0	49.4	0.68	0.64
	2	54.4	52.1	0.69	0.75
3.24%	3	91.4	93.8	2.31	2.38
	4	88.4	88.1	2.37	2.38
	5	84.7	84.9	2.29	2.4
	6	84.6	84.0	2.38	2.41
	7	84.1	73.5	2.33	2.4
	8	84.7	76.9	2.37	2.41
4.86%	9	93.7	92.9	3.88	3.81
6.48%	10	98.9	90.0	5.77	5.36
	11	91.0	80.0	5.82	5.12
	12	92.8	79.0	5.8	5.15
	13	81.6	78.5	5.83	5.18
	14	87.3	76.3	5.88	5.19
	15	86.9	72.1	5.9	5.2
	16	79.3	74.5	5.89	5.23
	17	79.1	72.5	2.94	5.24
	18	81.0	70.8	5.98	5.26
	19	66.8	64.2	6.01	5.3
9.72%	20	52.4	54.8	9.43	8.33
	21	24.5	27.1	9.86	8.64

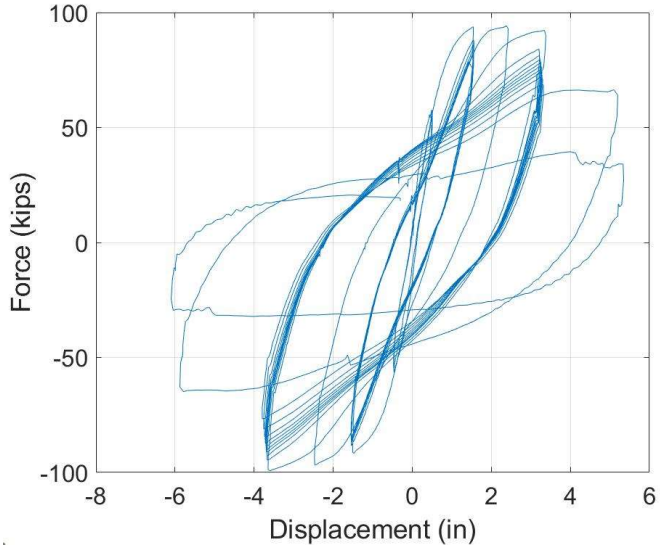

Figure 4.93. Specimen 30-21-LD Force-Displacement Curve with P-Δ Effects Removed

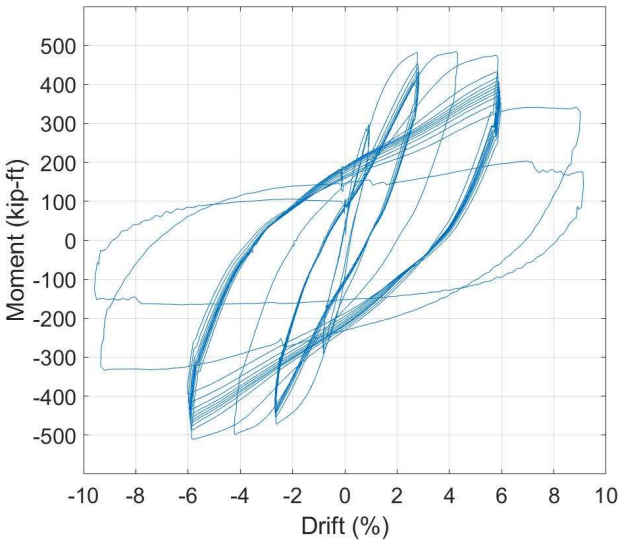

Figure 4.94. Specimen 30-21-LD Moment-Drift Curve with P-Δ Effects Removed

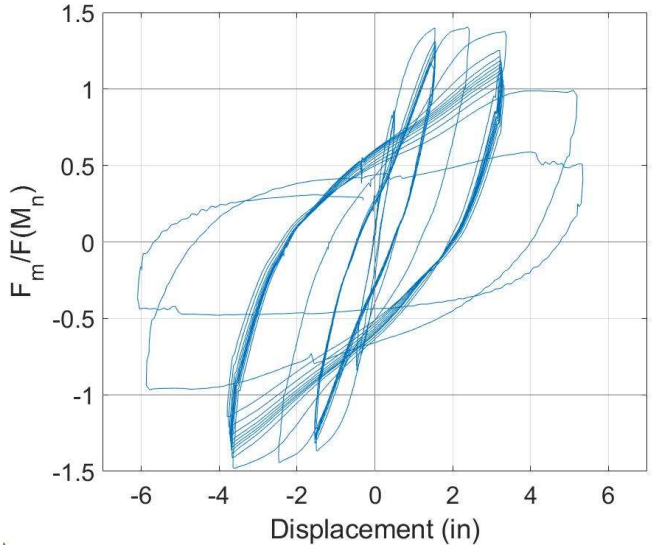

Figure 4.95. Specimen 30-21-LD Force-Displacement Curve with P-Δ Effects Removed Normalized by F_n

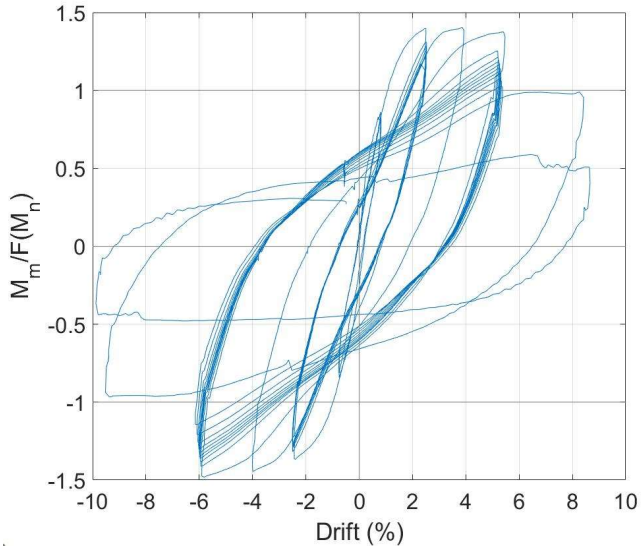

Figure 4.96. Specimen 30-21-LD Moment-Drift Curve with P-Δ Effects Removed Normalized by M_n

As shown in Table 4.8 and Figures 4.93-4.96, the largest moment, M_p, reached was 508.7 kip-ft or 1.47 M_n, at -5.8% drift. The nominal moment, M_n, was 345 kip-ft for Specimen 30-21-LD. It can be seen that the lateral resistance was approximately equal for the previous initial cycles at 2.4% and 3.9% drifts. The lateral resistance then degraded roughly 4% of M_p or 20 kip-ft with each following cycle at 5.5% drift. It then degrades roughly 20% of M_p or 100 kip-ft with each

cycle at 9.0% drift until it fails at a max drift of 9.9%. The behavior is similar in the negative drift direction as well The peak moment does line up with the peak lateral resistance when accounting for P-Δ delta effects, similar to Specimen 30-21.

Similar to Specimen 30-21-R, the lateral actuator force seemed to increase in magnitude as a step function for the first two cycles at 0.75 in. displacement. This is due to the small displacement that was occurring at the earlier cycles and the friction from the bearing coming into contact with the stainless steel on the side of the guiding channel as mentioned before in Specimen 30-21-R experimental observations. This caused the force-displacement curve to fluctuate as the force rose but did not have an impact on the peak loads or displacements and did not affect the results of the test.

Another visual observation was the stainless steel and PTFE on the inside of the axial bearing channel rig came unsecured from the East side of the channel. This is due to the bearing being placed too far to one side on top of the column. This led to the bearing riding against the greased stainless steel, which eventually forced the screws holding the stainless steel and PTFE to pop off. However, since the PTFE and stainless steel were greased, the axial bearing was still able to easily move back and forth during the cyclic loading. This issue had no noticeable effect on the measured results of the test.

Table 4.9 shows the width and location of the maximum and residual cracks measured for each drift level.

Table 4.9. Maximum Measured Crack Widths and Locations for Drift Level (30-21-LD)

Drift Level	Maximum Crack		Residual Cracks	
	Width (mm)	Location	Width (mm)	Location
0.7%	0.5	Base of Column	0.1	Base of Column
2.3%	2.4	Base of Column	2.0	Base of Column
3.8%	5.0	Base of Column	3.5	Base of Column
5.5%	Spall	Base of Column	Spall	Base of Column
9.0%+	Spall	Base of Column	Spall	Base of Column

4.6.1 *Low Drift Cycles (0-2.0% Drift)*

At 0.7% drift, the lateral load ranged from -0.8 to 0.8 times the nominal force, F_n, of 67.0 kips (-54.4 to 52.1 kips) as shown in Figure 4.97.

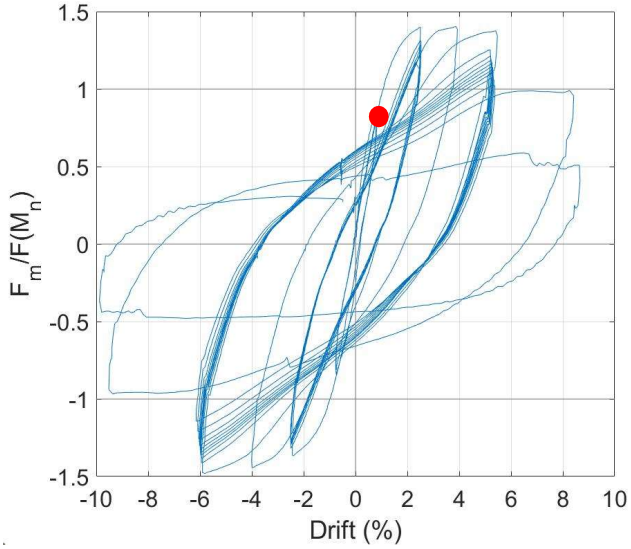

Figure 4.97. Specimen 30-21-LD Normalized Force-Drift Curve at 0.7% Drift

Horizontal cracks on the northern and southern faces formed roughly every $0.25D_{COL}$ (5 in.) going up the height of the column, with the maximum width of the cracks being 0.5 mm, which occurred $0.25D_{COL}$ (5 in.) from the base on both the North and South sides. Cracks also formed around the perimeter of the tube, which can be shown in Figure 4.98.

Figure 4.98. Specimen 30-21-LD Cracks at Edge of the Pile at 0.7% Drift

The strains measured at the peak displacement came very close but did not exceed the reinforcement yield strain of 0.0023 in./in. as shown in Figure 4.99. The largest strain measured was 0.0017 in./in., which occurred at -0.15D_{COL} on the N bar.

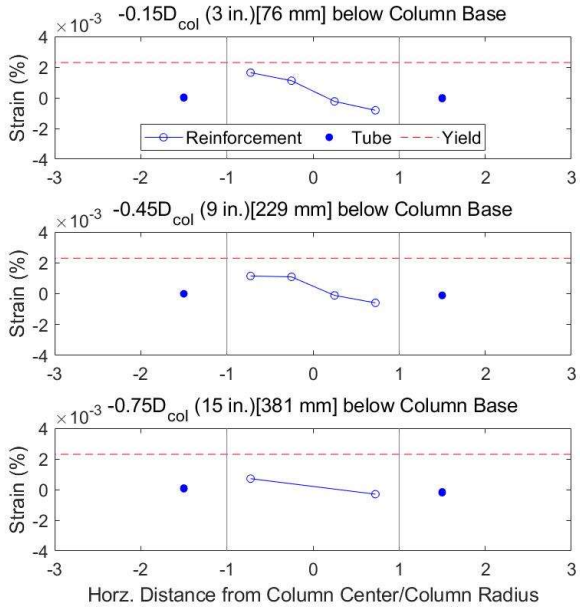

Figure 4.99. Specimen 30-21-LD Strain Distribution at 0.7% Drift

4.6.2 *Moderate Drift Cycles (2.0-4.0% Drift)*

After the first cycle at approximately 2.4% drift, the lateral load ranged from -1.4 to 1.4F_n (-91.4 to 93.8 kips) an increase of 0.6F_n from the previous cycle as shown in Figure 4.100.

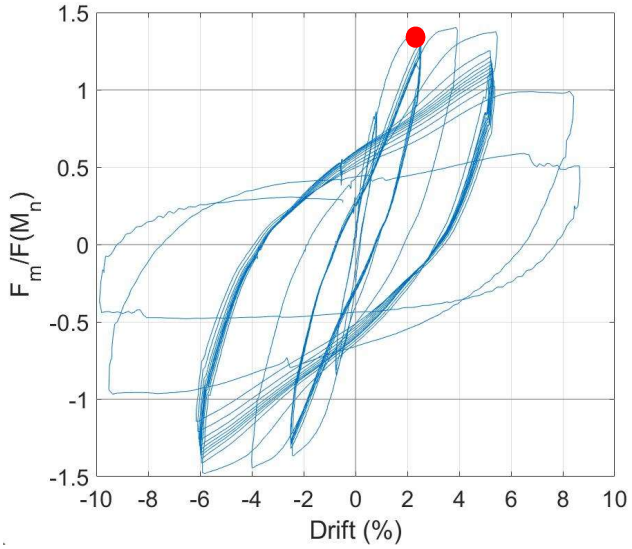

Figure 4.100. Specimen 30-21-LD Normalized Force-Drift Curve at 1st Cycle at 2.4% Drift

New cracks continued to form and already formed horizontal cracks continued to lengthen. The largest measured crack width was 1.3 mm, located at the Southern base of the column. Radial cracks formed around the column, from the edge of the tube to the base of the column. The first spalling also occurred at the base of the column on the northern face, which can be shown in Figure 4.101.

Figure 4.101. Specimen 30-21-LD 1st Spalled Region on Northern Column Face at 2.4% Drift

The reinforcement strain measured at the peak displacement on the N bar exceeded the yield strain of 0.0023 in./in. at $0.45D_{COL}$ and the other strain gauge located above. It is worth noting that while it was during this cycle the reinforcement yielded, this is not the yield displacement of the column, and nor is it an accurate representation of when the reinforcement should yield either. As shown with the other specimens, the reinforcement is closer to yielding around 0.8% drift.

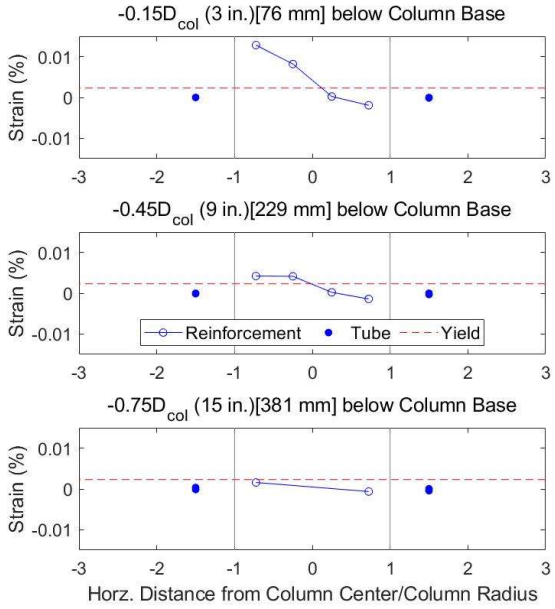

Figure 4.102. Specimen 30-21-LD Strain Distribution at 2.4% Drift

As cycles 3-6, at 2.4% drift, continued, four constant observations were noticed. The lateral load range for these cycles was -1.3 to $1.3F_n$ (-84.7 to 84.9 kips) a slight decrease from the first cycle at 2.4% drift, as shown in Figure 4.103.

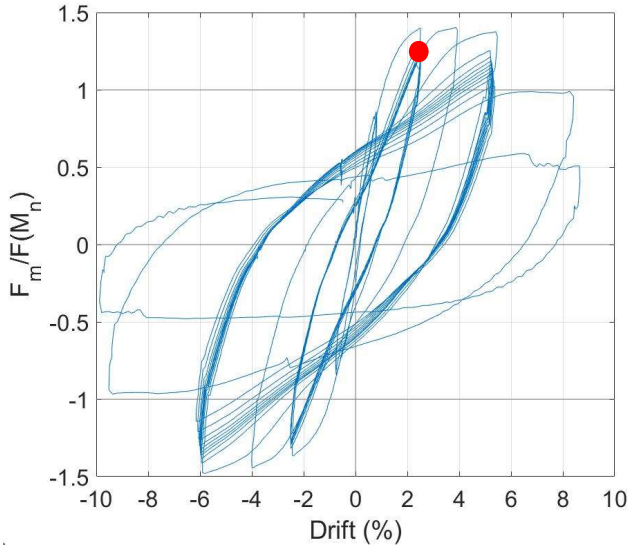

Figure 4.103. Specimen 30-21-LD Normalized Force-Drift Curve at 2.4% Drift

The horizontal cracks at the base of the column continued to widen to a width of 2.0 mm. The initial spalling at the base of the northern face of the column continued to increase in area and depth. The strains measured during these cycles were similar, with all strain gauge locations ranging from $-0.45D_{COL}$ to $0.45D_{COL}$ measured a strain greater than the reinforcement yield during the peak displacement.

The two most noticeable observations were the damage that occurred to the top of pile concrete and the lateral force degradation with repeated cycles. The damage to the top of the pile concrete, in comparison to the previous specimens, where there was little to no observed damage, is substantially greater. The damage to the top of the pile consisted of the edge of the pile concrete, by the tube spalling or breaking off and the crack at this location widening, and near the base of the column. While the concrete within the column's area was damaged so was the surrounding 0.5 in. at the base of the column. The damage can be shown in Figures 4.104a) and b). During these cycles, the lateral strength of the column was also decreasing. The first cycle at 2.4% drift had force peaks of -1.4 to $1.4F_n$ (-91.4 to 93.8 kips), while the 6^{th} and last cycle had force peaks of -1.3 to $1.1F_n$ (-84.7 to 76.9 kips), both decreasing over $0.1F_n$ from the first cycle.

Figure 4.104. Specimen 30-21-LD a) Concrete Damage at the Edge of the Pile and b) Concrete Damage Near Base of the Column at 2.4% Drift

At drift displacements of 3.8%, the lateral load ranged from -1.4 to $1.4F_n$ (-93.7 to 92.9 kips), which was approximately equivalent to the previous first cycle at 2.4% drift as shown in Figure 4.105.

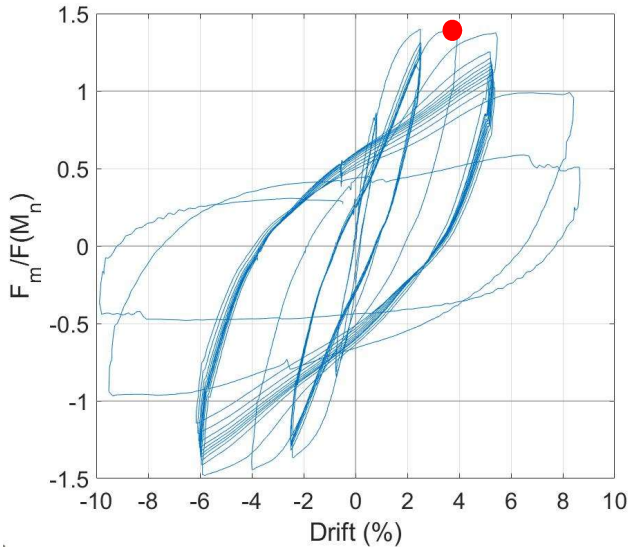

Figure 4.105. Specimen 30-21-LD Normalized Force-Drift Curve at 3.8% Drift

The cracks widened to a maximum width of 2.5 mm. The largest cracks were located on the northern and southern faces, both $0.3D_{COL}$ (6 in.) from the base of the column. The main observation during this cycle was the spalled region on the northern side increased greatly in area,

as shown in Figure 4.106. Also, a small spalled area formed on the base of the southern face of the column.

Figure 4.106. Specimen 30-21-LD Northern Column Face Spalled Region at 3.8% Drift

Similar to the previous cycle, the strains measured at the peak displacement of this cycle, exceeded the yield strain for all N and S bar locations, except for the N bar and S bar locations -0.75D_{COL} as shown in Figure 4.107. The strains reached up to 0.024 in./in., which occurred on the N bar at 0.3D_{COL}.

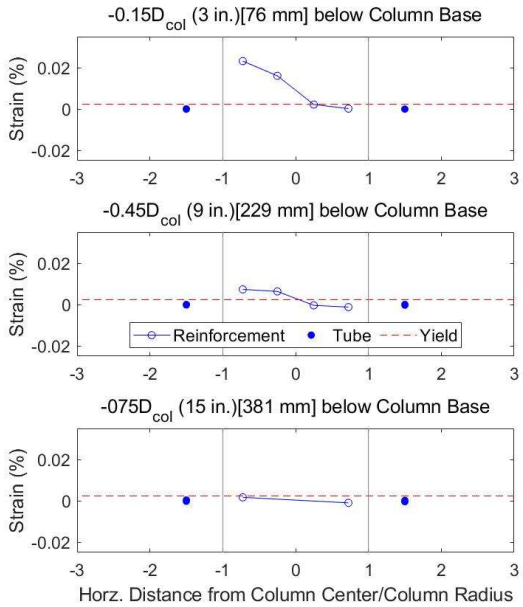

Figure 4.107. Specimen 30-21-LD Strain Distribution at 3.8% Drift

4.6.3 *Large Drift Cycles (Greater than 4.0% Drift)*

On the first cycle at 5.5% drift, the lateral load ranged from -1.5 to $1.3F_n$ (-98.9 to 90.0 kips), which was approximately equivalent to the previous cycle in tension and slightly less in compression, as shown in Figure 4.108. During this cycle, the maximum lateral force was reached of $-1.5F_n$ (98.9 kips). From this point on the lateral force would decrease slightly with each cycle in both compression and tension.

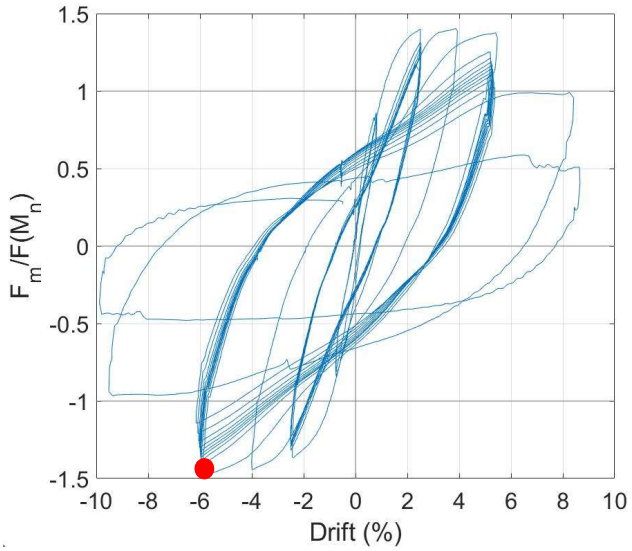

Figure 4.108. Specimen 30-21-LD Normalized Force-Drift Curve at 1st Cycle at 5.5% Drift

The column base spalled region and crack increased in size, to a maximum width of 4.0 mm and exposed the transverse reinforcement on the southern face. The second cycle at 5.5% drift exposed the longitudinal reinforcement on the southern face as shown in Figure 4.109. The maximum crack width at this drift was 5.0 mm and the spalled region had increased greatly in area. For the remaining cycles, the cracks were too large to be measured, but they all continued to increase in size and quantity.

Figure 4.109. Specimen 30-21-LD Exposed Longitudinal Reinforcement at 5.5% Drift

The strains measured at the peak displacement for all the cycles at 5.5% drift all had the same pattern. The strains exceeded the yield strain for all N and S bar locations, except the N bar and S bar locations -0.75D_{COL}. The strains reached up to 0.06 in./in., which occurred on the S bar at -0.3D_{COL}. Figure 4.110 shows an example of the strain distribution at 5.5% drift.

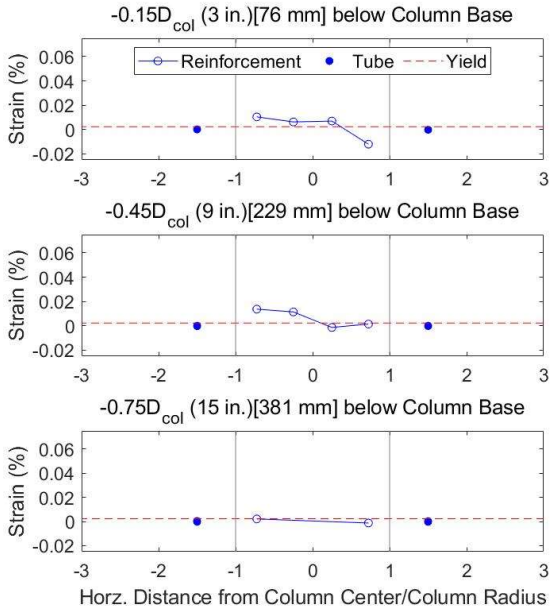

Figure 4.110. Specimen 30-21-LD Strain Distribution at 5.5% Drift

The third and fourth cycles at 5.5% drift, had a lateral load range of -1.4 to $1.2F_n$ (-92.8 to 79.0 kips), a decrease of $0.1F_n$ from the earlier cycles at 5.5% drift.

There was increased damage to the pile concrete and exposed the longitudinal reinforcement on the northern face of the column. As mentioned before, the pile concrete damage was both the concrete at the edge of the tube, but also the concrete surrounding the column, which now had expanded to roughly 1 in. around the base of the column. The increased spalled area and pile concrete damage are shown in Figures 4.111 and 4.112.

Figure 4.111. Specimen 30-21-LD Increased Spalled Region at 5.5% Drift

Figure 4.112. Specimen 30-21-LD Top of Pile Concrete Damage at 5.5% Drift

During the fourth cycle, a crack on the southern side of the transfer block was noticed extending the entire height of the transfer block, shown in Figure 4.113. There was no noticeable change in the instrumentation or results before, during, or after this was noticed.

Figure 4.113. Specimen 30-21-LD Crack on Southern Side of Transfer Block

On the fifth cycle at 5.5% drift, the lateral load ranged from -1.3 to $1.1F_n$ (-87.3 to 76.3 kips) a decrease of $0.1F_n$ from the previous cycle as shown in Figure 4.114.

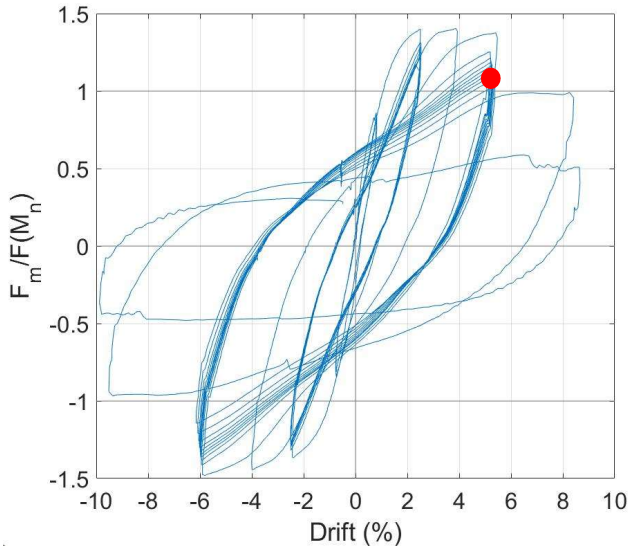

Figure 4.114. Specimen 30-21-LD Normalized Force-Drift Curve at 5th Cycle at 5.5% Drift

One of the longitudinal bars on the southern side of the column buckled slightly, as shown in Figure 4.115.

Figure 4.115. Specimen 30-21-LD Buckled Longitudinal Reinforcement on Southern Side of Concrete at 5.5% Drift

For the remaining five cycles at 5.5% drift, the lateral resistance of the column decreased around $0.03F_n$ (1-3 kips) per cycle, to a maximum resistance of $1.0F_n$ (66.8 kips) during the 10th cycle at 5.5% drift or 19th total cycle of the test. This was a decrease of $0.1F_n$ from the 5th cycle at 5.5% drift, as shown in Figure 4.116.

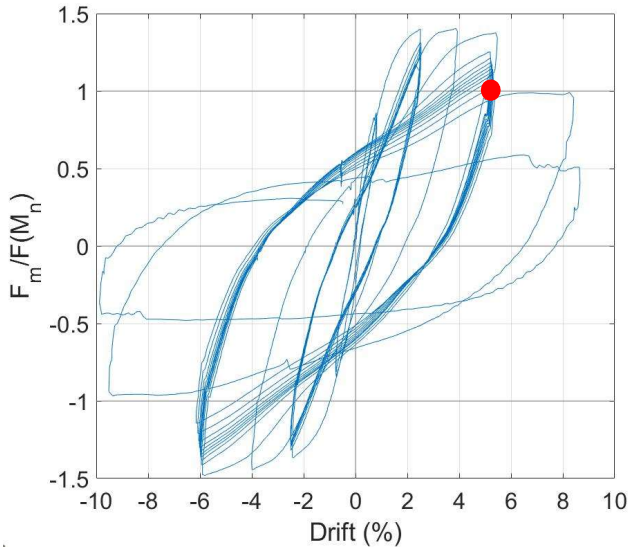

Figure 4.116. Specimen 30-21-LD Normalized Force-Drift Curve at 10th Cycle at 5.5% Drift

During these last five cycles at 5.5% drift, the bars on both the north and south sides of the column continued to buckle and the spalled area on both sides continued to increase in size. The state of the northern face of the column after the tenth cycle at 5.5% drift is shown in Figure 4.117.

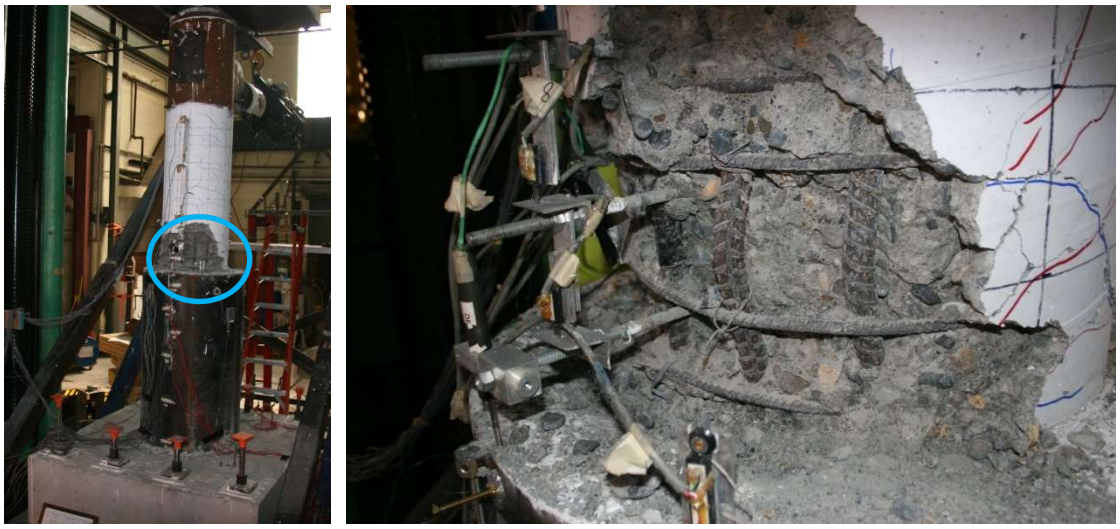

Figure 4.117. Specimen 30-21-LD Northern Face of Column after 10 cycles at 5.5% drift

As mentioned before in Section 3.8, originally the goal was to test the specimen to failure with repeated cycles at 5.5% drift. However, since the column was only losing a lateral strength of $0.03F_n$ per cycle, it was then decided to run 2 cycles at a 6 in. displacement or a target drift of 9.72%.

On the first cycle at 8.3% to -9.4% drift, the lateral load ranged from -0.8 to $0.8F_n$ (-52.4 to 54.8 kips), a decrease of $0.2F_n$ from the last cycle at 5.5% drift, as shown in Figure 4.118.

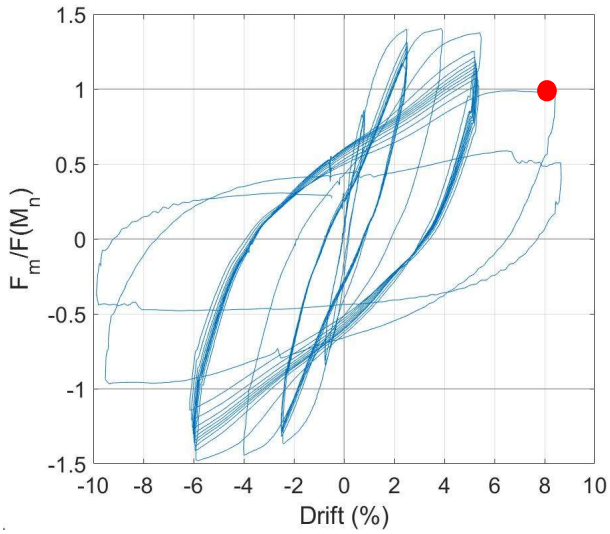

Figure 4.118. Specimen 30-21-LD Normalized Force-Drift Curve at 8.3% Drift

One of the longitudinal reinforcing bars on the Northside fractured in tension, which can be shown in Figure 4.119.

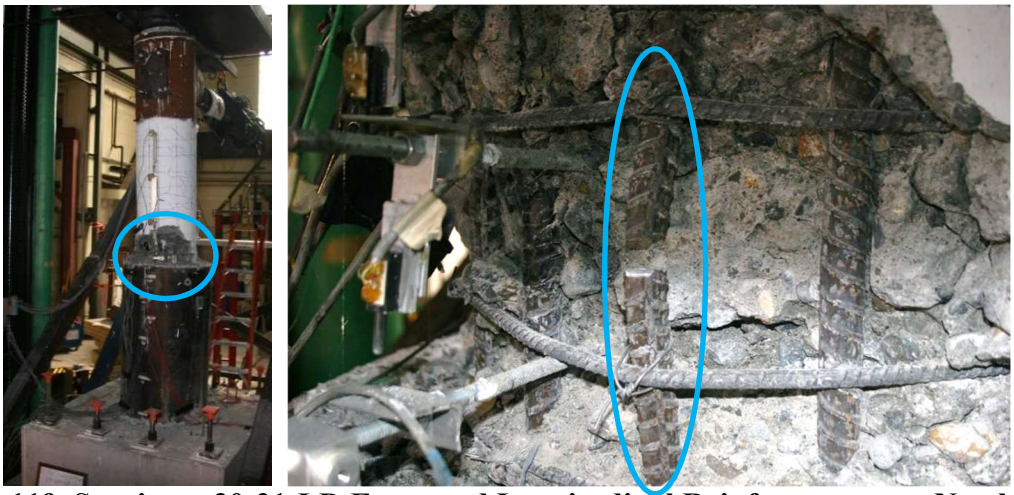

Figure 4.119. Specimen 30-21-LD Fractured Longitudinal Reinforcement on North side of Column at 9.4% drift

Loading was terminated after the second cycle when the column reached a drift of 9.9%. The last lateral load was $0.4F_n$ (27.1 kips), a decrease of $0.4F_n$ (27.7 kips) from the previous cycle. Another longitudinal reinforcing bar fractured during this cycle, this time on the southern side of the column, while all the remaining bars had completely buckled and the concrete at the base of the column had completely crushed. There was also widespread damage to the top of the pile

concrete especially around the base of the column. The final state of the column can be shown in Figure 4.120.

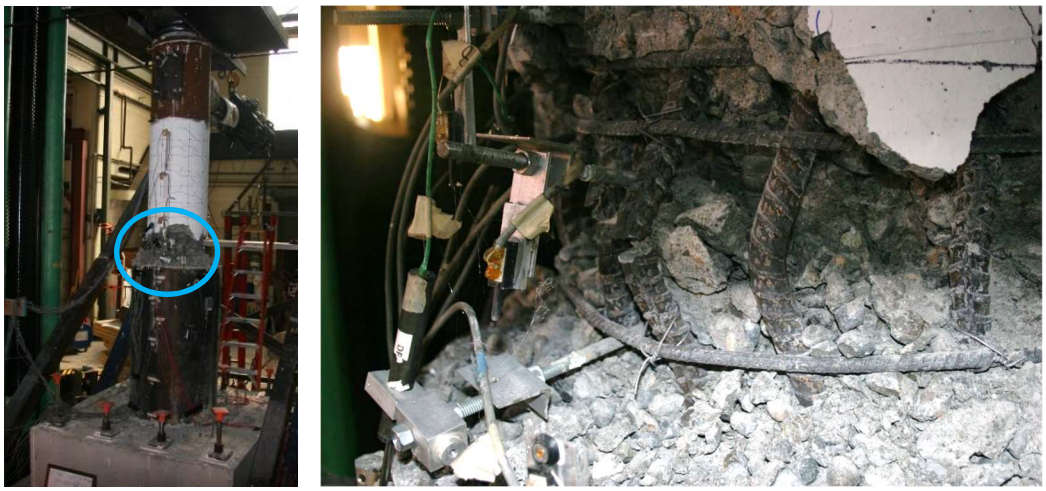

Figure 4.120. Specimen 30-21-LD Final State of Column after 9.9% Drift

Throughout all load cycles, the pile showed no visible damage. There was no buckling or yielding of the pile, with the largest measured strain being 0.00017 in./in., which occurred 52 in. below the top of the tube, during the 5.5% drift cycles. There was no noticeable slip between the pile concrete in comparison to the edge of the tube at any point of the test. The measured slip on the outside of the tube had a maximum reading of 0.05 in. for the whole test. As shown in Figure 4.121, the top of the pile concrete appears heavily damaged on the edges and around the base of the column.

Figure 4.121. Top of Specimen 30-21-LD Pile with Column Removed

Chapter 5. DATA ANALYSIS

This chapter compares the measured response of the test specimens, including strain distribution, displacement profiles, system behavior, and specimen damage. The strain distribution is the comparison of each specimen's column reinforcement strains and the tube strains on the outside of the pile at the peak displacement of the given. The displacement profiles consist of overall specimen displacement, curvature profiles, and a breakdown and comparison of the displacement contribution mechanisms. The system behavior is a comparison of the normalized moment-drift responses and energy dissipation curves. The specimen damage comparisons are the drift levels for the damage states of the pile concrete and column-pile connection.

5.1 SPECIMEN STRAINS

Strains were measured with strain gauges on both the column longitudinal reinforcement as well as on the outside of the tube. Strains on the outside of the tube were also measured using Vibrating Wire Gauges (VWG). The strain profiles and the strains distributions of the tube and reinforcement can be used to determine the flexural behavior of the column and assess if adequate embedment or development length is reached as well as if composite action is occurring between the column reinforcement and the CFST.

5.1.1 *Strain Distributions*

The following figures show the strains measured at the peaks of various drift levels and heights along the specimen. The plots may consist of up to six points per height and drift level for each specimen. Two of the points are the tube strains, which are shown as filled circles, and while it may only appear like there is one mark per side, there are actually two at each location, one from

the strain gauge and one from the VWG. This is due to the strains measured on the tube being significantly smaller than the strains measured on the reinforcement. The other points per specimen, there may be up to four at each level, are the reinforcement strains, which are shown as connected circles. If there are less than four points this is either due to the middle reinforcement, North-East (NE) and South-East (SE) bars, not having a strain gauge at this location, or a broken strain gauge at that location. On all plots, there are horizontal lines at the yield strain, .0024 in./in., of the reinforcement. The horizontal axis represents the horizontal distance the strain gauge is from the center of the column. The vertical lines at +/- 10 in. represent the sides of the column.

Figure 5.1 shows a cross-sectional view of the specimen and identifies the locations where the strain gauges are located. It is worth noting that the moment is increasing in magnitude going down the height of the specimen from the point of loading.

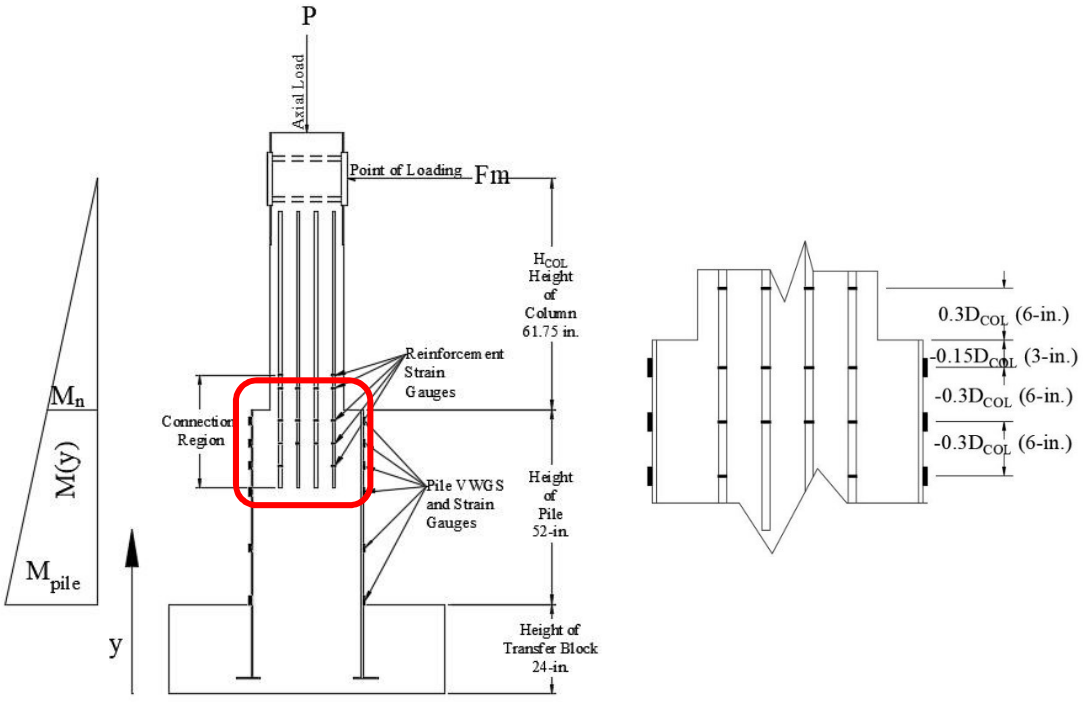

Figure 5.1. a) Cross-Sectional View of Specimen with Strain Gauge Heights and Strain Gauge Locations in Connection Region

The tube strains are examined to better understand the relationship between the concrete and the steel tube. A larger strain in the tube would signify less slip between the concrete and the steel since the steel would experience more strain staying in contact with the concrete. The tube strains in specimens 30-21, 30-21-R, and 30-21-LD can be compared directly since these specimens are of the same size and made of the same material. Specimen 48-21's strains are not able to be compared directly to the other specimens, due to it's larger size and different tube material. Specimen 48-21's strains can be compared to the other specimen's strains by multiplying Specimen 48-21's strains by the ratio between the two different CFST size stiffness's. The CFST's stiffness is calculated using the following equation (AASHTO 6.9.6.3.2-6):

$$EI_{eff} = E_s I_{st} + C' E_c I_c$$

EI_{eff} = Effective Stiffness of CFST (k-in^2)

E_s = Modulus of Elasticity of Steel (ksi)

I_{st} = Moment of Inertia of Steel Tube (in^4)

C' = Concrete Correction Factor = $0.15 + P/P_o + A_{st}/(A_{st}+A_c)$

E_c = Modulus of Elasticity of Concrete (ksi)

I_c = Moment of Inertia of Concrete in CFST (in^4)

P = Axial Load on Column (kips)

P_o= Axial Load Capacity of Column (kips)

A_{st} = Area of Steel Tube (in^2)

A_c= Area of Concrete in CFST (in^2)

Using this equation, the EI_{eff} of the 30 in. and 48 in. CFSTs were 1.91*108 k-in^2 and 8.92*108 k-in^2, respectively, resulting in a stiffness ratio of 4.67 between the two CFSTs, which was used to directly compare the strains of all four specimens.

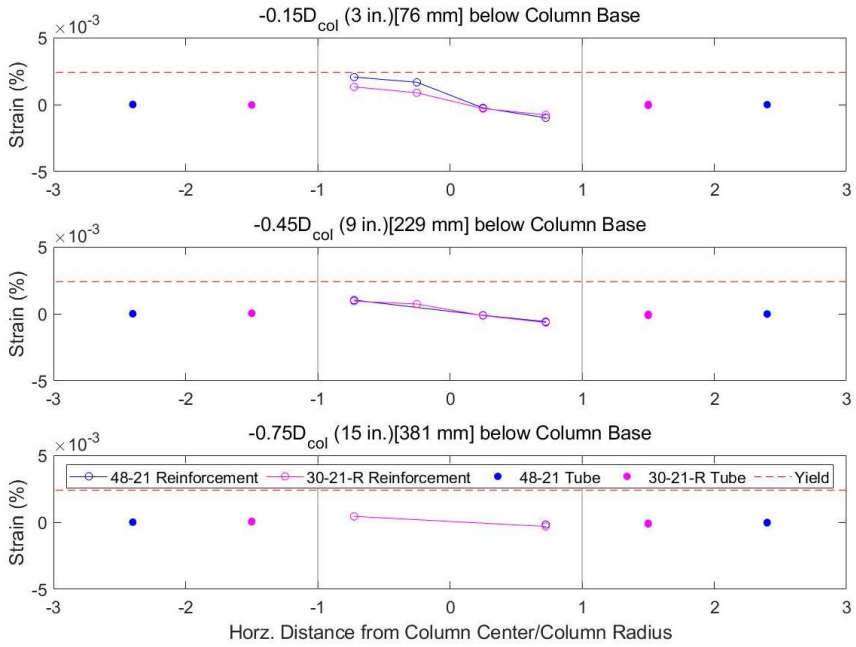

Figure 5.2. Strain Distribution at 0.5% Drift (Specimen 48-21 and Specimen 30-21-R)

As shown in Figure 5.2, at approximately 0.5% drift, the strains measured at these locations are all within the yield strain limits, showing that the reinforcement has not yielded during this cycle. Specimen 48-21's strains are slightly larger than Specimen 30-21-R's strains. Also shown is the strain decreasing in magnitude the deeper the reinforcement is into the pile.

Due to the size of the strain scale, the magnitudes of the tube strains are difficult to differentiate between the specimens. Specimen 48-21 and Specimen 30-21-R had similar tube strains for locations -0.15D_{COL} to -0.75 D_{COL}, ranging from $6.7*10^{-5}$ to $1.3*10^{-4}$ strain. The behavior of the tube strains is opposite of the reinforcement strains in that the magnitude of the strains increased the farther down the pile.

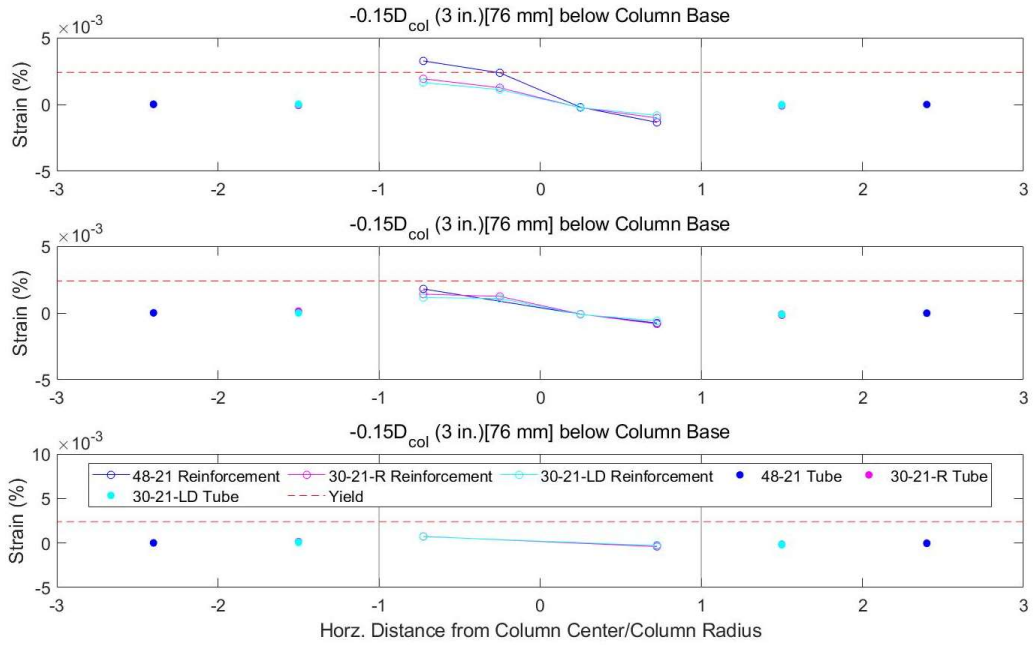

Figure 5.3. Strain Distribution at 0.8% Drift (Specimen 48-21, Specimen 30-21-R, and Specimen 30-21-LD)

As shown in Figure 5.3, at approximately 0.8% drift, the strains measured at these locations for Specimens 48-21 and 30-21-R have exceeded the yield strain limits, showing that the reinforcement has yielded during this cycle. The strains measured for Specimen 30-21-LD's reinforcement have not yielded but are very close to. For all shown specimens, the strains at $0.75D_{COL}$ (15 in.) below the column base are within the reinforcement yield strain limits. Similar to Figure 5.2, Specimen 48-21's strain is slightly larger than the strain measured in Specimen 30-21-R or Specimen 30-21-LD. Also shown for all specimens, the strain is decreasing in magnitude the deeper the reinforcement is into the pile.

It is worth noting that the strains measured for Specimen 30-21 are not shown on these plots, due to the previously mentioned testing error of not running elastic cycles, but it can be assumed that the reinforcement for Specimen 30-21 would have similar behavior to the other specimens and the reinforcement would have yielded or been close to yielding during this cycle.

For this drift level, Specimen 48-21 had the largest tube strains, reaching a maximum strain of $2.3*10^{-4}$ in/in at -0.75 D_{COL}, followed by Specimen 30-21-R's maximum strain of $2.2*10^{-4}$ in/in also at -0.75 D_{COL}. Specimen 30-21-LD had the smallest maximum strain of $2.0*10^{-4}$ in/in at -0.75 D_{COL}. The behavior of the tube strains is opposite of the reinforcement strain's behavior in that the magnitude of the strains increased the farther down the pile.

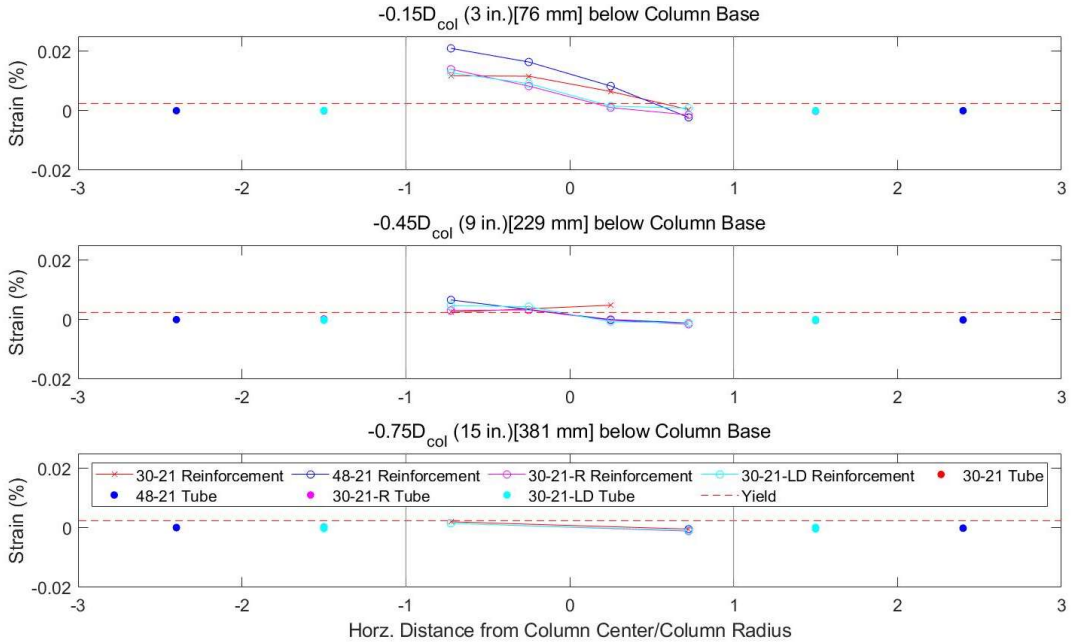

Figure 5.4. Strain Distribution at 2.2% Drift (Specimen 30-21, Specimen 48-21, Specimen 30-21-R, and Specimen 30-21-LD)

As shown in Figure 5.4, at approximately 2.2% drift, the reinforcement strains measured at the locations -0.45D_{COL} (9 in.) and above have significantly exceeded the yield strain, while the tube strains for all locations and the reinforcement strains at -0.75D_{COL} are still within the yield strain. Specimen 48-21's strains are larger than the other specimen's strains. The reinforcement strains are shown decreasing in magnitude as the reinforcement becomes more embedded in the pile.

For this drift level, Specimen 48-21 again had the largest tube strains, reaching a maximum strain of $7.9*10^{-4}$ in/in at -0.75 D_{COL}, followed by Specimen 30-21-R's and Specimen 30-21-LD's

maximum strain of $4.0*10^{-4}$ in/in also at -0.75 D_{COL}. Specimen 30-21 had the smallest maximum tube strain of $2.0*10^{-4}$ in/in at -0.75 D_{COL}. The tube strains increased in magnitude the farther down they are measured in the pile.

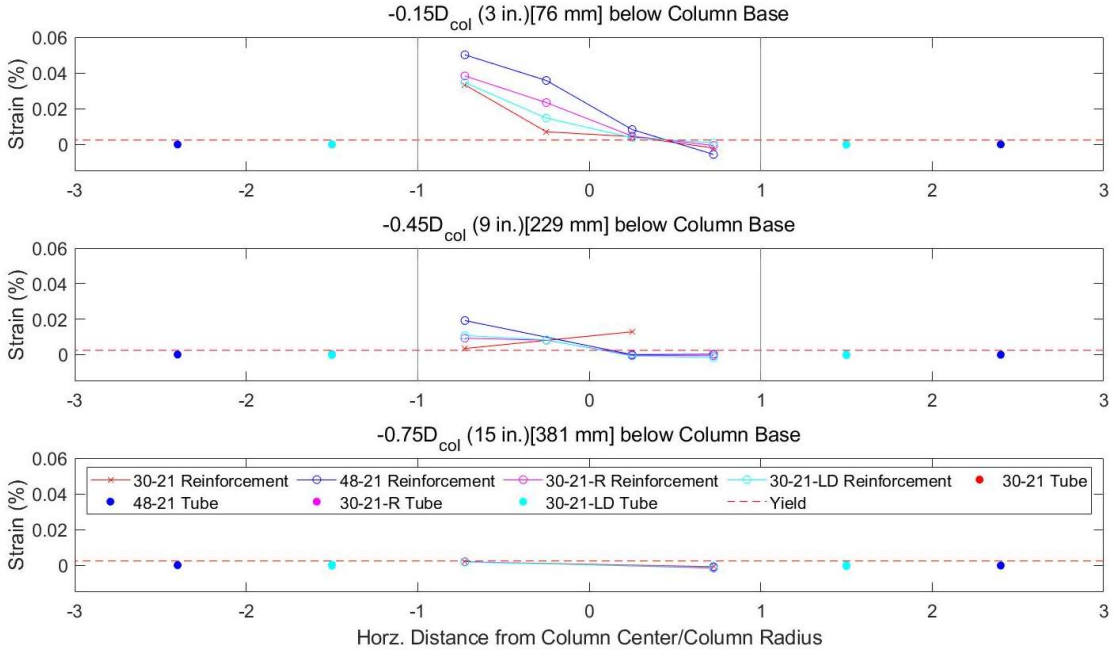

Figure 5.5. Strain Distribution at 5.0% Drift (Specimen 30-21, Specimen 48-21, Specimen 30-21-R, and Specimen 30-21-LD)

As shown in Figure 5.5, at approximately 5.0% drift, the behavior is very similar to the strain distribution at 2.2% drift, with the reinforcement strains measured at the locations -0.45D_{COL}, -0.15D_{COL}, and 0.30D_{COL} are exceeding the yield strain, and the reinforcement strains at -0.75D_{COL} are still within the yield strain. Specimen 48-21's strains are larger than the other specimens' strains. The reinforcement strains are also decreasing in magnitude as the reinforcement becomes more embedded in the pile.

For this drift level, Specimen 48-21 had the largest average tube strains, with a magnitude of $4.7*10^{-4}$ in/in, followed by Specimen 30-21's and Specimen 30-21-LD's average tube strain of $3.7*10^{-4}$ in/in. Specimen 30-21-R had the smallest average tube strain of $3.0*10^{-4}$ in/in. The tube strains increased in magnitude the farther down they are measured in the pile.

For all the strain distribution figures, Figures 5.2-5.5 above, there are several common observations. One, the strain in the reinforcement is approximately acting in plane. Two, the strains are largest in the transition region of the column-pile interface, from $0.30D_{COL}$ to $-0.15D_{COL}$. Three, the strains decrease in magnitude the deeper into the column-pile interface, where at $-0.75D_{COL}$ the reinforcement is either close to or no longer yielding. This decrease in reinforcement strain shows that the strain is transferring from the reinforcement to the tube and the CFST pile. Four, the reinforcement strains measured for Specimen 48-21 are consistently larger than the measured reinforcement strains of the other specimens. Five, at all the locations and drifts levels, the tube strains measured are incredibly small, compared to the strains in the reinforcement, but are still increasing in magnitude down the height of the pile. Six, Specimen 48-21 experienced the largest tube strains when accounting for it's larger size than the other specimens with 30 in. diameter piles, which all showed similar ranges in tube strain.

5.1.2 *Strain Profiles*

The following figures show profiles of strains in the reinforcement or the tube measured at the peaks of various drift levels. The plots may consist of up to 5 points per side of each specimen for the reinforcement strain profiles and 3 points per side of each specimen for the tube strain profiles. If there are less than 5 points on a reinforcement strain profile, this is due to a broken strain. Each specimen has a specific color and the north side strains are marked with circles and the south side strains are marked with squares. On the reinforcement strain plots, there is a vertical line at the yield strain, .0024 in./in., of the reinforcement. The tube strains used for these plots were measured using the VWGs on the side of the tube. On all plots, there is a horizontal line at 0, which is the base of the column. It is worth noting that the strain axes for the reinforcement and tube have different scales, due to the tube strains being significantly smaller in magnitude.

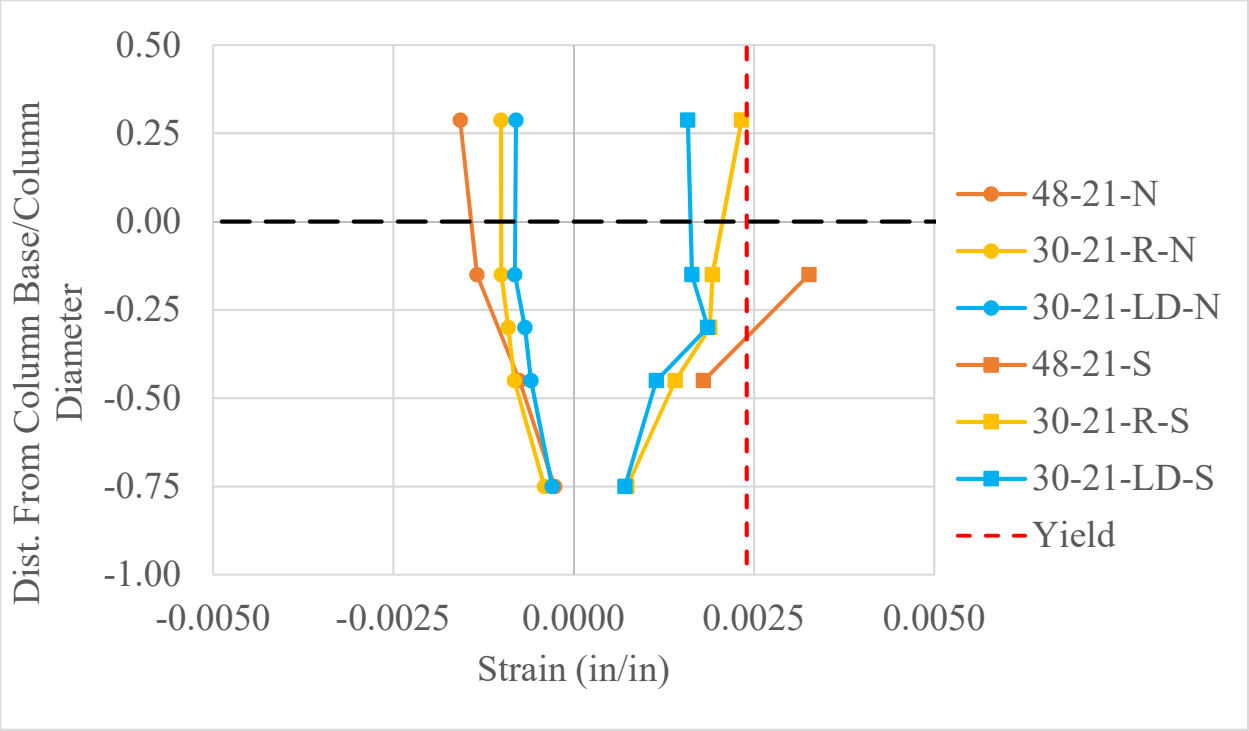

Figure 5.6. Reinforcement Strain Profile at 0.8% Drift (Specimen 48-21, Specimen 30-21-R, and Specimen 30-21-LD)

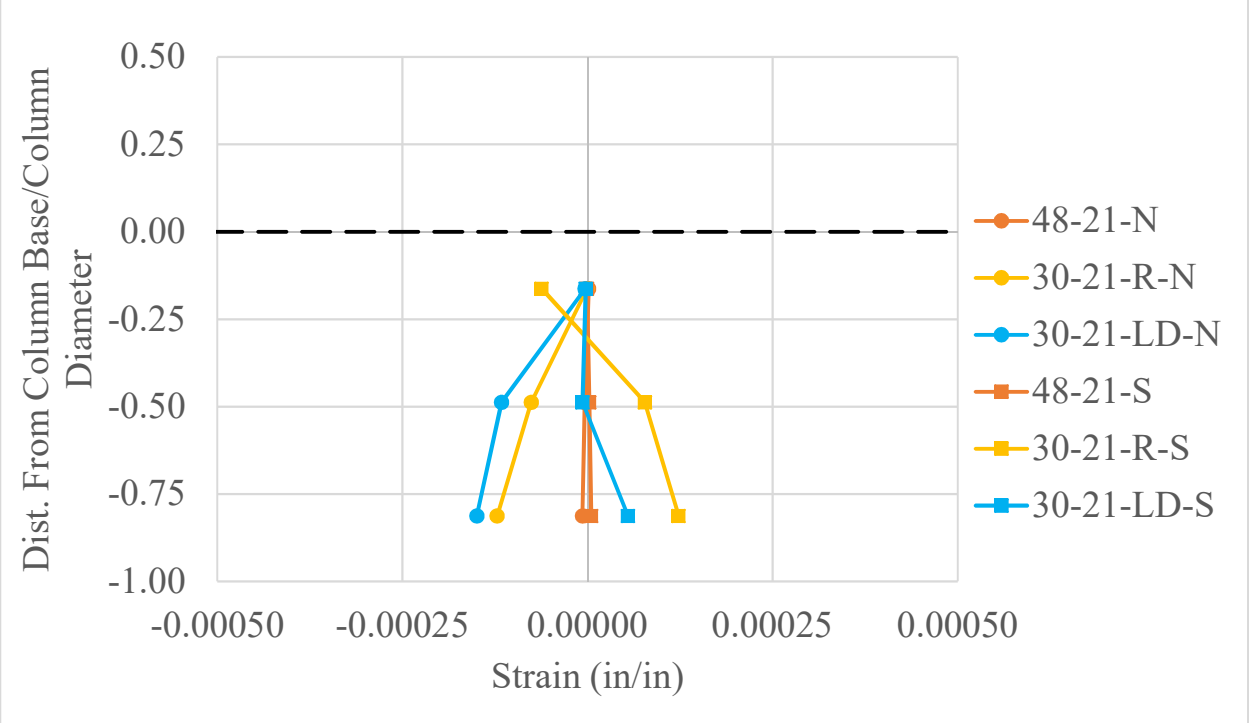

Figure 5.7. Tube Strain Profile at 0.8% Drift (Specimen 48-21, Specimen 30-21-R, and Specimen 30-21-LD)

As shown in Figures 5.6 and 5.7, the strain in the reinforcement is decreasing in magnitude as the reinforcement is farther embedded into the tube, while the strain in the tube is increasing in magnitude down the height of the tube. It can also be seen that the tube strain in Specimen 30-21-R's tube is larger than Specimen 30-21-LD's tube strain for the south side, which is the side that is loaded at this drift level, which is due to the rib transferring more force from the reinforcement to the tube.

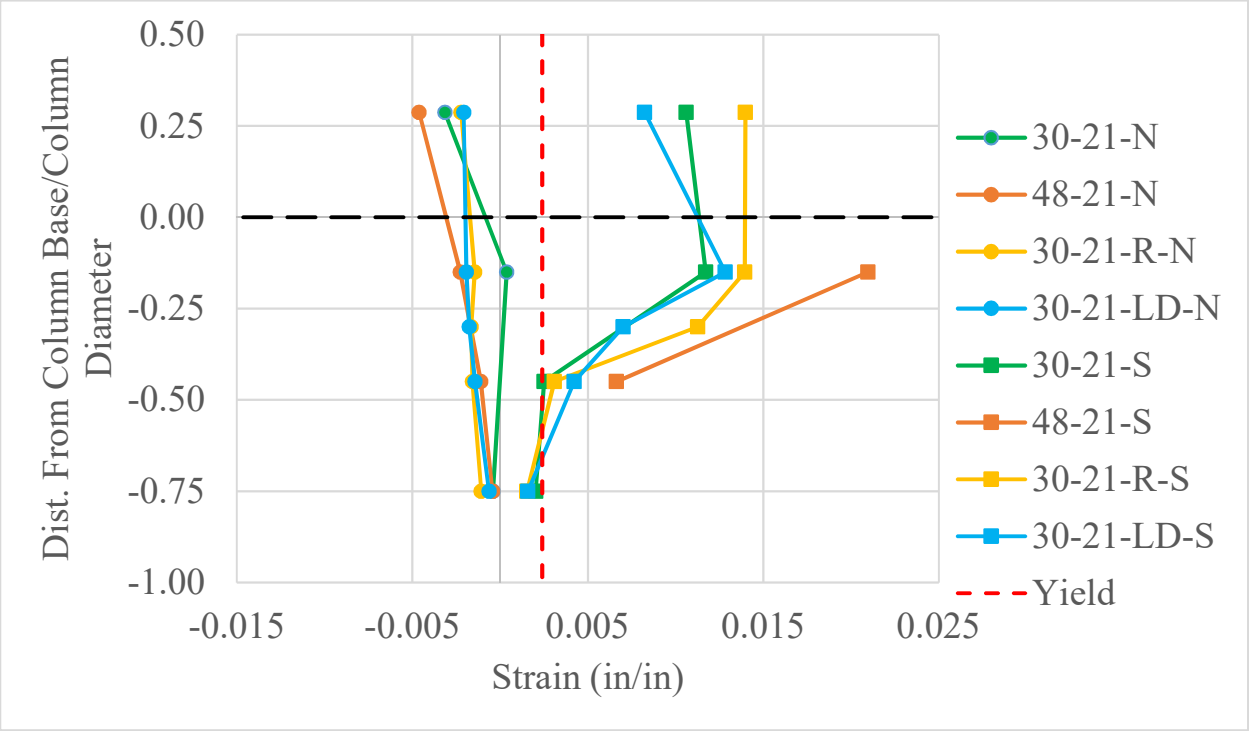

Figure 5.8. Reinforcement Strain Profile at 2.0% Drift (Specimen 30-21, Specimen 48-21, Specimen 30-21-R, and Specimen 30-21-LD)

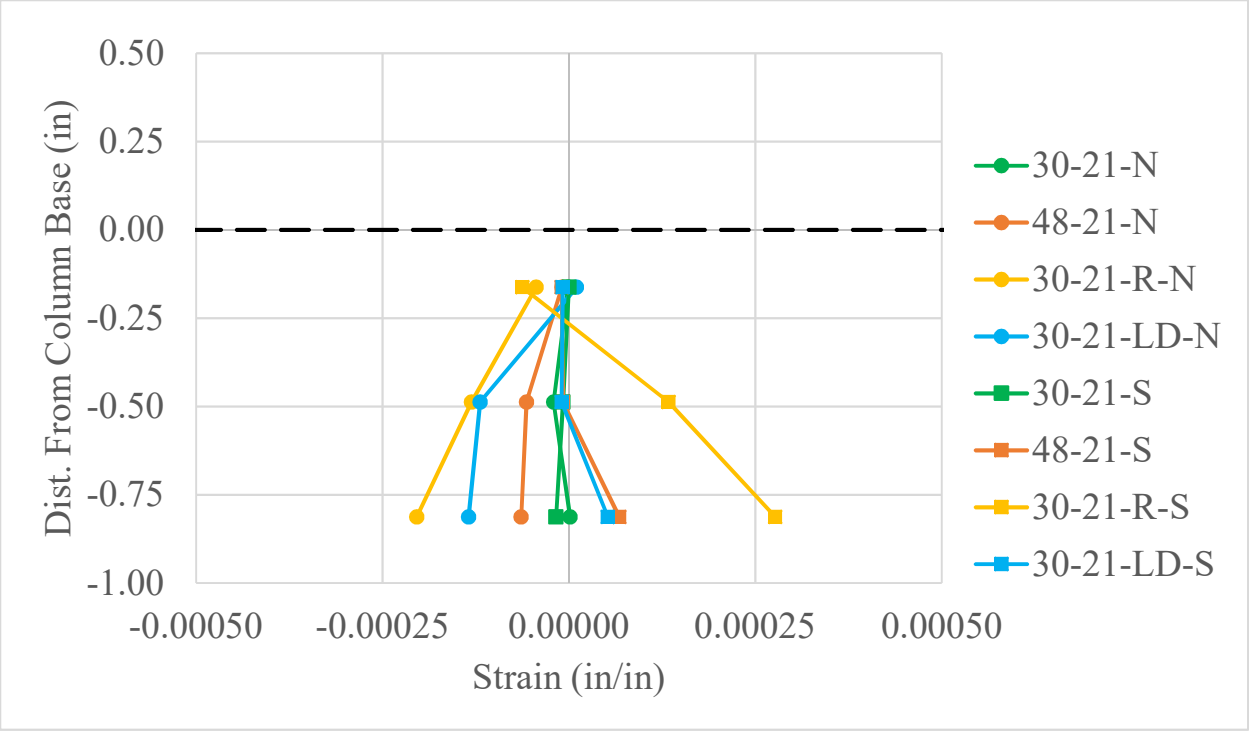

Figure 5.9. Tube Strain Profile at 2.0% Drift (Specimen 30-21, Specimen 48-21, Specimen 30-21-R, and Specimen 30-21-LD)

As shown in Figures 5.8 and 5.9, similar to the strain profiles at 0.8% drift, the strain in the reinforcement is decreasing in magnitude as the reinforcement is farther embedded into the tube, while the strain in the tube is increasing in magnitude down the height of the tube. The strains in the reinforcement are also decreasing in magnitude to the point the reinforcement is still in the elastic region at $-0.75D_{COL}$. It can also be seen that the strain in Specimen 30-21-R's tube is larger than the tube strains in specimens 30-21-LD and 30-21, this is due to the rib transferring more force from the reinforcement to the tube.

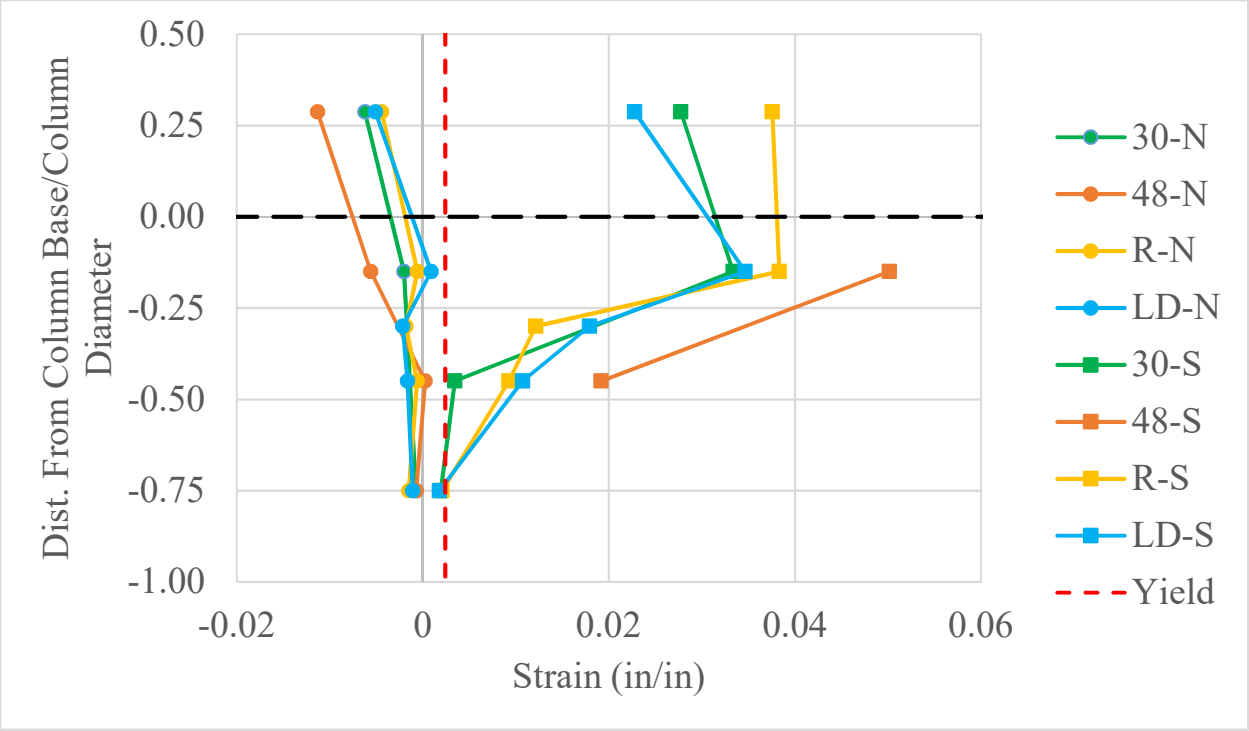

Figure 5.10. Tube Strain Profile at 2.0% Drift (Specimen 30-21, Specimen 48-21, Specimen 30-21-R, and Specimen 30-21-LD)

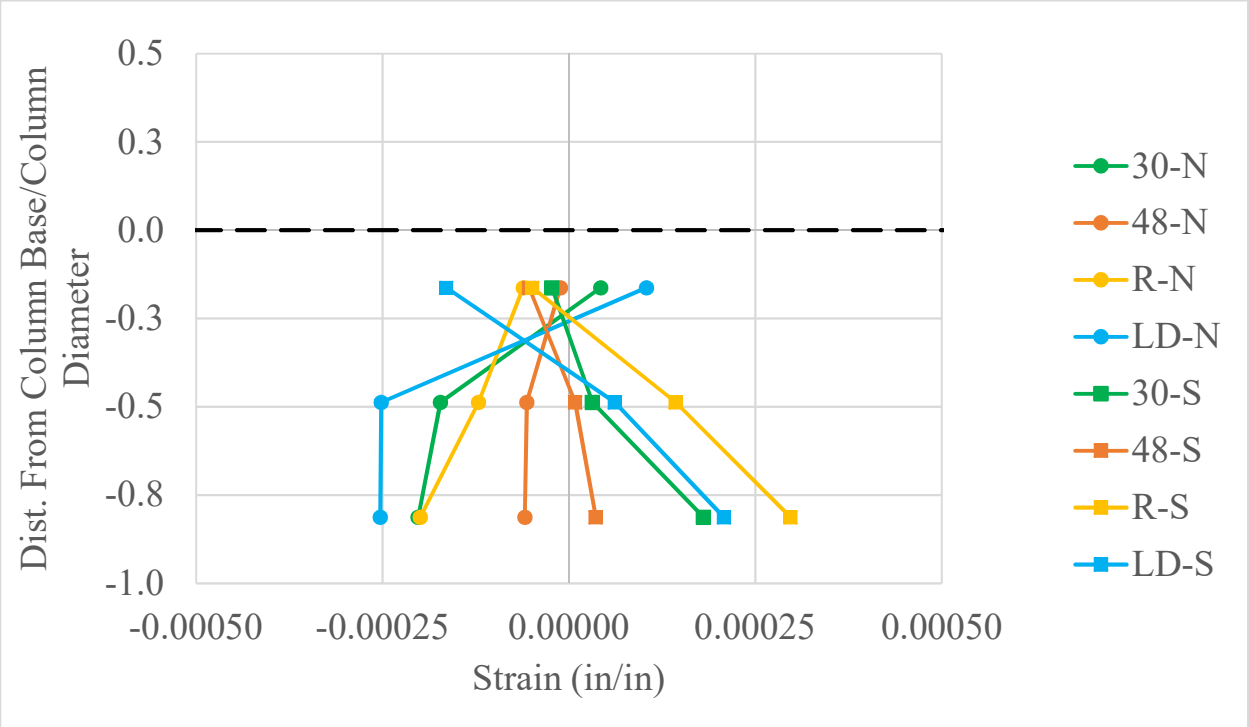

Figure 5.11. Tube Strain Profile at 5.0% Drift (Specimen 30-21, Specimen 48-21, Specimen 30-21-R, and Specimen 30-21-LD)

As shown in Figures 5.10 and 5.11, similar to the strain profiles at 0.8% and 2.0% drift, the strain in the reinforcement is decreasing in magnitude as the reinforcement is farther embedded into the tube, while the strain in the tube is increasing in magnitude down the height of the tube. The strains in the reinforcement are also decreasing in magnitude to the point the reinforcement is still in the elastic region at $-0.75D_{COL}$. It can also be seen that the strain in Specimen 30-21-R's tube is larger than the tube strains in specimens 30-21-LD and 30-21, this is due to the rib transferring more force from the reinforcement to the tube.

For all the strain profile figures, Figures 5.6-5.11, there are a few common observations. One, the reinforcement strains decrease in magnitude the deeper into the column-pile interface, where at $-0.75D_{COL}$ the reinforcement is still in the elastic range, while the tube strains increase in magnitude the farther down the tube. This behavior shows that the strain is transferring from the reinforcement to the tube and the CFST pile. Two, Specimen 30-21-R consistently had the largest tube strain for the side being loaded, followed by Specimen 30-21 and 30-21-LD, which had similar strain magnitudes. This shows that the ring aids the transfer of force from the column reinforcement to the tube or pile. Three, as stated in Section 5.1.1, the strains in Specimen 48-21 are the smallest of the four specimens due to the specimen's significantly larger stiffness.

The strain distribution plots and strain profiles exemplify five conclusions about the connection. One, the current embedment depth of the reinforcement is more than sufficient for this connection since the bottom strain gauge locations are either not exceeding the yield strain, therefore the reinforcement at this location is still in the elastic range. Two, at $-0.75D_{COL}$ the strain measured on both the reinforcement and tube are almost acting in-plane, while at any of the other locations above $-0.75D_{COL}$ the strains from the reinforcement and tube are not acting in plane. This relationship between the reinforcement and tube strains shows composite action between the

column connection and the CFST is close to occurring and might be occurring a farther into the tube. This is also exemplified by the behavior of the reinforcement and tube strains. The farther down into the connection the magnitude of the reinforcement strains is decreasing, while the tube strains are increasing. Three, Specimen 48-21's reinforcement strains are reaching higher magnitudes of strain than the other specimens as the drift levels are increasing, which means it has more of its deformability is coming from the connection. Four, due to the low levels of strain the tube experienced for all drift levels and locations, the pile was not near its maximum capacity and performed very well. Five, Specimen 48-21 experienced more tube strain than the other 30 in. diameter specimens when accounting for its larger stiffness, which shows that there was less slip between the tube and the connection concrete for Specimen 48-21. The tube strains for the 30 in. diameter specimens were of similar magnitude, but Specimen 30-21-R had the largest strains of the three specimens. This shows that the embedded rib is aiding the transfer of force from the reinforcement to the pile. As mentioned in Sections 4.5.3 and 4.6.3, the measured slip of Specimen 30-21-R, 0.003 in., was significantly less than the measured slip of Specimen 30-21-LD, 0.05 in. This shows another benefit that the embedded rib has on the connection.

5.2 DEFORMATION PROFILES

The external deformations of the specimen were measured using string and Duncan potentiometers as described in Chapter 3. Using the displacements measured from these instruments the displacement and average curvature of each specimen were calculated.

5.2.1 *Displacement Profiles*

Specimen displacements were measured using string potentiometers along the height of the column and pile. As mentioned before the string potentiometers were attached to an independent reference tower, as to not be affected by the testing rig setup.

Figures 5.12-5.15 show the displacement vs. height at the peaks and valleys of select drift cycles. The drift ratio is defined as displacement at the point of loading divided by column length, Δ/Lcol.

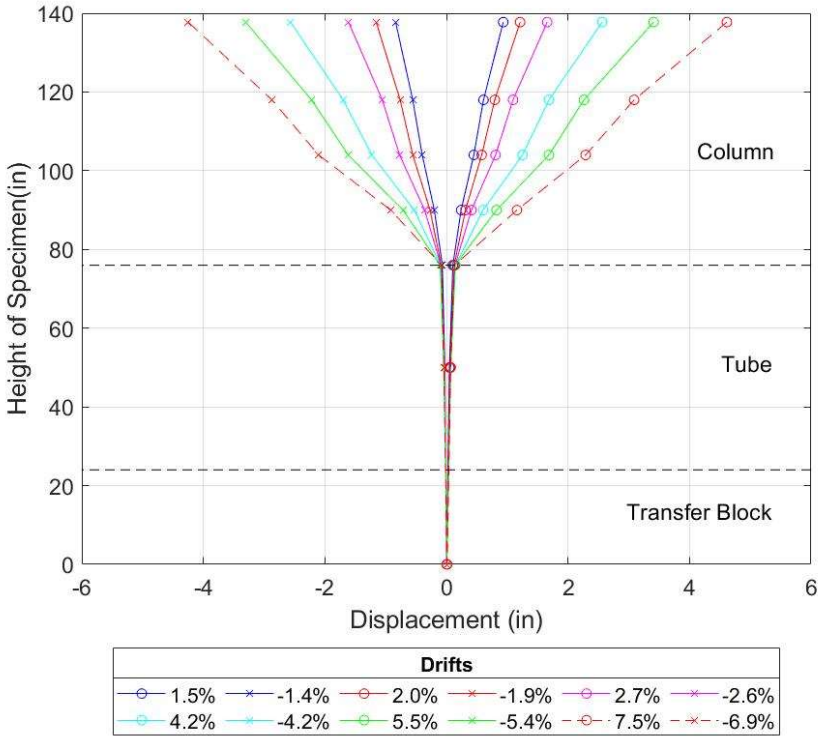

Figure 5.12. Specimen 30-21 Displacement Profile

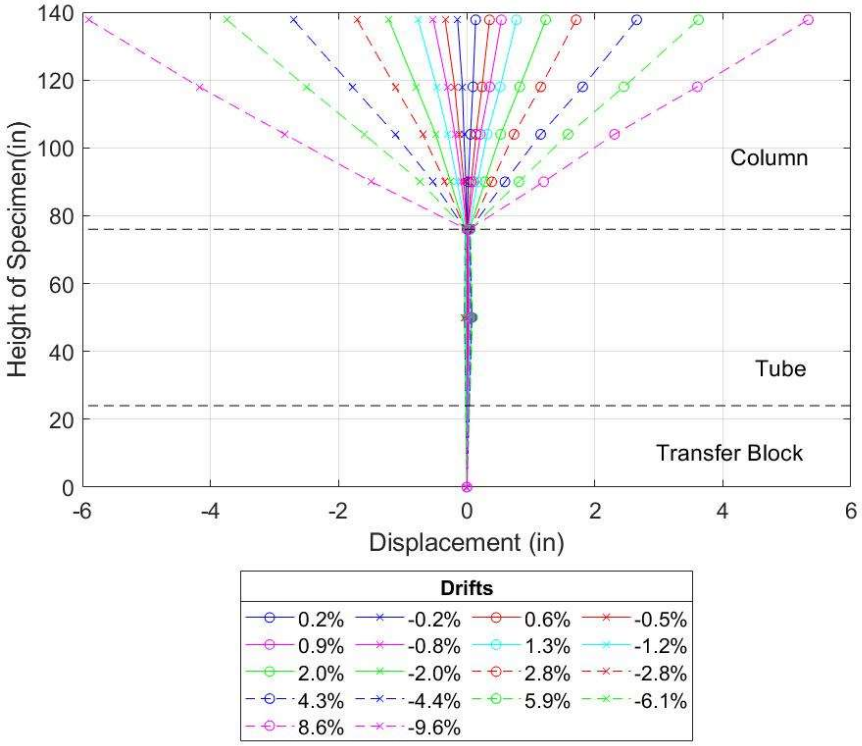

Figure 5.13. Specimen 48-21 Displacement Profile

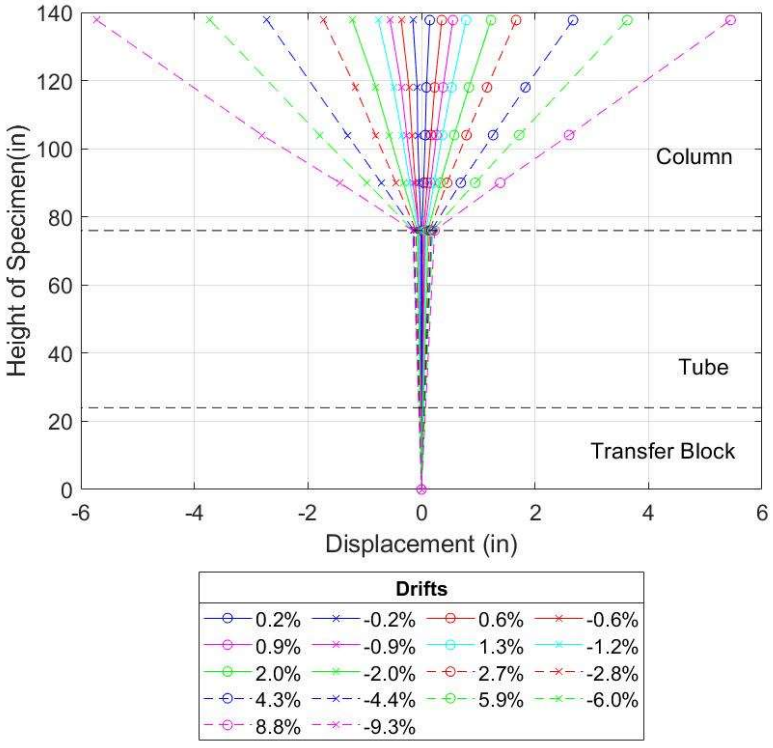

Figure 5.14. Specimen 30-21-R Displacement Profile

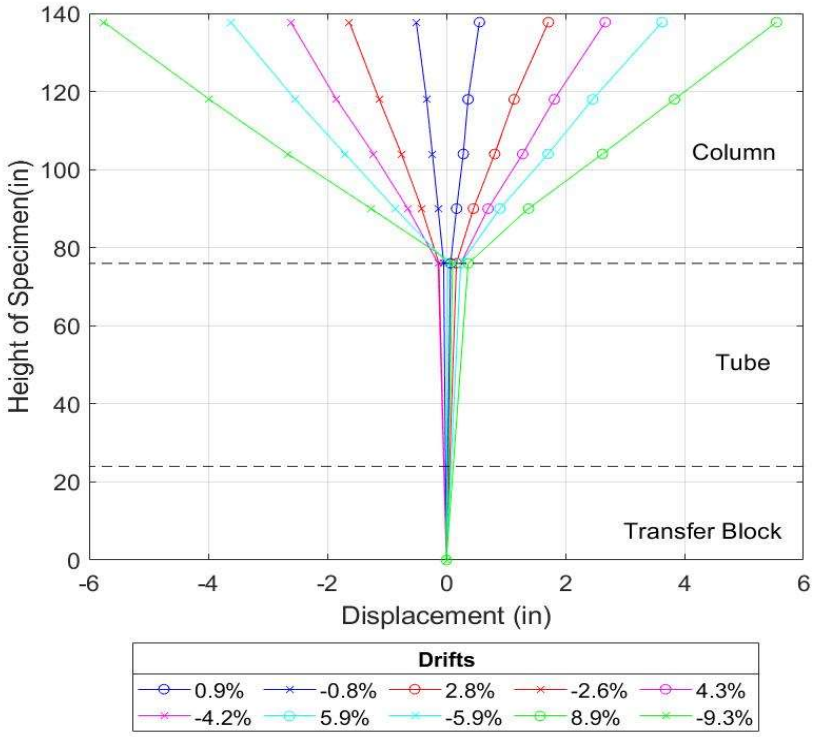

Figure 5.15. Specimen 30-21-LD Displacement Profile

There are a few observations to be noted from Figures 5.12-5.15. One, the displacement is almost entirely in the column, with minimal displacement in the tube and no displacement in the transfer block, which can be shown where the slope of the line increases drastically at the tube-column interface at approximately 76 in. Two, while minimal, the 30 in. tubes do have more lateral displacement than the 48 in. tube, which is due to the 30 in. tubes having a much smaller stiffness than the 48 in. tube. Three, of the three specimens with 30 in. tubes, Specimen 30-21-LD has the largest lateral displacement. Four, the tube and column segments are almost completely straight, this shows there is minimal rotation in the tube, the largest beings Specimen 48-21's rotation, and the majority of the column rotation is at the base of the column, where the slope changes drastically.

5.2.2 *Curvature Profiles*

Average curvatures for each specimen's column were computed using the vertical potentiometers going along the height of the column. The equation is given as:

$$\Phi = \left(\frac{\Delta_{N-DP} - \Delta_{S-DP}}{B}\right) * \frac{1}{H_{seg}}$$

Where

Φ= average curvature of the segment

Δ_{N-DP}= Vertical displacement on the north side of the specimen

Δ_{S-DP}= Vertical displacement on the south side of the specimen

B=horizontal distance between the two measurement locations

H_{seg}= height of the segment

The measurements from the instruments located between 11% and 17% of the column height (7 in. and 10.5 in. from the base of the column) were removed for Specimens 30-21, 48-21, and 30-21-R, and the instruments located between 6% and 11% of the column height (3.5 in. and 7 in.) from the base of the column were removed for specimen 30-21-LD. The removal of these instruments is due to incorrect measurements from the instruments during the test. The instrument measurements did not have the expected behavior as seen with the other instruments. Figure 5.16 is a comparison of instrument measurements at similar drift levels for Specimens 30-21 and 30-21-LD, which had identical construction.

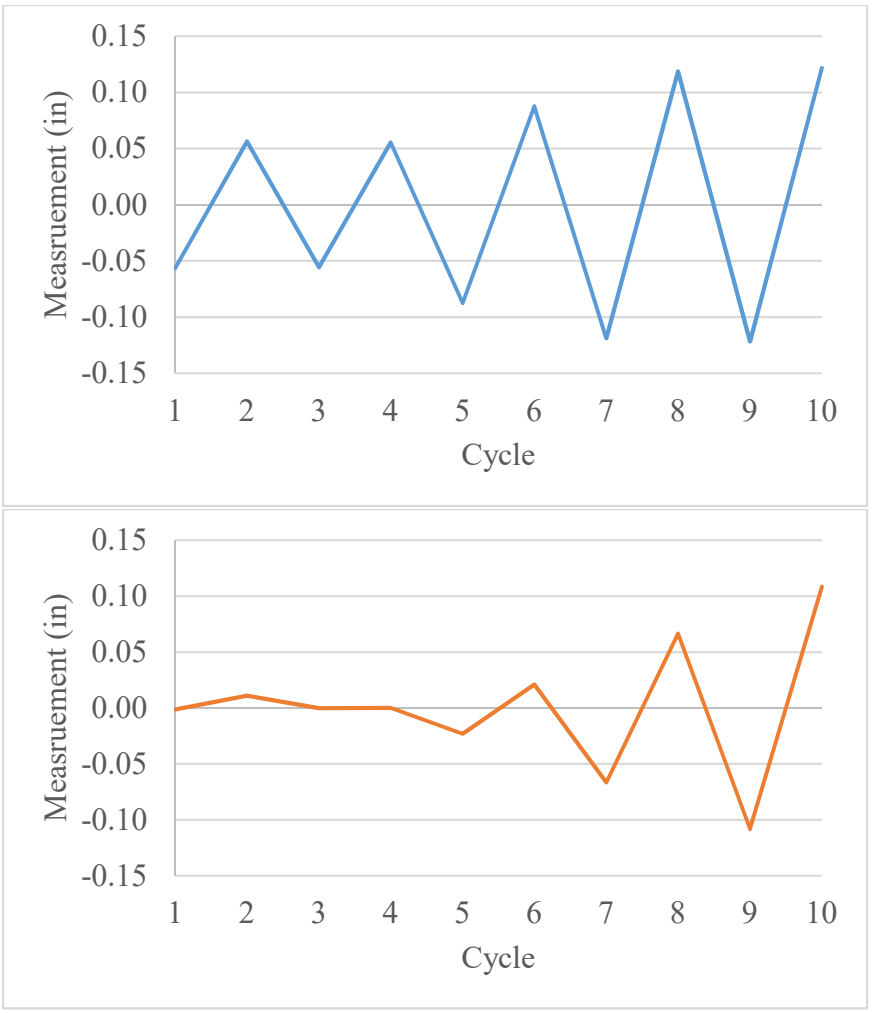

Figure 5.16. Comparison of a) Specimen 30-21's and b) Specimen 30-21-LD's Instrument Measurements Between 6% and 11% of the Column Height (3.5 in. and 7 in.) Above the Column Base

As shown in Figure 5.16, for cycles 1-6, which are drift levels 3.8% and smaller, Specimen's 30-21-LD measurements are significantly smaller than Specimen 30-21's measurements, but for cycles 7-10, which are drift levels 5% and greater, the measurements are comparable to each other. The other instruments measuring column flexure also have similar patterns to these two instruments. The plots were corrected by extending the average curvature from the above and below segments, whose instruments were not giving incorrect measurements to make up for the missing segment. The average column curvature vs. the percentage of column height figures for all specimens are shown in Figures 5.17-5.20.

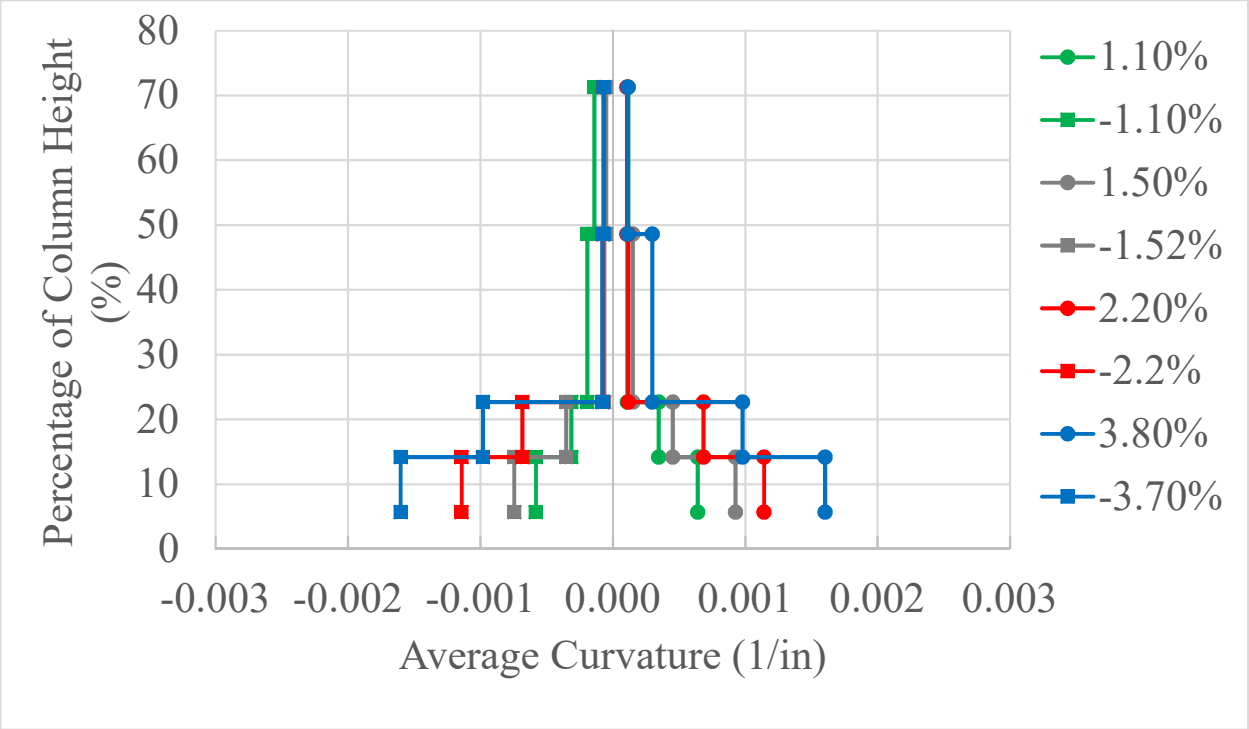

Figure 5.17. Specimen 30-21 Curvature Profile

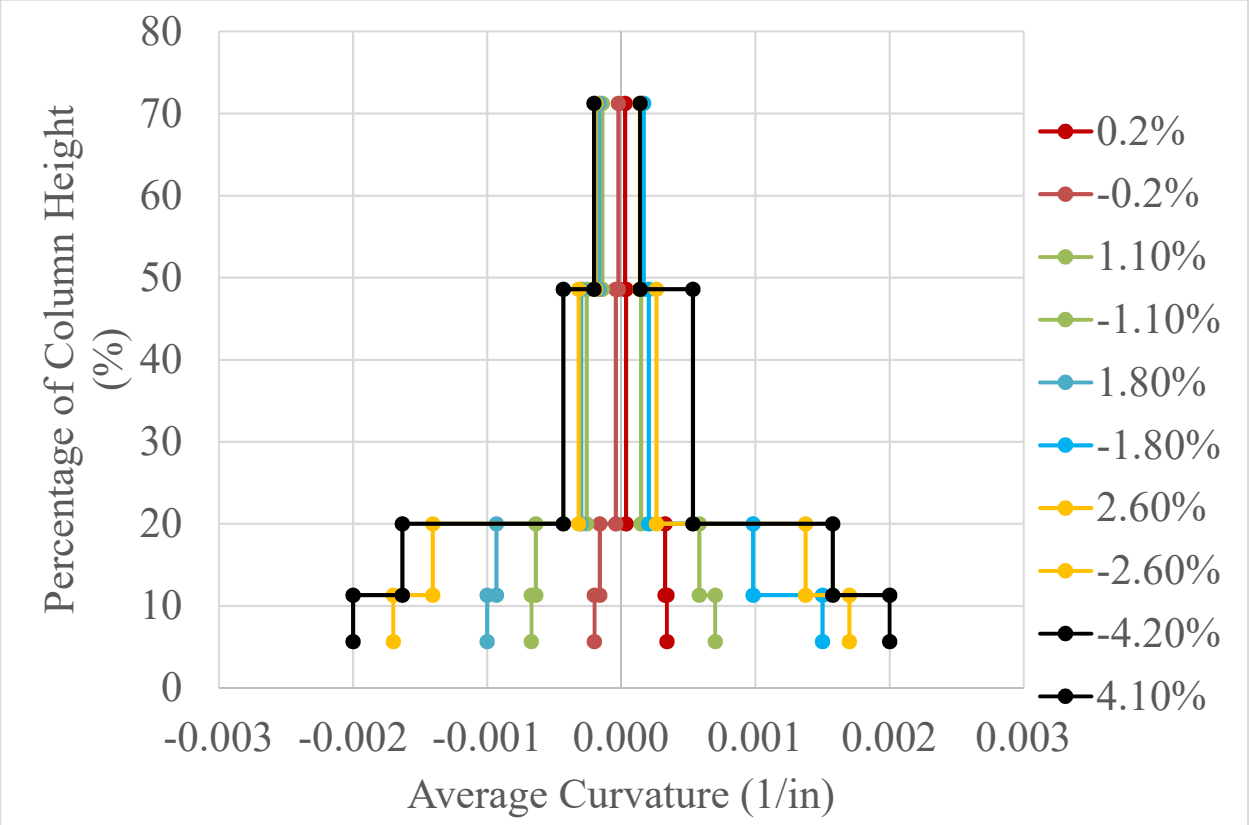

Figure 5.18. Specimen 48-21 Curvature Profile

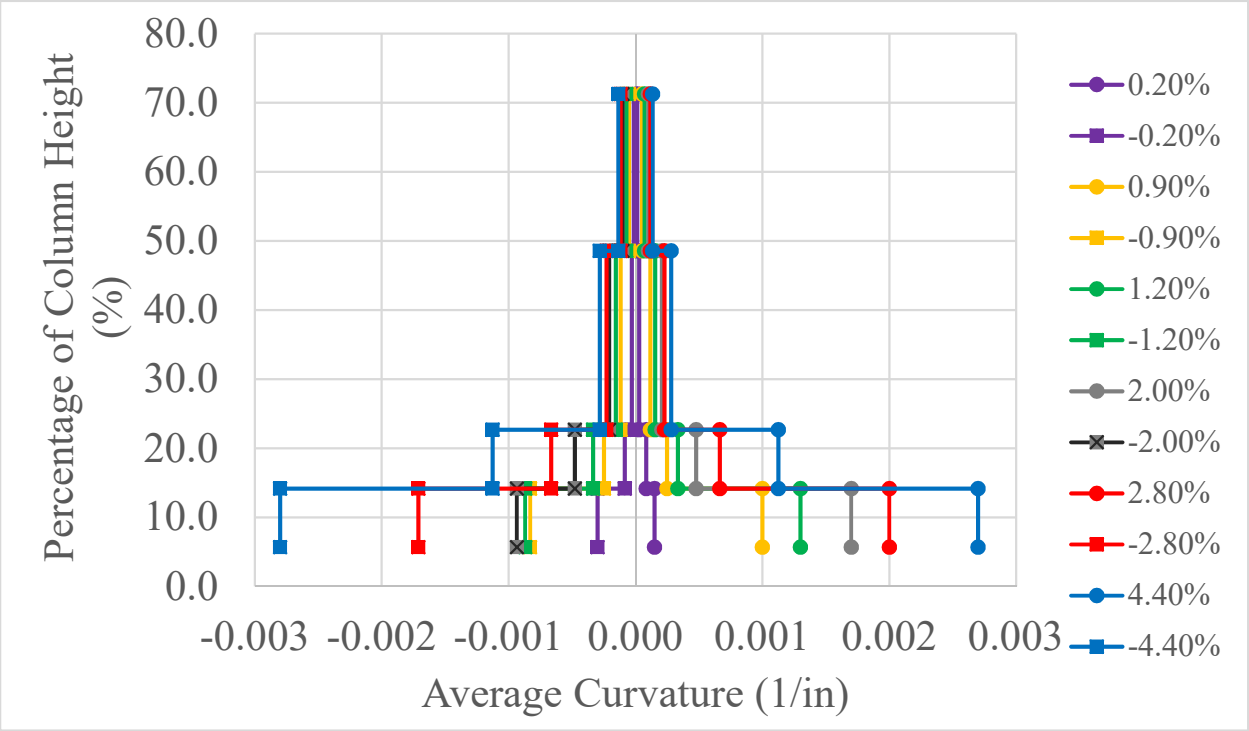

Figure 5.19. Specimen 30-21-R Curvature Profile

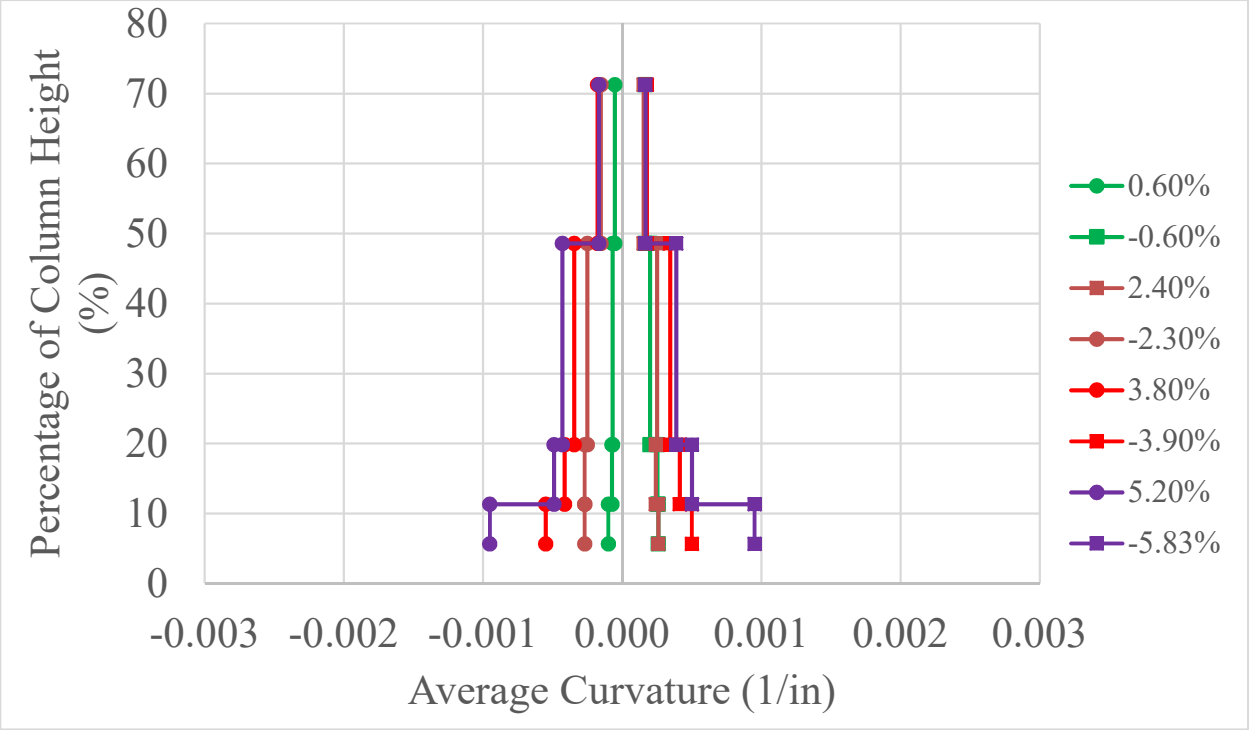

Figure 5.20. Specimen 30-21-LD Curvature Profile

As shown in Figures 5.17-5.20, for all the specimens, the average curvature was largest at the base of the column and increased with increase drift ratios. The average curvatures were relatively consistent for Specimens 30-21, 48-21, and 30-21-R. Specimen 30-21-LD's curvature range is significantly smaller for all drift levels, less than 5% drift. This is due to the incorrect instrument measurements described earlier in the section for the smaller drift levels. However, using the specimen displacement profiles, Figures 5.12-5.15 in Section 5.2.1, we can see that the majority of the rotation is at the base of the column, which confirms the general behavior of the curvature profiles. At the larger drift level, 5% and greater, the curvature at the base is still relatively smaller than the other specimens, this is reflected in Section 5.2.3, with Specimen 30-21-LD having slightly smaller displacement due to column flexure than the other specimens. The effects of this error are detailed in Section 5.2.3. The purpose of these figures is for calculating the displacement due to column flexure, which is described in Section 5.2.3.

5.2.3 *Contributions to Total Displacement*

The horizontal displacement at the point of loading for each of the specimens was broken down into four different types of deformations.

1. Pile Displacement, i.e. lateral displacement of CFST
2. Pile End Rotation, i.e. rigid body rotation of the specimen
3. Connection Displacement, i.e. deformation due to elongation and shortening of column reinforcement into the connection to the pile
4. Column flexural deformations

The pile displacement is measured using the string potentiometer that is attached to the top of the pile.

The pile end rotation uses the rotation of a point for a cantilevered beam with a concentrated load at the free end of the beam. It assumes that the pile stays elastic for all cycles.

The connection displacement was calculated using the rotation at the base of the column relative to the top of the tube. This rotation, along with the height of the column to the point of loading, was used to calculate the displacement due to the connection of the specimen. The connection displacement rotation is measured using the instruments located at 3.5 in. above the base of the column.

The column flexural displacement was calculated using the curvature profiles in Section 5.2.2 and the Second Moment-Area theorem. The column flexure displacement is calculated using the instruments located at 7 in. above the column base up the point of loading.

Not all the displacement contributions add up to the measured displacement magnitude, with some drifts having calculated displacement totals less than or greater than the measured displacement. This difference or error comes from all the calculations of the different mechanisms. It can still be seen in the figures that the general behavior of the contributions is consistent, with displacement due to the connection and displacement due to column flexure being the primary components of the specimen's combined displacement.

Not all drift levels are plotted to avoid repetition and cluttering of the figures. However, the different displacement contributions are similar at the same drift level, whether it is the first cycle or second cycle at that drift level, or, in the case of Specimen 30-21-LD, the multiple cycles following the first one. Also, none of the final cycles, drift greater than 9%, are plotted. This is because during these cycles the column was failing and falling apart, therefore the measurements taken during these cycles were inaccurate and not used.

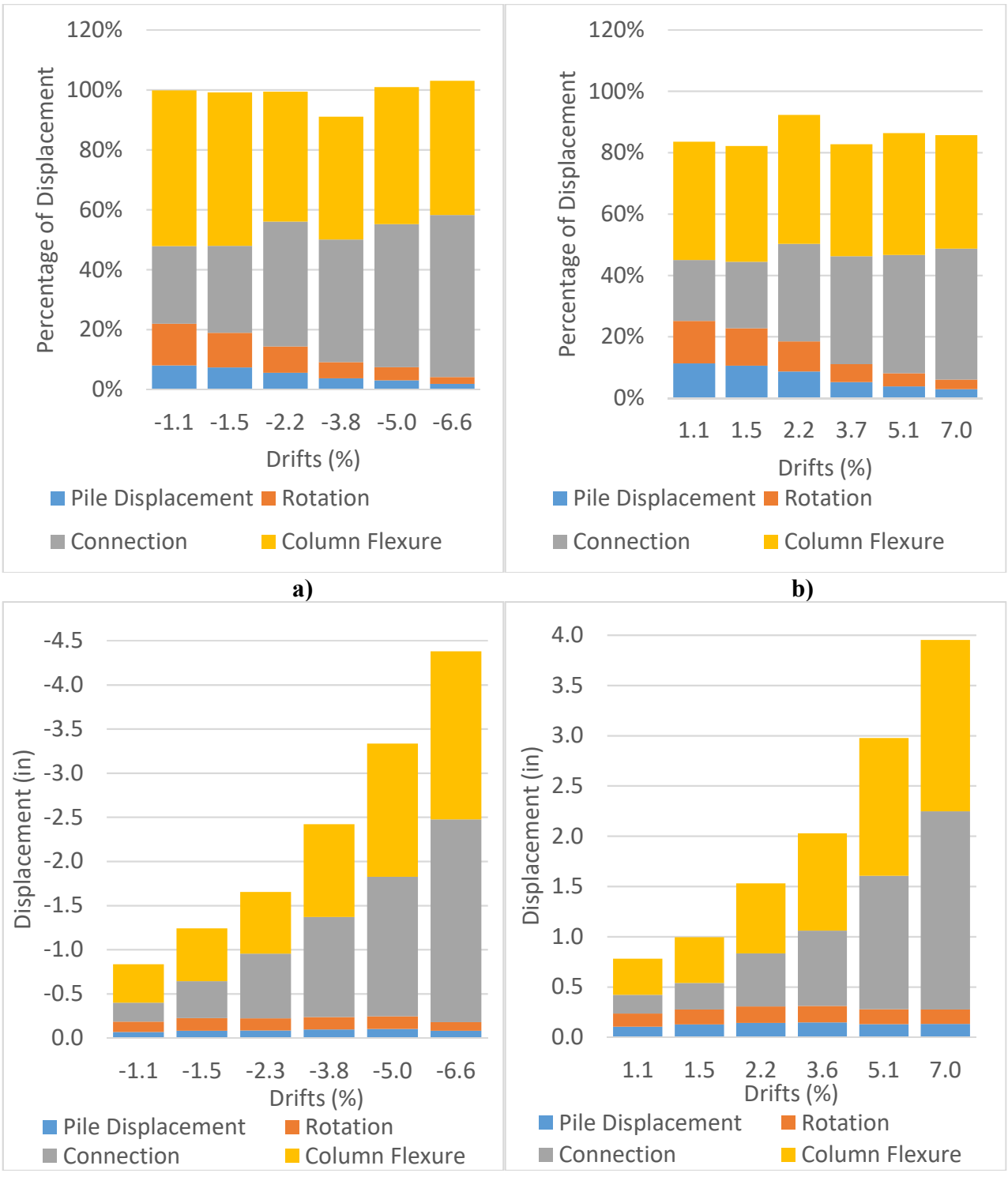

Figure 5.21. Specimen 30-21 Displacement Contributions: a) Negative Drift Percentages, b) Positive Drift Percentages, c) Negative Drift Magnitudes and d) Positive Drift Magnitudes

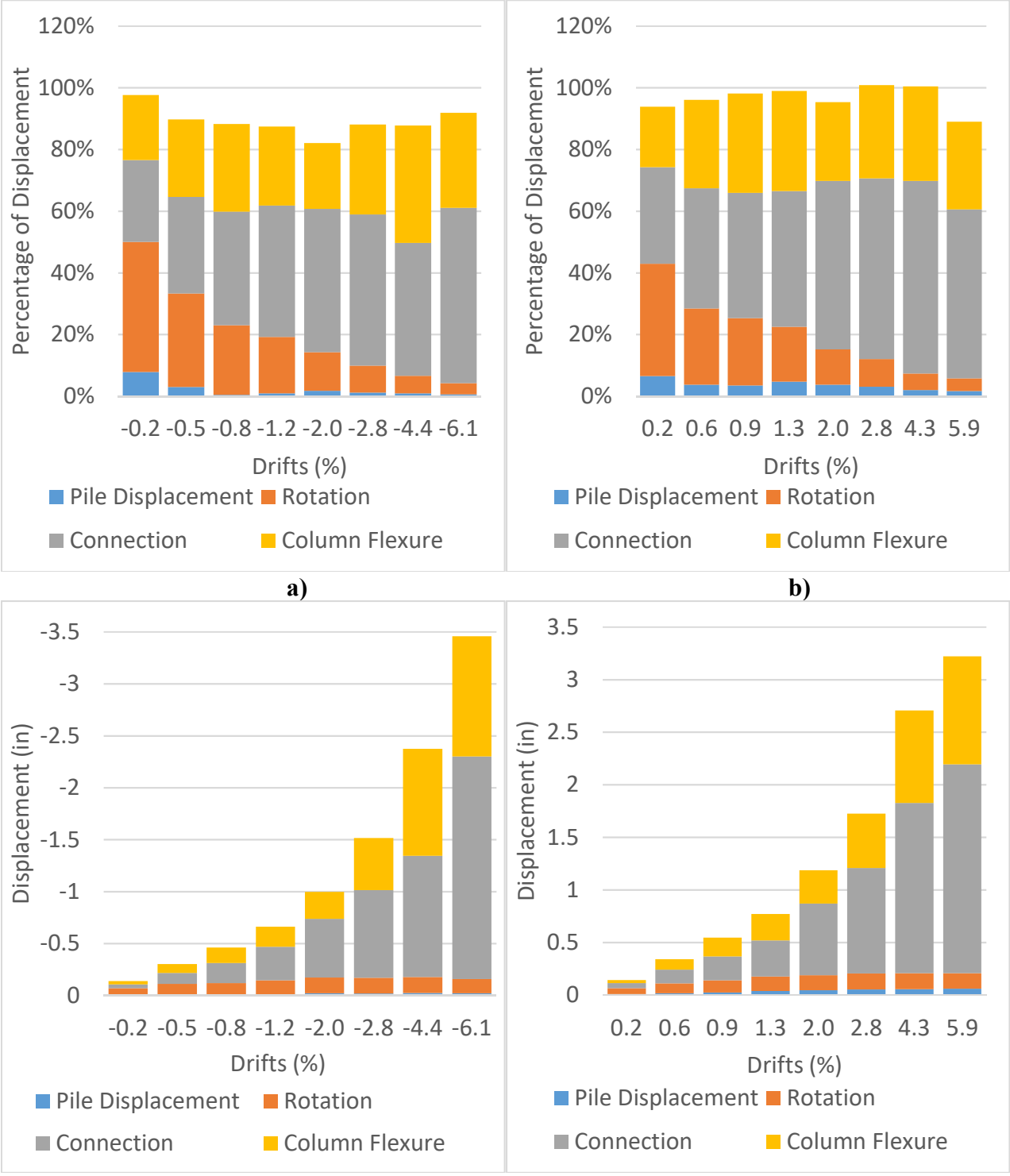

Figure 5.22. Specimen 48-21 Displacement Contributions: a) Negative Drift Percentages, b) Positive Drift Percentages, c) Negative Drift Magnitudes and d) Positive Drift Magnitudes

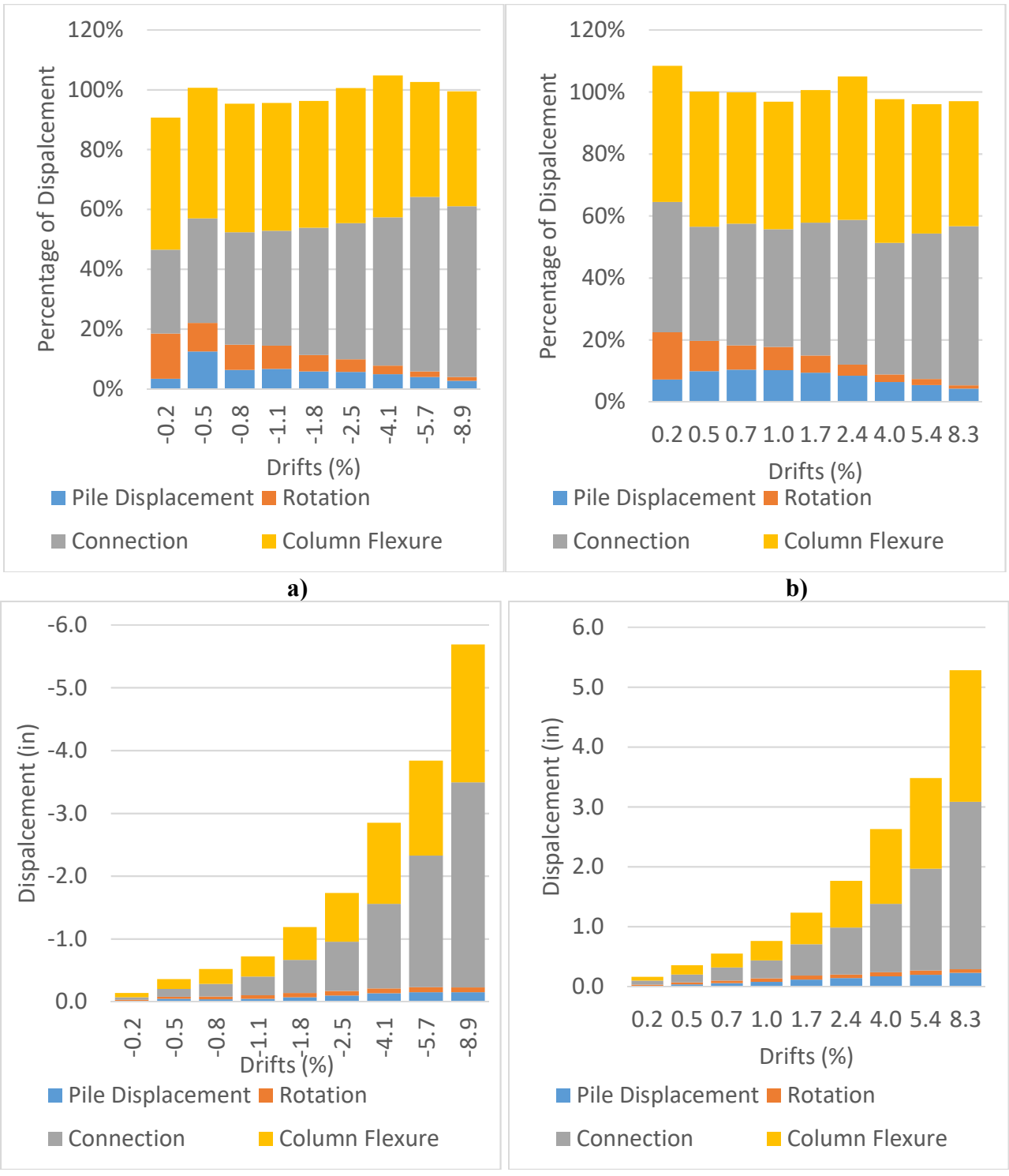

Figure 5.23. Specimen 30-21-R Displacement Contributions: a) Negative Drift Percentages, b) Positive Drift Percentages, c) Negative Drift Magnitudes and d) Positive Drift Magnitudes

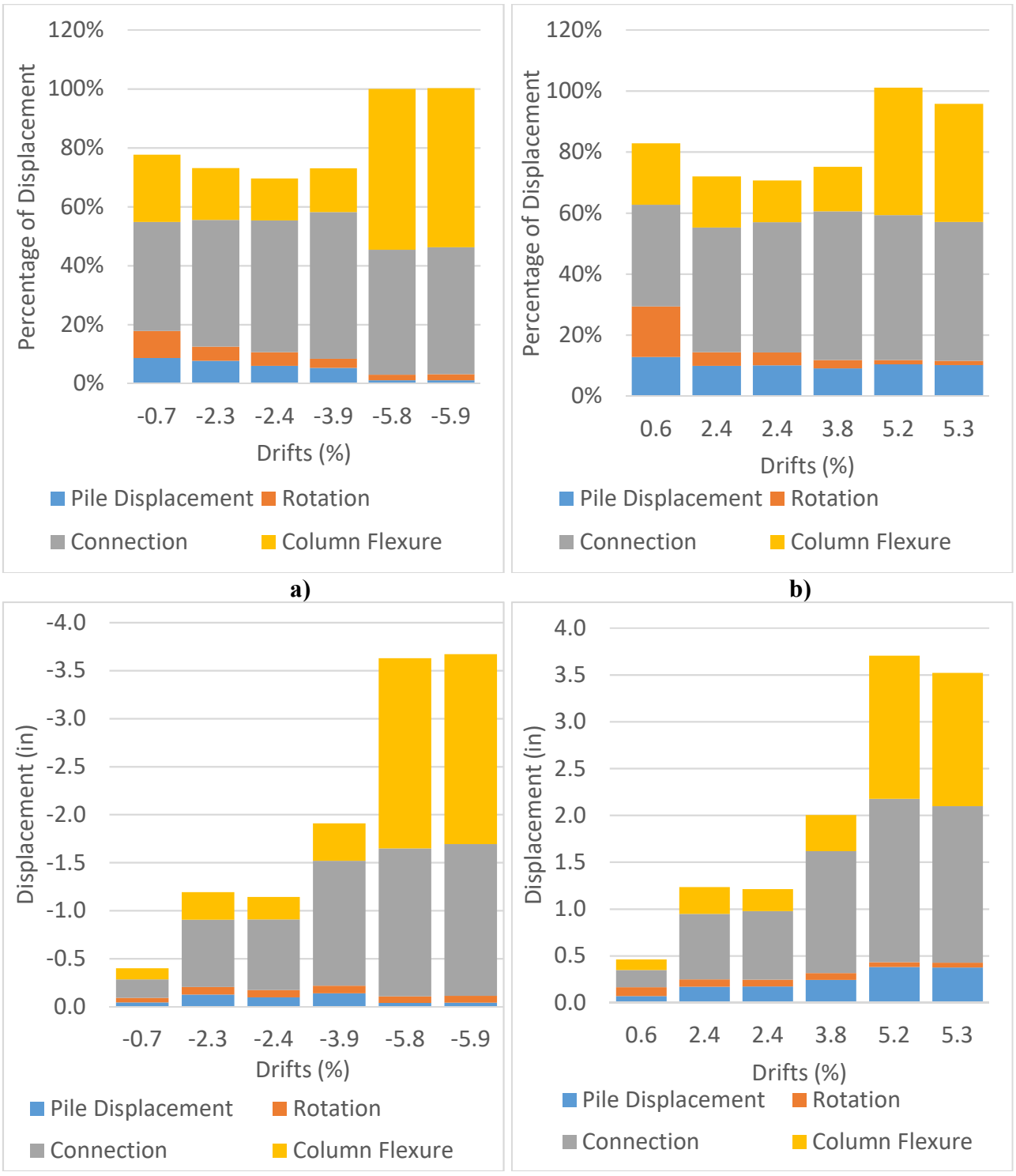

Figure 5.24. Specimen 30-21-LD Displacement Contributions: a) Negative Drift Percentages, b) Positive Drift Percentages, c) Negative Drift Magnitudes and d) Positive Drift Magnitudes

As shown in Figure 5.24 the displacement contribution figures for Specimen 30-21-LD, at drift levels less than 5.8% there is a significant difference, over 20%, in the calculated displacement and the measured displacement. This difference is due to the calculated column flexure displacement being significantly smaller than the other specimens. For the larger drift levels for Specimen 30-21-LD and the other specimen plots, displacement due to column flexure is typically around 40% of the total displacement, while for these small drift levels on Specimen 30-21-LD, the column flexure is 20% or less of the total displacement. This is caused by the error from the incorrect instrument measurements described in Section 5.2.2. However, since the source of error for the smaller drift levels has been identified, the displacement contributions graphs for 30-21-LD can be used in conjunction with the other specimen graphs to make some key points.

There are three key points to take away from the comparison displacement contribution plots, Figures 5.25 and 5.26. One, the displacement of the specimen is primarily due to the displacement due to the column connection, approximately 50% of total displacement, and the flexural displacement of the column, approximately 45% of total displacement. This is also confirmed by the displacement profiles in Section 5.2.1, where Figures 5.12-5.15 show minimal displacement due to the pile, and the contribution of pile rotation is largest for Specimen 48-21, followed by specimens 30-21, 30-21-R, and 30-21-LD. Two, as the displacement of the specimen increases, the displacement due to pile displacement and rotation decreases, while the displacement due to the column connection increases, and the displacement due to column flexure stays constant. Three, Specimen 48-21's displacement due to the column connection was a larger percentage of the total displacement than the other specimens with 30 in. piles. This observation, along with the strain distribution plots in Section 5.1, shows that there is more flexural deformability in Specimen 48-21's connection than the other specimens.

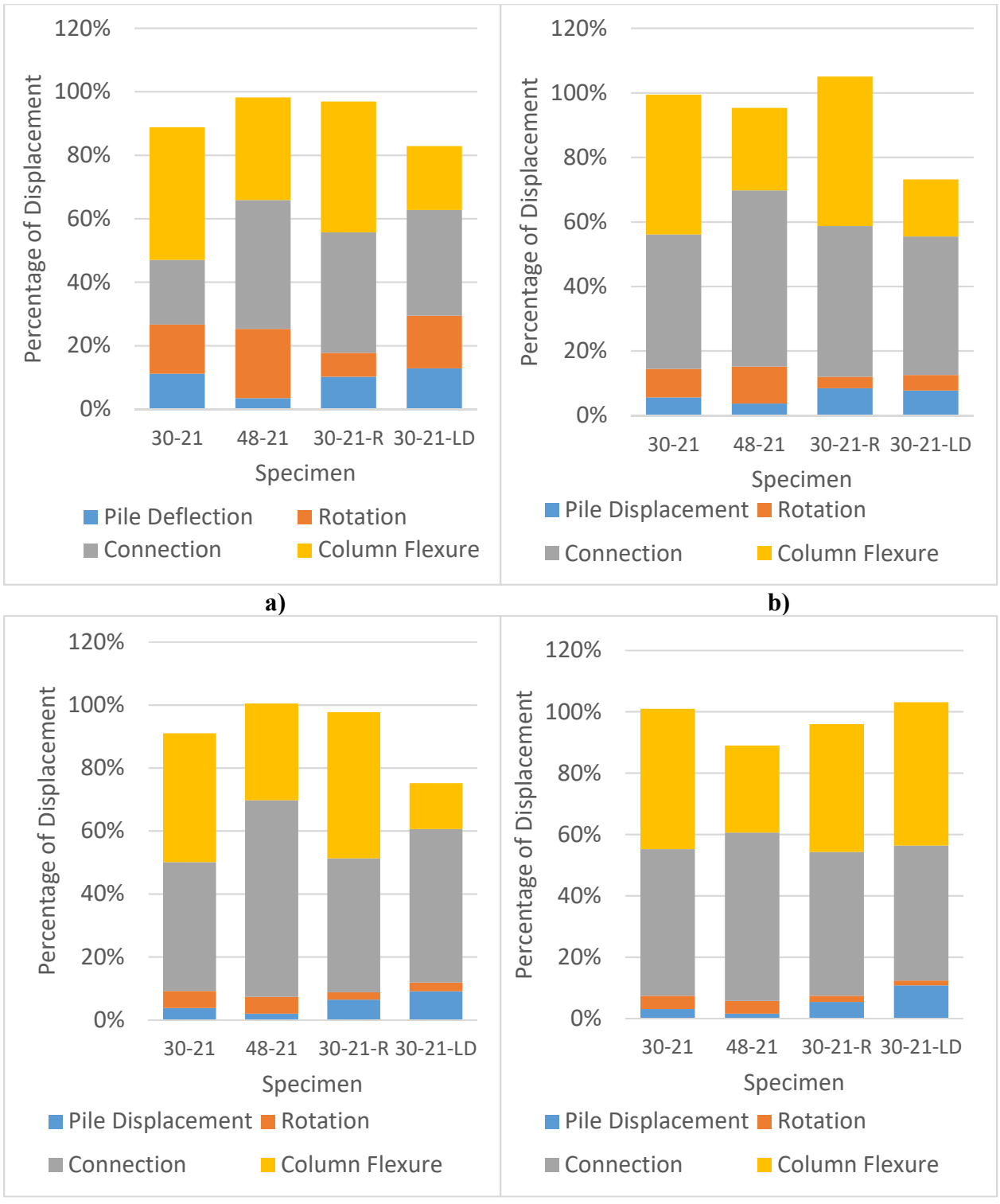

Figure 5.25. Comparison of Displacement Contributions Percentages at: a) approx. 1% Drift, b) approx. 2.5% Drift, c) approx. 4% Drift, and d) approx. 5% Drift

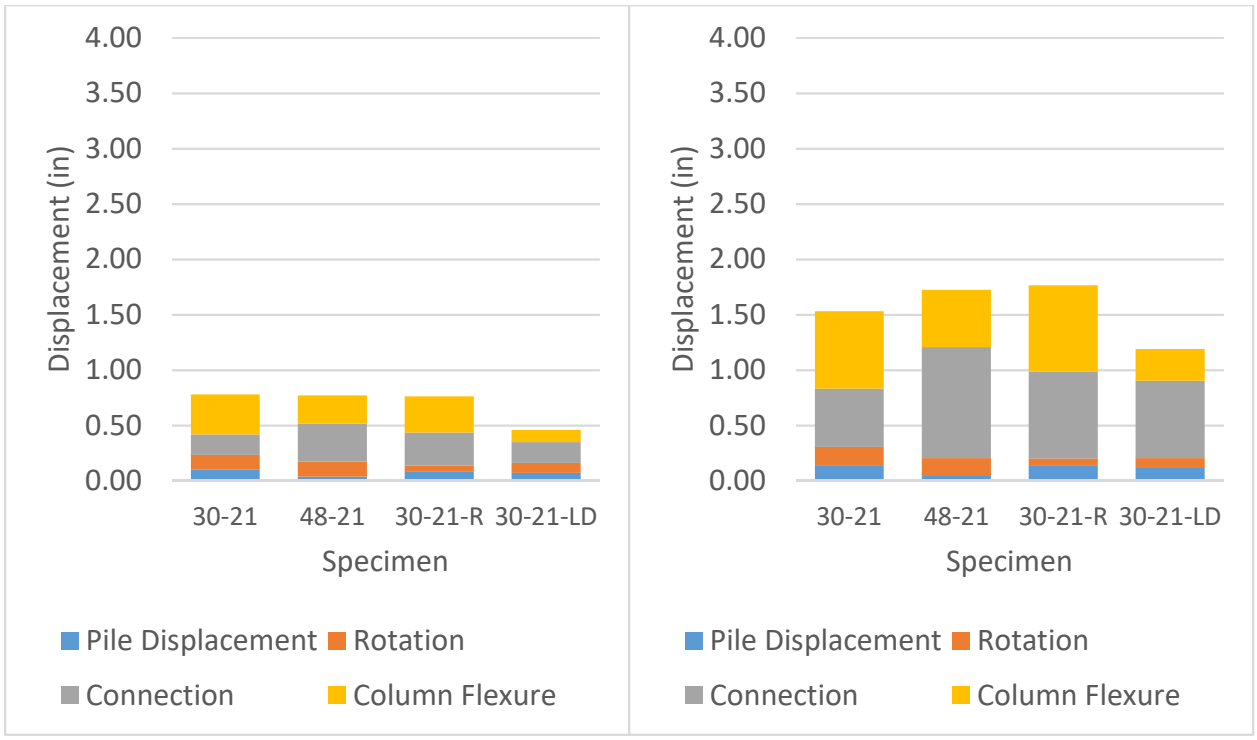

a) b)

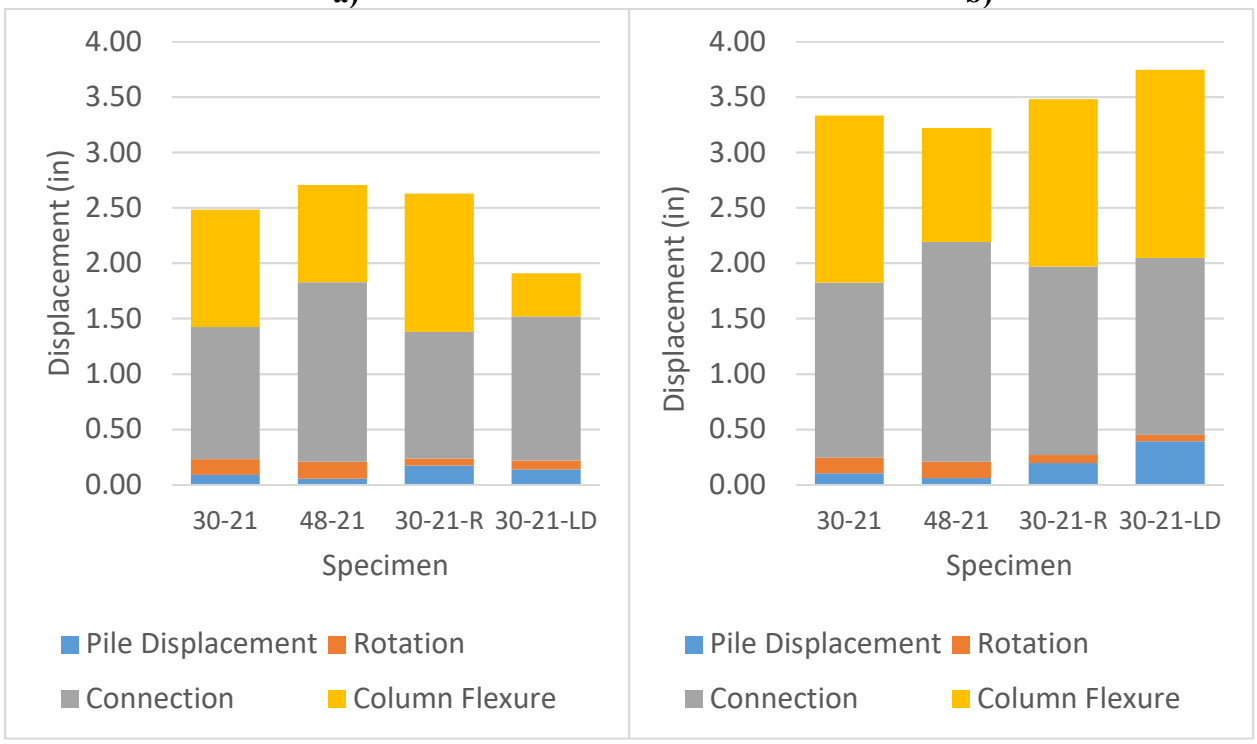

c) d)

Figure 5.26. Comparison of Displacement Contributions Magnitudes at: a) approx. 1% Drift, b) approx. 2.5% Drift, c) approx. 4% Drift, d) approx. 5% Drift

5.3 SYSTEM BEHAVIOR

The behavior of the system was quantified using the force-displacement or moment-drift responses and energy dissipation capabilities of each of the test specimens. For the moment-drift response, full hysteretic responses with removed P-Δ effects and normalized hysteretic responses were compared. The peak and ultimate drift and peak lateral strength values are also compared.

5.3.1 *Hysteretic Response*

Figure 5.27 shows the hysteretic curves from Specimens 30-21, 48-21, 30-21-R, and 30-21-LD, after P-Δ effects have been removed and normalized by the nominal moment, M_n, based on results from Response2000, a Reinforced Concrete Sectional Analysis Program. The M_n and Nominal Force, F_n, of each specimen were calculated using the day of test measured material strengths. M_n and F_n are listed in Table 5.1. The M_n was determined by when the longitudinal strain in the column reached 0.003 in./in. The F_n was calculated by dividing M_n by the height of the column, 61.75 in.

Table 5.1. Column Nominal Moments and Forces

Specimen	Nominal Moment (M_n) (kip-ft)	Nominal Force (F_n) (kips)
30-21	345.1	67.1
48-21	317.3	61.7
30-21-R	321.1	62.4
30-21-LD	345.0	67.0

Figure 5.27 shows a few observations to takeaway. One, the response in both positive and negative drift directions were largely similar, with the only major differences coming on the last two cycles when the specimen was reaching failure. Two, all the curves show “pinching” in the response, a common characteristic of concrete cyclic testing. This “pinching” indicates damage to

the concrete around the pile-column joint. Three, Specimen 30-21 showed degradation of lateral force resistance after reaching peak lateral force, while Specimens 48-21, 30-21-R, and 30-21-LD were able to maintain approximate lateral force resistance on the first cycle at each increased drift level, until the final cycles at 8% and larger drift. Four, for all the specimens, the peak moments are well above M_n for each column, around 40% greater. Specimen 48-21's and 30-21-LD's lateral measured moment only goes below the nominal moment once the column reaches 6% drift, while Specimens 30-21 and 30-21-R are able to go one and three cycles, respectively, before their measured moment decreases below the nominal moment.

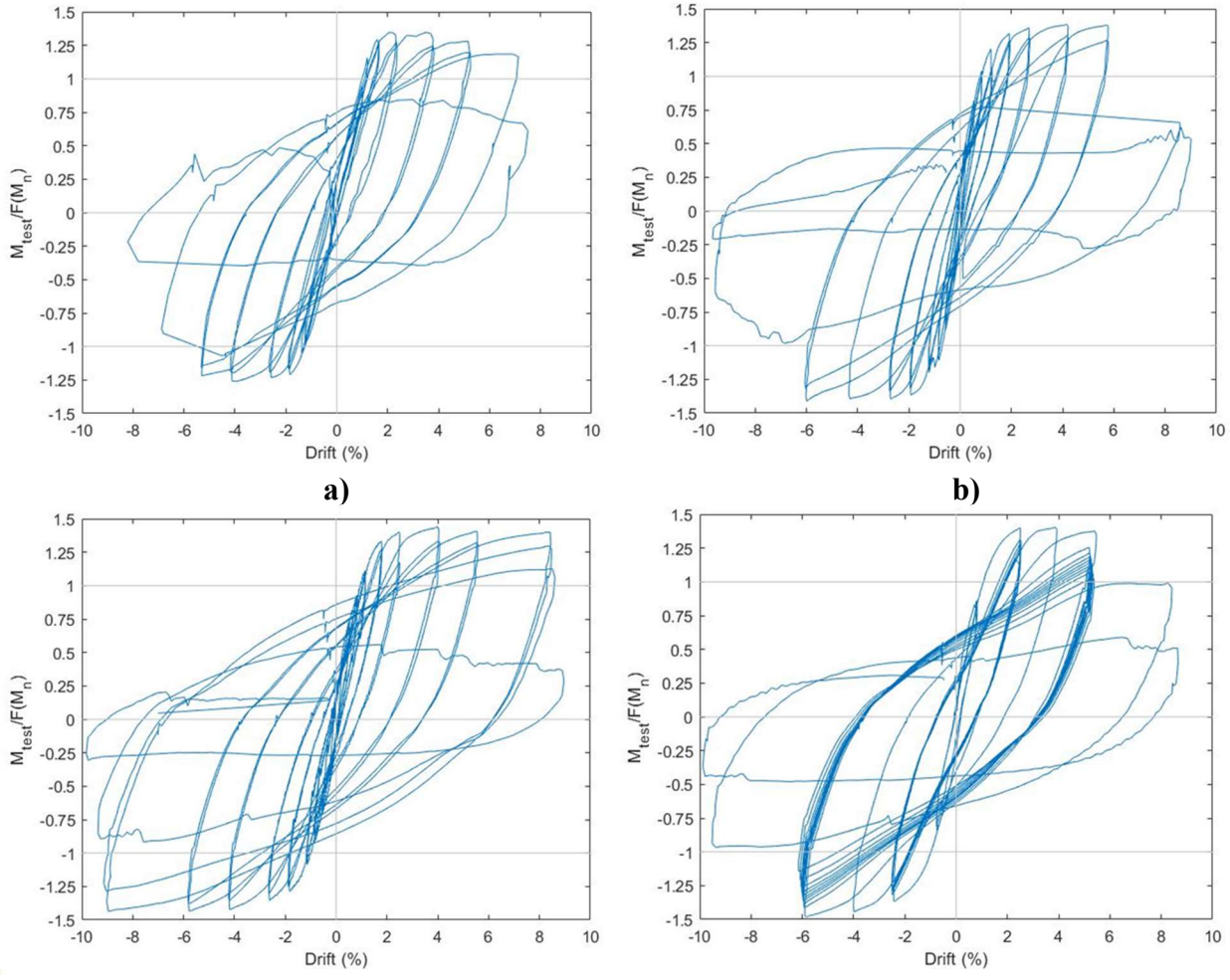

Figure 5.27. Normalized Moment-Drift Responses with P-Δ Effects Removed: a) Specimen 30-21, b) Specimen 48-21, c) Specimen 30-21-R, d) Specimen 30-21-LD

5.3.2 *Energy Dissipation*

The energy dissipated during the test was calculated by finding the area under the hysteretic curves of each specimen. Figure 5.28 shows the energy dissipated plotted against the drift of the specimen for the whole test.

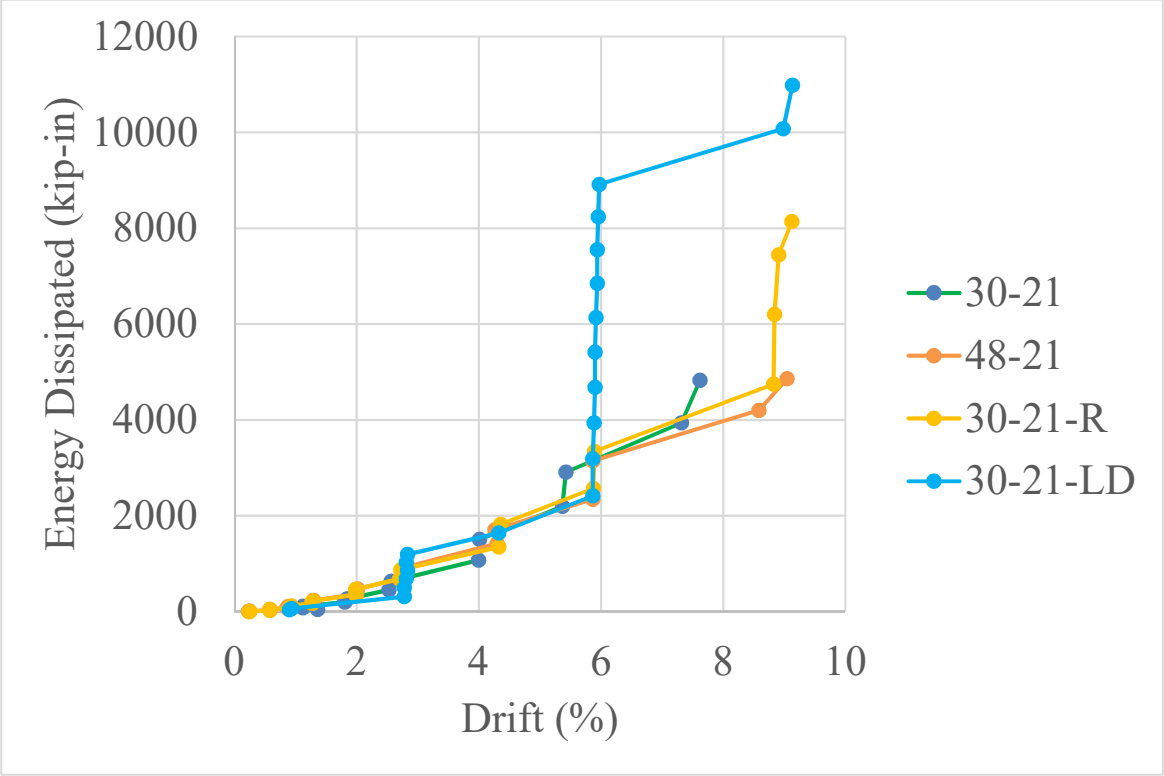

Figure 5.28. Total Energy Dissipation vs. Drift

As shown in Figure 5.28, the energy dissipation curves follow very similar paths, except for 30-21-LD, which is due to the different displacement history this specimen was tested under and shows that much more energy was dissipated due to the larger number of cycles it experienced. Specimen 30-21-R shows a spike at the end of the curve. This spike is due to the extra cycles ran at the end of the test at 9.0% + drift, which the other specimens were not able to do, and shows the increased strength and ductility the embedded ring provides the connection.

5.3.3 *First Drift Cycle Envelopes*

The force-drift envelopes of each specimen were developed using the peak displacement and normalized force at that displacement for the first cycle of the force-drift hysteretic curve. The envelopes for each specimen are in Figure 5.29. The key takeaway from the figure is the strength degradation seen in all the Specimens, except 30-21-R, after peak force is reached. Specimen 30-21-R also has the largest normalized lateral strength.

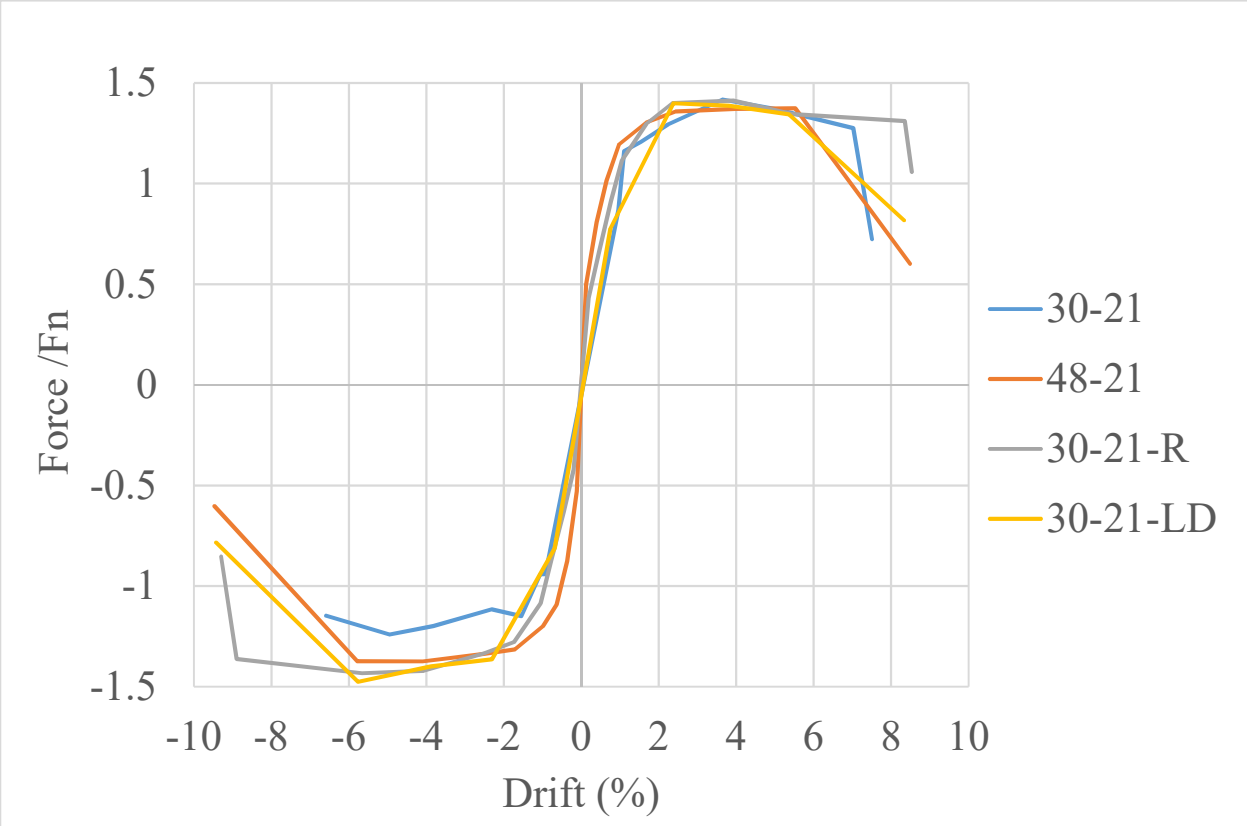

Figure 5.29. First Cycle Normalized Force-Drift Envelope

5.3.4 *Peak and Ultimate Drift and Peak Moment Values*

Peak drift is defined as the drift the column experienced at peak resistance. Ultimate drift is the largest drift the column experienced with a lateral strength greater than 50% of the peak strength. The drift values are summarized below in Table 5.2.

As shown in Table 5.2, Specimen 30-21 had significantly lower ranges with a peak drift range of 7.4% and an ultimate drift range of 13.6%. Specimen 30-21-R had the largest peak and ultimate drift ranges of 11.9% and 18.4%, respectively. Previously mentioned in Chapter 4, Specimen 30-21-R was able to undergo 4 total cycles at this range, 3 cycles of which were at a lateral strength greater than 50% of the peak strength, while the rest of the specimens were only able to endure 2 cycles.

Table 5.2. Peak and Ultimate Measured Drifts

Specimen	Drift (%)					
	Peak			Ultimate		
	Positive	Negative	Range	Tension	Compression	Range
30-21	3.65	3.77	7.42	7.03	6.59	13.62
48-21	5.65	5.91	11.56	5.69	5.95	11.64
30-21-R	5.87	6.03	11.90	8.91	9.50	18.41
30-21-LD	5.36	5.77	11.13	8.33	9.43	17.76

The peak measured moment is defined as the largest moment, with P-Δ effects removed, the column sustained. The peak measured moments, M_m, are shown in Table 5.3. The values are presented with the nominal moment, M_n, as calculated by Response 2000, as well as the normalized peak moment.

As shown in Table 5.3, all specimens showed significant overstrength, ranging from 38% to 47%, compared to M_n. All columns had the same design and used the same grade of reinforcement and concrete mix, therefore any difference in strength is due to the connection. Specimen 30-21-LD has the largest normalized lateral peak strength value followed by Specimens 30-21-R, 30-21, and 48-21. Specimens 30-21 and 48-21 have the largest normalized lateral ultimate strengths, however, these strengths are at significantly smaller drift ranges compared to Specimen 30-21-R.

Table 5.3. Peak and Ultimate Measured Moments with P-Δ Effects Removed

Specimen	Response 2000 Nominal Moment M_n (kip-ft)	Peak Measured Moment $M_{m\text{-}Peak}$ (kip-ft)	M_{m_Peak}/M_n	Ultimate Measured Moment, $M_{m\text{-}Ult.}$ (kip-ft)	$M_{m\text{-}Ult}/M_n$
30-21	345.1	489.5	1.42	440.5	1.28
48-21	317.3	436.5	1.38	405.9	1.28
30-21-R	321.1	460.2	1.43	339.8	1.05
30-21-LD	345.0	508.7	1.47	281.9	0.81

5.4 SPECIMEN DAMAGE

This section compares the various damage states mentioned in Chapter 4 for each specimen based on the drift at which states were reached.

The damage states discussed are as follows: Reinforcement Yielding, Spalling 1 (Exposure of Transverse Reinforcement), Spalling 2 (Exposure of Longitudinal Reinforcement), Bar Buckling, Bar Fracture, and Final State. These damage states are what was visually observed and the corresponding drift levels are also the peak drift of the given cycle, therefore not all damage states occurred at the peak drift, but did occur during that given cycle.

An additional damage state that is discussed is the damage to the pile and concrete fill inside of the pile. This state was observed after testing and the removal of the column from the specimen.

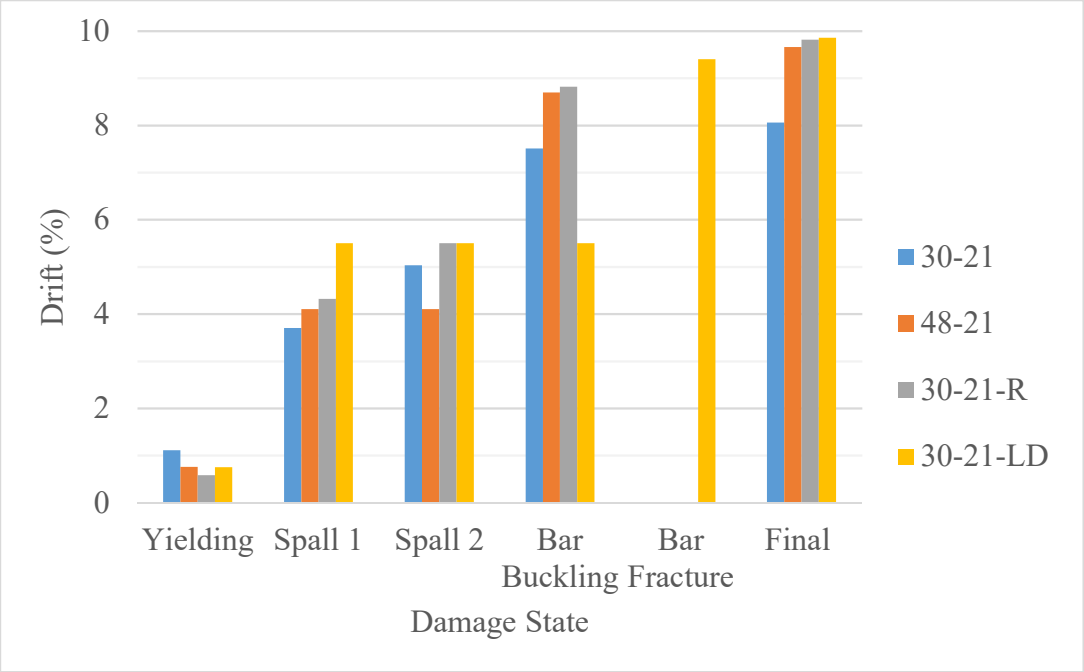

Figure 5.30. Damage Summary

Figure 5.30 shows that the reinforcement yielding occurs around 0.6 to 1.1% column drift. It is worth noting that this is not when the yield strain of the reinforcement was reached, but at the peak displacement of that cycle when the strain measured in the reinforcement was greater than the yield strain. Therefore, the reinforcement yielded during that cycle, but not necessarily at the peak drift of the cycle. Again as stated in earlier Sections 5.1 and 5.3.4, Specimen 30-21 did not have any cycles run at drift levels less than 1% drift. Had cycles been run at less than 1% drift, Specimen 30-21 would have probably yielded around 0.8% drift. This also does not represent the yielding of the column, but the drift level at which the reinforcement yielded.

Spall 1 is defined as when spalling had increased to the point that the transverse reinforcement was exposed. Spall 2 is defined as when spalling had increased to the point that the longitudinal reinforcement was exposed. For all specimens, except 30-21-R, both Spall 1 and 2 occurred at the same drift level. The drift levels for these damage states occurred between 4.1% and 6.0% column drift.

Buckling of the longitudinal reinforcement in the column occurred at similar drifts for Specimens 30-21, 48-21, and 30-21-R at approximately 8% drift, while Specimen 30-21-LD experienced buckling at 5.2% drift. It is worth noting that due to the different displacement histories, this was the 5th cycle at 5.2% drift for Specimen 30-21-LD. Another note about Specimen 48-21, as mentioned in chapter 4, while slight buckling was observed at 5.7% drift level it was not the pronounced buckling that occurred for all the other specimens, which occurred at 8.7% drift for Specimen 48-21

Bar fracture only occurred during testing for Specimen 30-21-LD. The most northern reinforcing bar fractured when the column drift reached 8.3%. When the column was then cycled to -9.4% drift, the most southern reinforcing bar fractured. As mentioned before in chapter 4, the most southern bar on Specimen 30-21-R did fracture the following day after testing but did not fracture during the actual test.

For all tests, testing was not stopped due to bar fracture, but to concrete crushing and lateral strength, resistance dropping below 30% of maximum resistance. Specimens 48-21, 30-21-R, and 30-21-LD failed around 9.7% column drift, with Specimen 30-21 failing around 8.1% drift. Specimen 30-21-R was able to undergo 4 full cycles at these given drift levels, while the other specimens were only able to undergo 2 full cycles before their lateral resistances had degraded to the point of failure.

After testing, the specimen was removed from the testing rig and the column was removed from the top of the pile. This allowed the top of the pile and any damage it might have experienced to be easily seen. As shown in Figure 5.31, Specimens 30-21 has some damage with radial cracks extending from where the column was to the edge of the tube and minor concrete fill damage around where the base of the column was. Specimen 48-21 has similar radial cracks to Specimen

30-21 but does not have any of the concrete fill damage. Specimen 30-21-R has no damage to the pile or the concrete fill. Specimen 30-21-LD has extensive damage consisting both of radial cracks and spalled concrete. The concrete has spalled both on the inside concrete fill around the column base and the outside of the concrete fill near the tube as well. This shows that the specimens that did not have the embedded rib in the pile or did not have a 48 in. pile diameter experienced significantly more damage to the top of pile concrete and pile-column interface.

a) **b)**

c) **d)**

Figure 5.31. Specimens with Columns Removed: a) 30-21, b) 48-21, c) 30-21-R and d) 30-21-LD

Chapter 6. COMPARISON OF RESULTS

This chapter compares the experimental and simulated results of the test specimens, which was done by a collaborating, visiting research student, Muzi Zhao, in parallel with this experimental program [14]. By comparing the measured experimental results and the simulated results, the behavior of the connection, globally and locally, can be better understood and areas of weakness or concern can be analyzed and addressed.

As described in Section 2.2.3, Zhao modeled RC column to CFST pile connections in LS-Dyna, which were the basis for the design of the test matrix. The tested specimens had slight differences in their as-built material strengths, dimensions of the reinforcement layout, and geometry. Zhao revised his previous models with the as-built conditions to better simulate the actual geometry and material strengths used as a comparison with the experimental results. These comparisons are important, they are needed to validate and improve the FEA model used for these connections which will improve the accuracy of future modeling efforts.

The following sections show comparisons of the overall system behavior and specimen damage. Specifically, the comparison of the measured and simulated results investigates the similarities and differences in stiffness, degradation, strength, and deformability, and the comparisons of the damage, look at axial stress, compressive and tensile damage indicators, CDP and TDP respectively, for each specimen. Issues with the simulation results are also discussed.

The comparison of the overall specimen behavior is shown by plotting the force-drift hysteric curve of each specimen. The force is normalized by the nominal force, F_n, of each column, which are tabulated in Table 5.1. The comparison of the specimen damage is shown by comparing photos from the experimental testing with figures showing compressive or tensile damage from the FEA. For all simulated damage figures, the size of the concrete elements are 1.33 in., while the

drawn grid on the experimental specimens has a spacing of 5 in. The specimen test matrix is shown in Table 6.1 for additional reference.

Table 6.1. Specimen Test Matrix

Specimen Name	Tube Diameter (in.) [mm]	Tube Diameter/ Tube Thickness	Reinforcement Bar Size	Embedment Depth (in.) [mm]	Rib Size (in.) [mm]	Rib Embedment Depth (in.) [mm]
30-21*	30 [762]	60	#7	21 [533]	NA	NA
48-21	48 [1219]	96	#7	21 [533]	NA	NA
30-21-R	30 [762]	60	#7	21 [533]	2 [50.8]	2 [50.8]
30-21-LD	30 [762]	60	#7	21 [533]	NA	NA

*Specimen 30-21 is reference specimen

6.1 SPECIMEN 30-21

6.1.1 *System Behavior Comparison*

As shown in Figure 6.1, numerical simulation results closely match the measured experimental results. There are differences in the negative drift during the last few cycles. As stated before in Chapter 4, during these cycles the axial binding issue occurred which affected these cycles, and estimated values were substituted for these cycles.

- The initial stiffness and onset of lateral strength resistance degradation are well matched for both the measured and simulated results.
- There is a slight difference in the peak lateral strength, with the measured results reaching a peak strength of $1.4F_n$ at 2.5% drift, while the simulated results only reach a peak strength of $1.27F_n$ at 4.3% drift. Both results had similar ranges of drift, with the measured drift ranging from -8.1% to 7.8% drift, and the simulated drift ranging from -8.9% to 7.8%.

Another issue that occurred during these last cycles for the FEA was distortion in concrete components of the model, which did not allow for the final cycle at 8% drift to be completed.

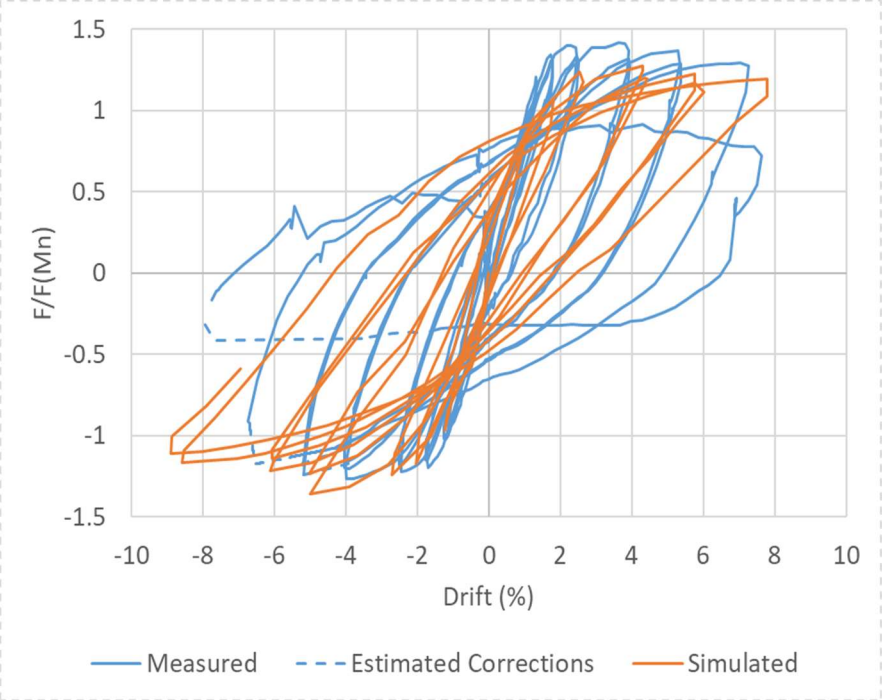

Figure 6.1. Specimen 30-21 Normalized by F_n Force-Drift Curve Comparison

6.1.2 *Damage Comparison*

At 2.2% drift, as shown in Figure 6.2a, the concrete spalled approximately up to 2 in. from the top of the pile.

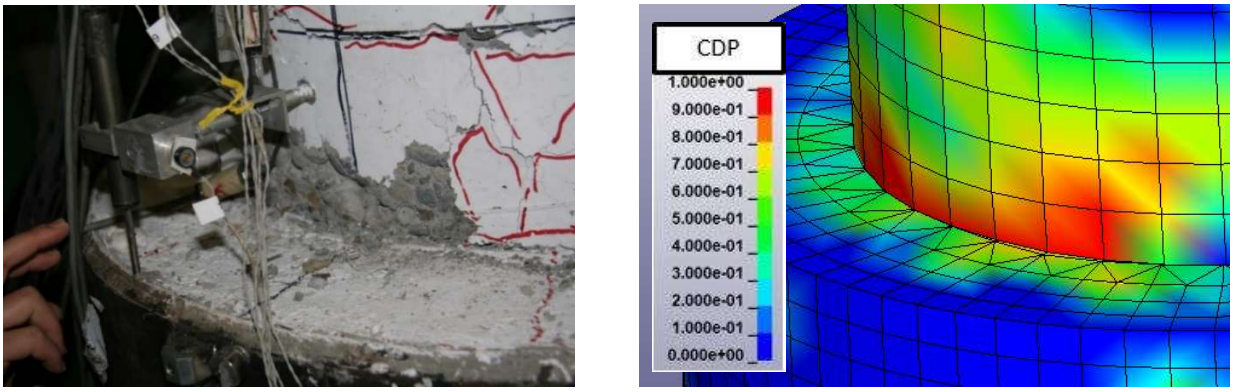

a) **b)**

Figure 6.2. Specimen 30-21 Compressive Damage at Base of Northern Column Face at 2.2% Drift: a) Observed and b) Simulated

Similar behavior is shown in Figure 6.2b with the red color representing the area of concrete that exceeded the normal strain of concrete indicating that region of the concrete has spalled. Also shown is the damage is concentrated at the base of the column, which is where the damage was focused in the experimental testing as well.

During the first cycle at 5.0% drift, as shown in Figure 6.3a, the spalled concrete area has increased in size, reaching up to 7 in. above the top of the pile.

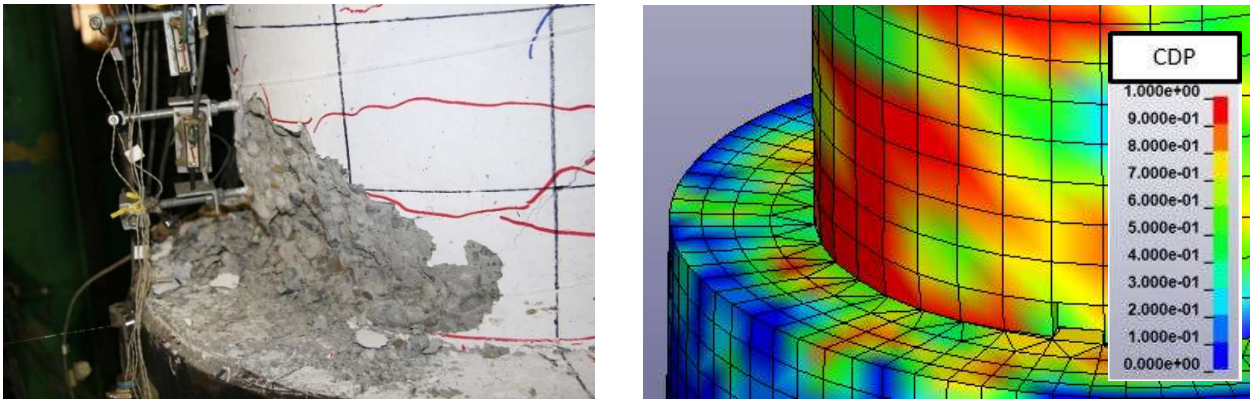

a) **b)**

Figure 6.3. Specimen 30-21 Compressive Damage at Base of Northern Column Face at 5.0% Drift: a) Observed and b) Simulated

The FEA damage, shown in Figure 6.3b, also shows an increased damaged area at the base of the column and the damage starting to spread to the concrete fill in the pile.

During the second to last cycle, which reached a drift of 7.0%, the concrete at the base of the column increased in spalled area furthering exposing both the longitudinal and transverse reinforcement as shown in Figure 6.4a.

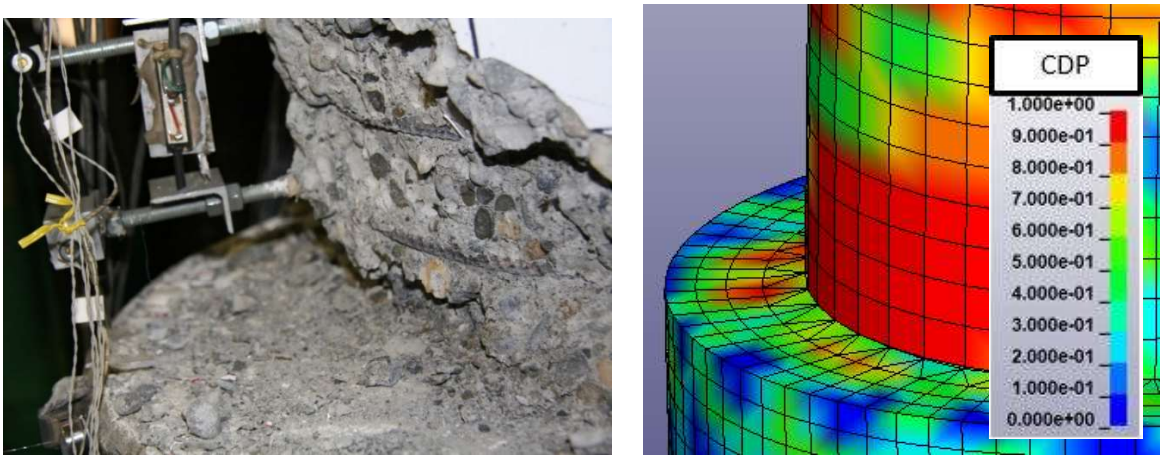

a) **b)**

Figure 6.4. Specimen 30-21 Exposed Longitudinal Reinforcement and Compressive Damage at Base of Northern Column Face at 7.0% Drift: a) Observed and b) Simulated

The FEA damage, shown in Figure 6.4b, shows the same area at the base of the column with increased damage, which would also lead to exposed reinforcement.

During the last cycle, which reached a drift of 8.0%, the concrete at the base of the column has completely spalled approximately 14 in. from the base of the column and the longitudinal reinforcement has buckled, as shown in Figure 6.5a.

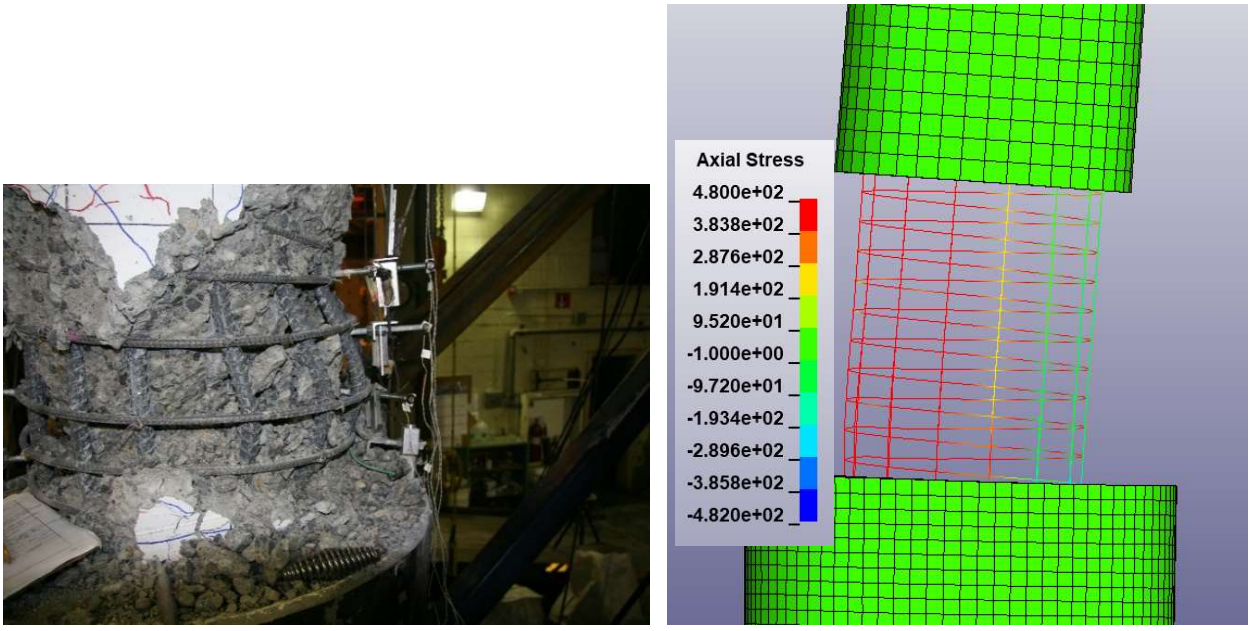

a) **b)**

Figure 6.5. Specimen 30-21 Buckled Reinforcement at Base of Southern Column Face at 8.0% Drift: a) Observed and b) Simulated Reinforcement Axial Stress

From the FEA axial stress, shown in Figure 6.5b, the southern longitudinal reinforcement is showing a compressive stress of 1 ksi, exemplifying that these bars have buckled since they are not taking any load.

6.2 SPECIMEN 48-21

6.2.1 *System Behavior Comparison*

As shown in Figure 6.6, the simulated response is similar to the measured results for Specimen 48-21 to the drift level of approximately 6%, with similar initial stiffness and no lateral strength resistance degradation as the drift level increases. There were issues with the model beyond 6% drift suggesting significant damage to the concrete between the reinforcement and tube, which was not seen in the test. As such, we will not compare the results beyond this drift level.

- There is a slight difference in the peak lateral strength, with the measured results reaching a peak strength of $1.33F_n$ at 2.8% drift, while the simulated results reach a peak strength of $1.41F_n$ at 3.7% drift.
- The measured and simulated results did not have similar ranges of drift, with the measured drift ranging from -9.4% to 9.0% drift, while the simulated drift ranged from -5.9% to 3.8%. This is due to the same issue that occurred for Specimen 30-21 where during the last cycles there was distortion in concrete components of the model, which again did not allow for the final cycles greater than 6% drift to be run.

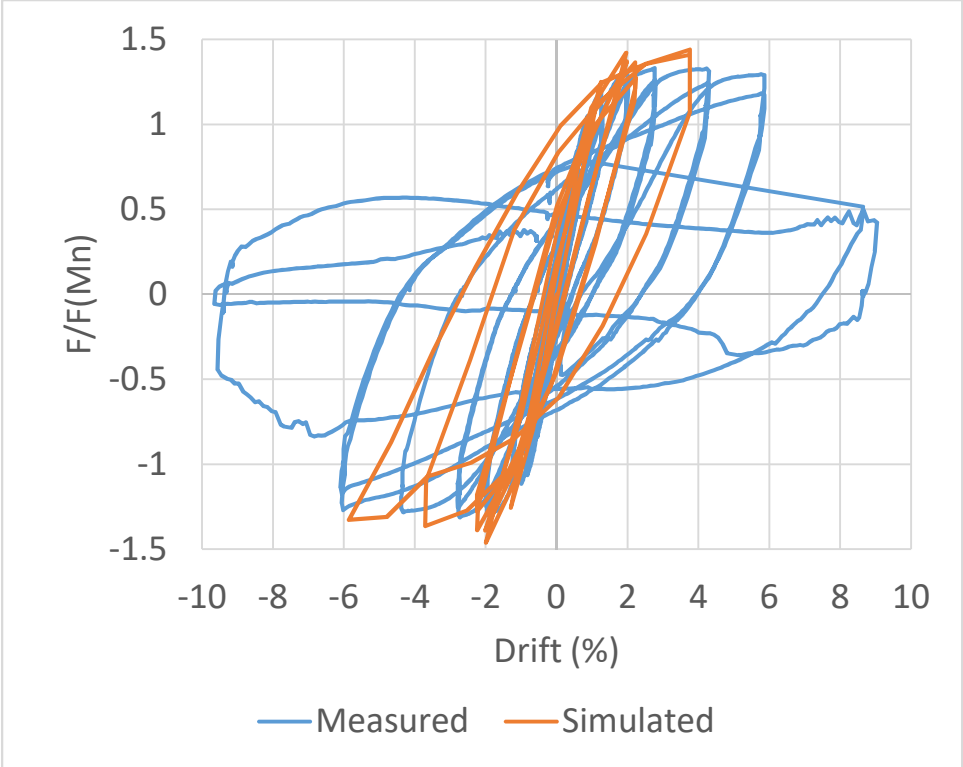

Figure 6.6. Specimen 48-21 Normalized by F_n Force-Drift Curve Comparison

6.2.2 *Damage Comparison*

At 1.1% drift, as shown in Figure 6.7, there is a radial crack on the top of the pile concrete, extending from the base of the column to the perimeter of the pile, as well as cracking around the base of the column.

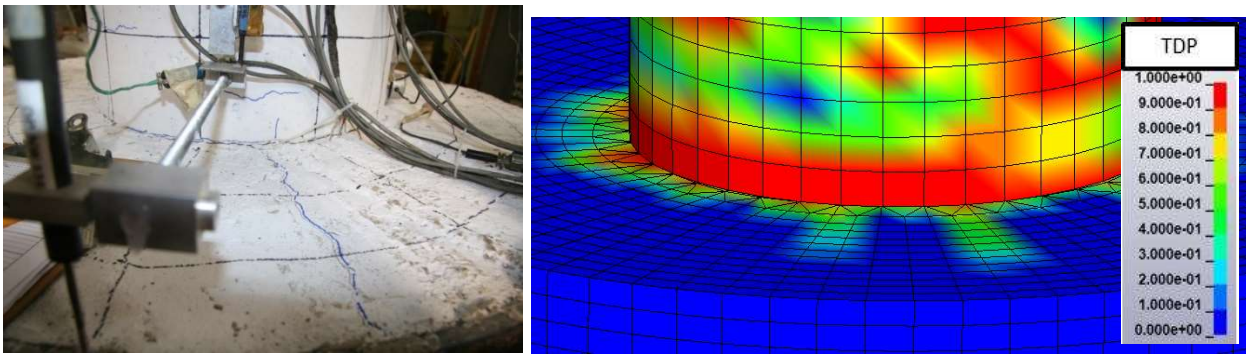

a) **b)**

Figure 6.7. Specimen 48-21 Radial Crack on Top of Pile Concrete at 1.1% Drift: a) Observed and b) Simulated Tensile Damage

As seen in Figure 6.7b, which is showing FEA tensile damage, there is significant damage around the base of the column as well as damage extending outward from the base. However, the damage to the top of the pile concrete does not extend out to the perimeter of the pile, as seen in Figure 6.7a.

At 2.6% drift, as shown in Figure 6.8a, there is spalling at the base of the column, reaching up to 6 in. above the column base.

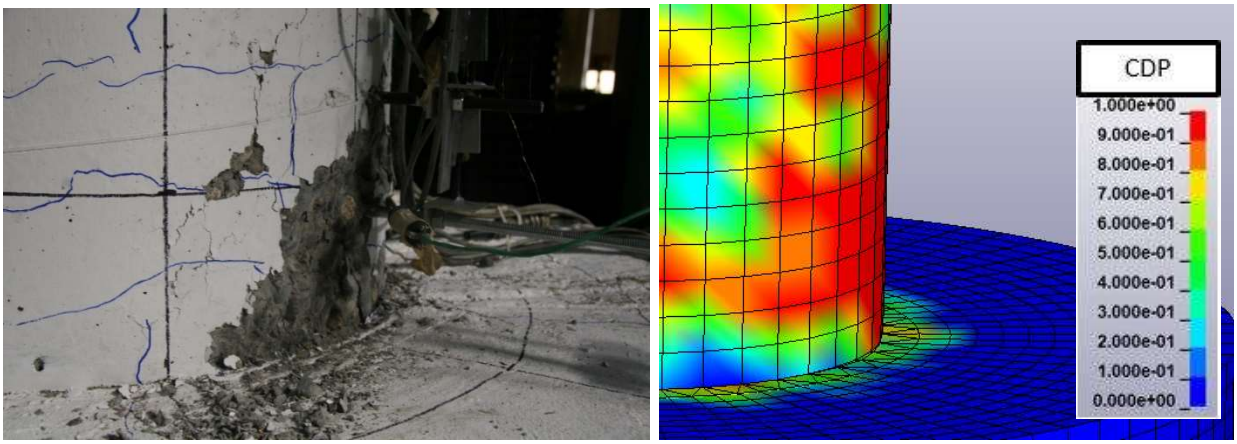

a) **b)**

Figure 6.8. Specimen 48-21 Compressive Damage at Base of Southern Column Face at 2.6% Drift: a) Observed and b) Simulated

Figure 6.8b shows there is also damage around the base of the column, which shows that the concrete has exceeded the normal strain of concrete indicating that region of the concrete has spalled. However, the damage seems to be more concentrated at the southern face of the column.

At 4.2% drift, as shown in Figure 6.9a, there is spalling at the base of the column, exposing both the longitudinal and transverse reinforcement.

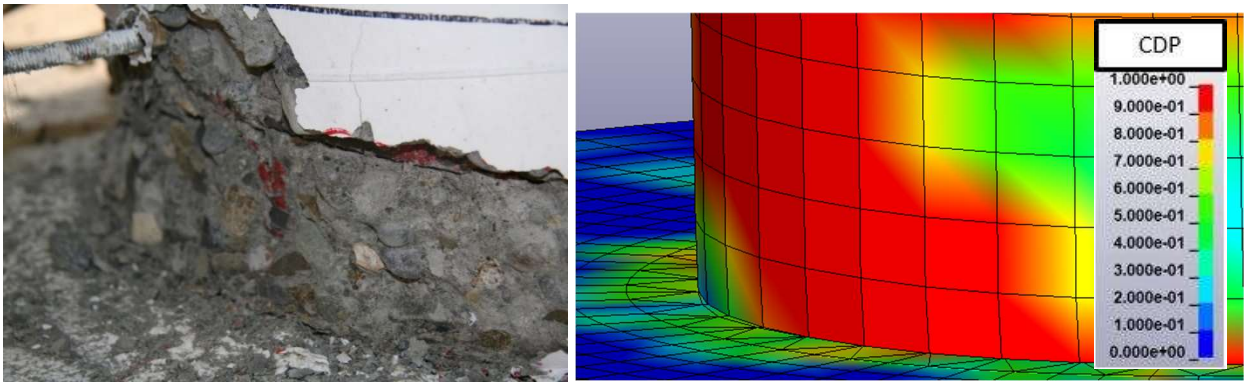

a) **b)**

Figure 6.9. Specimen 48-21 Exposed Reinforcement and Compressive Damage at Base of Northern Column Face at 4.2% Drift: a) Observed and b) Simulated

As shown in Figure 6.9b, there is compressive damage around the base of the column in the simulation, showing that the concrete has exceed the normal strain indicating that the region of concrete has spalled, which would also expose the reinforcement.

As seen in the overall system behavior results for Specimen 48-21, there was large distortion in the model elements at drift levels larger than 4.2%, as shown in Figure 6.10, and thus no damage figures were able to be compared at these drift levels.

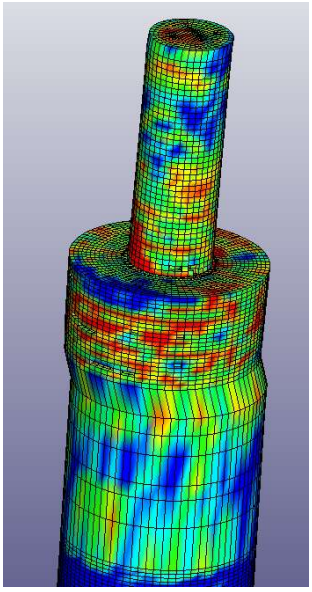

Figure 6.10. Specimen 48-21 Distorted Elements at 6.0% Drift

6.3 SPECIMEN 30-21-R

6.3.1 *System Behavior Comparison*

As shown in Figure 6.11, the simulated results closely follow the measured results for Specimen 30-21-R, with similar initial stiffness strength, cyclic response, and drifts corresponding to resistance degradation. The following summarized the results from the comparison:

- There is a larger difference in the peak lateral strength than compared to the other specimens, with the measured results reaching a peak strength of $1.36F_n$ at 4% drift, while the simulated results only reach a peak strength of $1.12F_n$ at 1.9% drift.
- Both results had similar ranges of drift, with the measured drift ranging from -9.7% to 8.9% drift, and the simulated drift ranging from -9.2% to 8.7%.
- The concrete distortion issues that occurred in the models of Specimens 30-21 and 48-21 were not observed in this model. This suggests that the distortion is exacerbated by the slippage of the concrete relative to the steel and this is mitigated by the embedded ring at the top of the pile, which helps mitigate the damage to the concrete in the pile.

There are two other key differences between the simulated and measured results. First, the simulated peak forces for cycles at 5.7% drift or smaller are slightly less than the measured results. Also, the test specimen sustained three cycles at 8.2% drift or greater before significant strength loss, while the simulated model sustained more than five cycles at similar drift levels and show no sign of lateral strength loss.

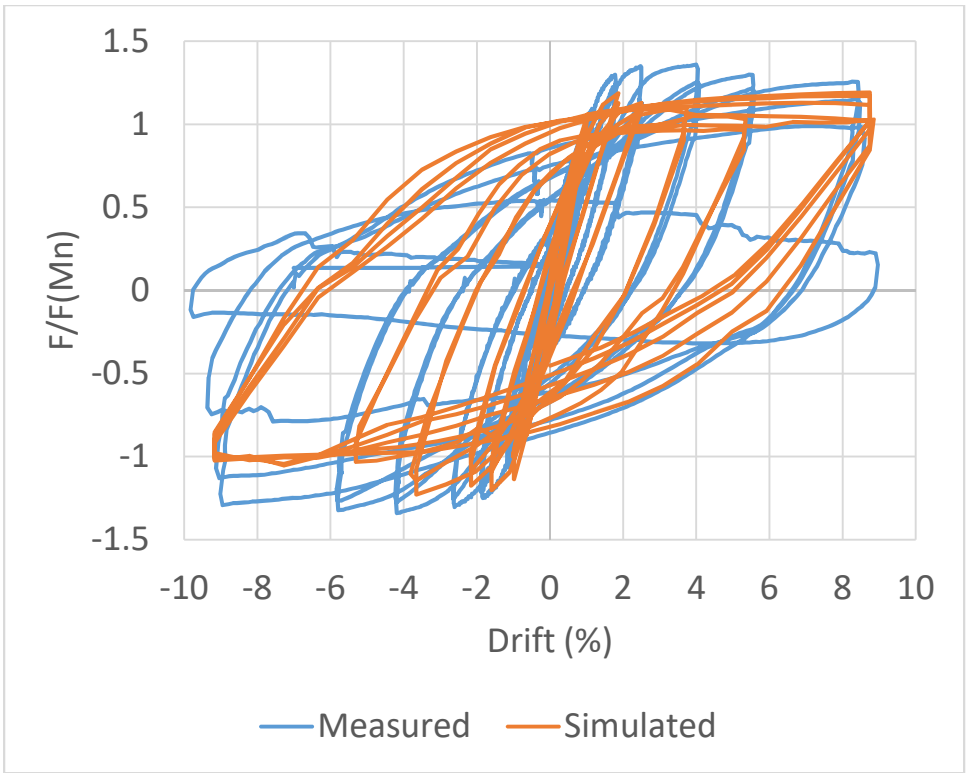

Figure 6.11. Specimen 30-21-R Normalized by F_n Force-Drift Curve Comparison

6.3.2 *Damage Comparison*

At 2.4% drift, as shown in Figure 6.12a, there is slight spalling at the northern base of the column, less than 2 in. from the top of the pile.

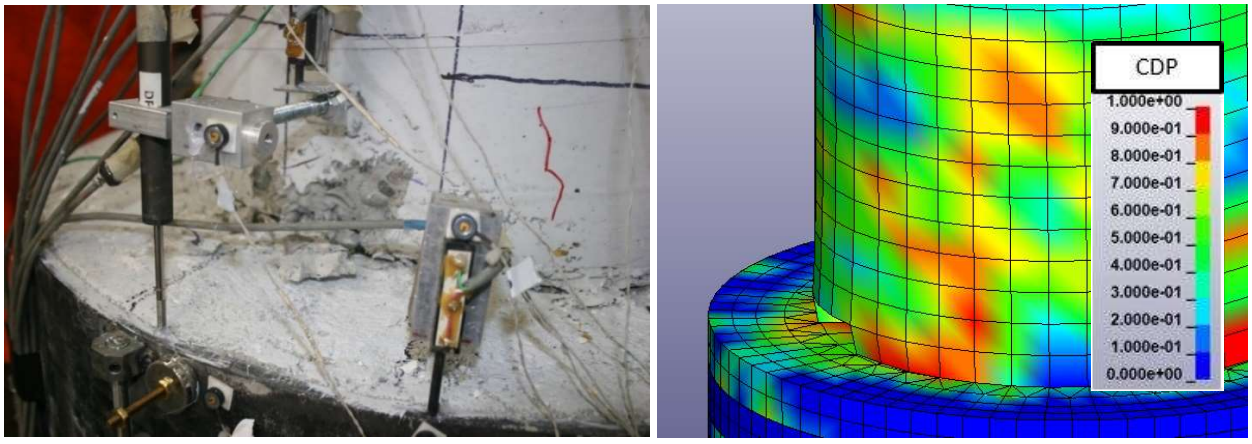

a) **b)**

Figure 6.12. Specimen 30-21-R Spalled Region and Compressive Damage at Base of North Face of Column at 2.4% Drift: a) Observed and b) Simulated

As shown in Figure 6.12b, the FEA compressive damage was also starting to occur at the northern base of the column.

At 5.5% drift, as shown in Figure 6.13a, there was significant spalling at the base of the column, approximately 7 in. up from the top of the pile, which exposed longitudinal and transverse reinforcement

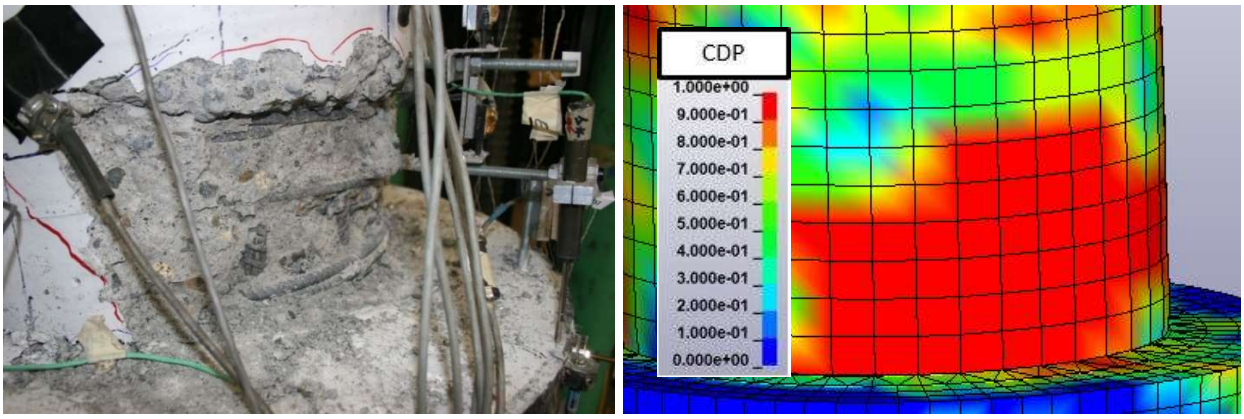

a) **b)**

Figure 6.13. Specimen 30-21-R Exposed Northern Longitudinal Reinforcement and Compressive Damage at 5.5% Drift: a) Observed and b) Simulated

The FEA compressive Damage, Figure 6.13b, shows a large damaged area at the northern base of the column, which would expose the reinforcement.

At 8.9% drift, the southern longitudinal reinforcement has buckled, shown in Figure 6.14a.

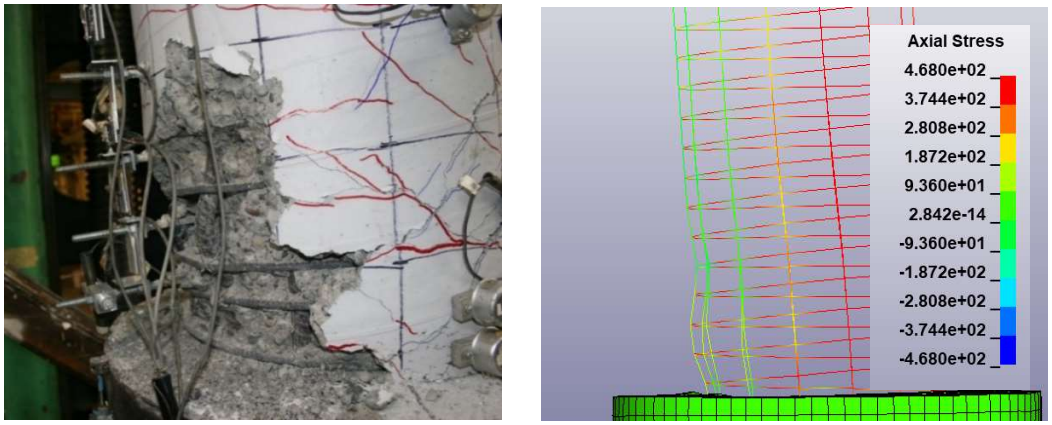

a) **b)**

Figure 6.14. Specimen 30-21-R Buckled Reinforcement at 8.9% Drift: a) Observed and b) Simulated Axial Reinforcement Stress

Figure 6.14b, showing the FEA axial stress, which shows the small axial stress in the southern longitudinal reinforcement and the buckled reinforcement as well.

6.4 SPECIMEN 30-21-LD

6.4.1 *System Behavior Comparison*

As shown in Figure 6.15, the simulated results closely follow the measured results with similar initial stiffness and slight lateral strength resistance degradation. There is a slight difference in the peak lateral strength, with the measured results reaching a peak strength of $1.33F_n$ at 2.5% drift, while the simulated results only reach a peak strength of $1.24F_n$ at 2.4% drift. The measured and simulated results did not have similar ranges of drift, with the measured drift ranging from -9.8% to 8.6% drift, while the simulated drift ranged from -5.3% to 5.2%. This is due to the same issue that occurred in the models of Specimens 30-21 and 48-21; those models have exhibited distortion in concrete components of the model. This distortion is due to increased concrete damage in the top of the pile, which is caused by the absence of the embedded rib and did not allow for the final cycles greater than 6% drift to be run.

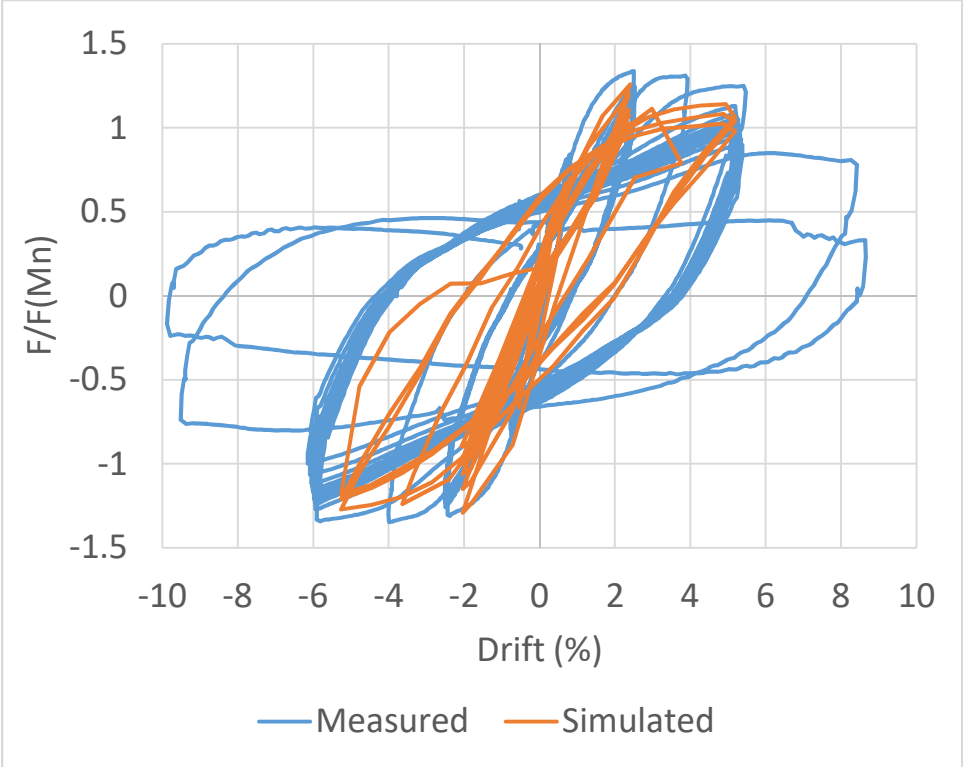

Figure 6.15. Specimen 30-21-LD Normalized by F_n Force-Drift Curve Comparison

6.4.2 *Damage Comparison*

At 2.4% drift, as shown in Figure 6.16a, the concrete is starting to spall on the northern base of the column.

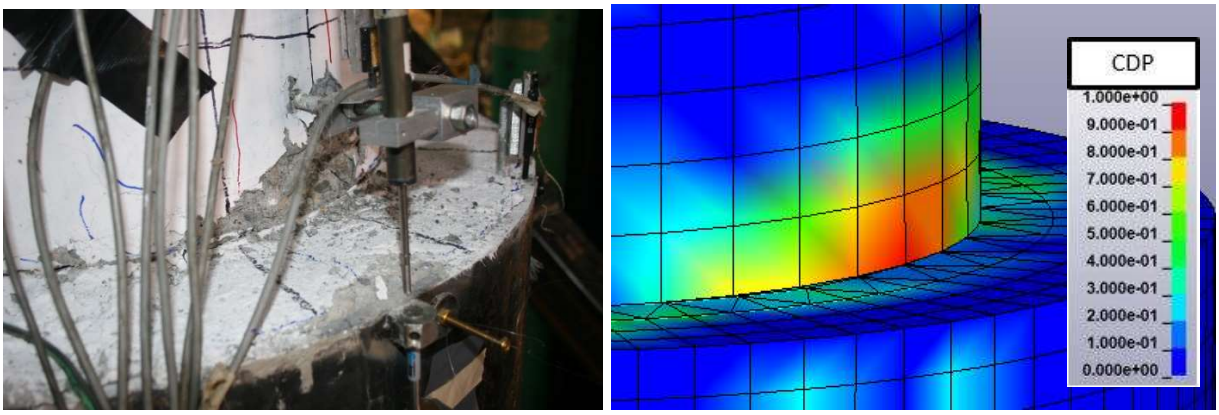

a) **b)**

Figure 6.16. Specimen 30-21-LD Initial Spall and Compressive Damage at Base of Northern Face of Column at 2.4% Drift a) Observed and b) Simulated

As shown in Figure 6.16b, the concrete has exceeded the normal strain of concrete indicating that region of the concrete has spalled and is concentrated at the northern base of the column.

At 5.5% drift, as shown in Figure 6.17a, spalling at the base of the column has increased over 7 in. above the base of the column and has exposed both the longitudinal and transverse reinforcement.

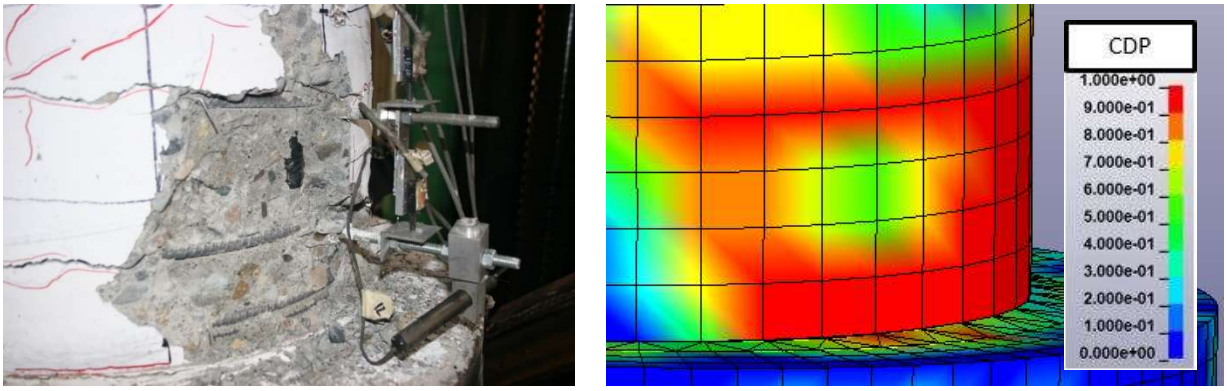

a) **b)**

Figure 6.17. Specimen 30-21-LD Exposed Longitudinal Reinforcement and Compressive Damage at 5.5% Drift: a) Observed and b) Simulated

As shown in Figure 6.17b, there is a large amount of FEA compressive damage in the same region, which would expose the reinforcement.

As seen in the overall system behavior results for Specimen 30-21-LD, there was large distortion in the model elements at drift levels larger than 5.5% and thus no damage figures were able to be compared at these drift levels.

6.5 COMPARISON SUMMARY

In terms of overall behavior, the simulated and measured results are similar in terms of strength and stiffness. However, in most cases, the simulated model began to lose strength before the measured specimens did. In addition there is information about the response of the connection from the simulated models that cannot be seen in the experimental tests. Lateral degradation is

evident in the simulated results for Specimens 30-21 and 30-21-LD, while there is no significant lateral strength degradation in the simulated results for Specimens 48-21, and 30-21-R. The measured peak strengths of each specimen are within $0.1F_n$ of the simulated peak strengths, except Specimen 30-21-R's results, which were $0.24F_n$ apart. The simulated results' drift ranges were similar for Specimens 30-21 and 30-21-R, however, the drift ranges for Specimens 48-21 and 30-21-LD were very different.

In terms of specimen damage, the observed damage from the experimental testing matched the simulated damage from the FEA results for all specimens. The photos from the experimental testing showing the onset, spread, and regions of concrete spalling around the column base closely matched the damage figures from the FEA model. The buckled reinforcement at large drift levels was seen both in the damage photos and the axial stress figures. While not shown for all specimens and drift levels, the tensile damage results from the FEA showed similar results to the cracking that occurred to the concrete fill in the pile.

The main issue between the model and the test specimen is the concrete element distortion for all the specimens without the embedded rib in the pile at large displacements. The element distortion issue is the result of high demands on the concrete for Specimens 30-21, 48-21, and 30-21-LD. As seen in both the measured and simulated results, specimens with an embedded rib are able to reach higher strengths and larger drift levels, all while not experiencing lateral strength degradation. This is also seen in the damage comparison figures, with the damage not being able to be compared at these large drift levels. There is also significantly less damage to the concrete at the top of the pile, as seen in there is no distortion in the concrete elements for the simulated results and reduced damage to the test specimen with the embedded ring, 30-21-R.

Chapter 7. SUMMARY, CONCLUSIONS, AND FUTURE WORK

The experimental research program was conducted to investigate the connection between a RC column and a CFST pile and the effects of various parameters. The following sections contain a summary of the tests performed and observed behavior, conclusions from the tests, and suggest future topics for similar research to explore.

7.1 SUMMARY OF RESEARCH

CFSTs have been shown to be excellent composite structural components as columns and as piles for bridges due to both their strength and ductility characteristics and their cost-effectiveness. One of the most common uses of CFST components in bridge construction is for deep piles. To advance accelerated bridge construction, there is an interest in a direct column to pile connection capable of sustaining large cyclic drift demands resulting from seismic demands. However, there is limited research on these connections.

This research program was undertaken to investigate the fundamental characteristics and structural performance of a direct connection. In all cases, the longitudinal column reinforcement was embedded the full development length according to AASHTO, i.e. this parameter was not varied. The four-specimen test matrix studied the following parameters:

- Pile diameter to column diameter ratio. This study used 20-inch diameter columns. Both 30 in. diameter pile and a 48 in. diameter piles were tested.
- Supplemental Bond. One specimen included a supplemental rib at the top of the steel tube inside the pile.
- The inelastic response of the connection under long-duration cyclic loading to simulate subduction zone motion.

A total of four, half-scale column-pile connections were tested. For all specimens, the column geometry and reinforcement were the same, a 20 in. diameter concrete column with a reinforcement embedment depth of 21 in. into the pile, while the pile component or test displacement history varied. All CFST piles were embedded into a RC transfer block. The concrete used for the pile fill and column all had the same design strength of 4000 psi. The reinforcing steel had a specified grade of A706 Gr. 60. The 30 in. diameter tube had a grade of API 5L x52 and the 48 in. diameter tube had a grade of API 5L X42. The steel used for the annular rings and embedded rib had a grade of A 572 Gr. 50. The specimen test matrix is shown in Table 7.1.

Table 7.1. Specimen Test Matrix

Specimen Name	Tube Diameter (in.) [mm]	Tube Diameter/ Tube Thickness	Reinforcement Bar Size	Embedment Depth (in.) [mm]	Rib Size (in.) [mm]	Rib Embedment Depth (in.) [mm]
30-21*	30 [762]	60	#7	21 [533]	NA	NA
48-21	48 [1219]	96	#7	21 [533]	NA	NA
30-21-R	30 [762]	60	#7	21 [533]	2 [50.8]	2 [50.8]
30-21-LD[#]	30 [762]	60	#7	21 [533]	NA	NA

*Specimen 30-21 is reference specimen
[#]Tested under long-duration displacement history based on M-9 earthquake research

The four specimens were tested under combined axial and lateral loading of the column. The axial load was applied using a 2400 kip Universal Testing Machine and the lateral loads were applied using a 200 kip MTS actuator attached to a self-reacting test frame. The axial load was approximately 7.5% of the gross axial capacity of the column based on measured strength. The axial load for each specimen is shown in Table 7.2.

Table 7.2. Specimen Test Matrix

Specimen	Axial Load
30-21	160
48-21	120
30-21-R	120
30-21-LD	160

The pile was embedded into a RC transfer block which was secured down to the test rig to avoid uplift. The transfer block was used to replicate the condition a CFST pile would experience under lateral loading.

While testing, the following observations were made:

- Yielding of the column reinforcement occurred during smaller cycles ranging between 0.6% to 1.1% column drift
- Spalling that exposed the column transverse reinforcement occurred during moderate cycles between 3.7% to 5.5% column drift
- Spalling that exposed the column longitudinal reinforcement occurred during moderate cycles between 4.1% to 5.5% column drift
- Extensive buckling of the column reinforcement occurred during larger cycles ranging 7.5% to 8.8% drift for all specimens not tested under long duration loading
- Specimen 30-21-LD experienced buckling at 5.2% drift due to its different displacement history
- Specimen 30-21-LD was the only specimen that had a longitudinal reinforcing bar fracture during testing, with both a bar on the north and south sides of the column fracturing during the last cycle
- All tests were terminated due to lateral strength resistance loss caused by bar buckling and concrete crushing during large drift cycles between 8.1% to 9.9% column drift

- Specimen 30-21-R was the only specimen able to withstand four cycles at 9% or greater drift before significant lateral strength loss
- Specimens 30-21 and 30-21-LD experienced significantly more damage, radial cracks, and concrete spalling, to the top of pile concrete than the other two specimens. Specimen 48-21 did have radial cracks on the top of the pile concrete, while Specimen 30-21-R did not show any damage
- For all specimens, the pile and transfer block showed no visible or measured damage

When comparing the strain distribution and profiles of each specimen, the following observations were made:

- The strain in the reinforcement decreased in magnitude the farther the reinforcement was embedded into the pile
- The tube strains increased in magnitude the farther down the pile
- At 15 in. below the column base, the strains measured on both the reinforcement and tube are approximately linear
- At all drift levels, the strain in the steel tube is very small, showing the pile is not near its maximum strength and is performing very well
- Specimen 48-21's reinforcement strain magnitudes were consistently higher than the other specimens' reinforcement strains at similar drift levels
- The strain in Specimen 30-21-R's tube was larger than Specimen 30-21's and Specimen 30-21-LD's tube strains

There were four different displacement contributions to the total displacement of the specimen (from the base to the top): (i) flexural response of the pile, (ii) end rotation of the pile, (iii) yielding of the reinforcement in the pile-column connection, and (iv) flexural response of the column. When

comparing the percentages of each deformation contributions of each specimen, the following observations were made:

- The displacement of the specimen is primarily due to two mechanisms: (1) yielding of the reinforcement in the pile and (2) the flexural displacement along the length of the column
- As the displacement of the specimen increases, the percentage due to pile displacement and rotation decrease, while the percentage due to the column connection increases, and the percentage due to column flexure stays constant
- The contribution of the connection was largest for Specimen 48-21, approximately 55% of displacement, while other specimens were approximately 45% of total displacement
- Calculation of Specimen 30-21-LD displacement due to column flexure at small drift cycles was incorrect due to error in the measurements from the instrumentation and not included

When comparing the overall specimen behavior of each specimen, the following observations were made:

- The flexural strength of all of the columns were 32% to 40% larger than the predicted
- Specimens 48-21 and 30-21-R were able to maintain lateral strength after the peak lateral resistance was reached at approximately 4.0% column drift for both, while Specimen 30-21 and 30-21-LD showed lateral strength degradation after the peak lateral resistance was reached, which occurred at 3.7% and 6% column drift respectively
- Specimens 30-21, 30-21-R, and 30-21-LD sustained one cycle at 8% drift, while Specimen 48-21 did not sustain any cycles at 8% drift or greater

When comparing the experimental results to the FEA model results, the following observations were made:

- The FEA system behavior of all specimens generally matched the measured experimental system behavior
- The simulated results for Specimens 30-21 and 30-21-LD showed lateral strength degradation after peak strength was reached
- The models of Specimens 30-21, 48-21, and 30-21-LD failed due to distortion in the concrete component of the model: the drift capacity of the models were less than the tests
- Specimen 30-21-R did not show any distortion in the concrete component of the model suggesting that it is the right connection design with the uncertainties in the field with respect to concrete strength and field placement including eccentricity
- The damage from the FEA closely resembled the damage from the experimental behavior in terms of concrete spall, cracking, and buckling of reinforcement

7.2 RESEARCH RESULTS AND CONCLUSIONS

The following conclusions were reached based on interpretation of experimental observations, measured response, and comparison to FEA:

- Composite action between the column and the CFST pile occurs at approximately 15 in. below the column base
- Without the addition of an embedded rib inside the pile, a 48 in. pile connection showed better overall performance than a 30 in. pile connection, both in terms of strength degradation, deformation capacity, specimen damage, and slip between the steel tube and the connection concrete. However, it is not possible to investigate the internal damage in any of these specimens. The model indications substantial internal damage to the connection I the specimens without the supplemental rib.

- With the addition of an embedded rib inside the pile, the connection showed improved performance with both an increase in strength and ductility, a decrease in the slip between the connection concrete and the steel tube, and a decrease in damage
- When testing the connection under long-duration cyclic loading, the connection was able to relatively sustain lateral resistance for multiple cycles at large drift levels
- The results of the FEA model closely matched the behavior of the different specimens' experimental results, showing similar behavior in terms of strength, ductility, lateral strength degradation of specimens with a smaller pile and without an embedded rib, and increased concrete damage for all specimens without the embedded rib
- Using CFST piles, in a direct column to pile connection, can reduce project costs and enable accelerated construction through the reduction of labor and materials due to the elimination of formwork and internal reinforcement inside the pile

7.3 Recommendations for Future Work

Several recommendations for future work were determined while testing and analyzing the results of the experimental program. The recommendations include:

- Experimental investigation of the effect an eccentric column would have on the connection with and without a supplemental rib
- Experimental investigation of different reinforcing bar sizes to determine the effect on embedment depth, which is based on the bar development length, on the connection
- Experimental investigation of using high-strength reinforcement to determine if an increase in column strength would improve the performance of the connection

- Experimental investigation of varying embedded rib depths to determine the optimal location for an additional mechanical bond mechanism in the connection
- Experimental investigation using different displacement histories, such as earthquake displacement histories, instead of increasing drift levels
- Experimental investigation using cyclic axial loading during the testing of the connection, simulating variable superstructure loads on the column

For all recommendations, experimental testing should look at the different parameters for piles of both 30 in. and 48 in. diameters to determine the extent of performance improvement using a larger diameter pile would be.

Based on experience constructing and testing in the UW structures laboratory, the following construction recommendation is also included:

- When constructing a specimen with a 48 in. diameter pile, decrease the transfer block height by 8 in., which will decrease the overall weight of the specimen by 2000 lbs. This will allow for the complete construction of the specimen on the structures lab floor before moving the specimen onto the test rig

BIBLIOGRAPHY

[1] American Association of State Highway and Transportation Officials. (2017). *AASHTO LRFD Bridge Design Specifications*. American Association of State Highway and Transportation Officials (AASHTO), Washington, DC.

[2] American Association of State Highway and Transportation Officials. (2015*). Guide Specifications for LRFD Seismic Bridge Design with 2012, 2014 and 2015 Interim Revisions*. American Association of State Highway and Transportation Officials (AASHTO), Washington, DC.

[3] American Concrete Institute. (2014). *Building Code Requirements for Structural Concrete (ACI 318-14)*. Farmington Hills, MI.

[4] California Department of Transportation (Caltrans). (2019). *Seismic Design Criteria*. Sacramento, CA

[5] Chang, M. (2021). *Seismic Performance of Column-to-Drilled-Shaft Connections in Reinforced Concrete Bridges,* Thesis, University of Washington.

[6] Kappes, L., Berry, M., and Stephens, J. (2013). *Performance of Steel Pipe Pile-to-Concrete Cap Connections Subjected to Seismic or High Transverse Loading,* Technical Report FHWA/MT-13-001/8203, Montana Department of Transportation.

[7] Kortum, Z. (2021). *Impacts of Cascadia Subduction Zone M9 Earthquakes on Bridges in Washington State: SDOF Idealized Bridges,* Thesis, University of Washington.

[8] Liu, Y. (2012). *Lateral Behavior of Reinforced Concrete Columns Supported on Type II Shafts*, M.S., University of California, San Diego.

[9] Mehraein, M. (2016). *Seismic Performance of Bridge Column-Pile-Shaft Pin Connections for Application in Accelerated Bridge Construction,* Dissertation, University of Nevada, Reno.

[10] Stephens, M. T. (2016). *Design Expressions and Dynamic Evaluation of CFST Bridges Subjected to Seismic Hazards,* Dissertation, University of Washington.

[11] Tran, H. V. (2015). *Drilled Shaft Socket Connections for Precast Columns in Seismic Regions,* Dissertation, University of Washington.

[12] Washington State Department of Transportation (WSDOT). (2020). *Bridge Design Manual (LRFD) M 23-50*. Olympia, WA.

[13] Yeutter, A. S. (2020). *A RC Slab to CFT Column Connection for Improved Seismic Behavior of Multi-Story Buildings,* Thesis, University of Washington.

[14] Zhao, M., Lehman, D., and Roeder, C. (2021). *Analytical Investigation of a New Direct Column-to-Cased Shaft Connection,* Engineering Structures, 245 (October 2021)

APPENDIX 1 –SPECIMEN DRAWINGS

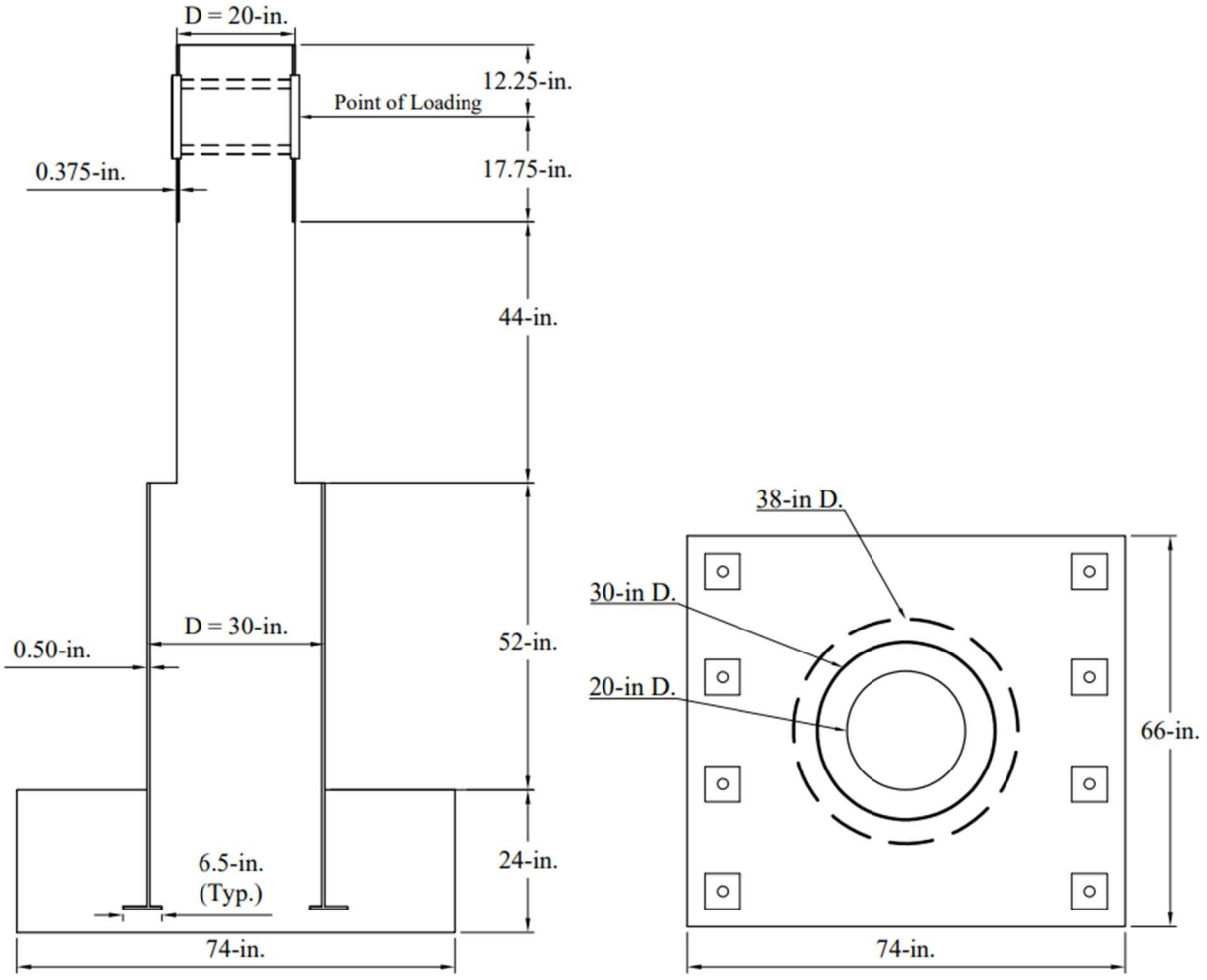

Figure A1.1 Specimen 30-21 and 30-21-LD Dimensions

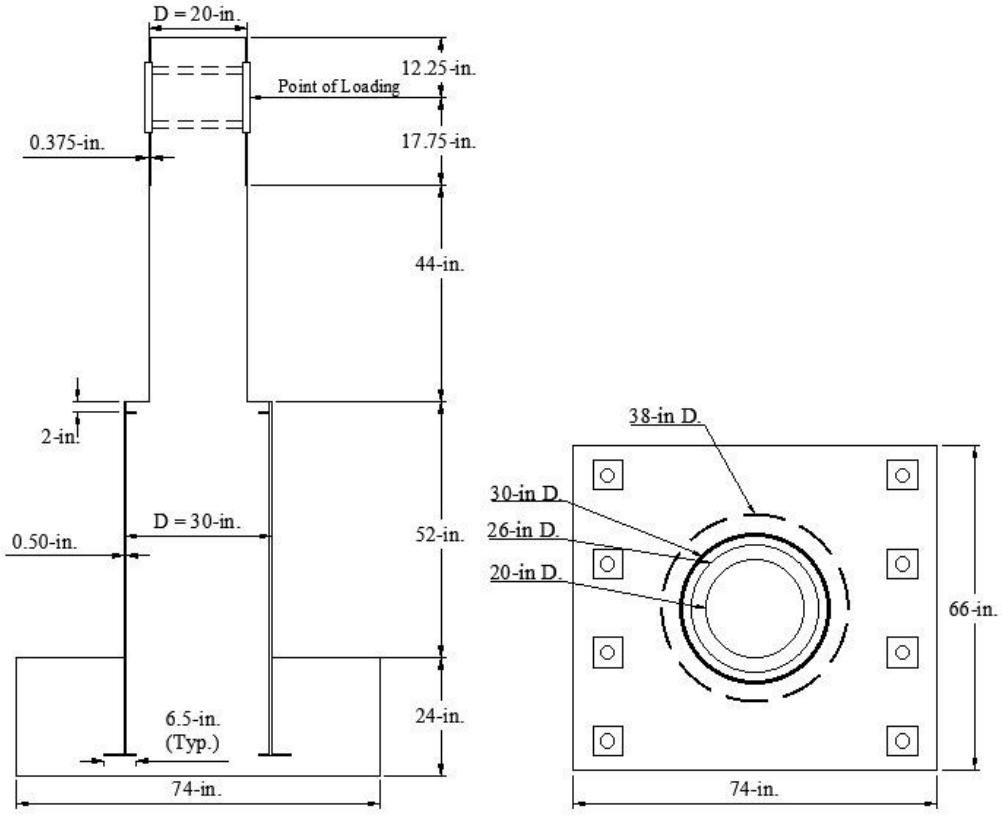

Figure A1.2 Specimen 30-21-R Dimensions

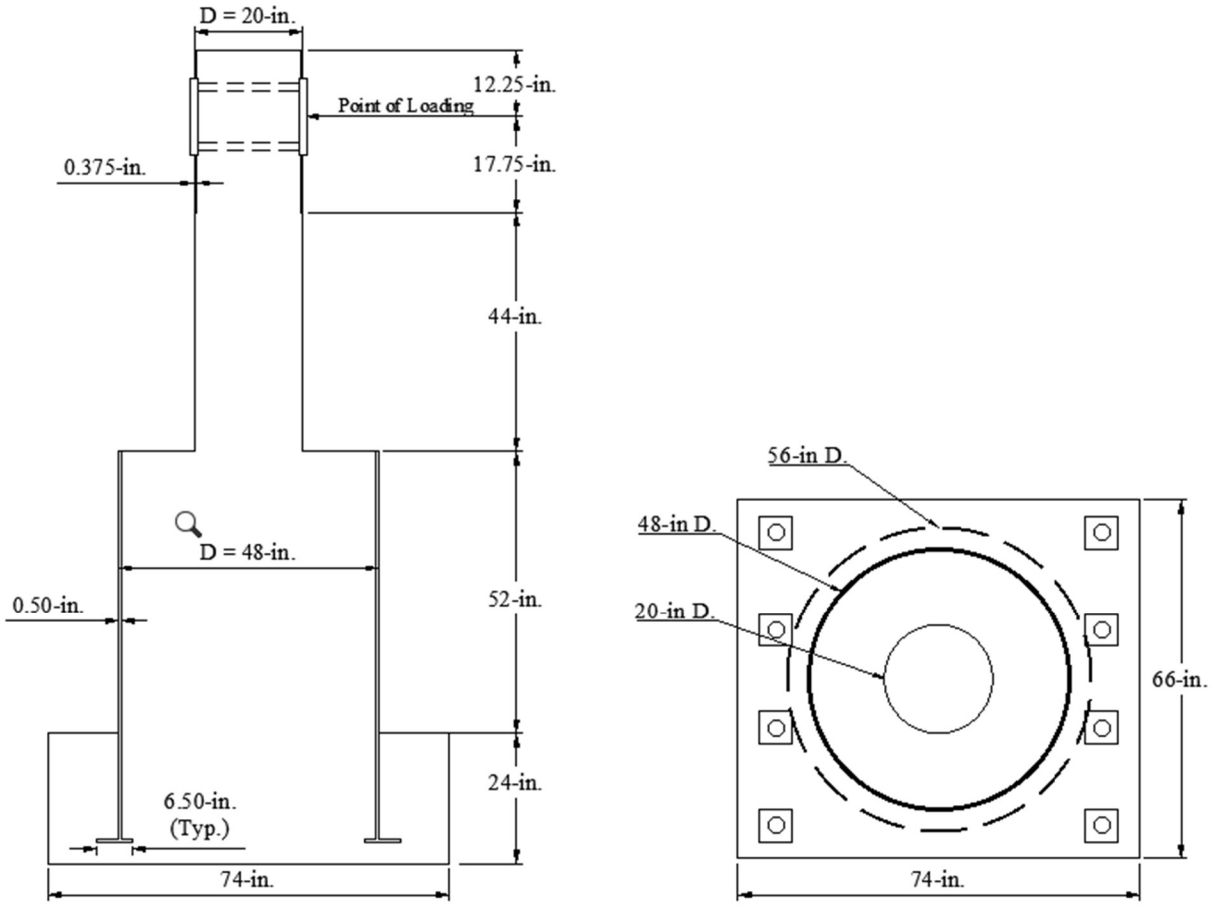

Figure A1.3 Specimen 48-21 Dimensions

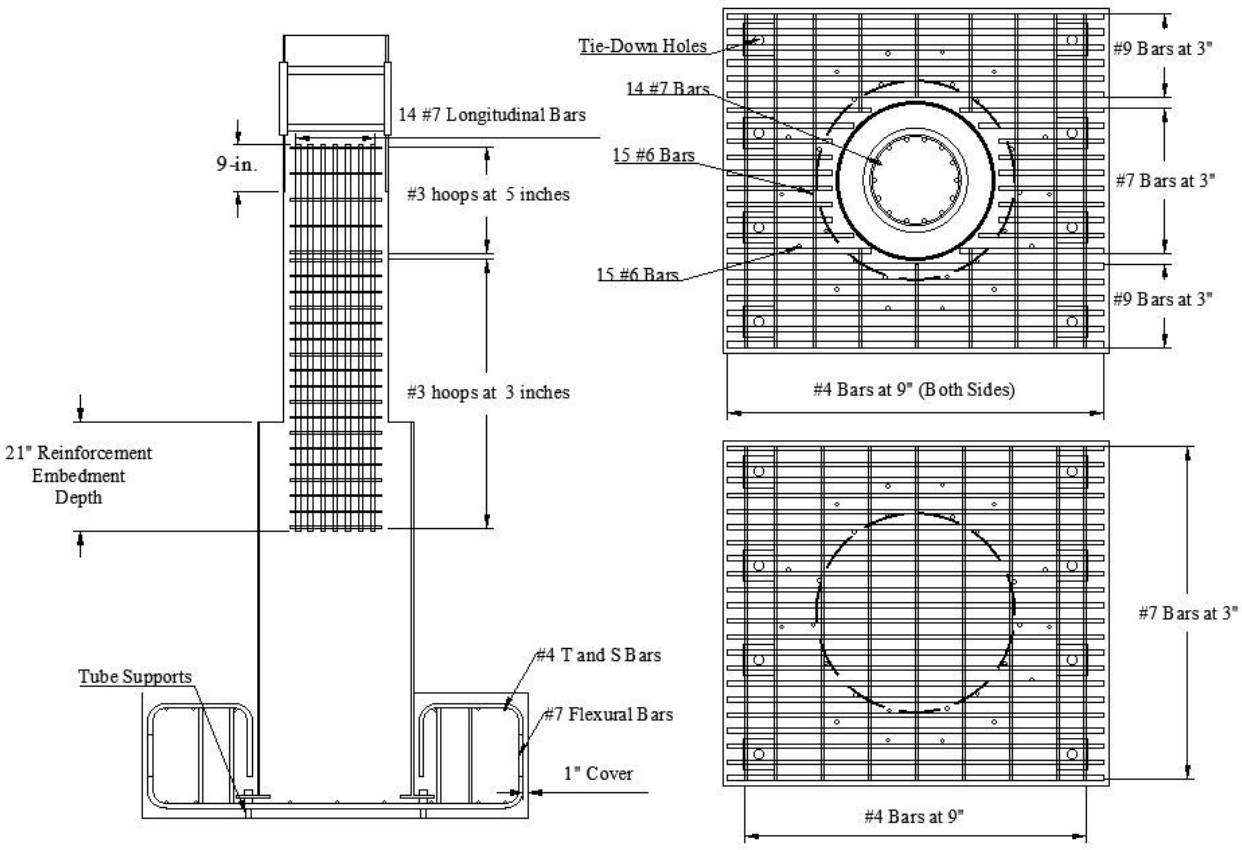

Figure A1.4 Specimen 30-21 and 30-21-LD Reinforcement Layout

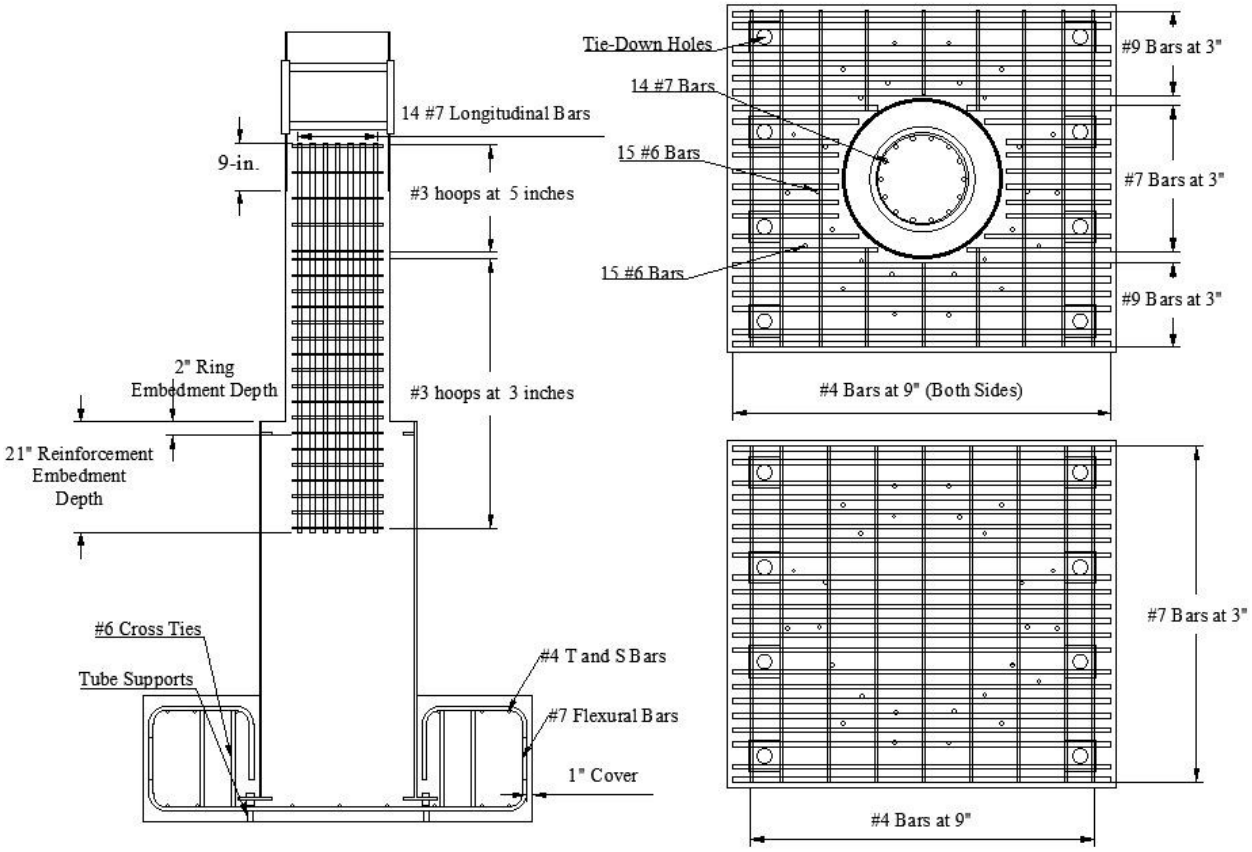

Figure A1.5 Specimen 30-21-R Reinforcement Layout

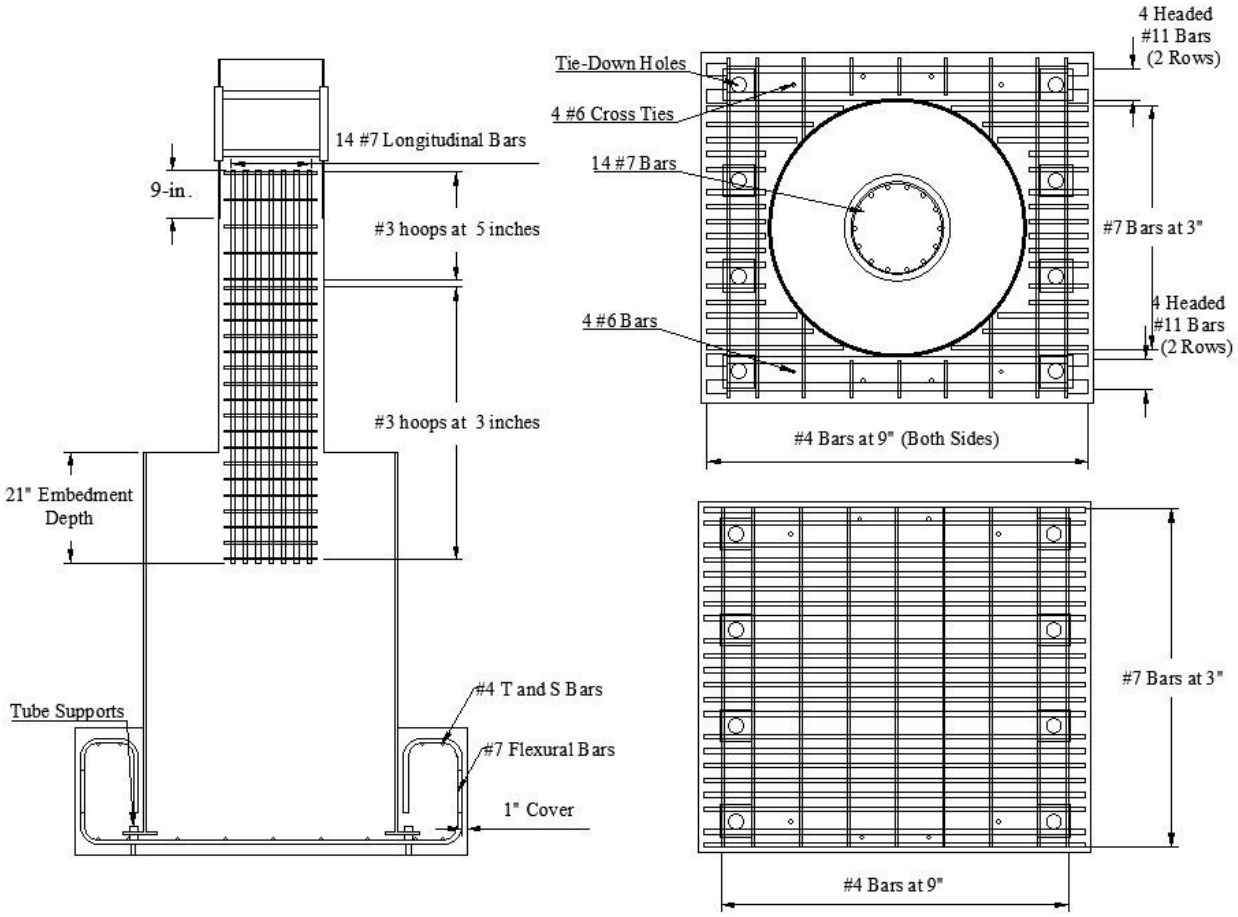

Figure A1.6 Specimen 48-21 Reinforcement Layout

APPENDIX 2 – SAMPLE CALCULATIONS

Spencer Lindsley
3/30/2020
Specimen Transfer Block
Calculations

Reinforcement Parallel to Loading

Design Moment	$M_u := 1000\ kip \cdot ft$
Steel Yield Stress	$F_y := 72\ ksi$
Width of Block	$W_b := 68\ in$
Depth of Block	$H_b := 24\ in$
Block Cover	$CC := 2\ in$
Diameter of #7 Bar	$D_{7.bar} := 0.875\ in$
Distance to Center of Reinforcement	$d := H_b - CC - \frac{D_{7.bar}}{2} = 21.6\ in$
Area of Steel Required	$As_{req} := \frac{M_u}{0.7 \cdot F_y \cdot 0.9 \cdot d} = 12.3\ in^2$
Area of Steel Required (per foot)	$As_{req.f} := \frac{As_{req}}{W_b} = 2.165\ \frac{in^2}{ft}$
Area of #7 Bar	$A_{b.7} := .6\ in^2$
Spacing of Bars	$Spacing := \frac{A_{b.7}}{As_{req.f}} = 3.325\ in$

Use #7 bars are 3 inches for top and bottom bars parallel to loading

Temperature and Shrinkage Reinforcement (Perpedicular to Loading)

Only need to account for temperature steel, use reinforcement layout from Angela Kingsley's 2005 thesis.
Use #4 bars are 9 inches for top and bottom bars parallel to loading

Figure A2.1 Transfer block Steel Reinforcement Calculations

APPENDIX 3 – TEST REPORTS

CFST Column to Pile Connection Test 1 Summary
Specimen 1: 30” Diameter Tube with 21” Reinforcement Embedment

Overview:

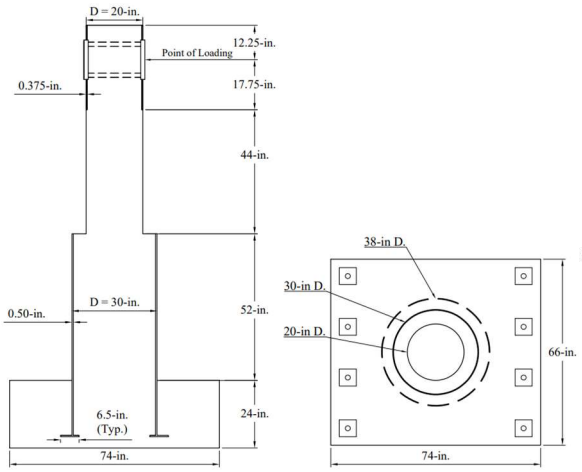

Fig. 1 Specimen Dimensions

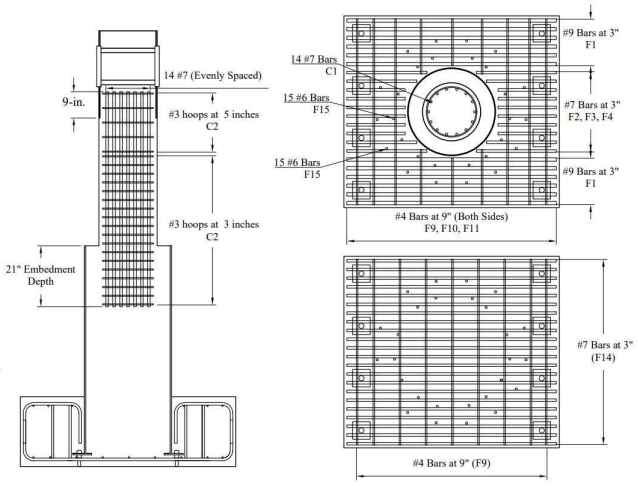

Fig. 2. Specimen Reinforcement

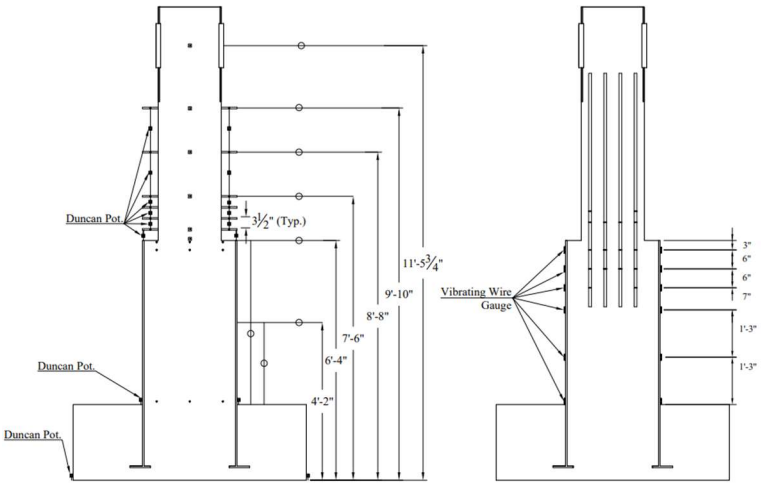

Fig 3. Specimen Instrumentation

Fig. 4. As-Built Specimen

Measured Response

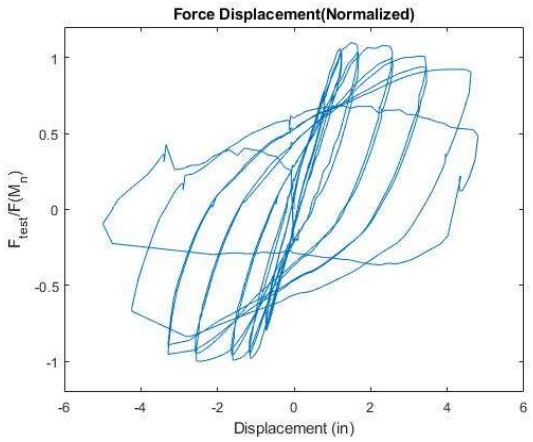

Fig 5. Normalized Force-Displacement

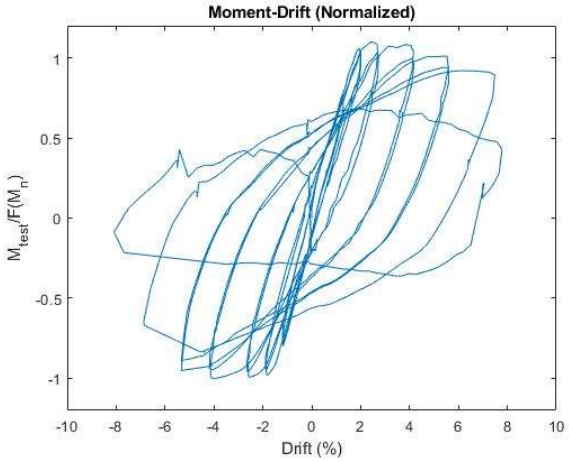

Fig. 6. Normalized Moment-Drift

Observed Response

Table 1. Specimen 1 Maximum Displacements, Drifts, and Forces

Set	Cycle	Target Displacement (in)	Target Drift (%)	Actual Displacement (in)	Actual Drift (%)	Force (kip)	Moment (k-ft)	Damage Description	Ref. Fig.
DR	1	1.1	1.78	0.68	1.11	75.6	401.0	H Cracks	
1	1	1	1.62	0.59	0.96	61.9	328.1	0.3mm H Crack	7
1	2	1	1.62	0.58	0.94	63.6	337.3	0.5mm H Crack	8
2	1	1.5	2.43	0.94	1.52	77.3	411.8	1 mm H crack and radial cracks	9
2	2	1.5	2.43	0.96	1.55	78.1	417.2	1 mm H crack and diagonal cracks	10
3	1	2	3.24	1.38	2.23	85.2	459.0	2 mm H crack	11
3	2	2	3.24	1.42	2.30	82.5	447.1	2 mm H crack and 1st spall	12,13
4	1	3	4.86	2.33	3.77	85.5	472.9	3mm H crack	14,15
4	2	3	4.86	2.36	3.82	78.2	437.8	3 mm H crack	16
5	1	4	6.48	3.11	5.03	83.1	472.9	4mm H crack	17
5	2	4	6.48	3.17	5.13	77.3	444.0	3 mm h crack	18
6	1	6	9.72	4.34	7.03	74.9	440.5	3+ mm crack at base of column	19
6	2	6	9.72	4.98	8.06	40.9	250.1	Concrete Crushed and Bars Buckled	20

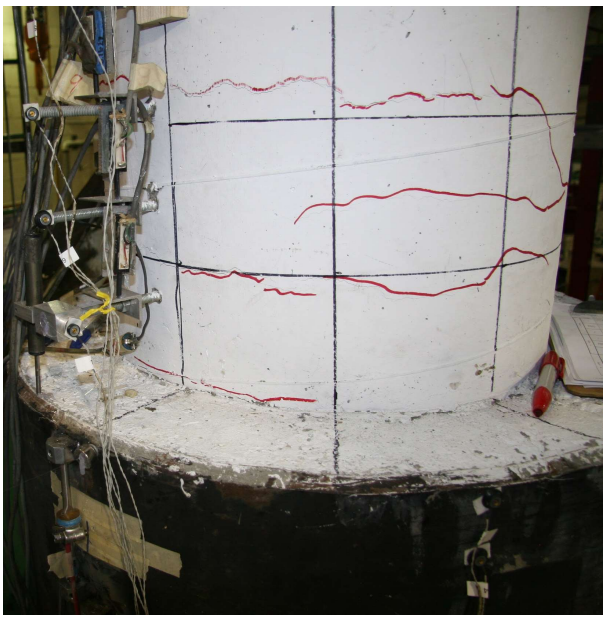

Fig. 7

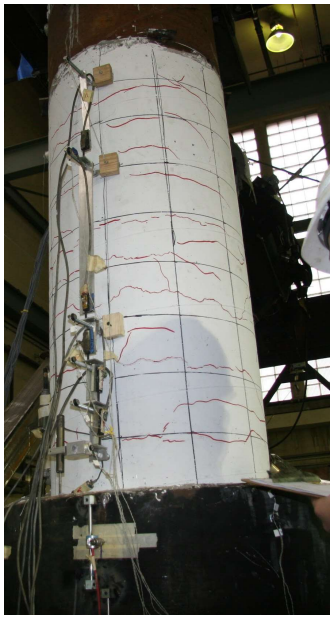

Fig. 8

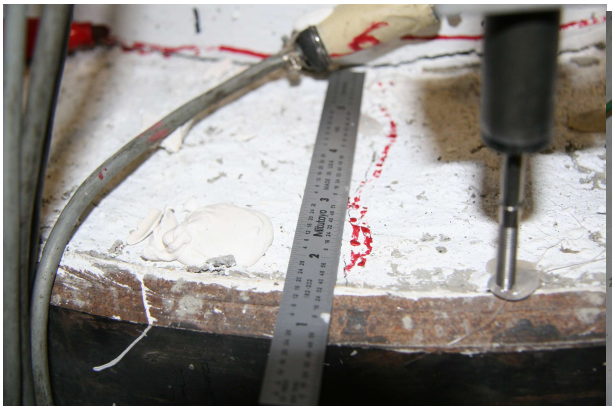

Fig. 9

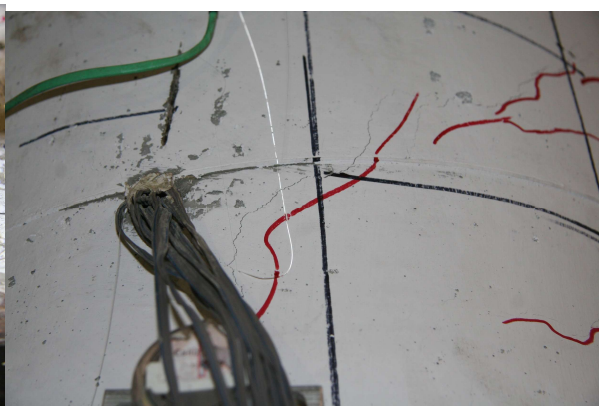

Fig. 10

Fig. 11

Fig. 12

Fig. 13

Fig. 14

Fig. 15

Fig. 16

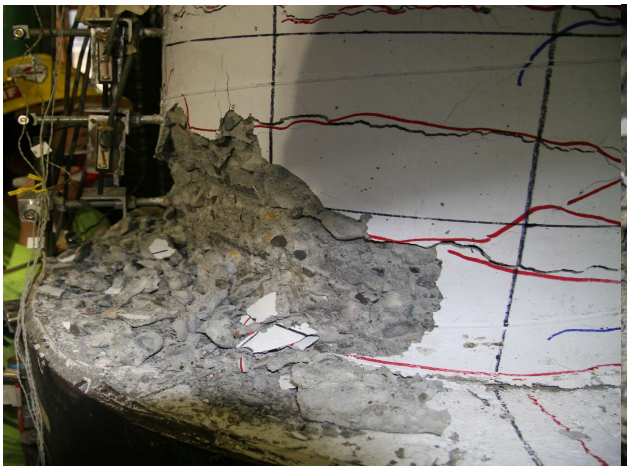

Fig. 17

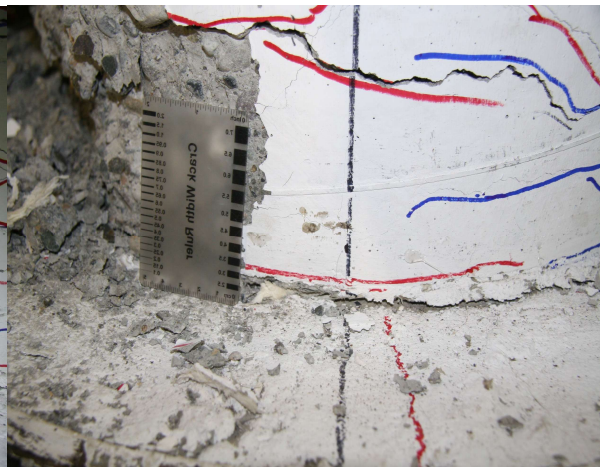

Fig. 18

Fig. 19

Fig. 20

CFST Column to Pile Connection Test 2 Summary
Specimen 2: 48” Diameter Tube with 21” Reinforcement Embedment

Overview:

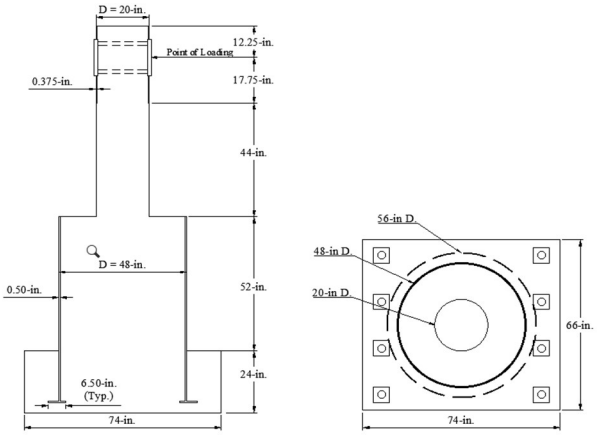

Fig. 1 Specimen Dimensions

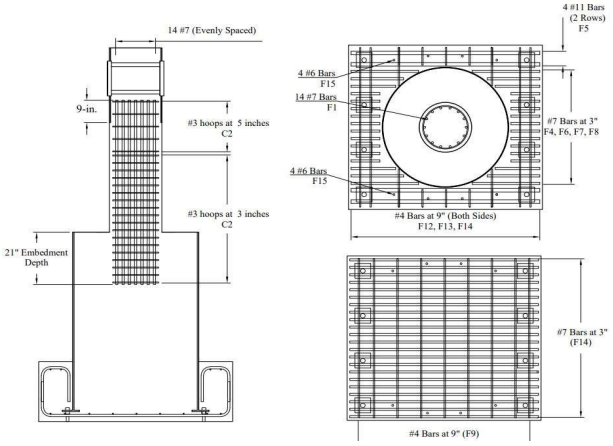

Fig. 2. Specimen Reinforcement

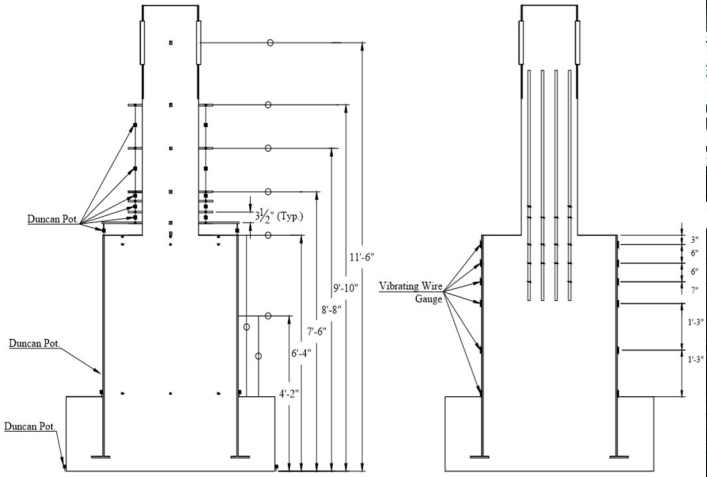

Fig 3. Specimen Instrumentation

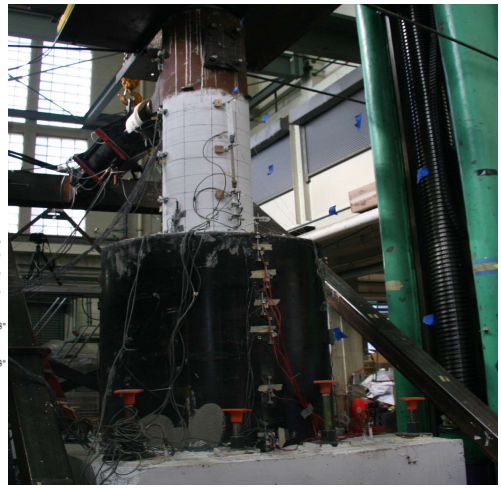

Fig. 4. As-Built Specimen

Measured Response

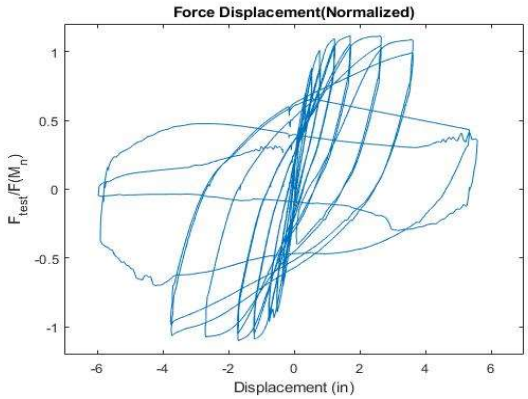

Fig 5. Normalized Force-Displacement

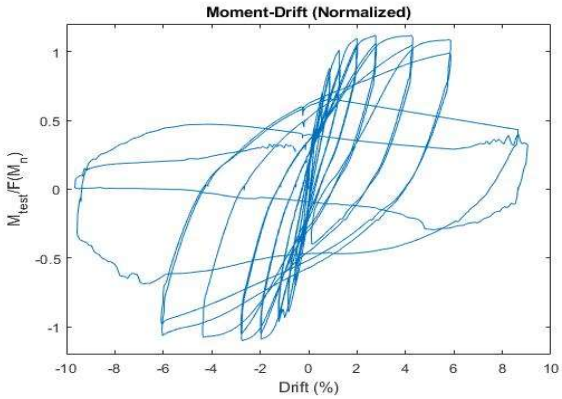

Fig. 6. Normalized Moment-Drift

Observed Response

Table 1. Specimen 1 Maximum Displacements, Drifts, and Forces

Set	Cycle	Target Displacement (in)	Target Drift (%)	Actual Displacement (in)	Actual Drift (%)	Force (kip)	Moment (k-ft)	Damage Description	Ref. Fig.
1	1	0.25	0.4	0.12	0.2	32.3	167.9	.1mm H crack	7
1	2	0.25	0.4	0.13	0.2	31.2	161.9	0.2mm H crack	8
2	1	0.5	0.81	0.30	0.49	53.3	277.9	0.35mm H crack	9
2	2	0.5	0.81	0.31	0.50	52.0	271.0	0.5mm H crack	10
3	1	0.75	1.21	0.47	0.76	66.4	346.8	0.7mm H crack	NA
3	2	0.75	1.21	0.47	0.76	61.7	322.7	0.8mm H crack Radial Crack	11
4	1	1	1.62	0.69	1.11	72.5	380.8	1.25mm H crack Diagonal Cracks	12
4	2	1	1.62	0.71	1.15	66.8	351.3	1.5mm H crack Radial Cracks	13
5	1	1.5	2.43	1.12	1.82	79.5	421.2	2mm H crack	14
5	2	1.5	2.43	1.14	1.84	78.7	417.5	2.5mm H crack Slight spall	15
6	1	2	3.24	1.62	2.62	80.5	431.3	3.25mm H Crack Spall at column base	16
6	2	2	3.24	1.63	2.64	79.0	424.3	3.5mm H crack	17
7	1	3	4.86	2.61	4.22	79.5	436.2	3.5mm H crack Reinforcement exposed	18
7	2	3	4.6	2.54	4.11	73.9	407.3	4mm H crack at base of column	19
8	1	4	6.48	3.65	5.91	77.8	436.5	5mm H crack	20
8	2	4	6.48	3.68	5.95	71.9	405.9	Major spalling Slight bar buckling	21
9	1	6	9.72	5.88	9.52	29.1	191.2	Bar buckled	22
9	2	6	9.72	5.96	9.66	24.3	169.0	Concrete Crushed and bars buckled	23,24

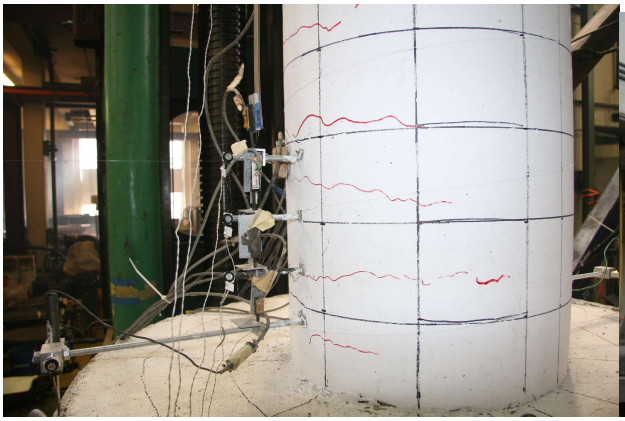

Fig. 7

Fig. 8

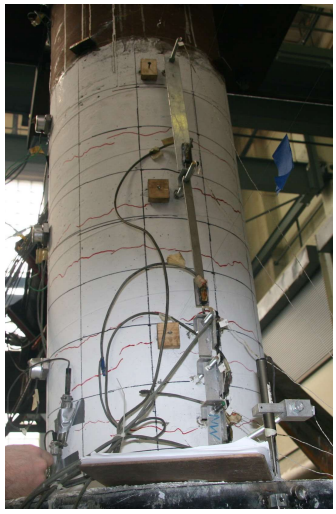

Fig. 9

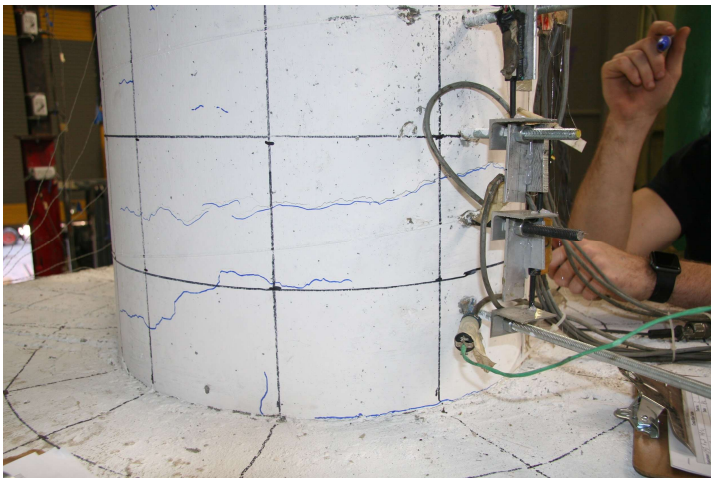

Fig. 10

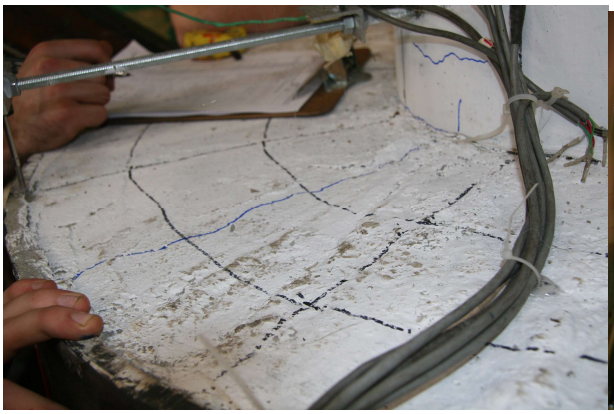

Fig. 11

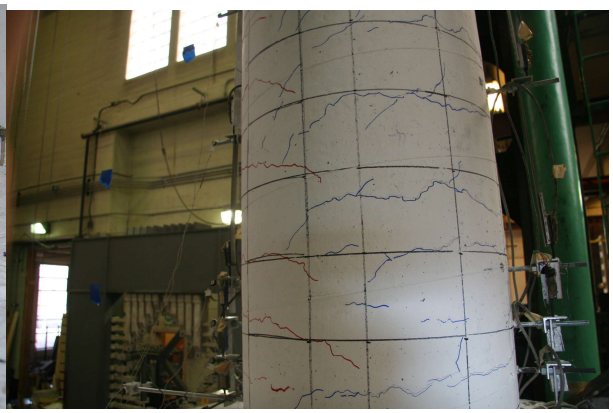

Fig. 12

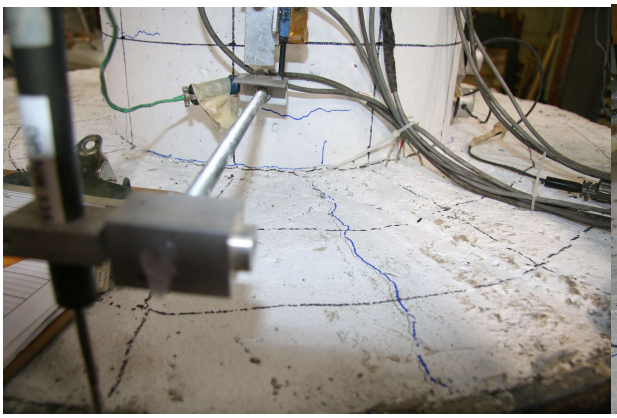

Fig. 13

Fig. 14

Fig. 15

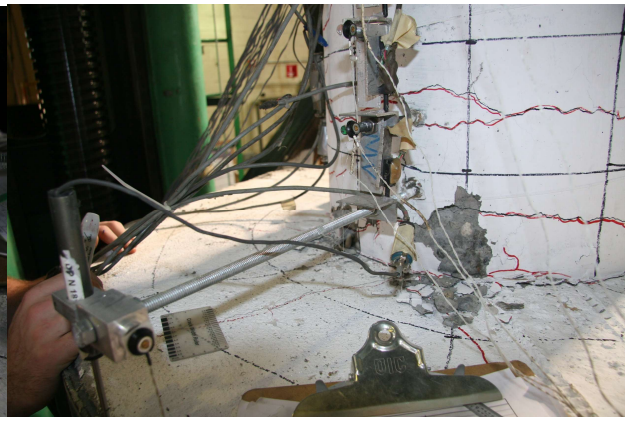

Fig. 16

Fig. 17

Fig. 18

Fig. 19

Fig. 20

Fig. 21

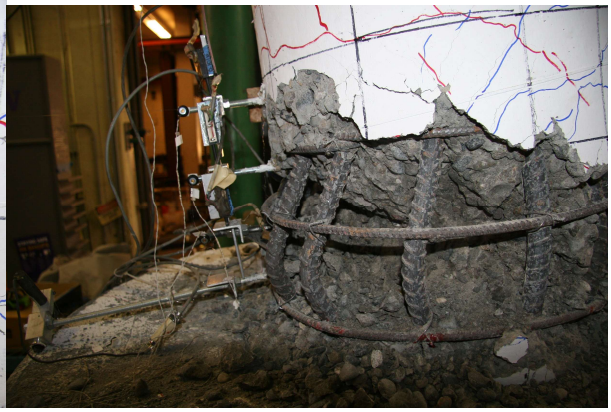

Fig. 22

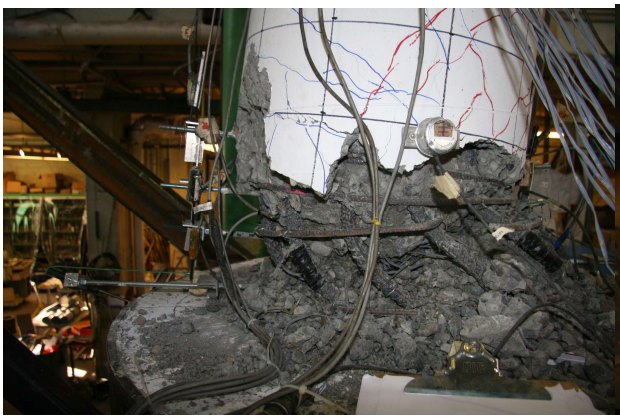

Fig. 23

Fig. 24

CFST Column to Pile Connection Test 3 Summary
Specimen 3: 30” Diameter Tube with 21” Reinforcement Embedment and 2” Embedded Rib

Overview:

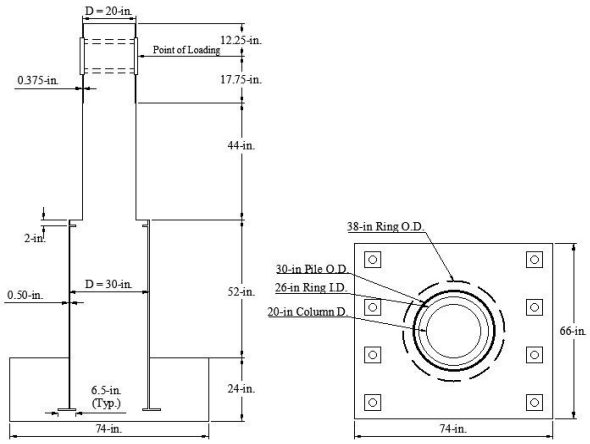

Fig. 1 Specimen Dimensions

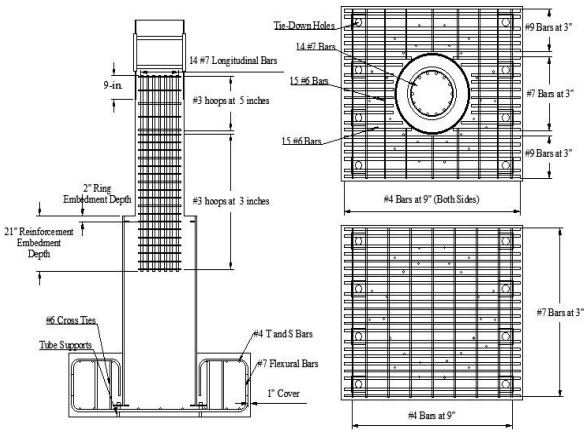

Fig. 2. Specimen Reinforcement

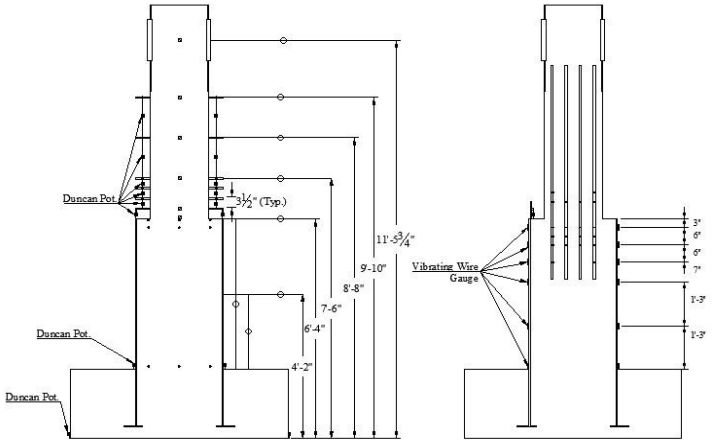

Fig 3. Specimen Instrumentation

Fig. 4. As-Built Specimen

Measured Response

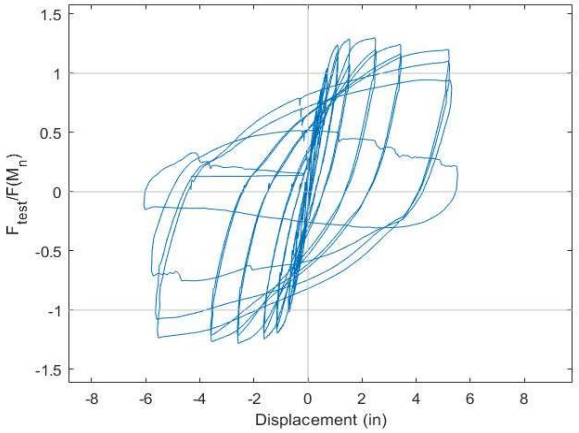

Fig 5. Normalized Force-Displacement

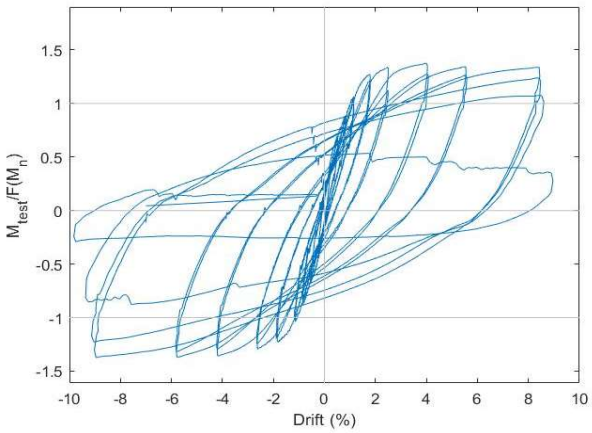

Fig. 6. Normalized Moment-Drift

Observed Response

Table 1. Specimen 3 Maximum Displacements, Drifts, and Forces

Set	Cycle	Target Displacement (in)	Target Drift (%)	Actual Displacement (in)	Actual Drift (%)	Force (kip)	Moment (k-ft)	Damage Description	Ref. Fig.
1	1	0.25	0.4	0.12	0.20	25.9	135.0	No Visible Cracks	NA
1	2	0.25	0.4	0.12	0.20	26.6	138.3	No Visible Cracks	NA
2	1	0.5	0.81	0.29	0.47	40.0	209.1	0.1 mm H Crack	7
2	2	0.5	0.81	0.29	0.46	40.8	213.2	0.1 mm H Crack	8
3	1	0.75	1.21	0.47	0.76	51.0	267.7	0.2 mm H Crack	9
3	2	0.75	1.21	0.48	0.78	56.0	293.6	0.3 mm H Crack	10
4	1	1	1.62	0.65	1.05	68.2	358.0	0.5 mm H Crack	11
4	2	1	1.62	0.67	1.08	66.3	348.4	0.6 mm H Crack Diagonal Cracks	12
5	1	1.5	2.43	1.07	1.74	78.8	416.9	0.9 mm H Crack	13
5	2	1.5	2.43	1.10	1.78	77.9	412.2	1.0 mm H Crack	14
6	1	2	3.24	1.55	2.51	84.3	449.6	1.5 mm H Crack North Base Spall	15 16
6	2	2	3.24	1.56	2.53	78.2	419.1	1.5 mm H Crack	17
7	1	3	4.86	2.51	4.06	83.5	456.5	2+ mm H Crack 2 in. deep crack and column base	18 19
7	2	3	4.6	2.53	4.10	77.2	423.4	2+ mm H Crack Transverse Reinforcement exposed, Spall and Vertical Cracks	20 21
8	1	4	6.48	3.50	5.66	82.5	460.2	2+ mm H Crack Column Base interface cracks	22
8	2	4	6.48	3.53	5.72	74.2	417.5	2+ mm H Crack Major Spall Exposed Reinforcement	23 24
9	1	6	9.72	5.50	8.90	76.4	437.5	2+ mm H Crack Buckled Reinforcement	25 26
9	2	6	9.72	5.57	9.03	70.4	408.4	2+ mm H Crack Reinforcement Buckling	27 28
10	1	6	9.72	5.74	9.30	57.2	339.8	Major Spalling and Bars Buckled	29 30
10	2	6	9.72	6.06	9.82	9.7	93.1	Concrete Crushed and Bars Buckled	31 32
Next-Day After Test								Bar Fracture	33

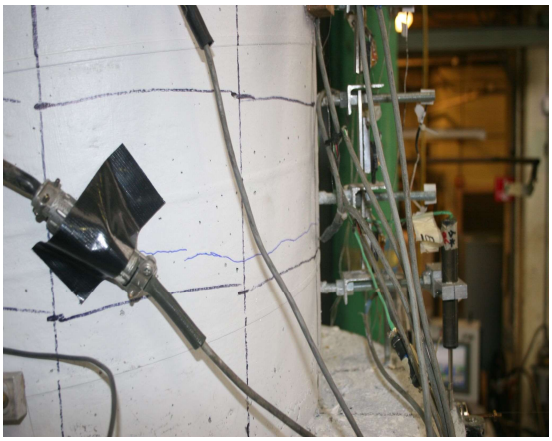

Fig. 7

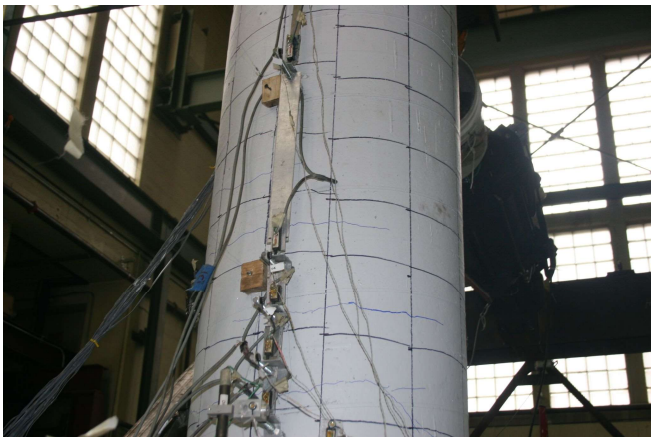

Fig. 8

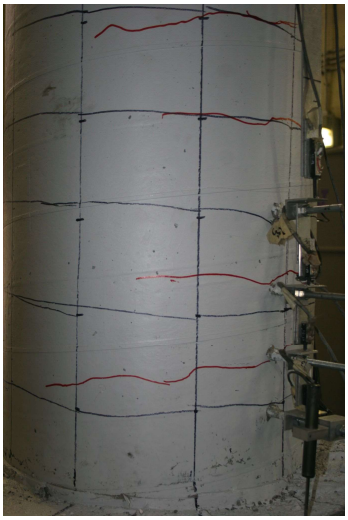

Fig. 9

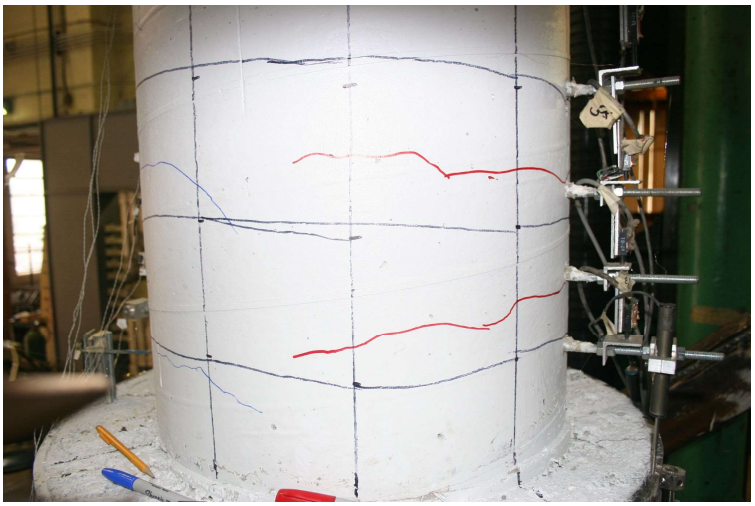

Fig. 10

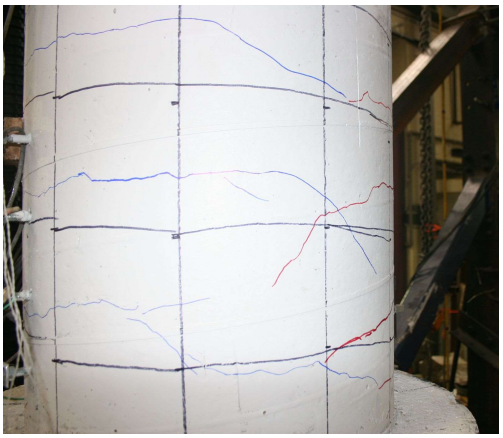

Fig. 11

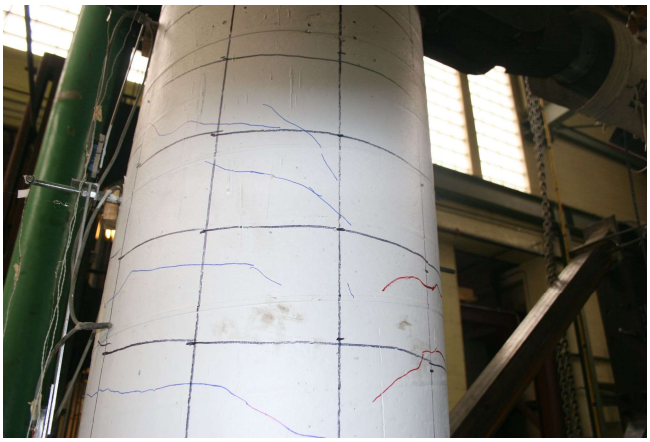

Fig. 12

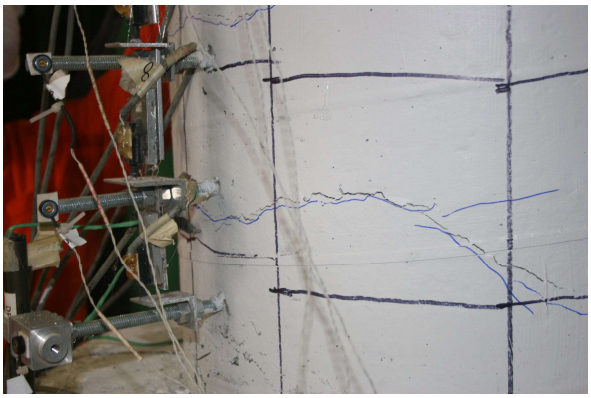

Fig. 13

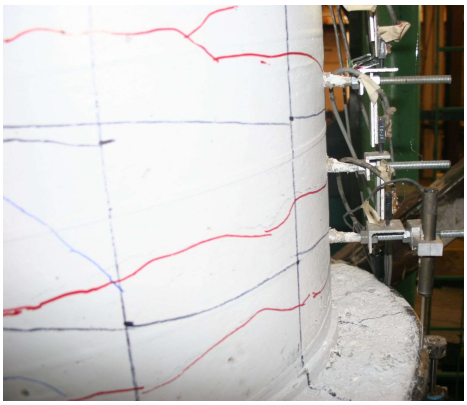

Fig. 14

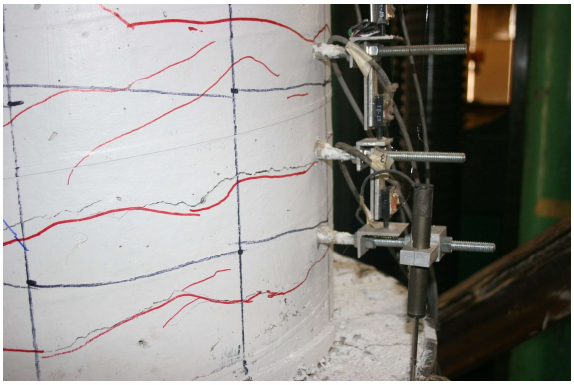

Fig. 15

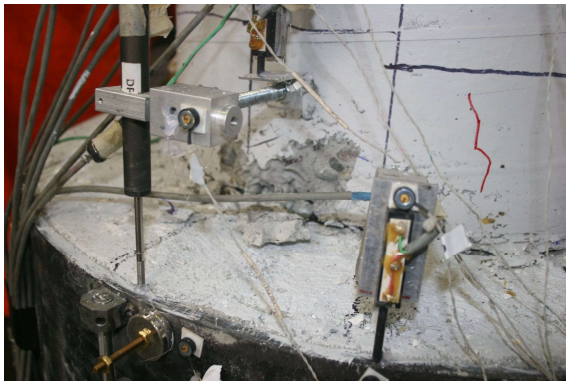

Fig. 16

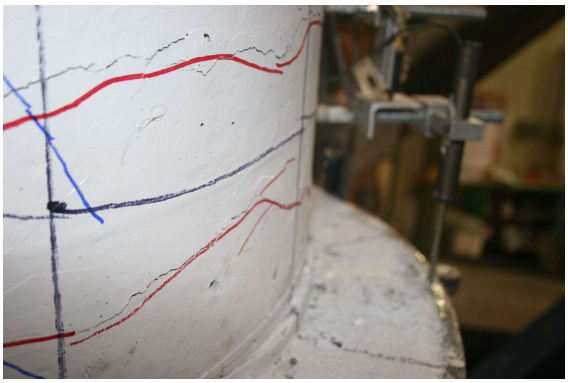

Fig. 17

Fig. 18

Fig. 19

Fig. 20

Fig. 21

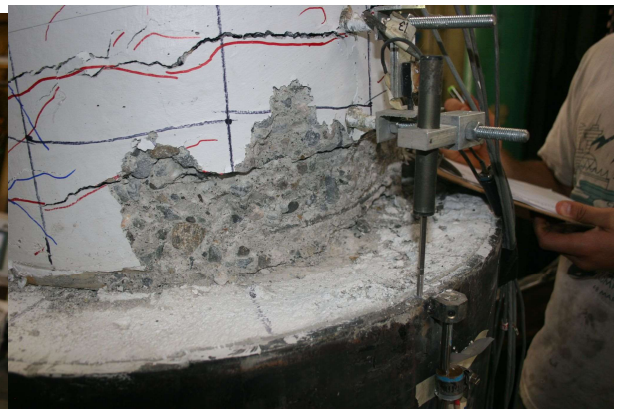

Fig. 22

Fig. 23

Fig. 24

Fig. 25

Fig. 26

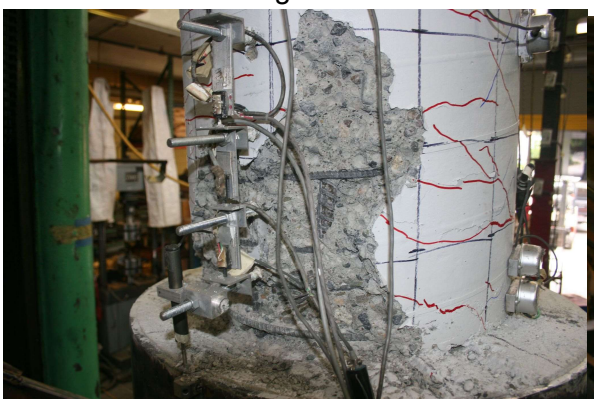

Fig. 27

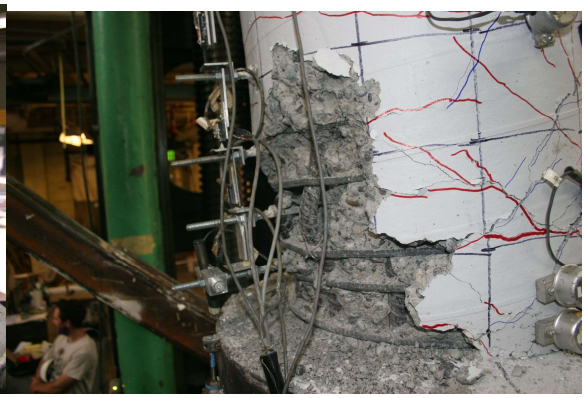

Fig. 28

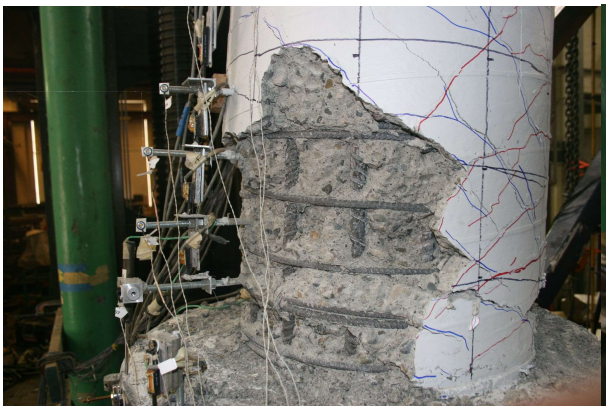

Fig. 29

Fig. 30

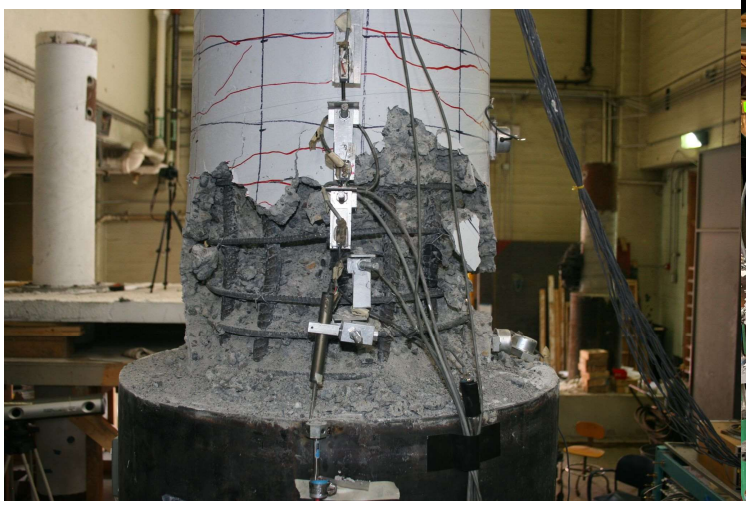

Fig. 31

Fig. 32

Fig. 33

CFST Column to Pile Connection Test 4 Summary

Specimen 4: 30” Diameter Tube with 21” Reinforcement Embedment under Long Duration Cyclic Loading

Overview:

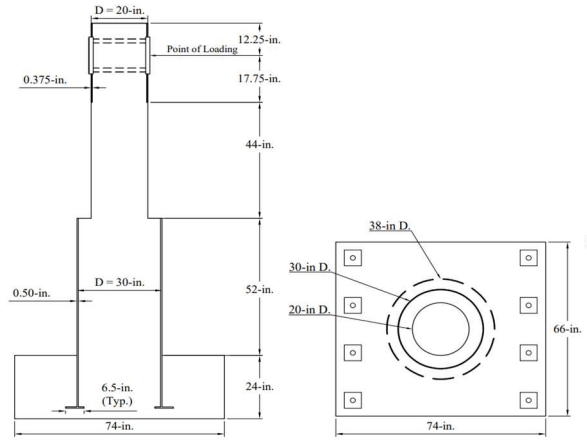

Fig. 1 Specimen Dimensions

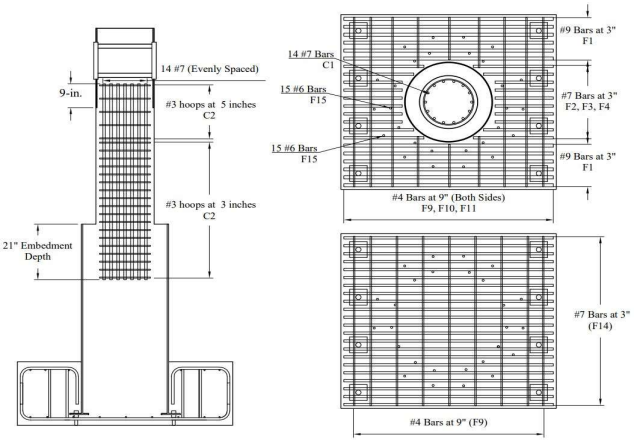

Fig. 2. Specimen Reinforcement

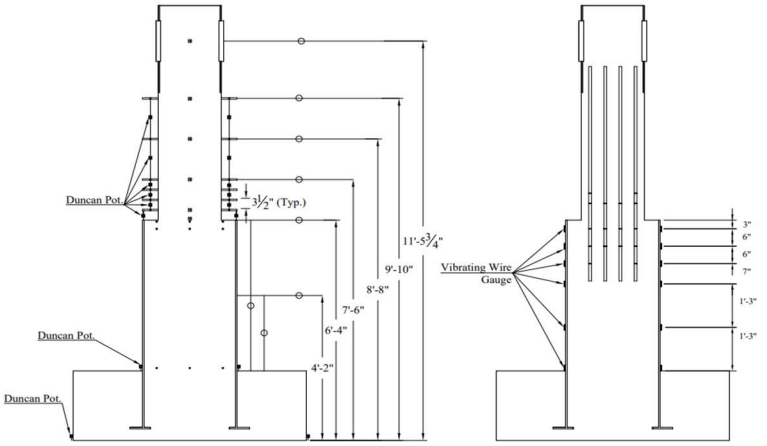

Fig 3. Specimen Instrumentation

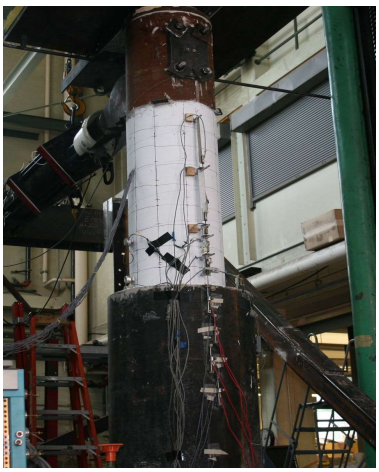

Fig. 4. As-Built Specimen

Measured Response

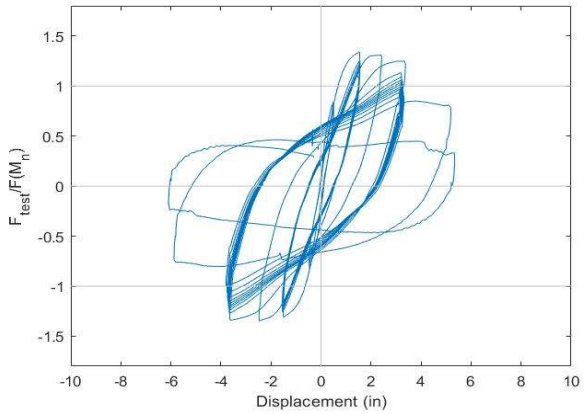

Fig 5. Normalized Force-Displacement

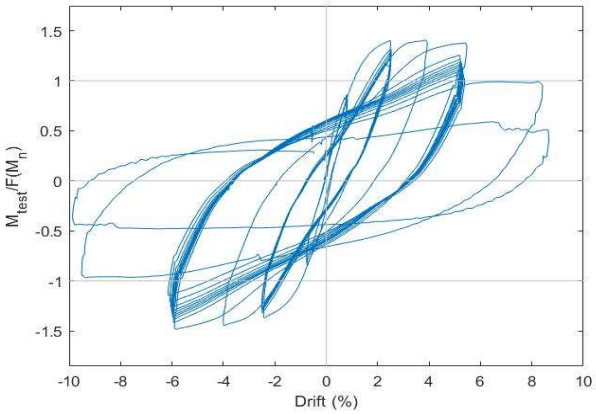

Fig. 6. Normalized Moment-Drift

Observed Response

Table 1. Specimen 1 Maximum Displacements, Drifts, and Forces

Set	Cycle	Target Displacement (in)	Target Drift (%)	Actual Displacement (in)	Actual Drift (%)	Force (kip)	Moment (k-ft)	Damage Description	RefFig
1	1	0.75	1.21	0.48	0.68	48.8	257.3	0.5mm H crack Pile Concrete crack	7 8
1	2	0.75	1.21	0.51	0.75	53.2	280.1	0.5mm H crack	9
2	1	2.0	3.24	1.54	2.38	89.6	482.4	1.3mm H crack 1st Spall Radial Cracks	10 11 12
2	2	2.0	3.24	1.54	2.38	84.3	454.9	1.6mm H crack Pile Concrete Damage	13 14
2	3	2.0	3.24	1.55	2.40	80.7	436.9	2.0mm H crack Column Base Damage	15 16
2	4	2.0	3.24	1.55	2.41	80.4	435.4	2.0mm H crack Edge of Pile Crack	17 18
2	5	2.0	3.24	1.54	2.40	80.1	432.8	2.0mm H crack	19
2	6	2.0	3.24	1.55	2.41	80.6	436.0	2.0mm H crack Deeper Spall	20
3	1	3.0	4.90	2.47	3.88	87.0	482.0	2.5mm H crack Larger Spall	21
4	1	4.0	6.48	3.65	5.77	89.2	50.87	4.0mm H crack Exposed Transverse Reinforcement	22
4	2	4.0	6.48	3.67	5.82	81.3	468.0	5.0mm H crack Exposed Longitudinal Reinforcement	23
4	3	4.0	6.48	3.66	5.80	83.2	447.4	Pile Concrete Damage	24
4	4	4.0	6.48	3.67	5.83	72.1	419.8	Exposed Reinforcement	25
4	5	4.0	6.48	3.70	5.88	77.7	449.5	Slight Bar Buckling	26
4	6	4.0	6.48	3.72	5.90	77.3	447.4	Longitudinal Bar Buckled	27
4	7	4.0	6.48	3.70	5.89	69.7	407.8	Increase in Spall and Buckling Magnitude	28
4	8	4.0	6.48	3.73	5.94	69.5	407.2	Increase in Spall	
4	9	4.0	6.48	3.76	5.98	71.3	416.7	Increase in Spall	
4	10	4.0	6.49	3.76	6.01	57.1	343.6	Increase in Spall	29
5	1	6.0	9.72	5.86	9.43	42.1	281.9	North Bar Fractured	30
5	2	6.0	9.72	6.10	9.86	15.5	139.7	South Bar Fractured Concrete Crushed	31 32

Fig. 7

Fig. 8

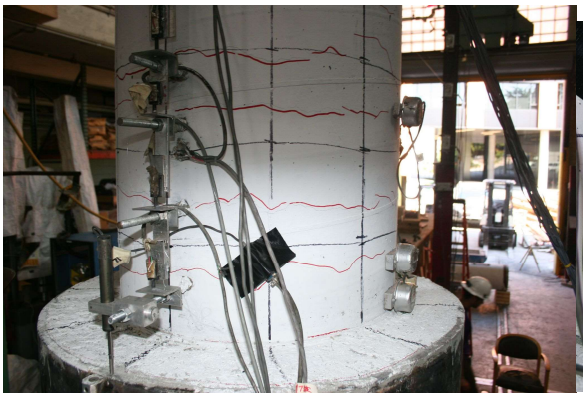

Fig. 9

Fig. 10

Fig. 11

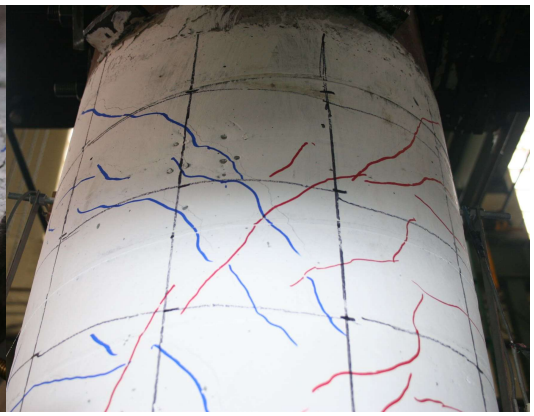

Fig. 12

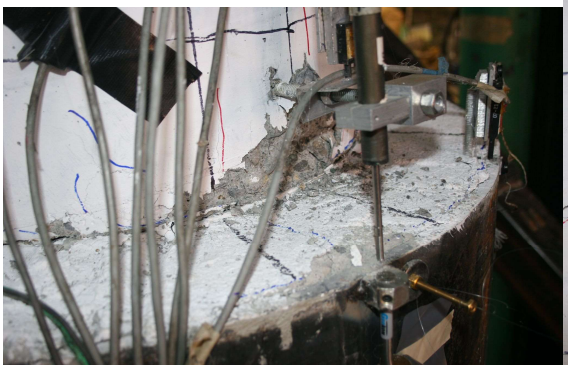

Fig. 13

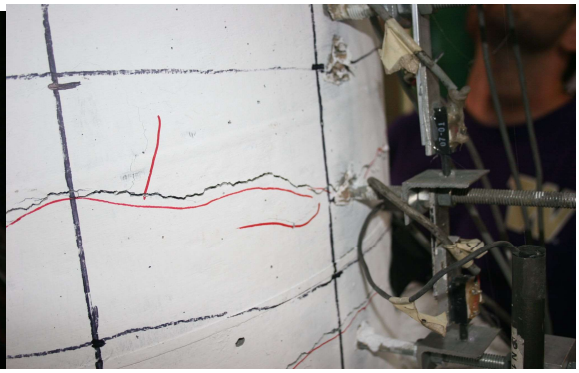

Fig. 14

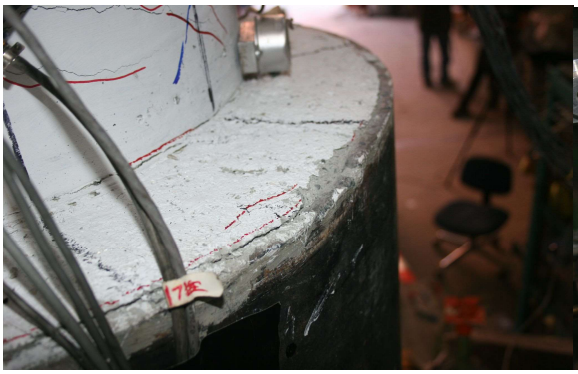

Fig. 15

Fig. 16

Fig. 17

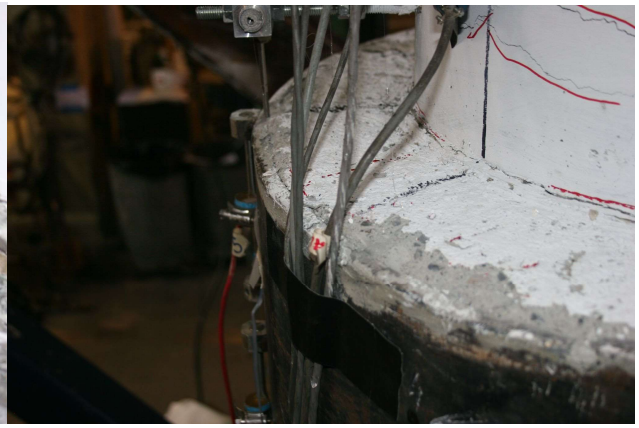

Fig. 18

Fig. 19

Fig. 20

Fig. 21

Fig. 22

Fig. 23

Fig. 24

Fig. 25

Fig. 26

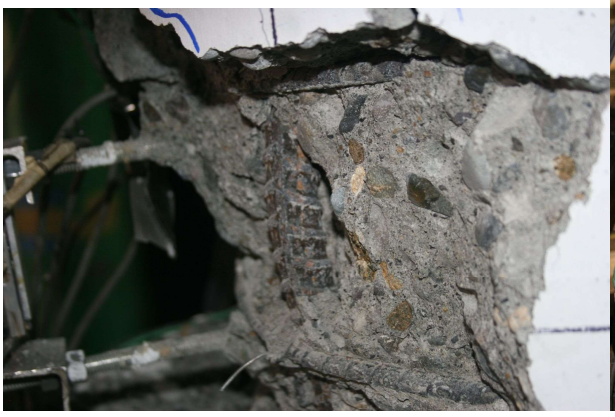

Fig. 27

Fig. 28

Fig. 29

Fig. 30

Fig. 31

Fig. 32